UNIVERSITY OF CAPE TOWN

MASTER'S DISSERTATION

Searching for Ultra-compact binary stars with the MeerLICHT Southern All-Sky Survey

Robbie Lees

supervised by

Prof. Paul GROOT (UCT, Radboud University, SAAO) and Prof. Patrick WOUDT (UCT)

May 12, 2022

Abstract

An effort was made to expand the known population of AM Canum Venaticorum (AM CVn) stars, a rare type of ultra-compact binary star. This was done by searching through the MeerLICHT Southern All-Sky Survey (ML SASS) data with a candidate selection process which made use of a selection technique based on the colours of stars. The candidates found were then observed with an extensive follow-up observation campaign which included both high-speed photometric observations and longslit spectroscopy. Over 20 weeks of observing were conducted, I conducted 9 of them myself and the rest were handled by other members of the MeerLICHT working group. These observations were conducted with multiple telescopes at the South African Astronomical Observatory (SAAO) in Sutherland. Over 100 targets were observed photometrically and over 150 spectra were obtained, out of a possible 251 primary candidates. The photometric lightcurves were then analysed by producing Lomb-Scargle periodograms for each of the observed target lightcurves searching for variability on the order of 5 to 65 minutes. All of the observed spectra were processed and searched for certain hydrogen, helium and metal absorption and emission lines. Unfortunately, no new AM CVns were found, although a new potential magnetic cataclysmic variable (CV) was discovered and one unknown but highly interesting spectrum was discovered. The lack of AM CVns was not unexpected as these binary stars are exceptionally rare with a little over 70 currently known AM CVns in the entire sky, and our statistical analysis predicted that we would have only detected approximately one AM CVn this far into the follow-up campaign. Potential further work and methods to improve both the candidate selection process and the follow-up campaign are outlined.

Acknowledgements

I would like to thank Prof. Paul Groot and Prof. Patrick Woudt for their unending and invaluable support. This work would not have been possible without all their incredible insight into the world of compact binary stars.

Prof. Patrick Woudt, Dr. Naomi Titus, Dr. David Buckley, Dr. Nic Erasmus, Dr. Stephen Potter, PhD candidate Simon de Wet, PhD candidate Orapeleng Mogawana, PhD student Anke van Dyk, and PhD student Petro Janse van Rensburg, all deserve thanks for their contributions as observers for the follow-up campaign.

I would also like to thank PhD student Hannes Breytenbach, PhD student Anja Genade, and Dr. Hannah Worters for all their support and training in the usage of the 1.0-m and Lesedi telescopes at SAAO.

My office mates, PhD student Tshiamiso Makwela, MSc student Reikantseone Diretse, and MSc student Timothy Roelf, were a huge help in keeping me sane and mentally healthy throughout a challenging two years.

I would like to thank Dr. Sally Macfarlane for her efforts as my mentor. Being a previous student of Paul and Patrick's, she was a great help in giving me perspective and making me feel better about working in research.

One final person who deserves recognition is my friend and confidant, James Harvey, who provided me with endless food, support and self-belief, and even let me live with him when I went remote observing at SAAO.

MeerLICHT is designed, built and operated by a consortium consisting of Radboud University, the University of Cape Town, the South African Astronomical Observatory, the University of Oxford, the University of Manchester and the University of Amsterdam.

This work uses observations made at the South African Astronomical Observatory (SAAO).

This work has been made possible by SARChI grant 111692 of the National Research Foundation.

Contents

1 Binary Stars

A large proportion of the stars that we see twinkling in the night sky are actually comprised of two or more stars. In fact, it has been proposed that potentially up to 85% of bright stars such as O or B type stars are actually binary star systems [1]. These binary stars abide by Kepler's laws and thus their orbits can be described almost in the same manner as the orbits of planets. For example, Kepler's third law describes how binary stars will have shorter periods the closer they are to one another. However, it was only as recently as the 1960s that binary stars with orbital periods less than roughly an hour were discovered [2]. To account for these short periods, astrophysicists realised that at least one of the components in these systems must be a stellar remnant such as a white dwarf, a neutron star or possibly a black hole. Typically these systems involve the transfer of matter from the companion, or donor, star onto the more compact, higher surface-gravity object. These companions can be a wide range of stellar objects from secondary white dwarfs or neutron stars to main-sequence or even brown dwarf stars. The focus of this project was finding AM CVn systems (AM Canum Venaticorum), a special type of ultracompact binary star, but it is important to understand what other systems we may encounter in our search.

1.1 AM CVns

In AM CVns both the primary and secondary star are compact objects, with the primary being a white dwarf and the companion being another dense, compact helium-rich star such as another white dwarf. The companion star is also known to be either a degenerate or semi-degenerate object [3]. AM CVns are some of the fastest rotating binary stars with orbital periods between 5 and 65 minutes [4]. These rapid orbital periods combined with their compact nature make AM CVn systems currently one of the few proposed sources of low-frequency gravitational wave (GW) radiation. AM CVn systems are one of a few classes of systems which evolve from a common envelope (CE). Another object which evolves from CEs is the Type Ia supernova (SNIa), and so by studying AM CVn systems, and other post-CE systems, we hope to better understand which population of post-CE objects could potentially lead to SNIa. However, in the AM CVn binaries we have detected thus far, there is not enough mass in the system to cause a SNIa. A SNIa explosion will only occur if the mass of the primary white dwarf exceeds the Chandrasekhar limit of 1.4 solar masses ($M_\odot$) [5].

1.1.1 GW sources

The Laser Interferometer Space Antenna (*LISA*) project will be the first ever gravitational wave observatory situated in space, and it is proposed that several hundred AM CVn binaries will be detectable with *LISA* [6]. The observatory will be able to detect GW radiation in a low frequency range of the spectrum, from 10^{-4} Hz to 1 Hz. This will allow for the observation and discovery of millions of ultracompact binary stars which reside within our Galaxy and possess orbital periods shorter than a few hours, with thousands of these sources being able to be individually resolved as well. To test the observatory and verify its capabilities, several sources which are predicted to have strong GW signals are proposed to be so-called "verification binaries" [7]. All of these sources will be individually resolvable and can most likely be detected on a timescale from weeks to maximum a few months. Amongst the current list of approved verification binaries are eight semidetached AM CVns. The eight semidetached AM CVns are: HM Cnc, V407 Vul, ES Cet, AM CVn, SDSS J190817.07+394036.4, HP Lib, CR Boo, and V803 Cen. Kupfer et al. [7] used parallaxes from Gaia DR2 to determine the expected signal-to-noise ratios (SNR) after a 4 year period of observation with *LISA* for approximately 50 candidate verification binaries and found an additional AM CVn binary, SDSS J135154.46–064309.0, that met the criteria to be a verification binary [7]. As the first space-bound GW observatory, *LISA* has the potential to shine light on under-studied concepts in physics such as GW radiation, and test theories such as Einstein's theory of general relativity. As a result, it is of the utmost importance to ensure that *LISA* works as intended which is why the study of these verification binaries is necessary.

1.1.2 Eclipsing AM CVns

The easiest means of measuring the binary parameters and properties of AM CVns is when the system is eclipsing. However, only a few are confirmed to be eclipsing and in only one of these systems has the primary WD been confirmed to be fully eclipsed by its donor star, Gaia14aae (ASASSN–14cn) [8]. Another three systems have been studied in detail, they are PTF1J1919+4815, YZ LMi and, most recently, ES Ceti. In PTF1J1919+4815, it is only the bright spot caused by the impact of mass transfer, and the edge of the disc which is eclipsed [9], in ES Ceti, an eclipse of only the outer accretion disc was recently discovered which makes ES Ceti the shortest period AM CVn which shows an eclipse [10], whereas in YZ LMi a partial eclipse of the primary WD is seen [11]. Due to the primary star being eclipsed, Gaia14aae and YZ LMi allowed for highly accurate measurements of the donor star mass and radius. The results of the measurements show that while the YZ LMi system is consistent with either the helium star channel or the WD channel for formation, Gaia14aae is only consistent with the evolved CV channel. This is unexpected as the evolved CV channel is theorised to be the most uncommon of the three formation channels, as discussed below. More recently, van Roestel et al. [12] have discovered five new eclipsing AM CVn systems all of which seem to be consistent with the helium star channel. With the discovery of more eclipsing AM CVns it is possible to further improve our understanding of the formation channels for these ultracompact binary stars.

1.1.3 Formation channels

There are three proposed formation channels for AM CVns [13]. The first of these channels is the theory that an AM CVn will evolve from a detached double white dwarf binary which undergoes angular momentum loss due to energy radiated away through gravitational waves. This results in the WD binary developing shorter and shorter orbital periods as the orbital separation diminishes until mass transfer starts at very short periods of a few minutes. It is at this point that the mass transfer will occur as direct impact which can cause further instability in the mass transfer resulting in a merger of the double white dwarf system in a large fraction of these systems. If no merger takes place then the binary will evolve to longer and more stable orbital periods as the mass transfer process slows down. In this instance, the donor star is required to be a relatively low mass helium-rich white dwarf [14]. In the models created by Nelemans et al. [14], it is indicated that this is the likeliest formation path for AM CVns.

The second channel involves a low mass non-degenerate helium star initiating mass transfer to the white dwarf [15]. In this channel, the binary then evolves to a period minimum of about ten minutes at which point the helium star becomes semi-degenerate. Once the period minimum is reached, the mass transfer rate starts to drop off rapidly and the period will increase. While this is ongoing, the helium star will also become increasingly degenerate. The final suggested channel for the formation of AM CVns is known as the hydrogen CV channel. In this channel, the AM CVn will form from a CV which has an evolved secondary star and after a certain amount of hydrogen mass loss due to evolution and accretion, the helium core of the star is exposed [16]. From this point, the evolution into an AM CVn follows a very similar track to that of the helium star path. This final track is generally considered less important than the others as it involves incredibly long timescales. Figure 1 depicts the different evolutionary paths for these three channels as well as that of a CV.

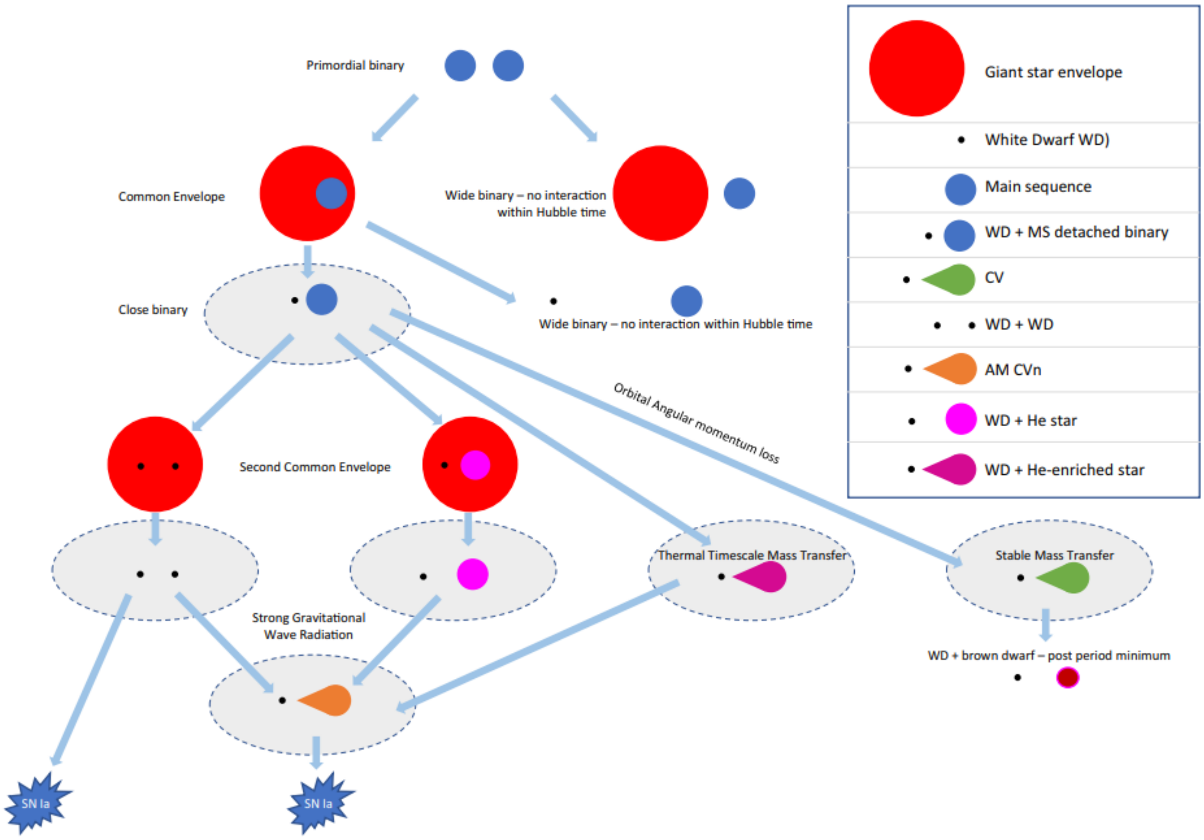

Figure 1: The different evolutionary pathways for AM CVn and CV formation. This is figure 1 as reproduced from Inight et al. [17].

In 2018, Ramsay et al. conducted a study of the 56 known AM CVn systems at the time with the release of Gaia's Data Release 2 (DR2) [4]. With 56 systems it was possible for a population study to be done especially with 41 of those systems having parallaxes and proper motions from Gaia DR2 [18]. In this study, a review was conducted of the known AM CVns which allowed the authors to confirm that the most reliable way to detect these rare binaries was through searching for hydrogen deficient stellar spectra and blue colour; these are two of the defining traits for AM CVns. They also deduced from the studies done searching for AM CVns and resolving their orbital periods, the most efficient way to determine orbital periods (if the system is not eclipsing or displaying outbursts) is through time series spectroscopy. However, that comes with many challenges as the majority of AM CVns are rather faint systems and in order to phase resolve the short orbital periods one requires short exposure times.

Another aspect of the paper dealt with the space density of AM CVn stars as a means of testing the different evolutionary pathways. Based on their studies and the references within, the space density of AM CVn stars is roughly in the range of 10^{-8} - 10^{-7} pc^{-3} [4] [19]. However, given that the methods used in the discovery of all the known AM CVns are all so varied such as variability, emission line detection, and photometric colour selections, it is not yet possible to say the sample has any sense of completeness. This means that the space density cannot yet be calculated with confidence for the entire sample. From the current estimates however, we can deduce that the very low space density is currently only compatible with the double white dwarf evolutionary track dominating the contribution to AM CVn systems [4]. Which leads to two possible conclusions, either the helium star and CV channels have much less of a contribution than first thought or our understanding of compact binary star evolution leading to stable mass transfer still requires work.

1.1.4 AM CVns distribution

From the table of known AM CVns from Ramsay et al. [4], we find that of the 56 known systems, 36 of them are in the northern hemisphere, i.e. they have a declination greater than 0°. See Figure 9 on page 19 for a visual representation of the AM CVn on-sky distribution. This bias towards the northern hemisphere is further confirmed by Kupfer et al. [7] in their paper on using ultracompact binary stars as a means to verify the efficacy of the upcoming Laser Interferometer Space Antenna (*LISA*) project [6]. This under-population of AM CVns in the southern sky is likely only due to the fact that studies that have searched for ultracompact binary stars, particularly AM CVns, have largely been focused on high Galactic latitudes and in the northern hemisphere. However, Ramsay et al. were able to study the distribution of AM CVns within our Galaxy with the parallaxes and proper motions that became available after the release of Gaia DR2 [18]. It was found that the majority of known systems reside in the thin disc, with a few more in the thick disc, however, none of the known AM CVns appear to reside in the Galactic halo. The evidence of this is seen in studying the different Galactic velocities of the systems as well as their angular momentum in the direction outward from the Galactic plane and the eccentricity of their galactic orbit. See Figure 2 for a schematic of the different Galactic structures.

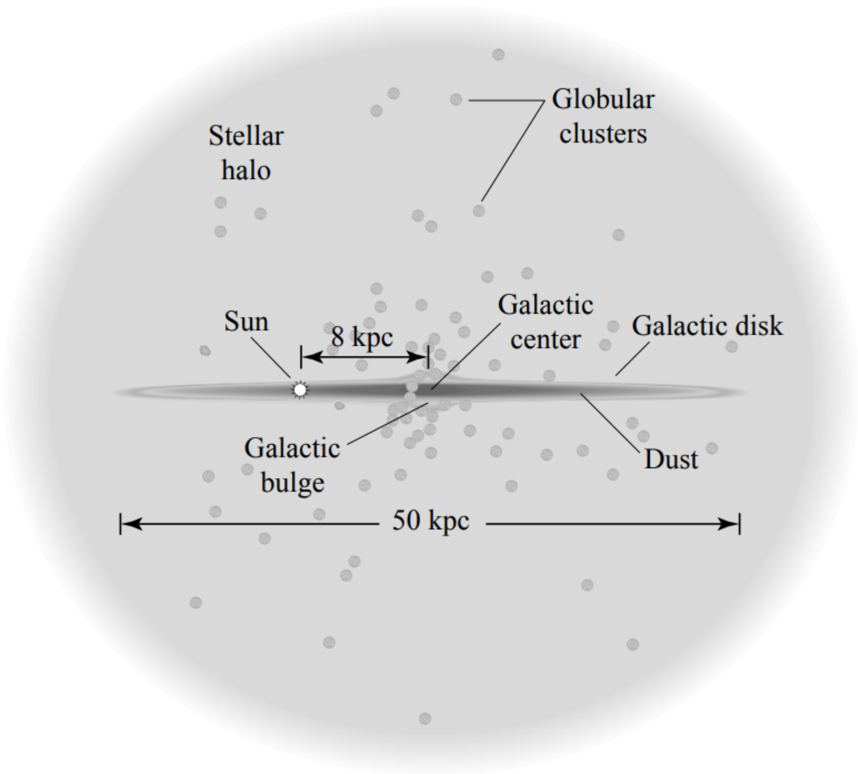

Figure 2: The structure of the Milky Way Galaxy, not to scale. Within the galactic disc, the thin disc reaches out to a height of roughly 350 pc, whereas the thick disc reaches a height of roughly 1 kpc. This is figure 6 reproduced from Chapter 25 of Carroll & Ostlie, Pearson New International Edition [20].

1.1.5 Finding AM CVns

Roelofs et al. [21] conducted a spectroscopic survey using the Sloan Digital Sky Survey (SDSS) which began in 2009, dedicated to the region of colour space in which AM CVn binaries were known to reside. This region of colour space was also one of the less covered by the general SDSS database. Thus, Roelofs et al. began a systematic search for the "hidden" population of AM CVns in this colour space. Roelofs et al. used a process that was based off a colour selection technique using the photometric data available to create a "colour box" in which the known AM CVns resided. Initially, Roelofs et al. selected roughly 2000 candidates upon which to conduct a more dedicated follow-up. By the beginning of 2013, a total of seven new AM CVn binary stars had been discovered when the survey was approximately 70% complete, which was below the initial estimate for the space density of these binaries [22]. When the project came to end, the total number of AM CVn stars discovered using SDSS, including those discovered before this survey began, was now at 17, with another three that were spectroscopically confirmed by SDSS but were initially discovered by other parties [4].

In 2009, the first results from the Catalina Real-Time Transient Survey (CRTS) were published [23]. CRTS was conducting a search for optical transients which had timescales from minutes to years. They made use of data coming from the Catalina Sky Survey (CSS) which was repeatedly observing approximately 26000 square degrees of the sky in the declination range from $-30°$ to $70°$, mostly avoiding the Galactic plane however by skipping fields with a Galactic latitude of $|b| < 10°$. To identify new optical transients, the authors searched for objects in the CSS which showed variability greater than 2 magnitudes when comparing new images to previous, deep co-added images from the CSS. By 2014, the CSS had increased its coverage to roughly 30000 square degrees from $-75°$ to $65°$ in declination. With new telescopes, the CRTS now had a limiting magnitude which varied from 19 to 21. At this time the CRTS had identified over 9000 new optical transients since its conception in 2007, among which were over 1000 new CVs and 3 new AM CVns [24]. These new optical transients were classified via means of a spectroscopic follow-up on a priority 85 systems identified with CRTS. CRTS is a currently ongoing project, which now has identified a total of 5 new AM CVns and confirmed the detection of another AM CVn detected by the Palomar Transient Factory (PTF).

The PTF conducted the first ever large-area, systematic search for AM CVn binaries with only photometric variability of a large-amplitude as a means of selecting candidates [25]. There are two pipelines which process the PTF data, a "transient" and a "photometric" pipeline. The transient pipeline processes data shortly after acquisition with difference imaging as a means of detecting transient events. Whereas the photometric pipeline produces lightcurves after the night of observing is complete using aperture photometry. It is from the photometric database that candidate AM CVn systems are selected by searching for outbursts of 2 magnitude greater than the median magnitude, provided the object has a second detection at least a day later that is 5σ above the median. Although, some of the AM CVns discovered by PTF were originally selected for follow-up by the transient pipeline as potential supernova systems. By 2018, they had found a total of eight new AM CVns [4], one of which was confirmed by CRTS as well. The large majority of the rest of their candidates were identified as CVs [26].

The All-Sky Automated Survey for Supernovae (ASAS-SN) has been operational since 2013 and it now has 24 telescopes across 6 different sites all over the globe [27]. Every night it attempts to survey the entire sky down to a limiting magnitude of about 18. As a result there is now a large catalogue of time-domain data available which has been used to search for transient objects. In this capacity, citizen science has played a large role in analysing this data with such platforms as the American Association of Variable Star Observers (AAVSO)[1] and the Variable Star Network (vsnet)[2]. There have been a total of 7 new AM CVns found through citizen efforts with the available ASAS-SN data, with one of them being separately confirmed by Gaia as well [28] [4]. There are a further 6 candidate AM CVns which were identified first as dwarf nova candidates by ASAS-SN and have now been followed up with lightcurves from the Zwicky Transient Facility (ZTF) [29].

The Zwicky Transient Facility (ZTF) began observing in 2018 in an effort to study the ever-changing transient sky [30]. With an automated difference imaging process, "alerts" are generated for sources which display a change of at least 5σ [31]. These alerts can then be used as a means to identify potentially outbursting star systems such as cataclysmic variables. Thus, van Roestel et al. [32] began a search for AM CVn binary stars with the ZTF alerts. By searching for outbursting stars with ZTF and then applying some strict

[1]Accessible at: http://www.aavso.org/
[2]Accessible at: http://www.kusastro.kyoto-u.ac.jp/vsnet

selection criteria, including using Gaia and Pan-STARRS1 colours to select only blue stars, they selected a total of 59 systems without classifications and expect to find approximately 15 new AM CVn binary stars. Thus far they have identified nine new AM CVns as well as one magnetic CV that displays only HeII lines in its spectrum. These classifications were made using a spectroscopic follow-up campaign on 35 of their sources. The AM CVns they discovered were also shown to have periods in the range of 29–50 minutes based on their respective outburst recurrence times.

For an overview of the majority of the known AM CVn systems, excluding those discovered since 2018, see Table 1 in Ramsay et al. [4][3].

1.2 Cataclysmic Variables

Cataclysmic variable stars (CVs) are a type of binary star where the primary star is a compact white dwarf (WD) and the companion, or donor, is usually a main sequence star, but can also be a sub-giant or brown dwarf star as the companion. Typically CVs show variations in brightness, some can dim by a factor of 10 over the course of half an hour, only to climb back up to a peak brightness a few minutes later. Others can vary from night to night. Some of these variations are periodic and have well-defined periods, and some variations are irregular and are difficult to predict. The largest contribution to these varied brightness variations is due to the flow of matter between the two stars, the light produced by this process can even dominate the brightness of the two stars in the system [33]. This is due to the large amount of friction due to the viscosity of the material which heats the gas, resulting in an increase in brightness as the flux of an object is proportional to its temperature. This matter accretion is the result of a loss of angular momentum in the system. There is a secondary effect which determines how this matter falls onto the WD, either a strong magnetic field from the WD pulls the matter directly onto the WD or an accretion disc forms surrounding the WD. The difference between magnetic and non-magnetic CVs is depicted in Figure 3.

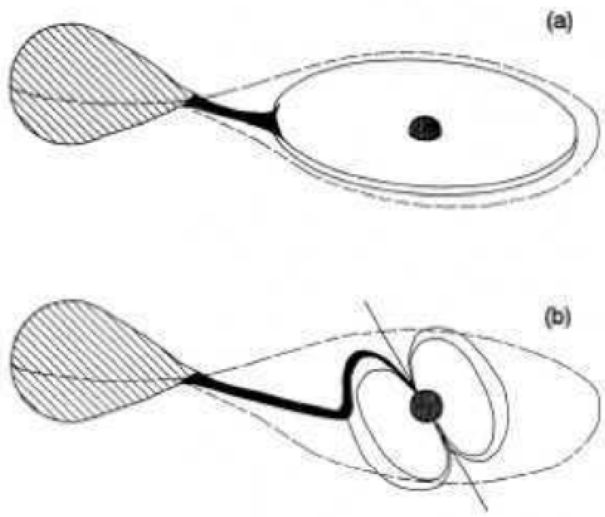

Figure 3: This figure shows the difference between non-magnetic and magnetic CVs. In (a) we see a non-magnetic CV in which matter flows across the accretion disc onto the primary star. In (b) we see a magnetic CV in which an accretion disc is prevented from forming and matter flows directly onto the primary star's magnetic pole. This is part of figure 1 reproduced from Singh [34].

In 2014, Drake et al. published a paper which revealed 855 possible CVs detected from the Catalina Real-time Transient Survey (CRTS) [35]. Around 137 of these candidates have been spectroscopically confirmed and it was found that the majority of the CRTS CVs were a dwarf novae (DNe) system rather than a magnetic CV. This was done by comparing the CRTS CVs to existing X-ray catalogues. These DNe systems, a subclass of non-magnetic CVs, experience a thermal instability inside the accretion disc and undergo a

[3]This table is also available online at: https://www.ast.cam.ac.uk/~ebreedt/web/AMCVn_datatable_Ramsay_etal_2018.fits

bright outburst. CVs are a common near-final state of evolved compact binary star systems and are also a class of post-CE objects.

1.2.1 Non-magnetic CVs

In non-magnetic CVs, matter flows from the donor star onto the WD via an accretion disc when the companion star's Roche Lobe overflows [34]. These discs can also form in magnetic CVs, but to a lesser extent. This accretion is due to the gravitational field coming from the highly compact WD. In certain instances the accretion disc that forms can contain instabilities that lead to DNe outbursts [35]. These DNe outbursts are called such in order to distinguish them from the far more explosive and rarer nova outbursts. The DNe outburst can cause the CV to jump up several magnitudes in brightness over the course of roughly a day and this increase can last weeks before it resettles to the pre-outburst level. DNe outbursts are caused by instabilities in the accretion disc which lead to an increased amount of matter flowing into the primary WD and raising the overall brightness of the system. This brightened period lasts until the disc has been drained of enough material allowing the instabilities to settle back into a quiescent and inactive state. It is also possible that a sudden increase in mass transfer from the donor star caused by increased irradiation from the disc during an instability can further contribute to the outburst's overall strength.

1.2.2 Magnetic CVs

Magnetic CVs come in two flavours, the polars (AM Herculis stars) and the intermediate polars (IPs or DQ Herculis stars). The polars have much stronger magnetic fields originating from the WD, up to 10^7 Gauss [36], whereas the intermediate polars have weaker fields and can form partial accretion discs. Polars direct their accretion from the donor star onto the poles of the WD which can cause soft X-ray emission in sync with the spin period of the WD, whereas in IPs the accretion onto the poles results in hard X-ray emission with the same regulation due to the spin period [37]. For a full discussion on the complex details behind the differences of these systems see Section 9 in Hellier (2001) [33].

1.3 Other ultracompact binaries

There is another class of compact binary object which is comprised of double degenerate extremely low mass (ELM) white dwarfs. These ELMs typically have a mass of $\lesssim 0.3 M_{\odot}$ and have largely helium-rich cores [38]. In 2009 a search for unbound hypervelocity stars by Brown et al. [39], had the unexpected result of discovering many of these ELM WDs. Their colour selection process, described in Brown et al. [40], was then the basis for a further survey searching for more ELMs. By 2017, they had discovered 82 of these double degenerate ELM WDs, 7 of which had orbital periods of less than an hour. In their population study, it was shown that the majority of these double degenerate ELMs will merge [41], particularly the He+CO WD binaries. There are three possible outcomes of this merger: a stable mass transfer AM CVn, a single massive white dwarf, or an fainter luminosity supernova explosion called a supernova ".Ia" [42], which are roughly 1/10 the brightness of a Type Ia Supernova for 1/10 the length of time [43]. However, the required conditions for a supernovae .Ia explosion are highly unlikely to ever be reached in ELMs. Thus it was concluded from the studies done on the merger rate of ELM WDs, and comparing them to the formation rate of AM CVns, .Ia supernovae and massive single WDs, that ELM WDs could be the progenitors of all observed AM CVns (and potentially .Ia supernovae), but the majority of ELM WDs will merge into a single massive object such as a single WD, a R CrB star, extreme helium stars, or He-rich subdwarfs [43].

X-ray binaries are another type of compact binary star similar to CVs and AM CVns, however in this case, the primary WD is replaced by a neutron star (NS) or more rarely a black hole (BH), and the companion is another type of main sequence (MS) star. The compact object is accreting matter from the MS star in a process which produces X-ray emission [44]. These binary star systems are some of the brightest X-ray emitters in the observable universe. Although XRBs can take two forms, the X-ray emission is generated when the matter from the MS companion is pulled onto the compact object. This accretion is caused either by the Roche-Lobe of the MS star overflowing into an accretion disc or matter being transferred onto the compact object directly by powerful stellar winds. The first mechanism describes a low-mass XRB and the second method is for a high-mass XRB. Typically XRBs are found almost exclusively in the plane of our galaxy. With further study of XRBs we might better our understanding of how these binary systems evolve and what their evolutionary end products are. The radiation emitted in the radio regime is generally weaker for NS XRBs than in BH XRBs for any given X-ray luminosity [44]. In 2006, a novel method for determining the accretion rate of an XRB separately from the X-ray flux was used to look for radiatively inefficient BH XRBs [45]. This allows astronomers to compare the X-ray emission from NSs and BHs in an effort to find these inefficient BH XRBs and use this inefficacy as possible evidence of an event horizon.

2 Candidate Selection Process

In order to find AM CVns in the Southern Hemisphere, we first needed a method to select candidates to observe because the nature of our project is one of follow-up based on objects meeting a certain criteria with MeerLICHT photometry. The method we employed was one of a colour-based selection with the u, g, r, i and q filters. Candidates were selected based on their position in $(u-g)$ vs. $(g-r)$ and $(g-r)$ vs. $(r-i)$ colour space, as well as an absolute magnitude cut-off where possible. The basis for this colour box, and the selection process that followed with the MeerLICHT Southern All-Sky Survey data, is described in the following sections.

2.1 Selection Box

2.1.1 Original Box

Our selection box was based on a similar project conducted by Roelofs et al. [21] which used a Sloan Digital Sky Survey (SDSS) colour selection criteria to search for candidates. The final sample of Roelofs et al. contained 1523 candidates of which they hypothesised that approximately 40 should be new AM CVn stars. This hypothesis was formed from a population study conducted by Roelofs, Nelemans, and Groot [19] on AM CVn stars which had been sampled by SDSS. In this population study, the SDSS sample was used to help quantify a theoretical population synthesis model for the spatial density of AM CVn stars. SDSS had, for the first time in AM CVn studies, provided a sample of six AM CVns which were homogeneous enough to allow for a reasonably detailed population study.

From studying the population of known AM CVn stars, Roelofs et al. [21] determined a colour selection region which had a few additional criteria in order to select their sample of candidates from SDSS. These conditions were as follows:

1. Object is a point source.
2. Object is not saturated in any filter.
3. $g < 20.5$
4. $u - g <$ minimum$[0.14, 1.35(g-r) + 0.32] - \sigma_{u-g}$
5. $-0.42 + \sigma_{g-r} < g - r < 0.02 - \sigma_{g-r}$
6. $-0.33 + \sigma_{r-i} < r - i < 0.03 - \sigma_{r-i}$

where the uncertainties, $\sigma_{u,g,r,i}$ are the photometric errors for the u, g, r, i magnitudes from SDSS. The above cuts are applied to SDSS dereddened colours, thus, the uncertainty for the colour terms $u-g$, $g-r$, $r-i$ actually contain a third error, the reddening error, which is taken to be a fraction of the reddening estimate. However, in our selection process we did not deredden colours and thus the reddening error was not a concern. Roelofs et al. [21] showed that the range of the extinction error, σ_E, would be between $0.16E$ and $1E$, where E is the extinction factor for a given colour. Given that the maximum extinction value for their reddening correction was around 0.5, the maximum shift that the extinction error could apply to the selection box would be $\sigma_{u-g} = \sqrt{\sigma_u^2 + \sigma_g^2 + \sigma_E^2}$, where $\sigma_E = 0.5$. The average extinction value was closer to 0.2, which would then imply a maximum reddening error of $\sigma_E = 0.2$.

2.1.2 Known AM CVns Table

In order to verify that the selection box we use is still relevant, Roelofs's original box was only based on 18 known AM CVns at the time, we needed a more up-to-date check for known AM CVn stars. Thus, we used a table of photometry for 56 known AM CVn systems from Ramsay et al. [4][4]. This table consists of all the relevant data for the known AM CVns, at the time of printing, including coordinates, period, and magnitudes from SDSS, SkyMapper and Pan-STARRS1, where available. These magnitudes are non-dereddened, however, the table does have columns for extinction and reddening factors based off Pan-STARRS1 data where available, or with the dust maps from Schlafly & Finkbeiner [46]. The large majority of the 56 AM CVns had SDSS magnitudes in u, g, r and i, which allowed us to compare the known AM CVns with our colour selection box once we created it.

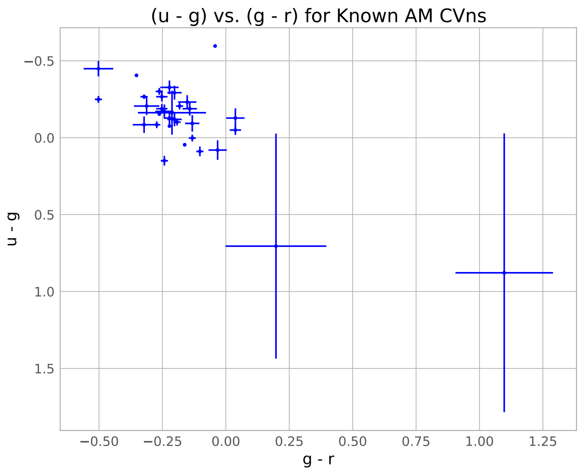

(a) SDSS colours, $u-g$ vs. $g-r$ for the known AM CVns from Ramsay et al. [4].

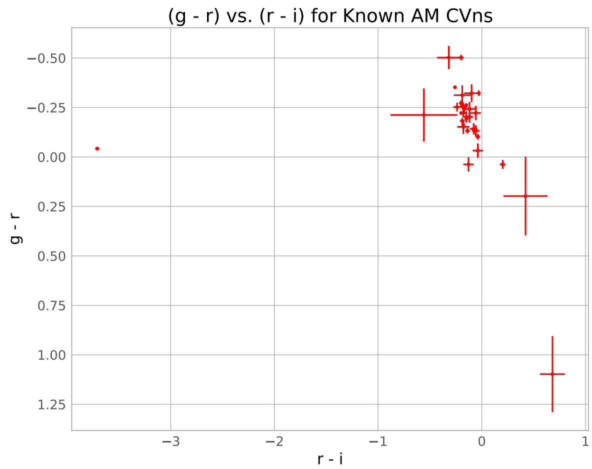

(b) SDSS colours, $g-r$ vs. $r-i$ for the known AM CVns from Ramsay et al. [4].

Figure 4: Colour-colour plots for the known AM CVns with SDSS colours from the table in Ramsay et al. [4]. There are 33 out of 55 known AM CVns in this selection.

These non-dereddened colours from the SDSS filter system have been shifted into the MeerLICHT filter frame of reference through a process described in the following section. The severe outlier in Figure 4b with an SDSS $r-i \approx -3.7$ is AM CVn. The table from Ramsay et al. [4] shows that the i-band magnitude is significantly fainter than the other magnitudes from SDSS for AM CVn. However, given that the available Pan-STARRS1 magnitudes all agree with the SDSS magnitudes, aside from a large discrepancy in the i-band, this would suggest the i-band magnitude for SDSS must have either been captured during a quiescent period or the i-band observation was compromised in some way. Upon checking on the SDSS SkyServer database, the data for the i-band does not appear to have any flags which would affect the value of AM CVn's i magnitude this significantly. Given that AM CVn has never been observed in outburst before, however, it is surprising that the i magnitude is significantly fainter than the other bands.

Using the table from Ramsay et al. [4], we searched for the known AM CVn systems in the MeerLICHT database. In Table 1 we show the AM CVn stars that were present in the selection as well as their available magnitudes. These are the 20 sources which have been detected in at least one band by MeerLICHT. There are an additional 13 sources which are in the right range, i.e. south of declination 30°, but have not yet been detected by MeerLICHT in any band. The rest of the known AM CVn systems in the Ramsay et al. table are too far north to be detected by MeerLICHT.

[4]This table is available at http://cdsarc.u-strasbg.fr/viz-bin/qcat?J/A+A/620/A141.

Table 1: Known AM CVn binaries detected in MeerLICHT.

Source	RA	Dec.	u_ML	g_ML	r_ML	i_ML	z_ML	q_ML
ES Ceti	02:00:52.24	−09:24:31.6	16.37	16.65	16.96	17.28	-	16.85
SDSS J1351−0643	13:51:54.46	−06:43:08.9	18.39	18.66	18.78	-	-	18.96
HP Lib	15:35:53.07	−14:13:12.2	-	-	-	-	-	13.71
ASASSN−14cc	21:39:48.25	−59:59:32.9	-	19.87	19.71	-	-	19.59
CX361	17:51:07.66	−29:40:37.3	-	17.43	17.26	17.39	-	17.43
CR Boo	13:48:55.22	+07:57:35.8	16.60	-	-	16.92	-	16.81
V803 Cen	13:23:44.54	−41:44:29.5	16.86	16.88	16.87	14.10	14.29	16.89
ASASSN−15kf	15:38:38.24	−30:35:49.7	-	-	-	-	-	19.41
CP Eri	03:10:32.77	−09:45:06.2	-	-	-	-	-	19.75
CRTS J0910−2008	09:10:17.45	−20:08:12.5	-	-	-	-	-	18.92
V406 Hya	09:05:54.75	−05:36:08.5	-	20.05	-	-	-	20.25
NSV1440	03:55:17.95	−82:26:11.3	-	18.47	18.51	-	-	18.67
V558 Vir	14:27:01.59	−01:23:10.2	-	-	-	-	-	20.34
SDSS J1240−0159	12:40:58.03	−01:59:19.2	16.80	16.78	16.82	16.87	17.15	16.85
ASASSN−14ei	02:55:33.28	−47:50:42.3	17.70	17.87	18.11	18.31	17.49	17.77
GP Com	13:05:42.40	+18:01:03.8	-	-	-	-	-	16.12
V396 Hya	13:12:46.44	−23:21:32.6	17.64	17.60	17.50	17.54	17.54	17.56
CRTS J0844−0128	08:44:13.66	−01:28:07.9	-	-	-	-	-	20.49
SDSS J1505+0659	15:05:51.57	+06:59:48.9	-	-	-	-	-	19.25
Gaia16all	06:27:20.51	−75:13:33.6	16.25	-	16.52	16.73	16.95	16.45

2.1.3 Creating our box

Although they are both ugrizq filter systems, the SDSS filters and the MeerLICHT filters actually have different zero points and transmission curves; thus we are required to shift the colour selection box into the MeerLICHT filter frame of reference before we can apply the same selection technique to the MeerLICHT Southern All-Sky Survey (ML SASS) data. In order to do this we need to find the shifts required for each filter magnitude we intend to use. The first step was to find a way to compare the magnitudes for each filter for a population of stars with magnitude measurements in both MeerLICHT and SDSS. As this was one of the first tasks we needed to complete, the ML SASS was still in its relative infancy meaning that there were not as many fields available in all 5 filters we intended to use. Thus our options for fields covered in u, g, r, i and q by MeerLICHT and also covered in u, g, r and i by SDSS were fairly limited. We made use of the data from 4 fields, 16018, 16020, 16052 and 20112, which had a combined total of $\approx$ 2900 stars across them giving us a fair starting sample size for magnitude comparison. All of these fields were covered by SDSS allowing us to extract the majority of the stars in each MeerLICHT field's SDSS magnitudes from the SDSS SkyServer using the SkyServer Search Form[5].

To compare the magnitudes of the stars we first cross-matched them across the MeerLICHT and SDSS data. This cross-matching process was done with Astropy's Astronomical Coordinate Systems module [47]. Using the SkyCoord task one can create a catalogue of coordinates in any commonly used coordinate unit system. These catalogues can then be cross-matched with one other catalogue at a time with the `search_around_sky` function which allows you to choose a maximum angular distance that two objects across catalogues can be matched. For our purposes, we set the maximum as 2 arcseconds. We then limited the stars we were looking at to those with magnitudes fainter than 14 in every band. These two steps reduced our starting sample size down from approximately 2900 stars to roughly 1700 stars. Firstly, we plotted the SDSS magnitudes and colours versus the MeerLICHT magnitudes and colours to determine whether or not any of the magnitude shifts required a colour term instead of just a linear shift.

[5]Available at `http://skyserver.sdss.org/dr16/en/tools/search/form/searchform.aspx`.

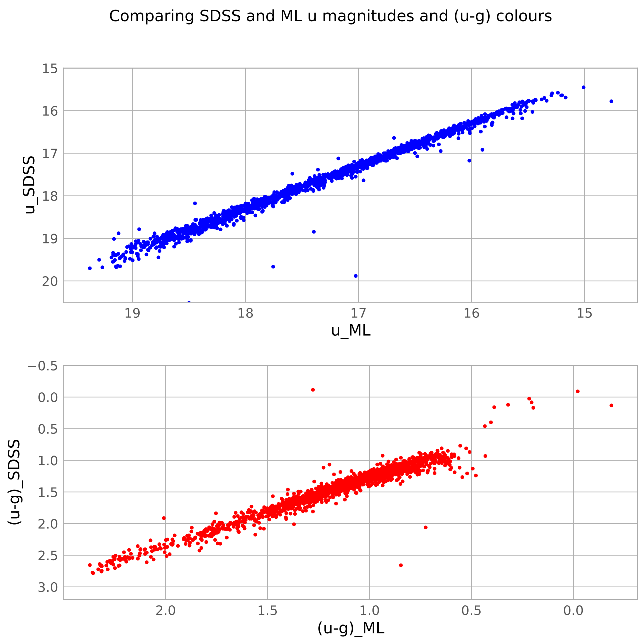

(a) Magnitude and colour comparison for u and $u - g$.

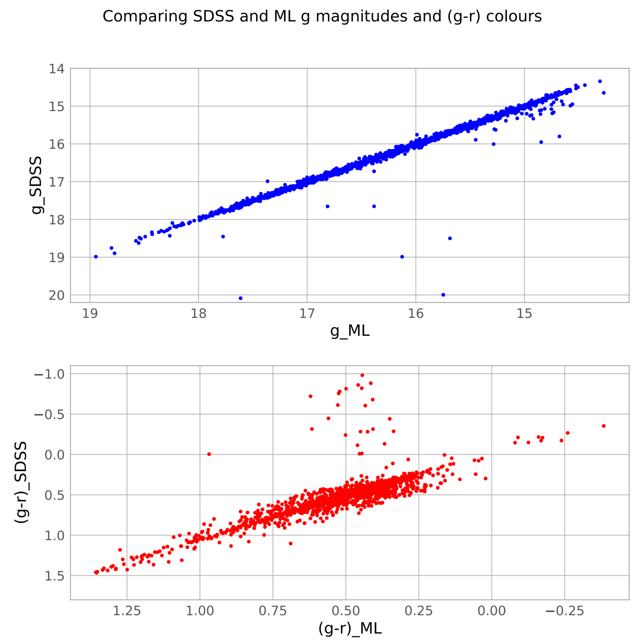

(b) Magnitude and colour comparison for g and $g - r$.

Figure 5: SDSS and MeerLICHT filter and colour comparisons for the u and g bands. A few outlying sources are not visible in the visible range.

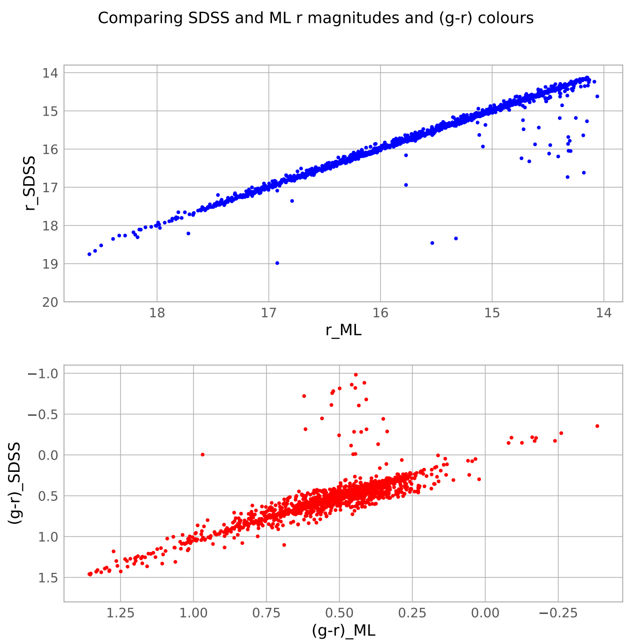

(a) Magnitude and colour comparison for r and $g - r$.

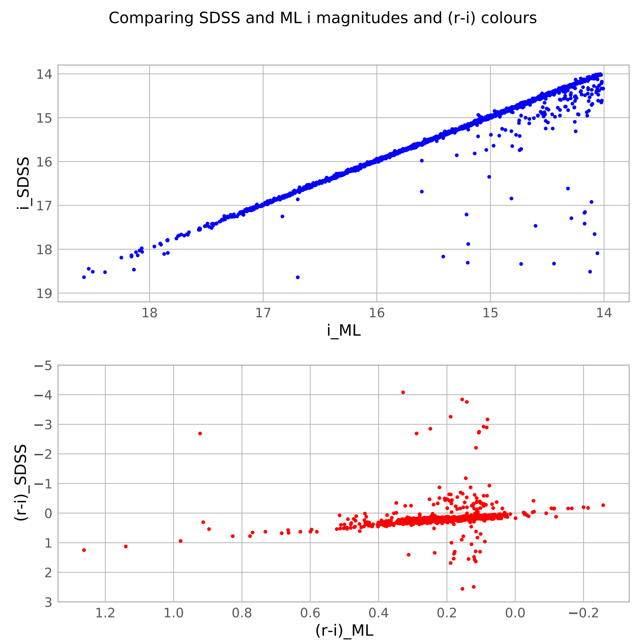

(b) Magnitude and colour comparison for i and $r - i$.

Figure 6: SDSS and MeerLICHT magnitude and colour comparisons for the r and i filters. Again, several outlying sources have been excluded from the visible range.

Both Figures 5a and 5b show multiple outliers far from the general trend. The u band shows a relatively large shift between the MeerLICHT and SDSS magnitudes as well as large scatter in the u-g plot seen in Figure 5. The g band has a much tighter relationship between magnitudes and a relatively smaller scatter in the g-r colours. From the plots for the u band we decided to include a colour term for the shift from u_SDSS into u_ML of (u-g)_SDSS. However, for both the r and i bands seen in Figure 6, we decided that to transform the SDSS filters into the MeerLICHT filter space we only required a simple shift and not a colour term as well. This was due in large part to the r and i bands having near identical coverage in wavelength and their comparisons showed a very tight relationship, with some scatter in the i band.

The SDSS wavelength ranges, as seen on the SVO Filter Profile Service [48], and the MeerLICHT wavelength ranges can be found in Table 2:

Table 2: Table showing the different wavelength coverages of the MeerLICHT and SDSS filters.

MeerLICHT Filter	λ_{min} [nm]	λ_{max} [nm]	SDSS Filter	λ_{min} [nm]	λ_{max} [nm]
u	350	410	u	305	403
g	410	550	g	378	555
r	563	690	r	542	699
i	690	840	i	669	839

From Figures 5 and 6, and in conjunction with knowing the differences in wavelength coverage of the two filter systems, it was determined that the g, r, and i bands only required a shift whereas the u band also required a colour term in the fitted shift. With this in mind, we determined the shifts to apply to the SDSS colour selection box with a process repeated three times. We made use of the `leastsq` function from the `scipy.optimize` module in SciPy [49] in order to perform a least squares fit on the shifts between SDSS and MeerLICHT magnitudes. The functional form of these shifts is as follows:

$$\begin{aligned} u_{\text{ML}} &= u_{\text{SDSS}} + a_u + b \times (u-g)_{\text{SDSS}} \\ g_{\text{ML}} &= g_{\text{SDSS}} + a_g \\ r_{\text{ML}} &= r_{\text{SDSS}} + a_r \\ i_{\text{ML}} &= i_{\text{SDSS}} + a_i \end{aligned}$$

where the a's are placeholders for the shifts and b is the factor of the colour term for the u shift. An initial fit was performed using the average of the differences for the a's and an initial guess of 1 for b. Using these first fitted parameters we shifted the SDSS magnitudes into the MeerLICHT filters frame and then performed a normalised fit on the residuals, the original MeerLICHT magnitudes subtracted from the shifted SDSS magnitudes. The normalised fit, from the `scipy.stats` module, produced a μ (mean) and σ (deviation) for each filter which we used to remove all datapoints more than 4σ from their respective μ's. This process was repeated twice more, each time removing these 4σ outliers until we performed the final fit on the remaining 1560 stars in the selection, and determined the final shifts of:

$$\begin{aligned} u_{\text{ML}} &= u_{\text{SDSS}} - (0.1127 \pm 0.0029) - (0.1326 \pm 0.0067) \times (u-g)_{\text{SDSS}} \\ g_{\text{ML}} &= g_{\text{SDSS}} - (0.0109 \pm 0.0017) \\ r_{\text{ML}} &= r_{\text{SDSS}} + (0.0115 \pm 0.0022) \\ i_{\text{ML}} &= i_{\text{SDSS}} + (0.0101 \pm 0.0049) \end{aligned}$$

We then used these fits to shift the SDSS colour selection criteria described above into the MeerLICHT filter system frame of reference. Initially, there was a minor error in the calculation of these shifts which resulted in a slightly shifted, larger selection box than intended, however, once corrected, 77 out of the 79 true candidates were in the original, larger selection of candidates. In Figures 7 and 8, we show the new shifted relationships for the SDSS and MeerLICHT magnitudes.

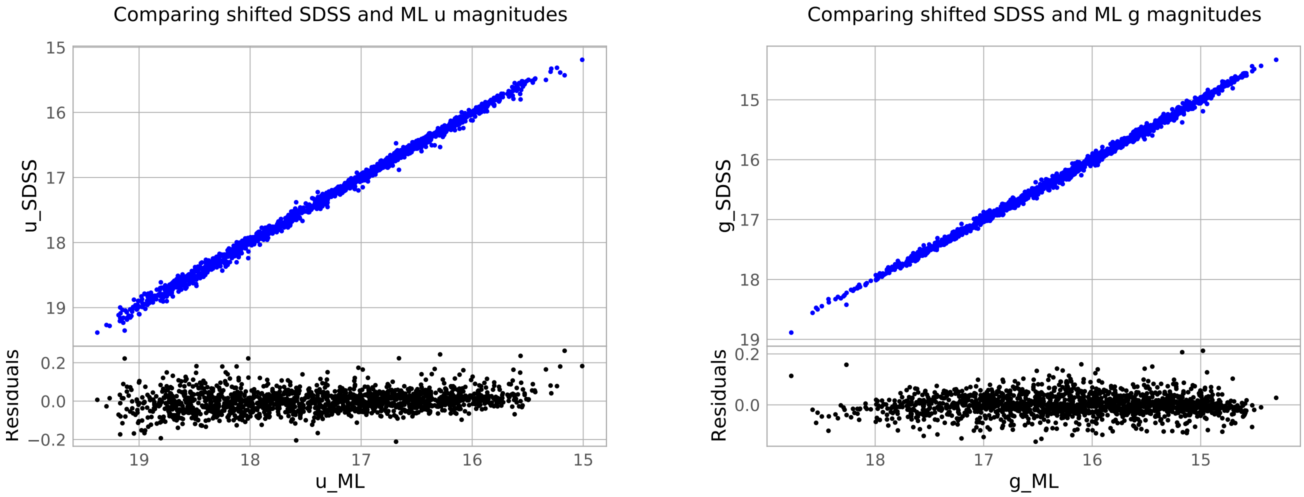

(a) Shifted SDSS magnitude comparison for u.

(b) Shifted SDSS magnitude comparison for g.

Figure 7: The shifted SDSS magnitudes compared to the MeerLICHT magnitudes for u and g of 1560 stars.

We see a very tight relationship now between for both u and g compared to the original comparison seen in Figure 5. The residuals show minor deviation away from 0 with a maximum deviation of roughly 0.2 for both u and g.

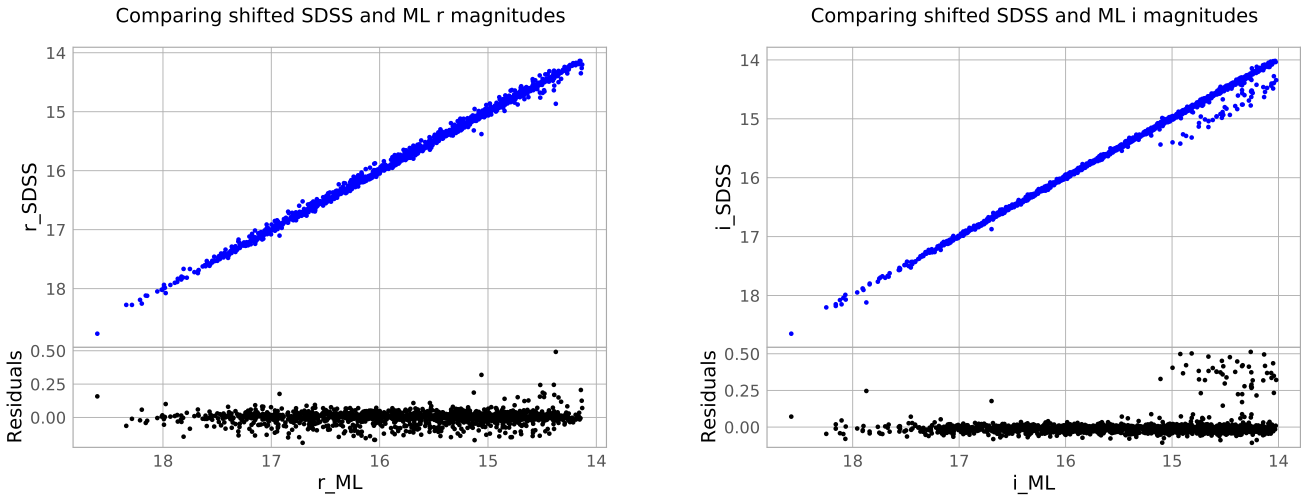

(a) Shifted SDSS magnitude comparison for r.

(b) Shifted SDSS magnitude comparison for i.

Figure 8: The shifted SDSS magnitudes compared to the MeerLICHT magnitudes for r and i of 1560 stars.

Here we see a slightly larger scatter at brighter magnitudes for r, and in particular, the i band. This is likely due to the majority of stars' having slightly more variable infrared emissions. However, we still see a much tighter overall relationship between the shifted SDSS magnitudes and the MeerLICHT magnitudes compared to their original positions in Figure 6.

2.2 MeerLICHT Southern All-Sky Survey

2.2.1 Coverage of ML SASS

Now that we have shifted the selection box into the MeerLICHT filter system frame of reference, we can apply this selection box to the MeerLICHT Southern All-Sky Survey (ML SASS) data. The ML SASS is a survey with the aim of observing the entire sky south of $+30°$ declination, in the MeerLICHT filter bands of ugrizq. In order to do so, the sky was divvied up into individual fields covering the entire area with each field having the MeerLICHT field of view of 1.65×1.65 degrees. To cover the entire sky south of $+30°$ declination takes 12740 fields, and each field will be observed at least once with a 60s observation in each filter. There are also a number of "special fields" which have a central interesting target or a group of interesting targets such as some fields dedicated to covering the Large and Small Magellanic Clouds. When any particular field is observed, there is a combination of filters taken at the same time but all six available filters are not observed at the same time. However, the q-band is always taken in combination with a few of the others so that every field observed will have a broadband q reference image for transient searches. This survey is still ongoing and as a result, our selection of candidates needed to be rerun every few weeks as the survey progressed.

The status of the ML SASS when we first ran our selection process can be seen in Figure 9. We first ran our candidate selection process in July of 2020 which produced 87 candidates from the initial colour selection box. At this point, there were 1264 fields which had been observed in the bands which we were interested in: u, g, r, i and q. One interesting fact to note is that the majority of the known AM CVns lie in the northern sky, speaking to either the lack of coverage in the southern hemisphere or the lack of studies done to search for AM CVns in the southern hemisphere.

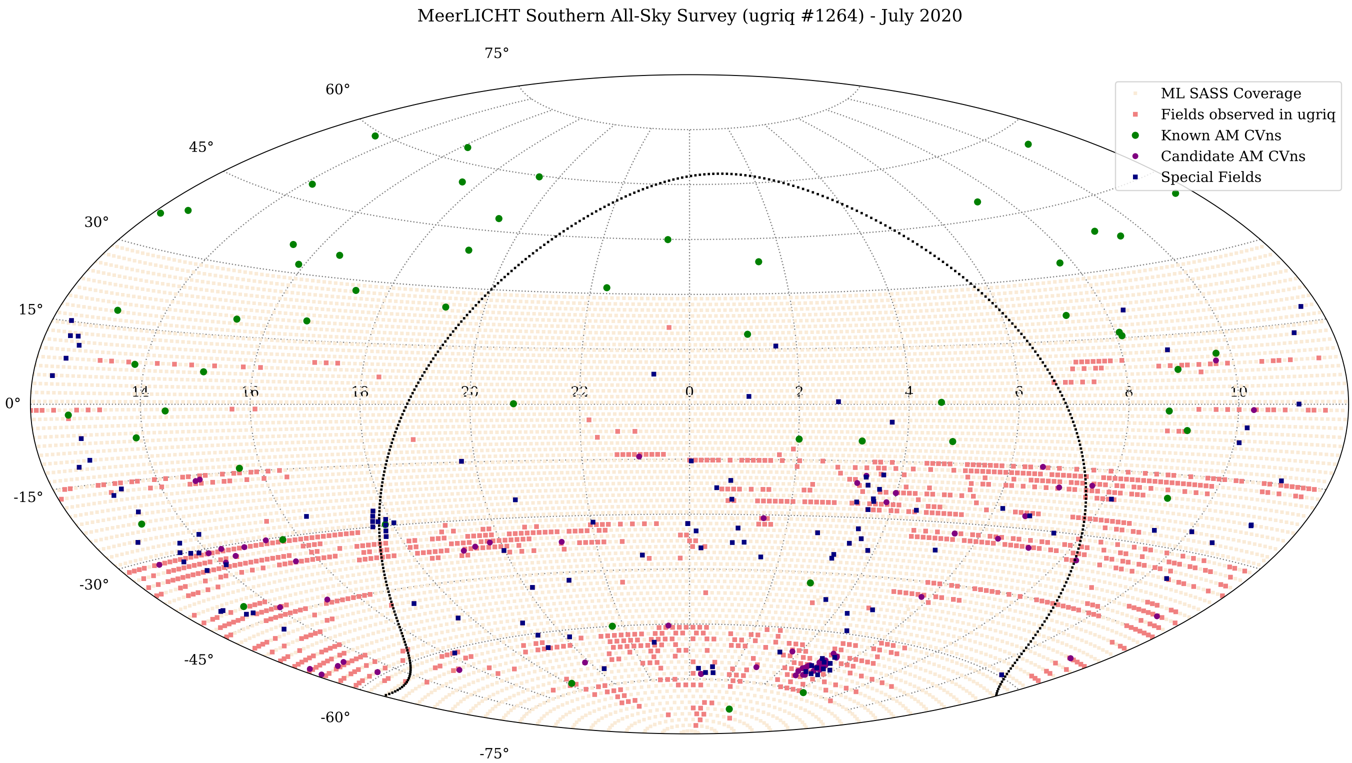

Figure 9: Status of ML SASS as of July 6th 2020.

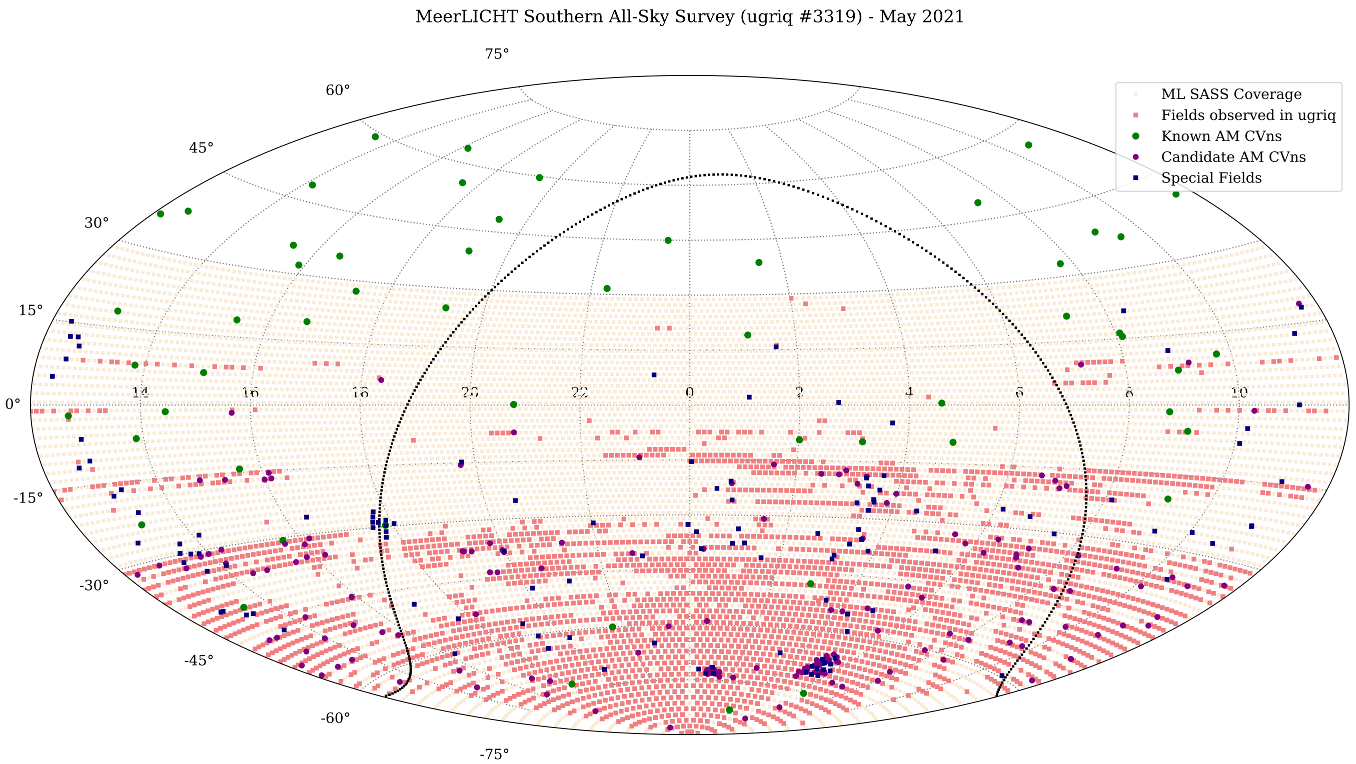

Figure 10: Coverage of ML SASS as of May 5th 2021. By this time, 3319 fields had been observed in the 5 filters we were using.

The selection process out of these 3319 fields produced 249 candidates for follow-up with the initial selection box. Upon re-running the selection process with the corrected box after having discovered the box was slightly out of place and larger than it should have been, 79 candidates were found. Of those 79, only 2 were not in the original selection box selection of 249.

2.2.2 Running the candidate selection process

In order to run our candidate selection process, we needed the u, g, r, and i reference images for each one of the fields which had been covered by all 4 of those bands. All of our data processing was done on the Ilifu JupyterLab service. Ilifu is a cloud-based computing platform for highly data-intensive research and is supported by the Inter-University Institute for Data Intensive Astronomy (IDIA)[6]. By utilising the Ilifu JupyterLab service, we have access to virtual machines allowing us to analyse the large datasets from ML SASS rapidly. All of the MeerLICHT data is also hosted on the I lifu cloud which makes accessing the ML SASS data very simple from the JupyterLab. To ensure that all the raw data is left unedited by our analysis, the reference catalogue tables for each field observed in u, g, r, and i were copied from the ilifu cloud on to a server in JupyterLab. From there we cross-matched the reference tables for all filters for all objects with a CLASS_STAR value above 0.8 and a FLAGS value of 0. This limits the reference tables to point-source objects which had no issues during the data reduction ensuring a clean selection of stars from which we select our candidates. The cross-matching process created a matched fits table of stars which had data in the 4 filters we were using - u, g, r and i - as well as q band data for reference. These cross-matched tables were then uploaded to the Gaia archive[7] and parallaxes were extracted from Gaia DR2/DR3 for all the stars where available.

[6]More information can be found at: https://www.ilifu.ac.za/.
[7]Available at: https://gea.esac.esa.int/archive/.

We show colour-colour and colour-magnitude plots for all the stars extracted from the ML SASS data as of May 5 2021. It is from these plots that we can extract our candidates. In order to have a more manageable number of targets on which to follow-up, we introduced another selection criterion. We separated the candidates into a primary and secondary group, the primary group all having absolute magnitudes in u and g of equal to or greater than 5. This criterion matches the known AM CVns range of absolute magnitudes as we can see in Figures 15, 16, 19 and 20.

Colour-colour plots for ML SASS data as of May 5 2021 are shown in Figures 11 and 13. These plots show roughly 3.5 million stars, showing both the primary 79 candidates and another 130 secondary candidates. Also seen are the known AM CVns with the relevant SDSS colours, shifted into the MeerLICHT frame, from the table in Ramsay et al. [4]. We see a near perfect overlap of the known AM CVns with our selected candidates, with a slightly larger deviation in Figure 13 due to the scatter in i band measurements, further ratifying our selection box.

Colour-magnitude plots for ML SASS data as of May 5 2021 can be seen in Figures 15 and 16. Absolute magnitudes were calculated using the parallaxes extracted from Gaia for each star. Once again we see that the overlap of our primary targets with the known AM CVns, shown here in black, is further evidence that our selection process is valid. We see the secondary candidates extend all the way up to an absolute magnitude of roughly –2.5. These are most likely bright white dwarfs and subdwarf stars. There was also a large amount of blue stars from the LMC and SMC which contaminated the sample of candidates and were weeded out.

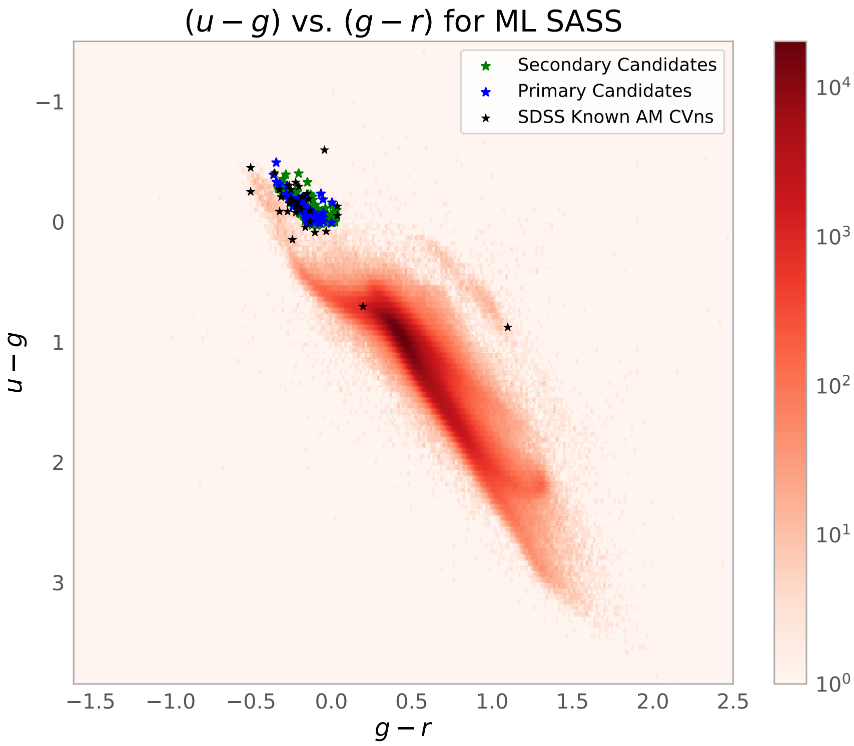

Figure 11: $u-g$ versus $g-r$ colour-colour plot for ML SASS.

We cropped this colour-colour plot to the region around the primary candidates and known AM CVn systems, and added in the AM CVn sources which have u, g, r and i MeerLICHT measurements, seen in Figure 12.

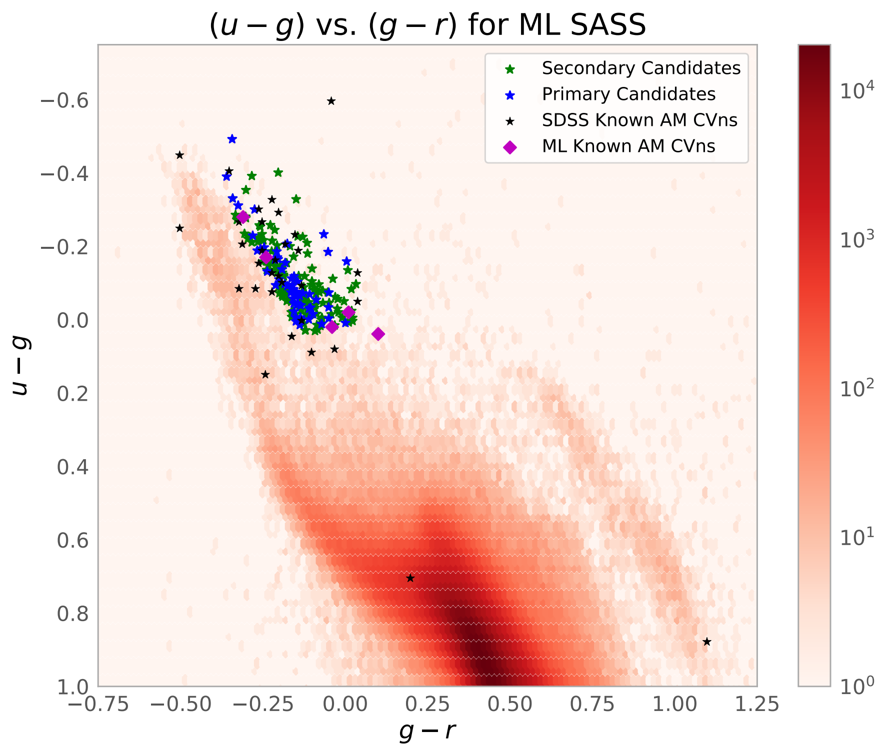

Figure 12: $u - g$ versus $g - r$ colour-colour plot for ML SASS.

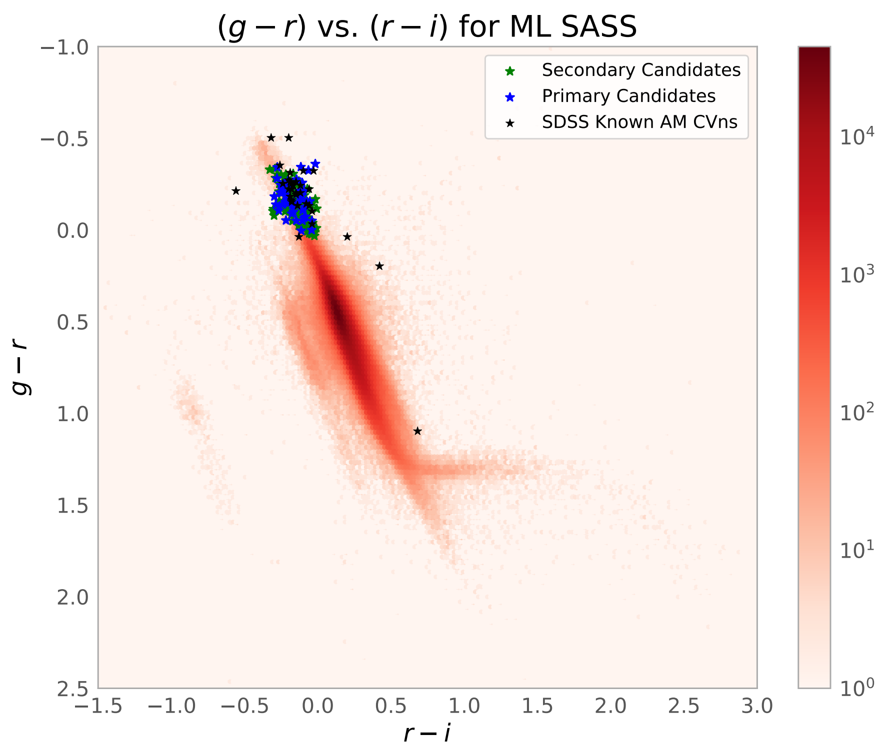

Figure 13: $g - r$ versus $r - i$ colour-colour plot for ML SASS.

We also zoomed into this plot to show the known AM CVn sources detected in ML and the primary candidates, as seen in Figure 14.

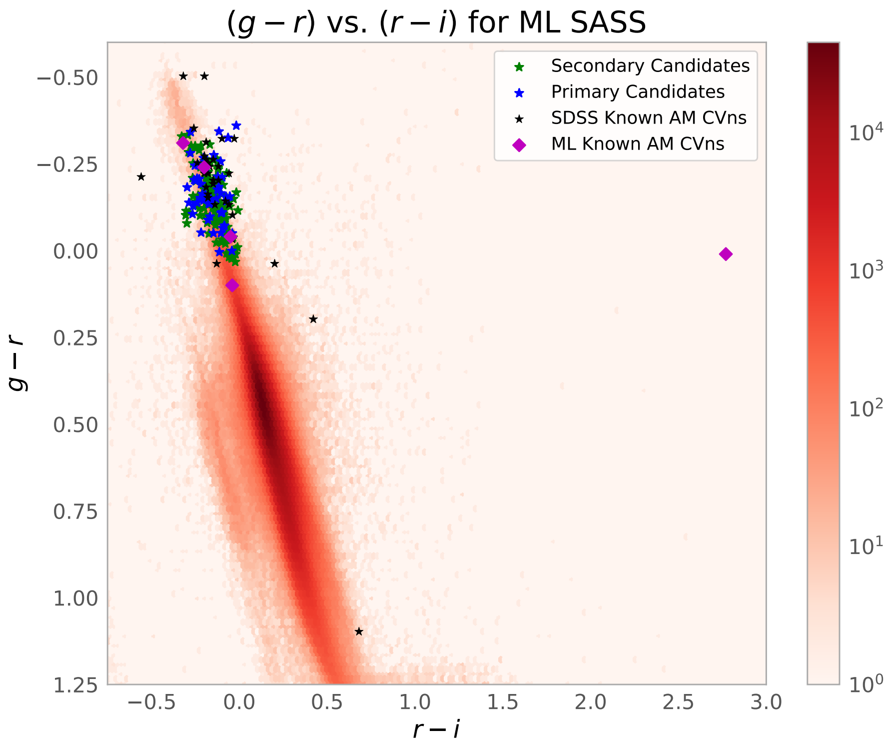

Figure 14: $g-r$ versus $r-i$ colour-colour plot for ML SASS.

From our zoomed-in plots in Figures 12 and 14, we can see that there appears to be an overlap between the MeerLICHT detected AM CVns and the primary selected candidates. However, from the $g-r$ versus $r-i$ positions of these ML sources in Figure 14, one object (V803 Cen) is far too red with $r-i=2.77$, and another object (V396 Hya) is also too red with $g-r=0.1$. The other three known AM CVns detected in MeerLICHT all reside just outside the colour selection box based on their position in the volume that the box creates in multiple colour-space. One possible reason for the over-redness of V803 Cen is that the filter magnitudes may not have been captured at the same time, thus it is possible that the i-band magnitude is during an outburst state whereas the r magnitude is during a quiescent state, this could cause the object to be redder than it is intrinsically. This could play a role in why none of the known AM CVns detected with MeerLICHT were selected by our selection box. It is possible that the magnitudes for the various filters are from different times and that could cause a "false colour" discrepancy.

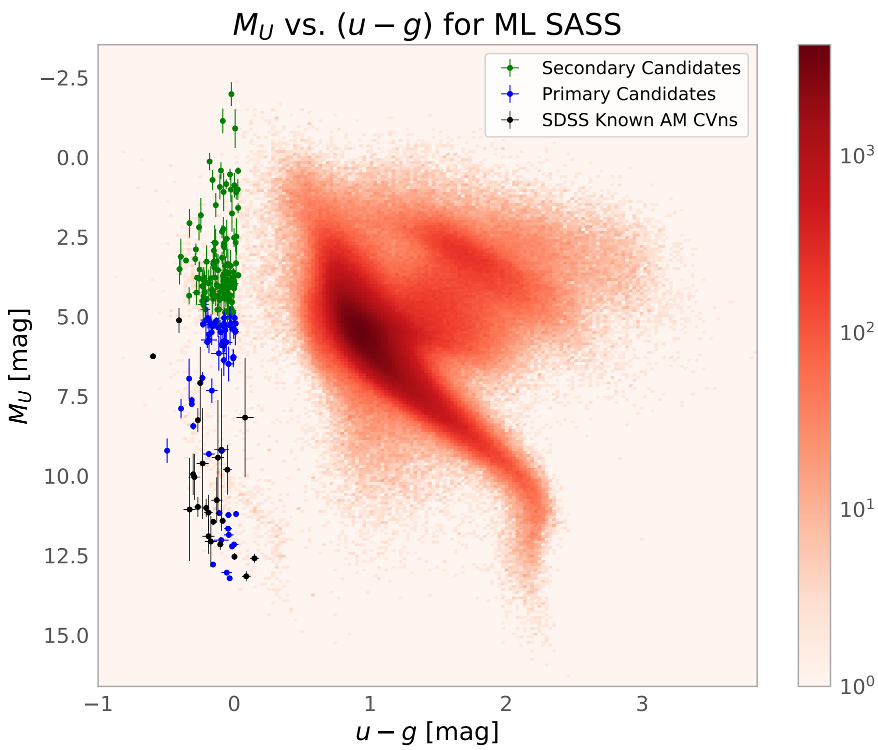

Figure 15: M_U versus $u-g$ colour-magnitude plot for ML SASS.

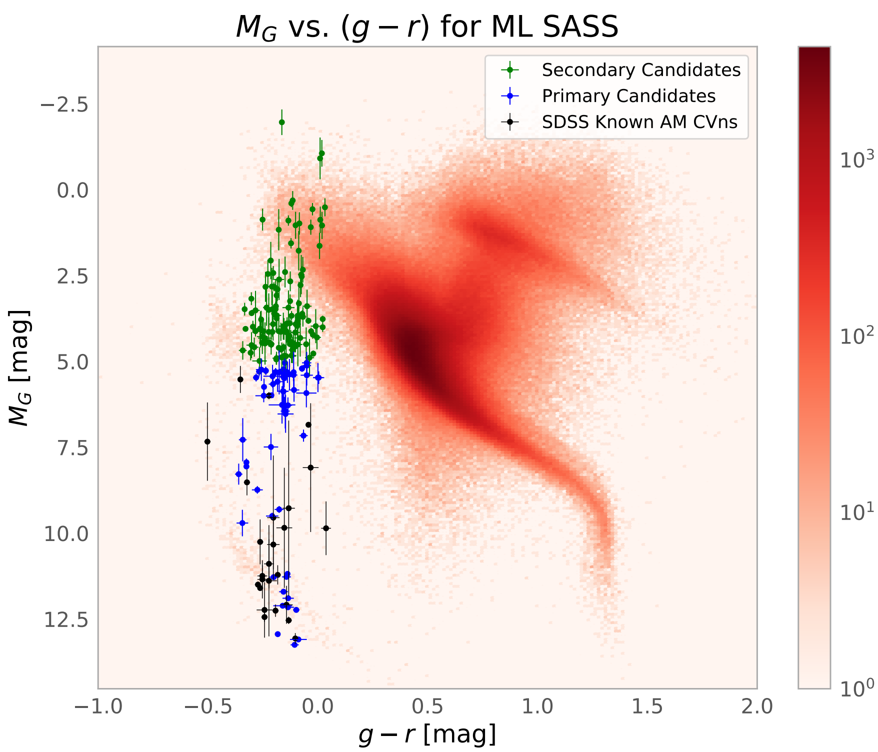

Figure 16: M_G versus $g-r$ colour-magnitude plot for ML SASS.

2.2.3 $ugrq$ Only

To demonstrate the limiting nature of the i band requirement, as the i band had the least coverage in ML SASS compared to the other filters we used, we also ran the selection process on the ML SASS data while dropping the i band requirement and selection criteria. This increased the number of fields in the sample on which to run the selection process which in turn increased the number of primary and secondary candidates we had. However, we kept the $ugriq$ and $ugrq$ candidates separate in order to keep track of where each candidate was found. There was some overlap in the selections which we noted in order to prevent following-up on the same target twice.

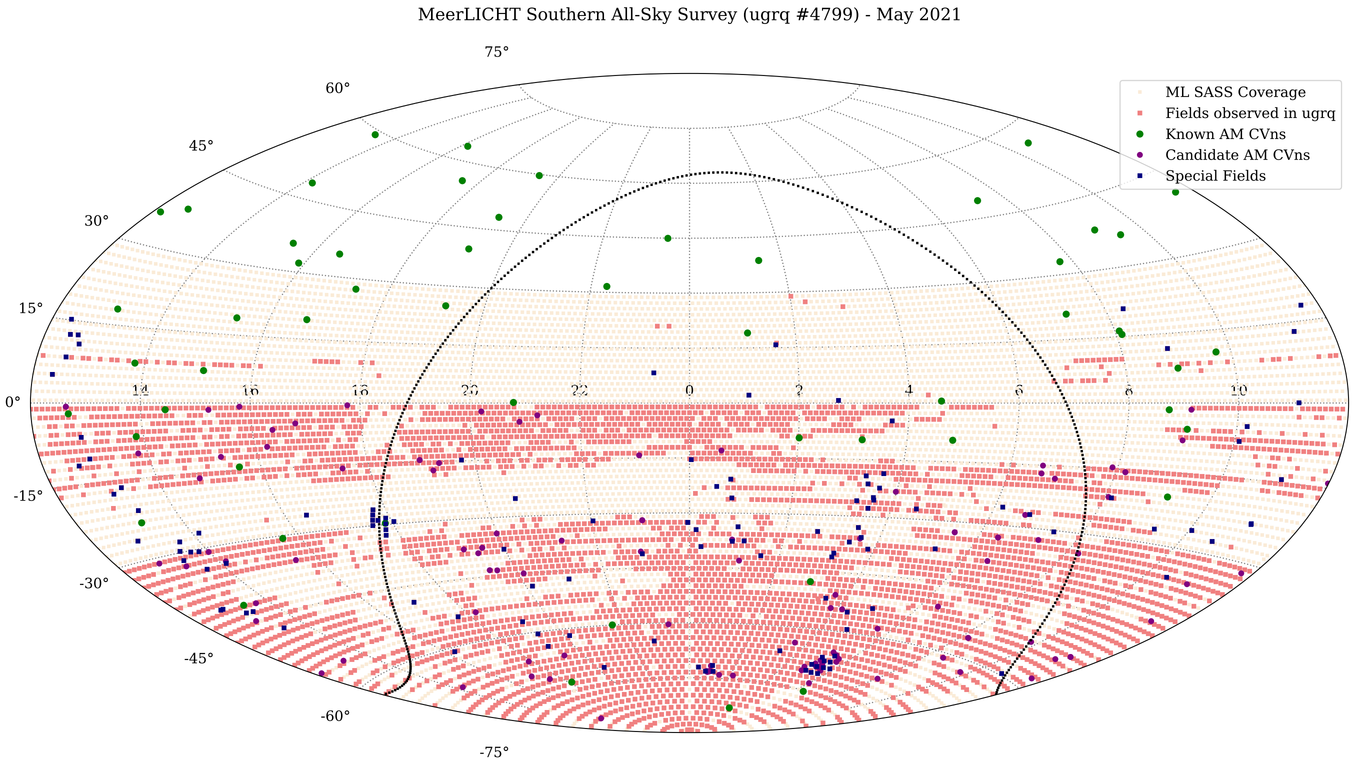

Figure 17: Status of ML SASS as of May 5th 2021 for only the u, g, r and q filters. There are 4799 fields in this selection compared to the 3319 seen in the u, g, r, i and q selection in Figure 10.

Colour-colour and colour-magnitude plots for $ugrq$ ML SASS can be seen in Figures 18, 19 and 20. Here we have a sample size of roughly 4.1 million stars, 116 primary candidates and 230 secondary candidates.

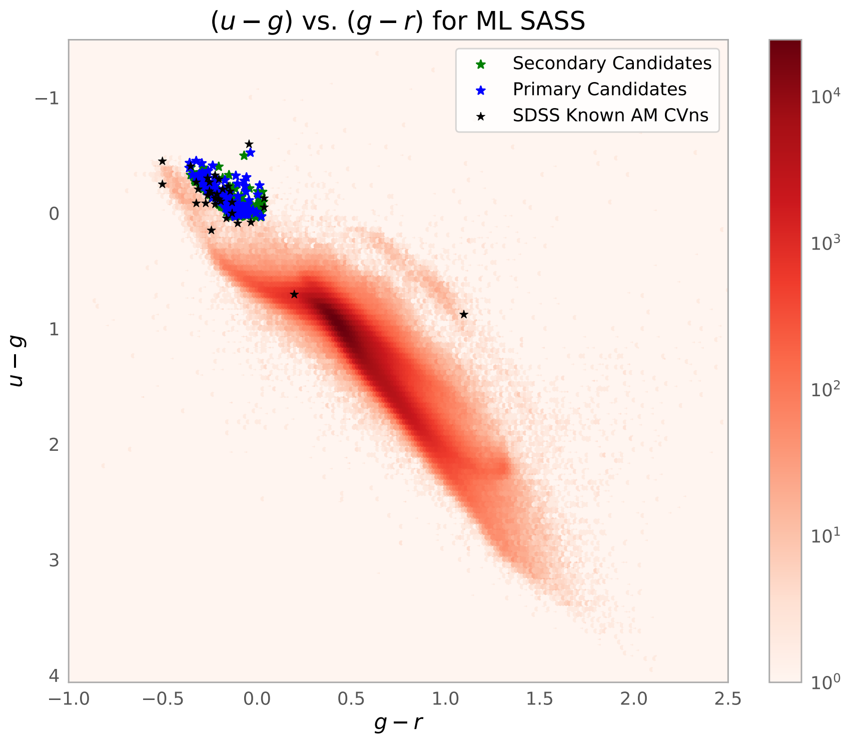

Figure 18: $u - g$ versus $g - r$ colour-colour plot for $ugrq$ ML SASS.

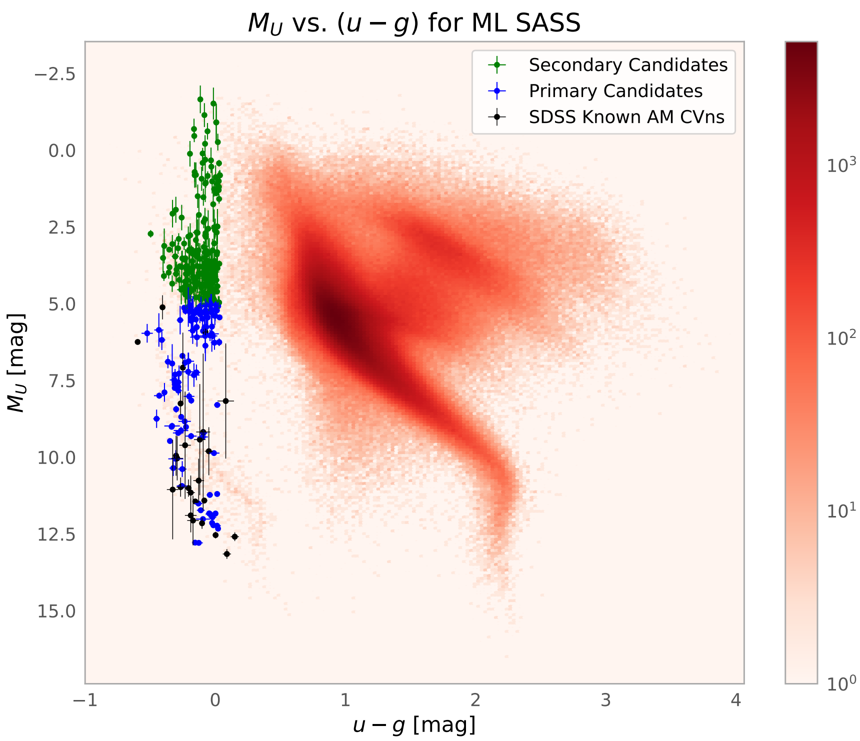

Figure 19: M_U versus $u - g$ colour-magnitude plot for $ugrq$ ML SASS.

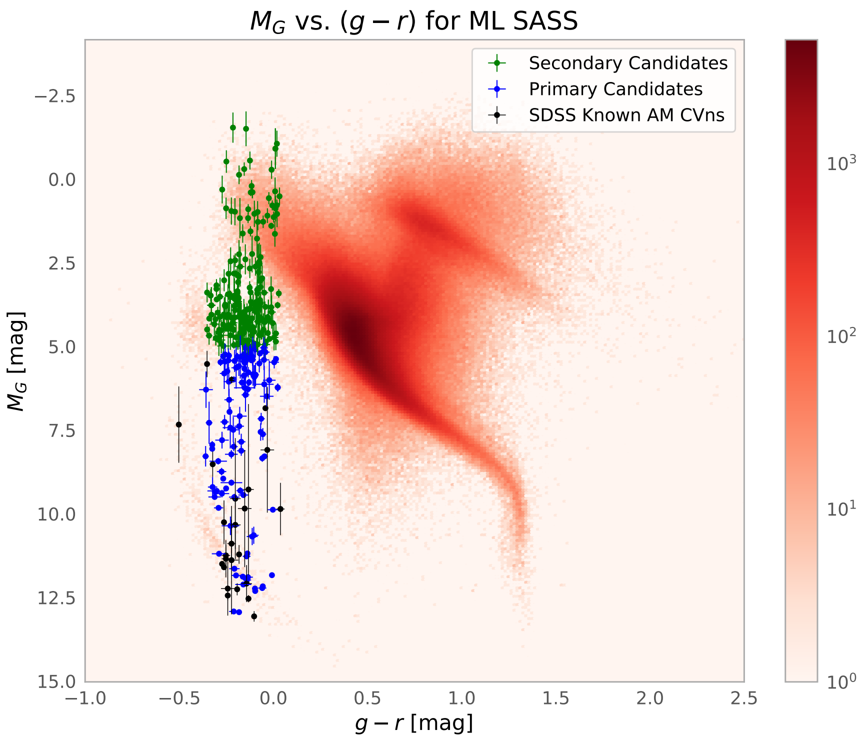

Figure 20: M_G versus $g - r$ colour-magnitude plot for $ugrq$ ML SASS.

2.3 Candidate Vetting and Bookkeeping

Once our candidates were selected, it was time to vet them and check whether or not these were already known objects. In order to keep track of them, we created several Google spreadsheets to keep relevant data for all our candidates easy to access and to have an easy way to update our follow-up campaign. First, we searched for each object on the SIMBAD Astronomical Database[8] using their coordinates looking for a match within 2 arcseconds. If there was a match, we added the SIMBAD name and identifier to the table of information for each AM CVn candidate. This was a way to check whether or not an object was known and if the type of the star was known. Thus we could prioritise observing those candidates which were either entirely unknown or their type was unknown first in the follow-up campaign. Figure 21 shows a screenshot of the primary AM CVn candidate sheet. A full list of all the $ugriq$ and $ugrq$ primary candidates can be found in Tables 8 and 9 respectively in Appendix A.

This sheet contains all 249 of the original primary candidates from the uncorrected selection box as well as the extra 2 candidates that were found to be new once we corrected the selection box. We include data for the apparent and absolute magnitudes of each candidate as well as their coordinates and a check for whether they had either spectroscopy or photometry data available. One final tool we used to prioritise our order of follow-up observations was an "Ideal Factor" check. This was the percentage error of each candidate's parallax. We prioritised those objects which had parallax errors equal to or less than 30% of their parallax. Access to these sheets can be requested from the author.

[8]Available at http://simbad.u-strasbg.fr/simbad/.

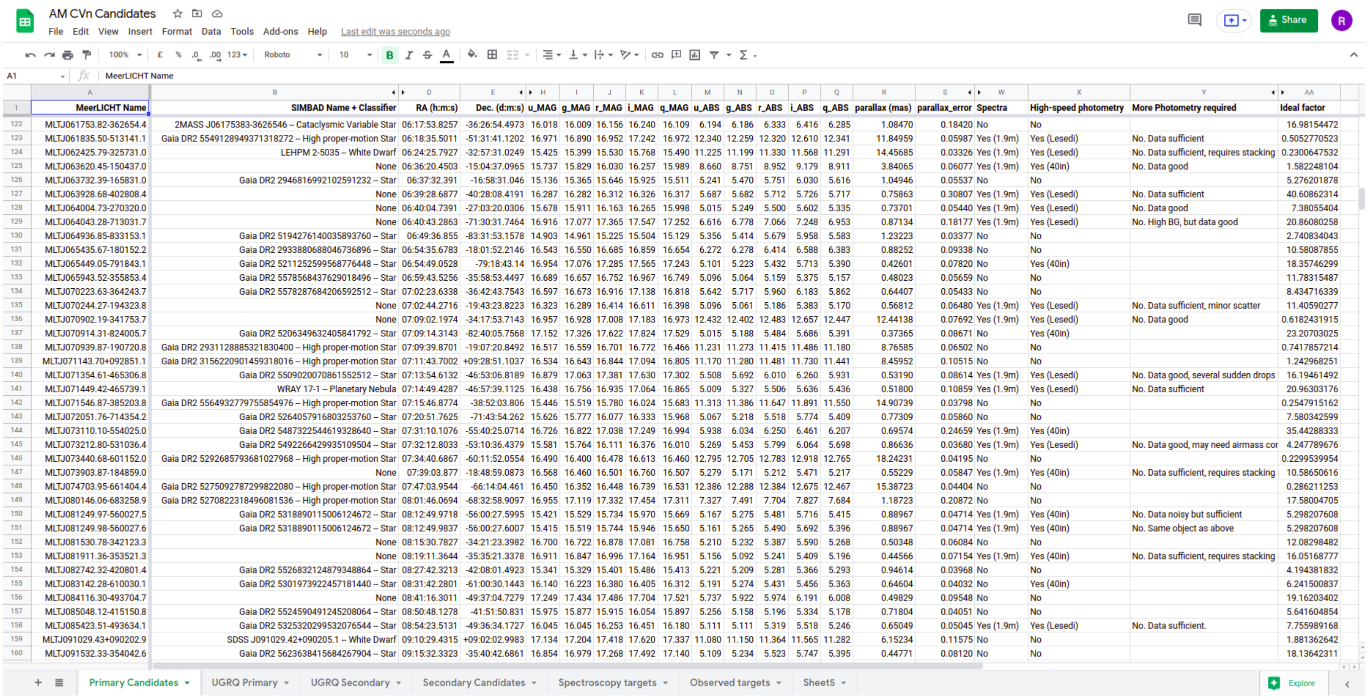

AM CVn Candidates

	MeerLICHT Name	SIMBAD Name + Classifier	RA (h:m:s)	Dec. (d:m:s)	u_MAG	g_MAG	r_MAG	i_MAG	q_MAG	u_ABS	g_ABS	r_ABS	i_ABS	q_ABS	parallax (mas)	parallax_error	Spectra	High-speed photometry	More Photometry required	Ideal factor
122	MLTJ061753.82-362654.4	2MASS J06175383-3626546 -- Cataclysmic Variable Star	06:17:53.8257	-36:26:54.4973	16.018	16.009	16.156	16.240	16.109	6.194	6.186	6.333	6.416	6.285	1.08470	0.18420	No	No		16.98154472
123	MLTJ061835.50-513141.1	Gaia DR2 5549128949371318272 -- High proper-motion Star	06:18:35.5011	-51:31:41.1202	16.971	16.890	16.952	17.242	16.972	12.340	12.259	12.320	12.610	12.341	11.84959	0.05987	Yes (1.9m)	Yes (Lesedi)	No. Data sufficient	0.5052770523
124	MLTJ062425.79-325731.0	LEHPM 2-5035 -- White Dwarf	06:24:25.7927	-32:57:31.0249	15.425	15.399	15.530	15.768	15.490	11.225	11.199	11.330	11.568	11.291	14.45685	0.03326	Yes (1.9m)	Yes (Lesedi)	No. Data sufficient, requires stacking	0.2300647532
125	MLTJ063620.45-150437.0	None	06:36:20.4503	-15:04:37.0965	15.737	15.829	16.030	16.257	15.989	8.660	8.751	8.952	9.179	8.911	3.84065	0.06077	Yes (1.9m)	Yes (40in)	No. Data good	1.582248104
126	MLTJ063732.39-165831.0	Gaia DR2 2946816992102591232 -- Star	06:37:32.391	-16:58:31.046	15.136	15.365	15.646	15.925	15.511	5.241	5.470	5.751	6.030	5.616	1.04946	0.05537	No	No		5.276201878
127	MLTJ063928.68-402808.4	None	06:39:28.6877	-40:28:08.4191	16.287	16.282	16.312	16.326	16.317	5.687	5.682	5.712	5.726	5.717	0.75863	0.30807	Yes (1.9m)	Yes (Lesedi)	No. Data sufficient	40.60862314
128	MLTJ064004.73-270320.0	None	06:40:04.7391	-27:03:20.0306	15.678	15.911	16.163	16.265	15.998	5.015	5.249	5.500	5.602	5.335	0.73701	0.05440	Yes (1.9m)	Yes (Lesedi)	No. Data good	7.38055404
129	MLTJ064043.28-713031.7	None	06:40:43.2863	-71:30:31.7464	16.916	17.077	17.365	17.547	17.252	6.616	6.778	7.066	7.248	6.953	0.87134	0.18177	Yes (1.9m)	Yes (Lesedi)	No. High BG, but data good	20.86080258
130	MLTJ064936.85-833153.1	Gaia DR2 5194276140035893760 -- Star	06:49:36.855	-83:31:53.1578	14.903	14.961	15.225	15.504	15.129	5.356	5.414	5.679	5.958	5.583	1.23223	0.03377	No	No		2.740834043
131	MLTJ065435.67-180152.2	Gaia DR2 2933880688046736896 -- Star	06:54:35.6783	-18:01:52.2146	16.543	16.550	16.685	16.859	16.654	6.272	6.278	6.414	6.588	6.383	0.88252	0.09338	No	No		10.58087855
132	MLTJ065449.05-791843.1	Gaia DR2 5211252599568776448 -- Star	06:54:49.0528	-79:18:43.14	16.954	17.076	17.285	17.565	17.243	5.101	5.223	5.432	5.713	5.390	0.42601	0.07820	No	Yes (40in)		18.35746299
133	MLTJ065943.52-355853.4	Gaia DR2 5578568437629018496 -- Star	06:59:43.5256	-35:58:53.4497	16.689	16.657	16.752	16.967	16.749	5.096	5.064	5.159	5.375	5.157	0.48023	0.05659	No	No		11.78315487
134	MLTJ070223.63-364243.7	Gaia DR2 5578287684206592512 -- Star	07:02:23.6338	-36:42:43.7543	16.597	16.673	16.916	17.138	16.818	5.642	5.717	5.960	6.183	5.862	0.64407	0.05433	No	No		8.434716339
135	MLTJ070244.27-194323.8	None	07:02:44.2716	-19:43:23.8223	16.323	16.289	16.414	16.611	16.398	5.096	5.061	5.186	5.383	5.170	0.56812	0.06480	Yes (1.9m)	Yes (Lesedi)	No. Data sufficient, minor scatter	11.40590277
136	MLTJ070902.19-341753.7	None	07:09:02.1974	-34:17:53.7143	16.957	16.928	17.008	17.183	16.973	12.432	12.402	12.483	12.657	12.447	12.44138	0.07692	Yes (1.9m)	Yes (Lesedi)	No. Data good	0.6182431915
137	MLTJ070914.31-824005.7	Gaia DR2 5206349632405841792 -- Star	07:09:14.3143	-82:40:05.7568	17.152	17.326	17.622	17.824	17.529	5.015	5.188	5.484	5.686	5.391	0.37365	0.08671	No	Yes (40in)		23.20703025
138	MLTJ070939.87-190720.8	Gaia DR2 2931128885321830400 -- High proper-motion Star	07:09:39.8701	-19:07:20.8492	16.517	16.559	16.701	16.772	16.466	11.231	11.273	11.415	11.486	11.180	8.76585	0.06502	No	No		0.7417857214
139	MLTJ071143.70+092851.1	Gaia DR2 3156220901459318016 -- High proper-motion Star	07:11:43.7002	+09:28:51.1037	16.534	16.643	16.844	17.094	16.805	11.170	11.280	11.481	11.730	11.441	8.45952	0.10515	No	No		1.242968251
140	MLTJ071354.61-465306.8	Gaia DR2 5509020070861552512 -- Star	07:13:54.6132	-46:53:06.8189	16.879	17.063	17.381	17.630	17.302	5.508	5.692	6.010	6.260	5.931	0.53190	0.08614	Yes (1.9m)	Yes (Lesedi)	No. Data good, several sudden drops	16.19461492
141	MLTJ071449.42-465739.1	WRAY 17-1 -- Planetary Nebula	07:14:49.4287	-46:57:39.1125	16.438	16.756	16.935	17.064	16.865	5.009	5.327	5.506	5.636	5.436	0.51800	0.10859	Yes (1.9m)	Yes (Lesedi)	No. Data sufficient	20.96303176
142	MLTJ071546.87-385203.8	Gaia DR2 5564932779755854976 -- High proper-motion Star	07:15:46.8774	-38:52:03.806	15.446	15.519	15.780	16.024	15.683	11.313	11.386	11.647	11.891	11.550	14.90739	0.03798	No	No		0.2547915162
143	MLTJ072051.76-714354.2	Gaia DR2 5264057916803253760 -- Star	07:20:51.7625	-71:43:54.262	15.626	15.777	16.077	16.333	15.968	5.067	5.218	5.518	5.774	5.409	0.77309	0.05860	No	No		7.580342599
144	MLTJ073110.10-554025.0	Gaia DR2 5487322544619328640 -- Star	07:31:10.1076	-55:40:25.0714	16.726	16.822	17.038	17.249	16.994	5.938	6.034	6.250	6.461	6.207	0.69574	0.24659	Yes (1.9m)	Yes (40in)		35.44288333
145	MLTJ073212.80-531036.4	Gaia DR2 5492266429935109504 -- Star	07:32:12.8033	-53:10:36.4379	15.581	15.764	16.111	16.376	16.010	5.269	5.453	5.799	6.064	5.698	0.86636	0.03680	Yes (1.9m)	Yes (Lesedi)	No. Data good, may need airmass cor	4.247789676
146	MLTJ073440.68-601152.0	Gaia DR2 5292685793681027968 -- High proper-motion Star	07:34:40.6867	-60:11:52.0554	16.490	16.400	16.478	16.613	16.460	12.795	12.705	12.783	12.918	12.765	18.24231	0.04195	No	No		0.2299539954
147	MLTJ073903.87-184859.0	None	07:39:03.877	-18:48:59.0873	16.568	16.460	16.501	16.760	16.507	5.279	5.171	5.212	5.471	5.217	0.55229	0.05847	Yes (1.9m)	Yes (40in)	No. Data sufficient, requires stacking	10.58650616
148	MLTJ074703.95-661404.4	Gaia DR2 5275092787299822080 -- High proper-motion Star	07:47:03.9544	-66:14:04.461	16.450	16.352	16.448	16.739	16.531	12.386	12.288	12.384	12.675	12.467	15.38723	0.04404	No	No		0.286211253
149	MLTJ080146.06-683258.9	Gaia DR2 5270822318496081536 -- High proper-motion Star	08:01:46.0694	-68:32:58.9097	16.955	17.119	17.332	17.454	17.311	7.327	7.491	7.704	7.827	7.684	1.18723	0.20872	No	No		17.58004705
150	MLTJ081249.97-560027.5	Gaia DR2 5318890115006124672 -- Star	08:12:49.9718	-56:00:27.5995	15.421	15.529	15.734	15.970	15.669	5.167	5.275	5.481	5.716	5.415	0.88967	0.04714	Yes (1.9m)	Yes (40in)	No. Data noisy but sufficient	5.298207608
151	MLTJ081249.98-560027.6	Gaia DR2 5318890115006124672 -- Star	08:12:49.9837	-56:00:27.6007	15.415	15.519	15.744	15.946	15.650	5.161	5.265	5.490	5.692	5.396	0.88967	0.04714	Yes (1.9m)	Yes (40in)	No. Same object as above	5.298207608
152	MLTJ081530.78-342123.3	None	08:15:30.7827	-34:21:23.3982	16.700	16.722	16.878	17.081	16.758	5.210	5.232	5.387	5.590	5.268	0.50348	0.06084	No	No		12.08298482
153	MLTJ081911.36-353521.3	None	08:19:11.3644	-35:35:21.3378	16.911	16.847	16.996	17.164	16.951	5.156	5.092	5.241	5.409	5.196	0.44566	0.07154	Yes (1.9m)	Yes (40in)	No. Data sufficient, requires stacking	16.05168777
154	MLTJ082742.32-420801.4	Gaia DR2 5526832124879348864 -- Star	08:27:42.3213	-42:08:01.4923	15.341	15.329	15.401	15.486	15.413	5.221	5.209	5.281	5.366	5.293	0.94614	0.03968	No	No		4.194381832
155	MLTJ083142.28-610030.1	Gaia DR2 5301973922457181440 -- Star	08:31:42.2801	-61:00:30.1443	16.140	16.223	16.380	16.405	16.312	5.191	5.274	5.431	5.456	5.363	0.64604	0.04032	No	Yes (40in)		6.241500837
156	MLTJ084116.30-493704.7	None	08:41:16.3011	-49:37:04.7279	17.249	17.434	17.486	17.704	17.521	5.737	5.922	5.974	6.191	6.008	0.49829	0.09548	No	No		19.16203402
157	MLTJ085048.12-415150.8	Gaia DR2 5524590491245208064 -- Star	08:50:48.1278	-41:51:50.831	15.975	15.877	15.915	16.054	15.897	5.256	5.158	5.196	5.334	5.178	0.71804	0.04051	No	No		5.641604854
158	MLTJ085423.51-493634.1	Gaia DR2 5325320299532076544 -- Star	08:54:23.5131	-49:36:34.1727	16.045	16.045	16.253	16.451	16.180	5.111	5.111	5.319	5.518	5.246	0.65049	0.05045	Yes (1.9m)	Yes (Lesedi)	No. Data sufficient.	7.755989168
159	MLTJ091029.43+090202.9	SDSS J091029.42+090205.1 -- White Dwarf	09:10:29.4315	+09:02:02.9983	17.134	17.204	17.418	17.620	17.337	11.080	11.150	11.364	11.565	11.282	6.15234	0.11575	No	No		1.881362642
160	MLTJ091532.33-354042.6	Gaia DR2 5623638415684267904 -- Star	09:15:32.3323	-35:40:42.6861	16.854	16.979	17.268	17.492	17.140	5.109	5.234	5.523	5.747	5.395	0.44771	0.08120	No	No		18.13642311

Figure 21: Screenshot of the AM CVn candidates Google sheet.

One unexpected outcome of the selection process was that those stars which were in the right region for the selection box, but had no parallax and so could not be sorted into either the primary or secondary candidate lists, were automatically added to the primary candidate list as a result of Python's handling of NaN values. This resulted in us having a total of 251 primary candidates, of which 185 had parallaxes and were thus prioritised over the ones without, by the time we last ran the selection process with the December 2021 update to ML SASS coverage which only increased the number of fields covered by 2 since the May 2021 update.

3 Photometry

Once our selection process had determined suitable candidates for follow-up investigation, high-speed photometry was obtained for each of the candidates in order to search for variability in the lightcurves. This photometry was conducted at the South African Astronomical Observatory (SAAO) site in Sutherland. Due to travel restrictions and lockdown regulations due to the COVID-19 pandemic, much of the photometry was done remotely from the SAAO site in Cape Town. We made use of both the 1.0-m telescope and the new Lesedi 1.0-m telescope to observe our candidates.

3.1 Observations

Because we are searching for periodic variability on the timescale of 5 to 65 minutes, we observed our candidates over a three hour period with a cadence of between 10 and 30 seconds depending on the brightness of the target star. By making use of a three hour time span, we can confirm whether any apparent periodicity in the range we are probing is consistent. Both telescopes are equipped with Sutherland High Speed Optical Cameras (SHOC) [50] which are high-speed, visible-wavelength instruments. The detectors on the SHOC cameras have a 2048×1024 shape with a pixel size of 13-μm, however, used in the frame-transfer mode they have an imaging area of 1024×1024 pixels. On both the telescopes used for the photometry, the observational setup was the same. The binning used was either 2×2 or, when the atmospheric seeing was particularly poor or the target star was very faint, 4×4. We avoided using the 8×8 binning mode as this caused an over-binning issue in which a nearby star's aperture could overlap with either the target star or the suitable comparison stars. This overlap was particularly noticeable and problematic when observing in crowded fields. Although the SHOC cameras are outfitted with an electron-multiplying (EM) capability, this was not used for either telescope as it was not necessary. The data output is a fits cube of all the frames taken of the target during the exposure. All of the candidates for which we have conducted photometric observations are shown in Table 3. The "Variability?" column was used as an indicator for potential variability based on a visual inspection of the differential lightcurves and the error analysis plots described later in Data Reduction & Analysis in Section 3.3. Those objects with a "Yes" in the "Variability?" column were then subject to a more detailed analysis of their lightcurves and periodograms.

3.1.1 1.0-m

The 1.0-m telescope at the Sutherland site has a Cassegrain focus with an f-ratio of f/16 [51]. It is fitted with a SHOC CCD. This instrument has 2.85×2.85 arcminute field of view on the 1.0-m telescope and a platescale of 0.167 arcseconds per pixel. The 1.0-m telescope is fitted with two filter wheels, however, only one was available for usage, the Geneva B1 wheel. This wheel contains SDSS filters u, g, r, i, z, an Hα (20nm) filter, an [O III] 501nm filter, and an empty filter. The g filter was used for our observations. The pre-amplifier gain on the 1.0-m SHOC camera was set to 2.4 with a readout rate of 1 MHz at 16-bit.

3.1.2 Lesedi

The Lesedi 1.0-m telescope is a new 1-metre alt-az telescope which has only recently undergone commissioning [52]. It has two identical Nasmyth foci and an f-ratio of f/8, with a total possible field of view diameter of 42.9 arcminutes. However, for our purposes we used the SHOC CCD instrument fitted to Lesedi which limits the field of view to 5.7×5.7 arcminutes with a platescale of 0.335 arcseconds per pixel. Lesedi has a Bessell filter wheel with UBVRI and clear filters. We used the V filter for all observations conducted with Lesedi. The pre-amplifier gain for Lesedi's SHOC camera was set to 2.5 with a readout rate of 1 MHz at 16-bit.

3.1.3 Observed Targets

Table 3: MeerLICHT selected targets observed.

Target	Date	Telescope	Binning	Cadence (s)	# Exps.	Exp. Time (hr)	Variability?
MLTJ012956.10–305512.3	24/08/2020	1.0-m	8x8	15	724	3.017	No
MLTJ032047.03–185527.0	01/11/2020	1.0-m	4x4	30	360	3.000	No
MLTJ034315.70–660204.8	02/11/2020	Lesedi	4x4	30	382	3.183	No
MLTJ034917.85–541825.6	30/12/2020	1.0-m	4x4	20	354	1.967	No
MLTJ035122.99–254054.7	27/01/2021	Lesedi	4x4	20	540	3.000	No
MLTJ035904.91–231225.1	28/01/2021	Lesedi	2x2	20	540	3.000	No
MLTJ040830.70–542139.7	29/01/2021	Lesedi	2x2	30	360	3.000	No
MLTJ044403.48–703939.6	02/01/2021	1.0-m	4x4	20	427	2.372	No
MLTJ045327.58–684953.3	30/01/2021	Lesedi	2x2	30	360	3.000	No
MLTJ045837.48–685904.4	25/11/2020	1.0-m	2x2	30	360	3.000	No
MLTJ045926.12–654943.5	01/02/2021	Lesedi	2x2	20	540	3.000	No
MLTJ050418.69–671903.9	04/02/2021	Lesedi	2x2	20	450	2.500	No
MLTJ050555.42–683706.0	05/02/2021	Lesedi	2x2	30	280	2.333	No
MLTJ050926.31–651124.1	04/02/2021	Lesedi	2x2	10	900	2.500	No
MLTJ053450.55–580140.6	28/01/2021	Lesedi	2x2	20	540	3.000	Yes
MLTJ053541.03–685734.4	08/02/2021	Lesedi	2x2	20	500	2.778	No
MLTJ054725.58–484720.4	31/01/2021	Lesedi	2x2	30	366	3.050	No
MLTJ061835.50–513141.1	09/02/2021	Lesedi	2x2	30	300	2.500	No
MLTJ062425.79–325731.0	02/02/2021	Lesedi	2x2	15	647	2.696	No
MLTJ063620.45–150437.0	29/11/2020	1.0-m	4x4	30	360	3.000	No
MLTJ063928.68–402808.4	08/02/2021	Lesedi	2x2	20	500	2.778	No
MLTJ064004.73–270320.0	05/02/2021	Lesedi	2x2	10	853	2.369	No
MLTJ064043.28–713031.7	01/11/2020	Lesedi	4x4	30	490	4.083	No
MLTJ065449.05–791843.1	01/05/2021	1.0-m	2x2	20	260	1.444	No
MLTJ070244.27–194323.8	06/02/2021	Lesedi	2x2	20	450	2.500	No
MLTJ070902.19–341753.7	02/11/2020	Lesedi	4x4	30	365	3.042	No
MLTJ070914.31–824005.7	02/05/2021	1.0-m	2x2	30	360	3.000	No
MLTJ071354.61–465306.8	06/02/2021	Lesedi	2x2	20	450	2.500	No
MLTJ071449.42–465739.1	07/02/2021	Lesedi	2x2	30	300	2.500	No
MLTJ073110.10–554025.0	24/02/2021	1.0-m	2x2	30	320	2.667	No
MLTJ073212.80–531036.4	29/01/2021	Lesedi	2x2	20	540	3.000	No
MLTJ073903.87–184859.0	01/01/2021	1.0-m	8x8	25	576	4.000	No
MLTJ080146.07–683258.9	31/03/2021	1.0-m	4x4	30	145	1.208	No
MLTJ080146.07–683258.9	31/03/2021	1.0-m	2x2	30	360	3.000	No
MLTJ080401.92–211831.9	01/04/2021	1.0-m	4x4	30	334	2.783	No
MLTJ080401.92–211831.9	05/04/2021	1.0-m	4x4	30	360	3.000	No
MLTJ080401.92–211831.9	06/04/2021	1.0-m	4x4	30	360	3.000	No
MLTJ081249.97–560027.5	27/11/2020	1.0-m	4x4	30	295	2.458	No
MLTJ081911.36–353521.3	30/12/2020	1.0-m	4x4	20	538	2.989	No
MLTJ083142.28–610030.1	23/04/2021	1.0-m	2x2	20	450	2.500	No
MLTJ085423.51–493634.1	09/02/2021	Lesedi	2x2	20	550	3.056	No
MLTJ094115.19+090152.5	07/02/2021	Lesedi	2x2	30	300	2.500	No
MLTJ100814.09–375754.2	04/06/2021	Lesedi	2x2	30	360	3.000	No
MLTJ102251.75–322602.6	02/04/2021	1.0-m	4x4	30	360	3.000	No
MLTJ105609.30–451430.5	05/06/2021	Lesedi	2x2	20	540	3.000	No
MLTJ110105.32–355045.3	06/06/2021	Lesedi	2x2	30	360	3.000	No
MLTJ111610.64–525935.7	02/01/2021	1.0-m	4x4	10	540	1.500	No
MLTJ111610.64–525935.7	02/01/2021	1.0-m	4x4	5	540	0.750	No
MLTJ111845.64–420550.0	30/01/2021	Lesedi	2x2	30	360	3.000	No
MLTJ112405.68–431729.4	02/04/2021	1.0-m	8x8	30	360	3.000	No
MLTJ121018.82–554428.5	02/02/2021	Lesedi	2x2	20	560	3.111	No
MLTJ121432.53–541942.5	22/04/2021	1.0-m	2x2	15	733	3.054	No
MLTJ121558.78–491453.4	04/04/2021	1.0-m	4x4	30	500	4.167	Yes
MLTJ121558.78–491453.4	06/04/2021	1.0-m	4x4	30	540	4.500	Yes
MLTJ123403.30–450133.3	31/03/2021	1.0-m	4x4	30	353	2.942	No
MLTJ124631.99–480413.5	04/06/2021	Lesedi	2x2	10	1031	2.864	No
MLTJ125002.08–310255.5	22/04/2021	1.0-m	2x2	10	720	2.000	No
MLTJ125544.63–555351.4	23/04/2021	1.0-m	2x2	25	440	3.056	No
MLTJ130106.77–481034.8	07/06/2021	Lesedi	2x2	20	540	3.000	No

MLTJ130116.33–480811.7	07/06/2021	Lesedi	2x2	20	540	3.000	No
MLTJ130129.04–515244.5	11/06/2021	1.0-m	2x2	30	360	3.000	No
MLTJ131438.71–554554.9	14/07/2021	Lesedi	2x2	30	360	3.000	No
MLTJ132425.35–592124.4	01/05/2021	1.0-m	2x2	20	540	3.000	No
MLTJ135704.98–510325.9	10/06/2021	1.0-m	2x2	30	360	3.000	No
MLTJ135917.77–305409.6	13/06/2021	1.0-m	4x4	30	332	2.767	No
MLTJ140516.70–434023.6	22/04/2021	1.0-m	2x2	15	730	3.042	No
MLTJ140801.86–331717.0	29/07/2020	1.0-m	8x8	30	411	3.425	No
MLTJ141822.54–303211.9	30/07/2020	1.0-m	4x4	10	1000	2.778	No
MLTJ144139.77–161530.4	24/03/2020	1.0-m	8x8	30	369	3.075	No
MLTJ144603.78–680359.5	06/06/2021	Lesedi	2x2	20	540	3.000	No
MLTJ144641.89–305708.2	01/08/2020	1.0-m	4x4	15	735	3.063	No
MLTJ144700.45–160149.1	05/06/2021	Lesedi	2x2	20	540	3.000	Yes[9]
MLTJ150307.49–502107.2	08/06/2021	Lesedi	2x2	30	360	3.000	No
MLTJ151629.11–442615.4	31/07/2020	1.0-m	4x4	10	1175	3.264	No
MLTJ153133.70–353213.7	06/04/2021	1.0-m	4x4	30	240	2.000	No
MLTJ161604.14–794236.8	04/06/2021	Lesedi	2x2	10	901	2.503	No
MLTJ161737.30–734440.4	05/06/2021	Lesedi	2x2	20	450	2.500	No
MLTJ170507.64–695031.0	23/04/2021	1.0-m	2x2	15	740	3.083	No
MLTJ181411.28–531653.9	12/06/2021	1.0-m	4x4	30	480	4.000	No
MLTJ181723.44–872557.7	14/07/2021	Lesedi	2x2	30	480	4.000	No
MLTJ185535.63–813507.0	14/07/2021	Lesedi	2x2	30	360	3.000	No
MLTJ190610.74–373414.1	08/06/2021	Lesedi	2x2	30	360	3.000	No
MLTJ190752.82–373956.0	29/07/2020	1.0-m	4x4	20	900	5.000	No
MLTJ192433.98–432444.6	30/04/2021	1.0-m	2x2	20	420	2.333	No
MLTJ192504.69–365151.4	17/07/2021	Lesedi	2x2	30	360	3.000	No
MLTJ192608.60–352013.2	06/06/2021	Lesedi	2x2	20	462	2.567	No
MLTJ193431.86–433643.9	13/06/2021	1.0-m	4x4	30	360	3.000	No
MLTJ194921.72–684412.2	23/08/2020	1.0-m	8x8	15	472	1.967	No
MLTJ203654.63–432231.6	03/06/2021	Lesedi	2x2	20	823	4.572	Yes
MLTJ203654.63–432231.6	04/06/2021	Lesedi	2x2	20	480	2.667	Yes
MLTJ203654.63–432231.6	05/06/2021	Lesedi	2x2	20	453	2.517	Yes
MLTJ203654.63–432231.6	06/06/2021	Lesedi	2x2	20	445	2.472	Yes
MLTJ211648.89–365233.6	21/08/2020	1.0-m	8x8	10	1267	3.519	No
MLTJ220803.20–322800.1	28/11/2020	1.0-m	4x4	30	203	1.692	No
MLTJ230345.82–141447.1	22/08/2020	1.0-m	8x8	30	514	4.283	No
MLTJ230816.36–042339.3	29/11/2020	1.0-m	4x4	30	360	3.000	Yes
MLTJ230816.36–042339.3	30/11/2020	1.0-m	4x4	30	325	2.708	Yes
MLTJ232129.59–602302.9	24/08/2020	1.0-m	8x8	30	361	3.008	No

3.2 Data Management

Due to the ever-increasing quantities of data being produced by all the photometric follow-up, data management became more and more important as the project progressed. After each night of observing, all relevant data was copied from the telescopes' data banks onto a local machine where it would be reduced. All data was also backed up onto a Google Drive hosted by the BlackGEM group as part of a data backup system for all transient projects related to MeerLICHT and BlackGEM. The data were organised into folders by year and then into sub-folders by day. For example, data taken on the 8 November 2020 would be in the directory "/2020/Data/1108/". Due to the observational constraints, we could only observe up to three targets each night we had observing time on either the 1.0-m or Lesedi telescopes.

3.3 Data Reduction & Analysis

A first attempt at reducing the data produced by the photometric follow-up was made using a pipeline designed to reduce SHOC data. However, this pipeline proved outdated and challenging to use. One of the

[9]This object is a RD+WD binary discovered by ZTF [53].

first failings was its dependency on IRAF packages being installed, which can be difficult to install and have running effectively on newer systems. The SHOC pipeline especially had troubles extracting lightcurves out of crowded fields and it did not have a functional method of producing differential lightcurves. Thus, we moved on to the adapTive Elliptical Aperture PHOTometry (TEA-Phot) pipeline [54].

3.3.1 TEA-Phot

TEA-Phot is a pipeline developed by Dominic Bowman (Instituut voor Sterrenkunde, KU Leuven, Belgium) and Daniel Holdsworth (Jeremiah Horrocks Institute, University of Central Lancashire, UK) which is optimised for extracting light-curves for ground-based photometry. It is exceptionally easy to use and is designed for high-cadence photometry performed by SHOC, however, it is easy enough to adapt for other similar instruments at different observatories. One of the reasons that TEA-Phot proved far more efficient to use was that it is entirely coded in Python with zero outside dependencies. At its base, TEA-Phot takes advantage of the powerful Source Extraction and Photometry (SEP) [55] library with the Astropy [47] and Matplotlib [56] packages providing the rest of the necessary tools. TEA-Phot can be run from the command line in the following manner:

```
python3 TEA-Phot.py SAAO SHOC SHD_20210128.0009.fits --image_dir Data/0128/ --bias
SHD_20210128.0001.fits --flat SHD_20210128.0003.fits --bias_dir Data/0128/ --flat_dir
Data/0128/ --object MLT_J0359-2312 --coord ‘03:59:04.9108 -23:12:25.1121’ --do_plot
True --source_sigma 5.0 --out_dir Lightcurves/MLT_J0359-2312/1/
```

In the example above the first three positional arguments after calling the TEA-Phot script are placeholders for observatory, instrument and filename respectively. The rest of the arguments are callable and changeable. The "`do_plot`" argument decides whether or not you want to produce the quick-look lightcurves which we use to test the success of the lightcurve extraction. The "`source_sigma`" argument sets the significance level for a brightness point to be classed as a source, i.e. a source which has an SNR of 5 or higher in the above example would be marked for extraction. There are further arguments one can use in the reduction process, however, they were not necessary for our purposes.

When running the pipeline as shown above, after creating a master bias and master flat and performing the necessary corrections to the science frames, a pop-up window will appear asking the user to choose first the target star and then a single comparison star as seen in Figure 22a. The next step will ask whether the user wants to use an annular or 'sky star' method to determine the sky background level. In most cases we used the annular method, however, on occasion when the field was particularly crowded, we selected a sky star in an empty patch of sky to avoid the light contamination in the sky background near to either the target or comparison stars. After choosing the background calculation method, a pop-up window with curves of growth for both the target and the comparison stars will be displayed. Using this window, we select an aperture size at which the curve becomes linear thereby ensuring that all the flux from the relevant star is used to determine instrumental magnitudes and produce lightcurves. As seeing degrades, this curve of growth has gentler slope until it becomes linear, however, we ensured that the same relative point on the curve was chosen for both the target and comparison star. An example of this curve of growth plot is shown in Figure 22b, in this instance the third point on each plot was chosen as the aperture area for both stars.

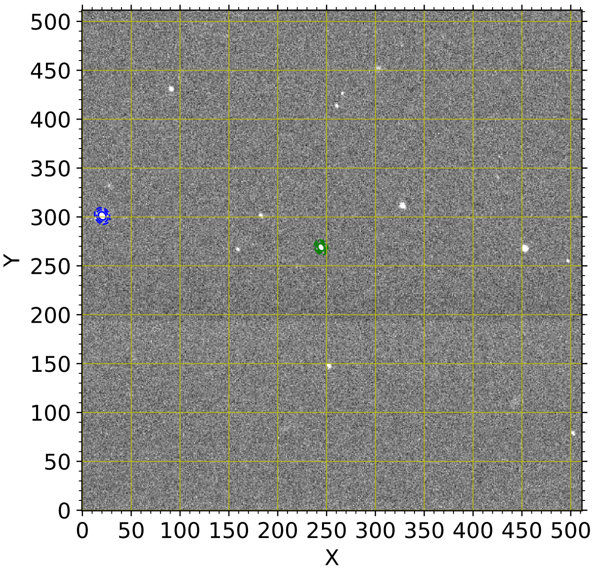

(a) The target selection window for MLTJ0359–2312, the target star is selected in green and the comparison in blue.

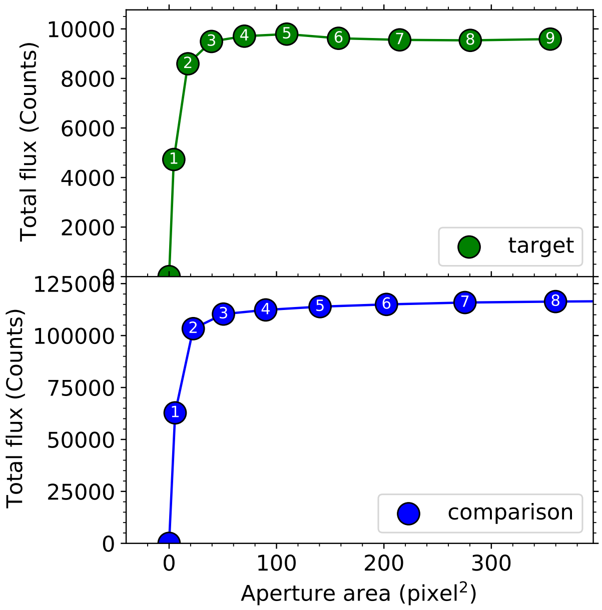

(b) The curve of growth produced by TEA-Phot.

Figure 22: TEA-Phot's lightcurve production process for MLTJ035904.91–231225.1 (MLTJ0359–2312).

After selecting the aperture sizes, TEA-Phot will then run through every frame in the corrected science fits cube and extract instrumental magnitudes for both the target and comparison stars. Occasionally, a frame would be ignored due either to multiple apertures being detected for either the target star or the comparison star, or due to no aperture being detected for the target or comparison stars. The former case occurs when there is another nearby star or a sudden spot of flux which has an aperture overlap with one of the selected stars. This can usually be avoiding by increasing the "`source_sigma`" value so that the impostor is not bright enough to be marked as a detection. A potential drawback of this strategy though would be if the target star dims too much due to possible variability, it might then be ignored as a significant detection. However, this was not a problem as none of the target stars in crowded fields observed dimmed severely enough to be ignored.

The latter case, when the target or comparison star is not detected, happens when the position and radius in which either is expected to be found has no detection. The two causes that we encountered were either when the telescope shifts suddenly and causes the frame to jump or when clouds intervened and prevented detection. In the case of the Lesedi telescope, a few of the observations were affected by a complete azimuthal rotation as a result of the cables needing to be unwrapped. This only affects a few frames and did not affect the observations in any significant way. The 1.0-m has a different issue when an observation crosses a line at around 0.5 hour angle (HA), the telescope shifts slightly and causes the image to jump around before settling back into position once again. However, this also only affects a few frames and did not prove to be an issue for the observations which had this shifting.

TEA-Phot pipeline concludes by producing a plot of the differential magnitude of the comparison star and the target star, and a .dat file containing the instrumental magnitudes for both stars, the differential magnitude, error estimates for all magnitudes, the time (in BJD) of the datapoint, and the target's airmass. An example differential lightcurve produced by TEA-Phot is shown in Figure 23a. The default for all the images produced is to be saved as .eps files, however, we edited the pipeline's code so that the images were saved as PDFs instead. We repeated this process for each target at least twice and, when possible, a third time in order to ensure that we had at least two or three comparison stars for each target. Each time we selected a comparison star that was brighter than the target star. Once we have two or three comparisons, depending on availability, for our target star we then use the data files produced by TEA-Phot to conduct further analysis of the lightcurves. Unfortunately, the TEA-Phot pipeline does not yet have the capability to perform multiple comparisons simultaneously, so this process can be become quite cumbersome.

3.3.2 Lightcurve Analysis

In order to further investigate the lightcurves of our targets produced by TEA-Phot, using Python, we first needed to combine all the comparisons for each target into one weighted average lightcurve. To ensure that the datapoints matched across the comparisons, we first applied a mask to the individual datasets for each comparison based on the timestamps provided in BJD format. The Barycentric Dynamical Time (TDB) is a uniform time frame that takes into account relativity, the fact that a moving clock measures time at a different speed. TDB uses the Barycentric Julian Date (BJD), which is a date reference point corrected to the centre of mass of the Solar System. By masking for time frames, we ensured that, in case one of the comparisons did not have a datapoint for a specific timestamp, due to one of the possible errors mentioned earlier, the timestamps across all the comparisons would match and any that did not would be ignored. The first comparison would be masked by the second, and third if available, the second would be masked by the first, and third if available, and the third would be masked by the first and second.

Once we had ensured that the datapoints for each comparison matched, we could begin combining them into a single consolidated differential lightcurve. To do so, we weighted the differential magnitudes for each datapoint by the instrumental magnitude of the comparison star. Thus, the brighter comparison stars would have a stronger contribution to the weighted average differential lightcurve than the fainter comparison stars. Bearing in mind that all the instrumental magnitudes produced were negative, the larger negative number implies a brighter object. Thus, we use the absolute values of the comparison stars' magnitudes to weight the differential values in the following formulae. Where only two comparison stars were available this was a relatively simple calculation:

$$\overline{\Delta \mathrm{m}} = \frac{\Delta \mathrm{m}_1 \mathrm{m}_{1c} + \Delta \mathrm{m}_2 \mathrm{m}_{2c}}{\mathrm{m}_{1c} + \mathrm{m}_{2c}}$$

Where m_{1c} and m_{2c} are the absolute values of the comparison stars' instrumental magnitudes, and $\Delta\mathrm{m}_1$ and $\Delta\mathrm{m}_2$ are the differential magnitudes for each comparison, which are calculated via $\Delta\mathrm{m}_i = \mathrm{m}_{target} - \mathrm{m}_{ic}$. In the case of a third comparison being available, there is a third value to add to both to the denominator and numerator:

$$\overline{\Delta \mathrm{m}} = \frac{\Delta \mathrm{m}_1 \mathrm{m}_{1c} + \Delta \mathrm{m}_2 \mathrm{m}_{2c} + \Delta \mathrm{m}_3 \mathrm{m}_{3c}}{\mathrm{m}_{1c} + \mathrm{m}_{2c} + \mathrm{m}_{3c}}$$

In order to properly calculate the errors of this new weighted average, we made use of the general rule for error propagation:

$$\delta(\overline{\Delta \mathrm{m}}) = \left| \frac{\mathrm{d}\overline{\Delta \mathrm{m}}}{\mathrm{d}x} \right| \delta x$$

Where δ denotes the error of the variable or value. This type of error propagation will only work, however, when the individual δm_i's are small ($\lesssim 0.1$ mag). When the error is above this, the non-linear nature of the magnitude scale begins to affect the calculations too strongly and all these calculations should rather be done in flux values first, then converted back into magnitudes. In the case of only two comparisons being available, this produced the following error formula:

$$
\begin{aligned}
\delta(\overline{\Delta \mathrm{m}}) =& \delta(\Delta \mathrm{m}_1)\left|\frac{\mathrm{m}_{1c}}{\mathrm{m}_{1c}+\mathrm{m}_{2c}}\right| + \delta(\Delta \mathrm{m}_2)\left|\frac{\mathrm{m}_{2c}}{\mathrm{m}_{1c}+\mathrm{m}_{2c}}\right| \\
&+ \delta(\mathrm{m}_{1c})\left|\frac{\Delta \mathrm{m}_1\mathrm{m}_{2c}-\Delta \mathrm{m}_2\mathrm{m}_{2c}}{(\mathrm{m}_{1c}+\mathrm{m}_{2c})^2}\right| + \delta(\mathrm{m}_{2c})\left|\frac{\Delta \mathrm{m}_2\mathrm{m}_{1c}-\Delta \mathrm{m}_1\mathrm{m}_{1c}}{(\mathrm{m}_{1c}+\mathrm{m}_{2c})^2}\right|
\end{aligned}
$$

This becomes a little more complex when we add a third comparison:

$$
\begin{aligned}
\delta(\overline{\Delta \mathrm{m}}) =& \delta(\Delta \mathrm{m}_1)\left|\frac{\mathrm{m}_{1c}}{\mathrm{m}_{1c}+\mathrm{m}_{2c}+\mathrm{m}_{3c}}\right| + \delta(\Delta \mathrm{m}_2)\left|\frac{\mathrm{m}_{2c}}{\mathrm{m}_{1c}+\mathrm{m}_{2c}+\mathrm{m}_{3c}}\right| + \delta(\Delta \mathrm{m}_3)\left|\frac{\mathrm{m}_{3c}}{\mathrm{m}_{1c}+\mathrm{m}_{2c}+\mathrm{m}_{3c}}\right| \\
&+ \delta(\mathrm{m}_{1c})\left|\frac{\Delta \mathrm{m}_1\mathrm{m}_{3c}+\Delta \mathrm{m}_1\mathrm{m}_{2c}-\Delta \mathrm{m}_2\mathrm{m}_{2c}-\Delta \mathrm{m}_3\mathrm{m}_{3c}}{(\mathrm{m}_{1c}+\mathrm{m}_{2c}+\mathrm{m}_{3c})^2}\right| \\
&+ \delta(\mathrm{m}_{2c})\left|\frac{\Delta \mathrm{m}_2\mathrm{m}_{1c}+\Delta \mathrm{m}_2\mathrm{m}_{3c}-\Delta \mathrm{m}_1\mathrm{m}_{1c}-\Delta \mathrm{m}_3\mathrm{m}_{3c}}{(\mathrm{m}_{1c}+\mathrm{m}_{2c}+\mathrm{m}_{3c})^2}\right| \\
&+ \delta(\mathrm{m}_{3c})\left|\frac{\Delta \mathrm{m}_3\mathrm{m}_{1c}+\Delta \mathrm{m}_3\mathrm{m}_{2c}-\Delta \mathrm{m}_1\mathrm{m}_{1c}-\Delta \mathrm{m}_2\mathrm{m}_{2c}}{(\mathrm{m}_{1c}+\mathrm{m}_{2c}+\mathrm{m}_{3c})^2}\right|
\end{aligned}
$$

Using the above equations, we calculated the weighted average differential lightcurves and errors for each observed target. An example of such a lightcurve can be seen in Figure 23b.

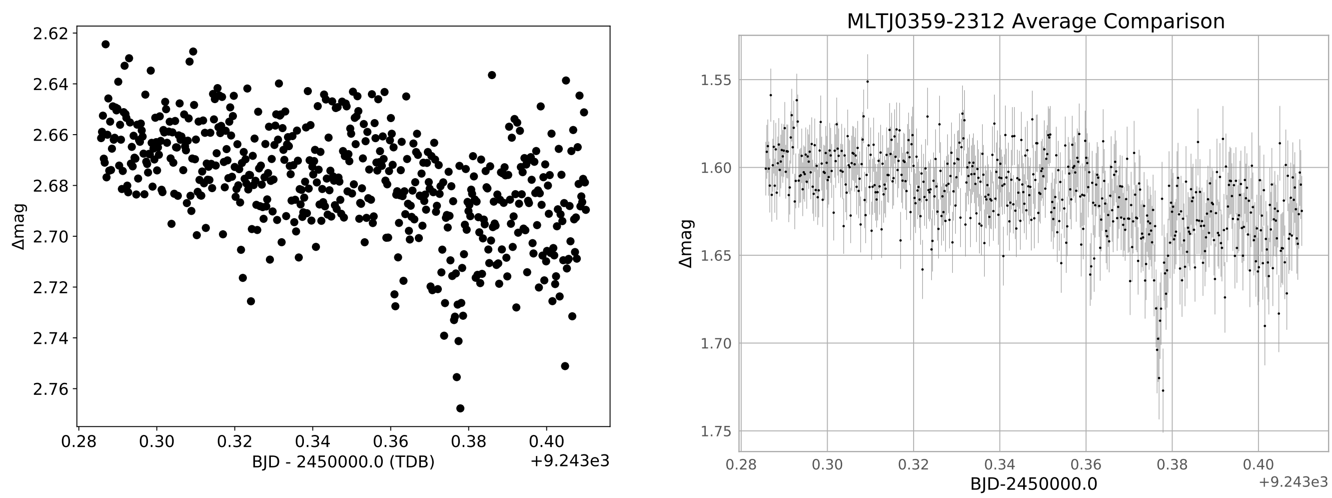

(a) Standard TEA-Phot produced differential lightcurve for MLTJ0359–2312.

(b) A weighted average differential lightcurve for MLTJ0359–2312.

Figure 23: Comparing the standard TEA-Phot produced differential lightcurve with the computed weighted average differential lightcurve for MLTJ0359–2312.

As a first step to analysing these new weighted average differential lightcurves for each target, we plotted a histogram of the difference between each individual datapoint and the median differential magnitude value. With this histogram we can check the spread of the values, if there is minimal spread then this histogram will be similar to a tight Gaussian in shape. However, if there is large spread, indicative of possible variability if the lightcurve is variable in shape, then the histogram will have a flatter and wider Gaussian-like shape. An example of such a histogram can be seen in Figure 24a. We then attempted to fit a Gaussian to the histogram using Scipy's [49] in-built `norm.fit` function in the `scipy.stats` module. This `norm.fit` function fits a Gaussian to Gaussian-shaped data and output its estimates for the mean (μ) and width (σ) of the Gaussian. With this width in hand, we calculated difference between the error sizes of the differential lightcurves and the widths of the fitted Gaussians for each target. This difference provides us with a further indication of whether or not the target is likely to be variable. If the width of the Gaussian is consistently and significantly larger than the error sizes then the target is far more likely to be variable. However, if the error sizes are equivalent to or larger than the width than the target is not likely to be variable. An example plot of this error comparison is shown in Figure 24b.

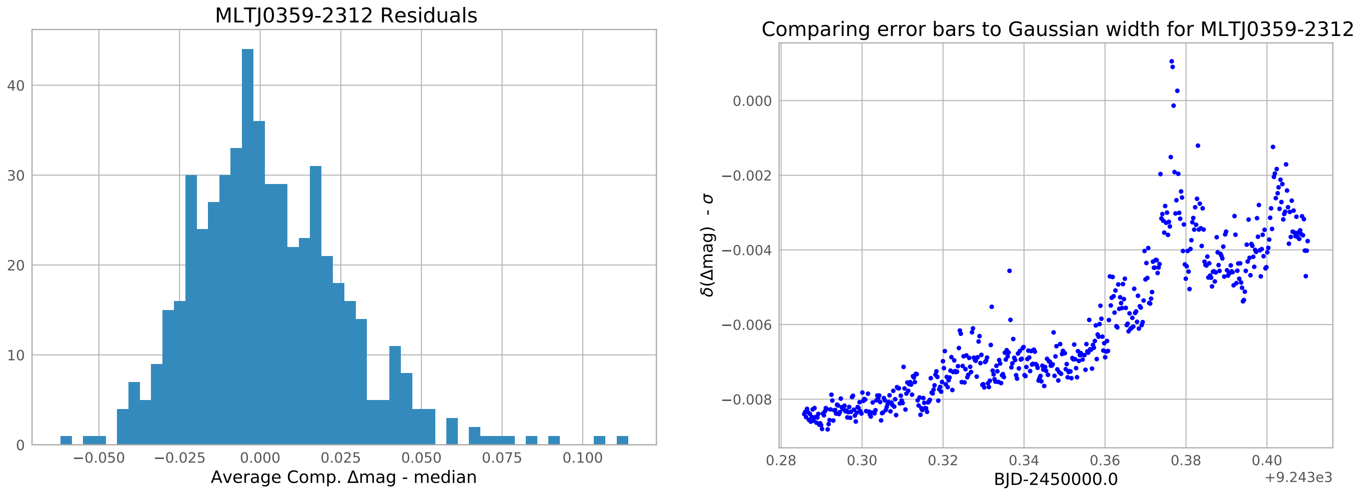

(a) Histogram of $\overline{\Delta m}-$median for MLTJ0359–2312, showing a strong Gaussian shape.

(b) Comparing error sizes to Gaussian width for MLTJ0359–2312.

Figure 24: Histogram and error comparisons for MLTJ0359–2312. From the histogram in (a), we see a strong and narrow Gaussian shape, which is indicative of non-variability in the lightcurve. This is matched by the error sizes being consistently similar to the width of the Gaussian in (b). Throughout the course of the observation, the error sizes actually become larger than the width. This increasing error size is likely due to an increase in atmospheric seeing as the night progresses.

3.3.3 VARTOOLS Fourier Analysis

To search for periodic signals in our data, the VARTOOLS Light Curve Analysis Program [57] was used to process and analyse our observed lightcurves. VARTOOLS has a wide variety of tasks and operations which can be used to analyse multiple aspects of time series data, however, only the LS and Killharm routines were used to analyse our lightcurves. The LS routine calculates a Generalised Lomb-Scargle periodogram for the provided lightcurve [58], looking for periodic sinusoidal signals. This periodogram is calculated over a provided range of frequencies in the manner described below. VARTOOLS's LS routine uses a modified version of the fasper algorithm described in Press et al. [59]. VARTOOLS can be run through the command line and the usage of the LS routine is as follows:

```
vartools -LS minp maxp subsample Npeaks operiodogram [outdir]
```

Where the minp is the minimum period from which the maximum frequency is calculated of 1/minp. The minp value is given in cycles per day, for example, a lightcurve with 30s exposures would have a minp value of 0.00069444 which corresponds to a maximum frequency of $1/0.00069444 = 1440$ cycles per day. This corresponds to a period of 60s which is a sampling rate of 2×30s. We set the maxp to 1 cycle per day which corresponds to 24 hours and the fmin is calculated from the maxp with fmin = 1/maxp. The subsample value determines the frequency step-size, Δf, by dividing the subsample value by the time-span of the observation. The majority of our objects were observed over 3 hours, and we used a subsample value of 0.02, giving us a step-size of 0.02/(3/24) as the time-span of the observation is calculated as a fraction of a day. The Npeaks keyword denotes the number of strong peaks that the LS periodogram must find in the data. For each peak, the program will output the period found, the logarithm of the false-alarm probability, and the spectroscopic signal-to-noise (SNR) ratio for that peak. The operiodogram (or "output periodogram") keyword is a value of either 0 or 1, 0 if one does not wish to create a separate output file of each lightcurve and 1 if one desires an output periodogram file for each lightcurve. If the operiodogram value is 1, then the outdir keyword is required to indicate where the output periodogram file must be saved. This output file contains three columns, the first is the frequency given in cycles per input light curve time unit (in our case, a day), the second is the non-normalised P(omega) calculated according to equation 5 in Zechmeister & Kürster (2009) [58], and the final column is the logarithm of the false alarm probability.

The other task that was used with VARTOOLS, was the Killharm routine which whitens light curves against one or more periods by removing some of the harmonic effects created by periodic signals. Thus we remove the harmonic signals in the light curve itself and output the whitened lightcurve to a file with the added suffix ".killharm.model". This whitened lightcurve shows the sinusoidal variation of the strongest apparent period, essentially producing a perfect sinusoid. Finally, we also used the readformat keyword when running VARTOOLS to indicate the format of the input lightcurve. The readformat keyword takes four separate numbers as an input, firstly the number of lines to skip at the beginning of the file (i.e. the header line), and the next three numbers denoted the column numbers for time, magnitude and sigma, in that order. All together, using the VARTOOLS program to produce a periodogram would look like this:

```
vartools -i MLT_J0359-2312/MLTJ0359-2312_lightcurves.ascii
-readformat 1 1 2 3 -LS 0.00069444 1. 0.02 1 1 MLT_J0359-2312/outdir
-Killharm ls 0 0 1 MLT_J0359-2312/outdir -oneline -header
```

This would produce two outputs, the whitened lightcurve and the periodogram file, in the sub-directory "outdir" for each target. In our plots of the periodograms we normalise the power by dividing by the max power of the frequency periodogram and we convert the frequency unit from cycles per day to mHz by dividing the input frequency by 86400 (seconds in a day) and multiplying by 1000. An example of the plots that one can produce with the outputs of running VARTOOLS is shown in Figure 25.

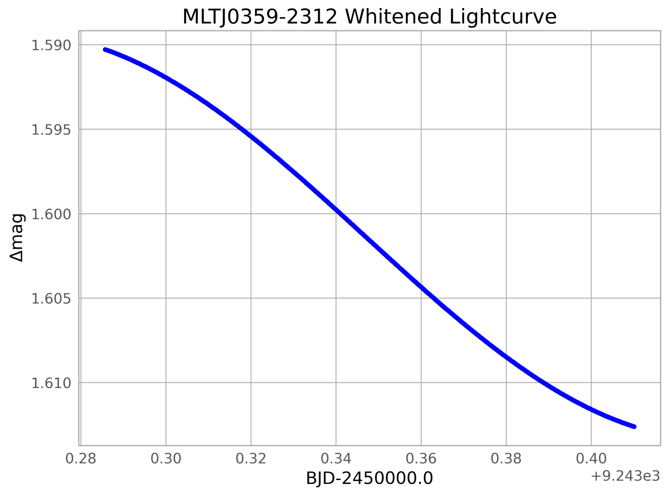

(a) Harmonically cleaned lightcurve for MLTJ0359–2312 showing a general downward trend in magnitude.

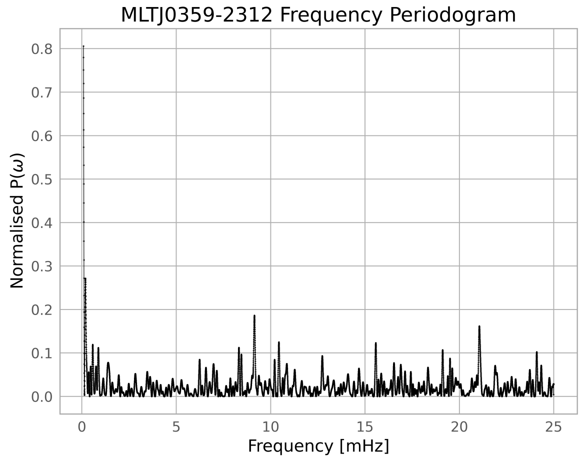

(b) Power spectrum produced by Fourier analysis with VARTOOLS for MLTJ0359–2312.

Figure 25: An example of the input lightcurve for one of our targets, MLTJ035904.91–231225.1 (MLTJ0359–2312), can be seen in Figure 23b. Here we see the results of running the VARTOOLS routines on the lightcurve seen in Figure 23b: the output of the harmonically whitened lightcurve for MLTJ0359–2312 produced by the Killharm routine in VARTOOLS is shown in (a), and the frequency periodogram produced with the LS routine is visible in (b). There are no clear, strong peaks in (b) aside from the alias at the frequencies close to 0. This is the alias caused by the maximum period or minimum frequency of 1 day, as well as the signal alias caused by the length of the observation, 3 hours.

For those targets which had apparent spikes at certain frequencies, a Gaussian fitting routine was run on the frequency periodogram in order to measure the frequency with an uncertainty. This frequency can then be converted into a period with a simple equation, $p = (1/(f/1000))/60 = \frac{60}{f/1000} = \frac{60000}{f}$, where f is the frequency in mHz and p is the period in minutes. For convenience, the plots shown in the Interesting results section have been cropped down to a frequency range showing the strongest peaks.

3.4 Interesting results

3.4.1 MLTJ053450.55–580140.6: Known CV TW Pic

MLTJ053450.55–580140.6 (MLTJ0534–5801) was observed on 28/01/2021 with the Lesedi telescope over a three hour exposure with a cadence of 20 seconds, this gives us 540 frames in the fits cube. MLTJ0534–5801 is actually a known Cataclysmic Variable Star, TW Pic [60].

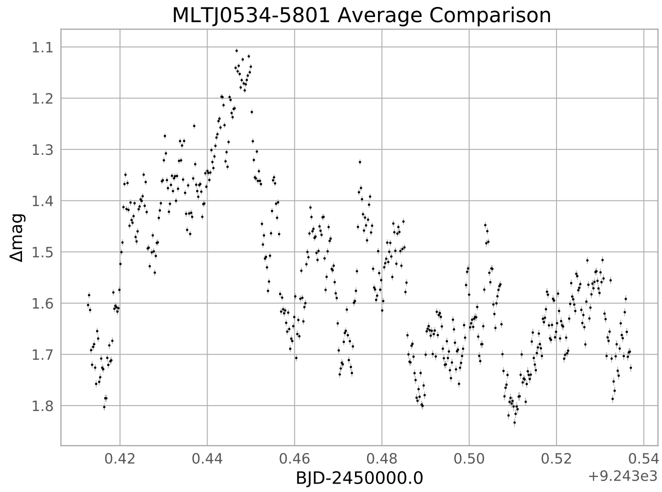

(a) Weighted average differential lightcurve for MLTJ0534–5801 from 2 available comparison stars.

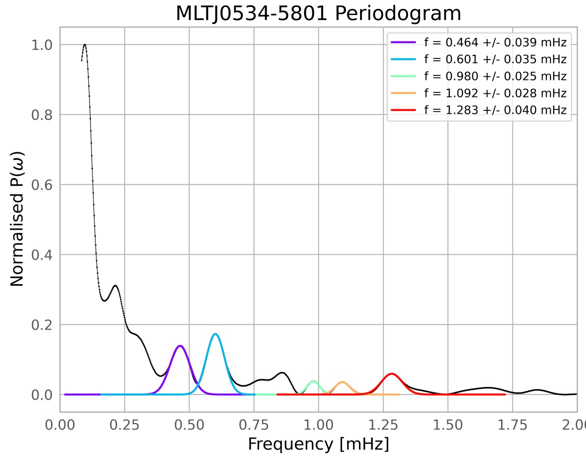

(b) Periodogram produced by Lomb-Scargle analysis for MLTJ0534–5801.

Figure 26: Differential lightcurve and Fourier power spectrum for MLTJ0534–5801.

The lightcurve in Figure 26a shows clear short period variability at around 25 minutes, as well as a longer term variability which we cannot constrain with this singular three hour observation. The periodogram in Figure 26b shows some notable peaks at 0.464 mHz, 0.601 mHz, 0.980 mHz, 1.092 mHz, and at 1.283 mHz. These correspond to periods of 35.90, 27.72, 17.00, 15.26, and 12.99 minutes respectively. We need more data to say with precision which of these are genuine periods and which are just aliases. It is likely that the 27.72 minute period is the general short variability which we can see in the lightcurve. It is also the strongest of the selected peaks with an amplitude of roughly 0.17.

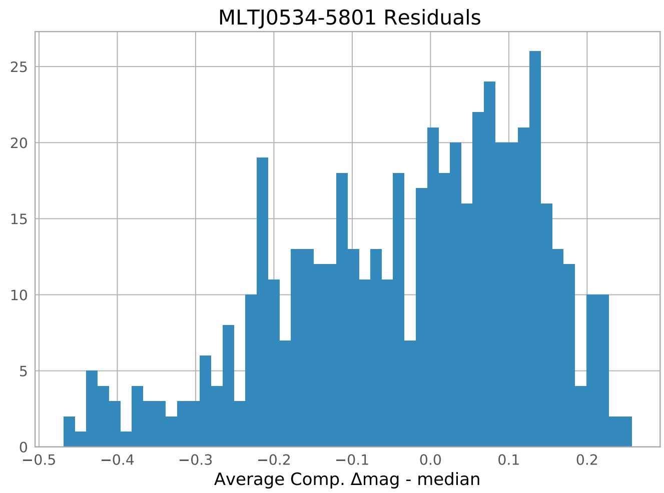

(a) Histogram of $\Delta m - \text{median}$ for MLTJ0534–5801, showing a large spread and roughly Gaussian shape.

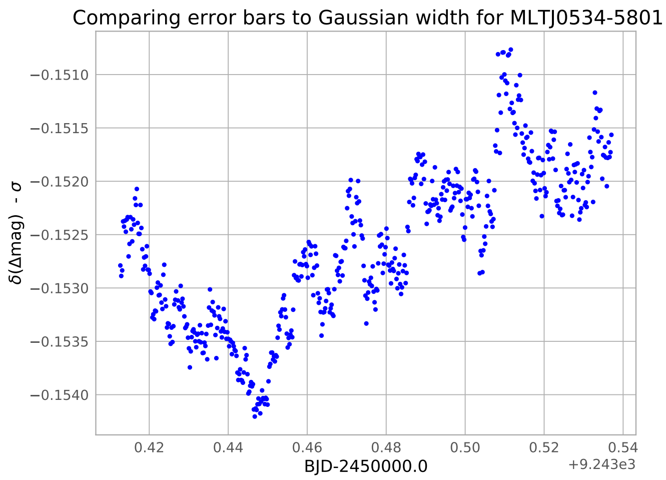

(b) Comparing error sizes to Gaussian width for MLTJ0534–5801.

Figure 27: Histogram and error comparison plot for MLTJ0534–5801.

From the histogram in Figure 27a we see a large spread in values to its roughly Gaussian shape. This is indicative of variability. Correspondingly, the error comparison plot in Figure 27b shows the error sizes being consistently and only slightly less than the width of the rough Gaussian fit to the histogram.

3.4.2 MLTJ071354.61–465306.8

MLTJ071354.61–465306.8 (MLTJ0713–4653) was observed on 06/02/2021 with the Lesedi telescope over a two and a half hour exposure with a cadence of 20 seconds, resulting in a fits cube with 450 frames. It is a relatively unknown 17th magnitude star with a parallax of 0.531 mas, resulting in a absolute magnitude of just fainter than 5 in the g band. This puts it right on the border of our selection box.

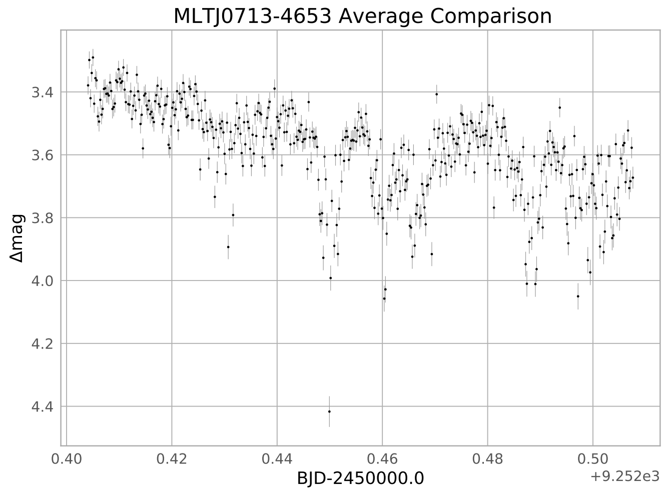

(a) Weighted average differential lightcurve for MLTJ0713–4653 from 3 available comparison stars.

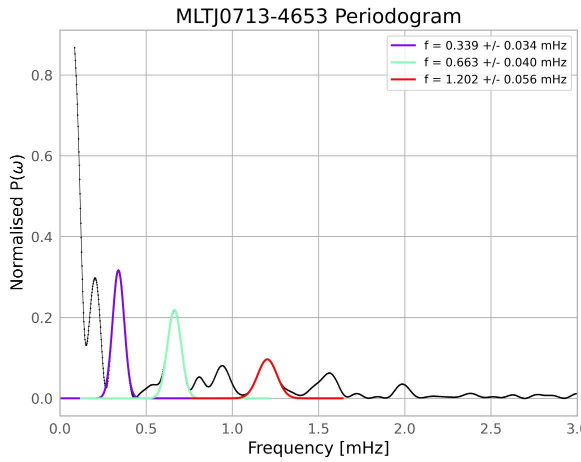

(b) Periodogram produced by Lomb-Scargle analysis for MLTJ0713–4653.

Figure 28: The differential lightcurve and power spectrum for MLTJ0713–4653.

In Figure 28a, the lightcurve appears noisy but may hint at a semi-regular dip. This is either the result of seeing fluctuations, variable changes in weather, or intrinsic inconstant variability. In Figure 28b, we see a few strong peaks at 0.339 mHz, 0.663 mHz, and at 1.202 mHz. These correspond to periods of 49.17 minutes, 25.14 minutes, and 13.86 minutes, respectively.

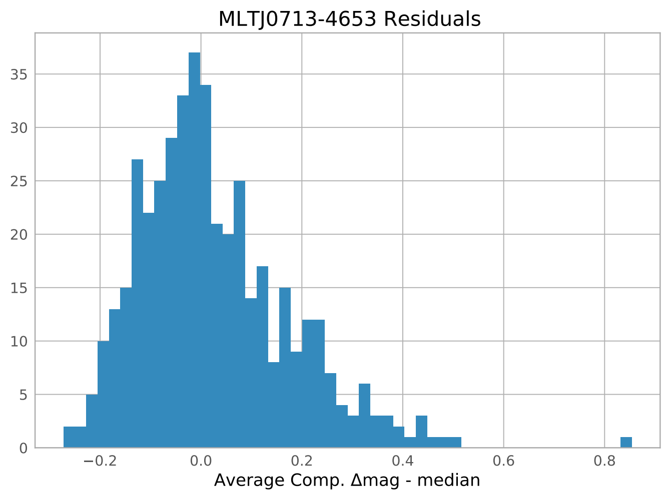

(a) Histogram of Δm$-$median for MLTJ0713–4653, showing a narrower structure.

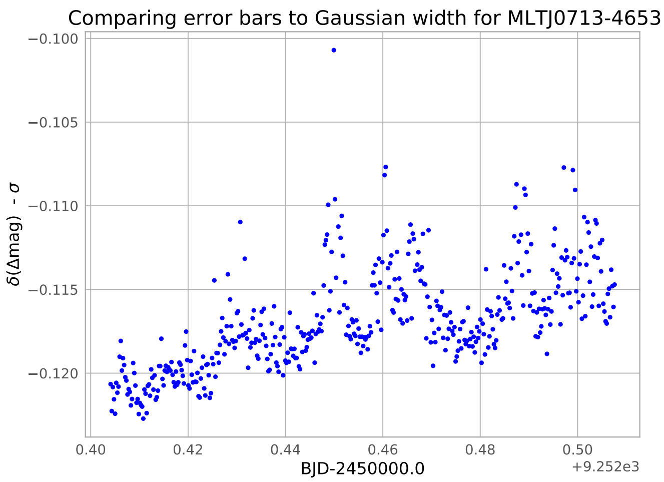

(b) Comparing error sizes to Gaussian width for MLTJ0713–4653.

Figure 29: A histogram showing the residuals and a plot of the error comparison for MLTJ0713–4653.

In Figure 29a, we see the histogram of the residuals, which shows a narrower shape then what we expect for variable lightcurves. The error plot in Figure 29b further indicates that there is variability in the lightcurve. This is indicated by the Gaussian width being consistently of a similar value to the error bars.

3.4.3 MLTJ080401.92–211831.9

MLTJ080401.92–211831.9 (MLTJ0804–2118) was observed on three separate nights in April 2021. For almost three hours it was observed on 01/04/2021 at 30s cadence, then again for three hours at 30s on 05/04/2021 and finally on 06/04/2021 for three hours at a 30s cadence. All the observations were take on the 1.0m telescope with a 4x4 binning. After the first night's data was analysed it became evident there might be minor variability in the star and thus it was observed on two more nights of that observing week. This star is known only by its GAIA classification on SIMBAD. It has a g-band magnitude of 17.141 and a parallax of 1.798 mas. This target actually comes from our selection of $ugrq$ candidates instead of the full $ugriq$ candidates as at the time the selection process was run, it did not have an observation in the i band.

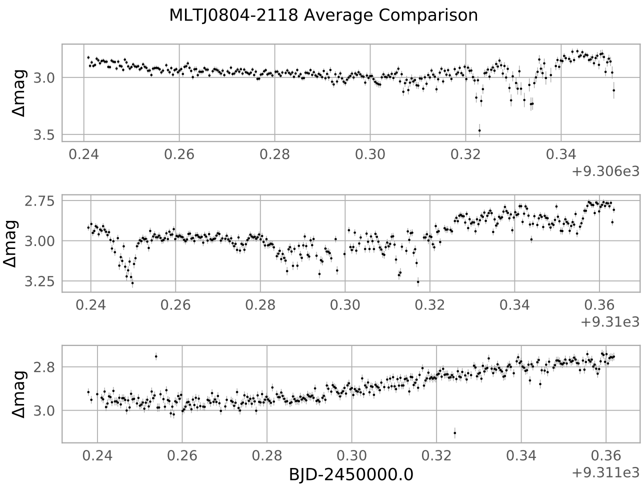

(a) Weighted average differential lightcurve for MLTJ0804–2118 across three nights.

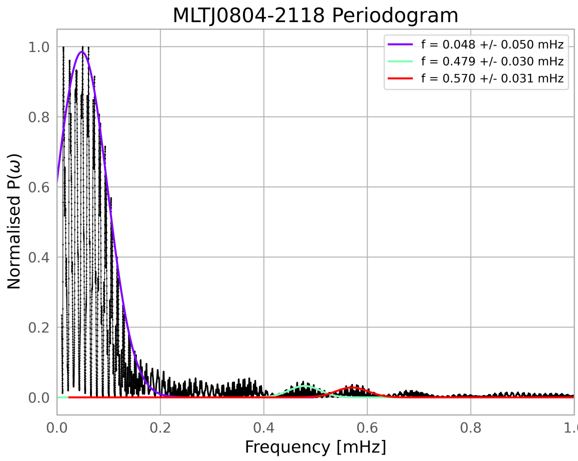

(b) Periodogram produced by Lomb-Scargle analysis for MLTJ0804–2118.

Figure 30: Lightcurve for MLTJ0804–2118 across the three nights it was observed in (a) and the resulting periodogram produced by VARTOOLS of those three nights in (b).

While there does not appear to be very prominent short term variability in Figure 30a, throughout the course of a single three hour exposure there is a more gradual change in magnitude. Upon closer inspection of each individual night we see minor fluctuations in each night which may account for the small peaks in the periodogram at 0.479 mHz and 0.570 mHz seen in Figure 30b. These correspond to periods of 34.829 minutes and 29.229 minutes respectively. However, given their very small amplitudes we can say nothing definitive about whether these periods represent some intrinsic variability. There is also a stronger peak at 0.048 mHz (346.88 minutes), but the uncertainty on this is larger than the actual measurement. We would need more observations at a more even sampling in order to verify the veracity of this spike.

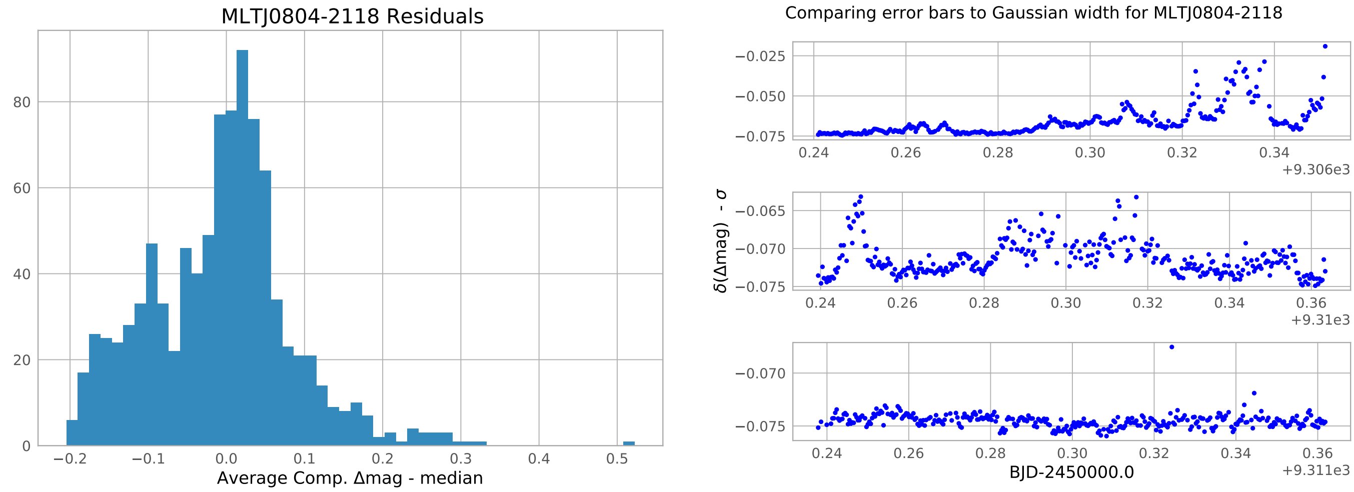

(a) Histogram of Δm$-$median for MLTJ0804–2118, showing a relatively large spread.

(b) Comparing error sizes to Gaussian width for MLTJ0804–2118.

Figure 31: Plots showing the histogram of residuals and the error size comparison for MLTJ0804–2118.

The histogram in Figure 31a shows a relatively large spread and an uneven shape around the median lightcurve value. This is mildly indicative of low-level variability. This low amplitude variability is further evidenced by the comparison plot of the error sizes to the Gaussian width of the histogram as seen in Figure 31b. The error sizes are consistently similar in value to the Gaussian width, with the largest deviation being just over 0.075.

3.4.4 MLTJ121558.78–491453.4

MLTJ121558.78–491453.4 (MLTJ1215–4914) was observed twice, first on 04/04/2021 and then two nights later on 06/04/2021, with the 1.0-m telescope. On the first night MLTJ1215–4914 was observed for just over four hours, and four and a half hours on its second night. MLTJ1215–4914 is only known by its GAIA designation on SIMBAD with a parallax of 3.263 mas and it has a MeerLICHT g-band magnitude of 16.334. MLTJ1215–4914 came from our secondary batch of primary targets, those with observations only in $ugrq$ and not in the i band.

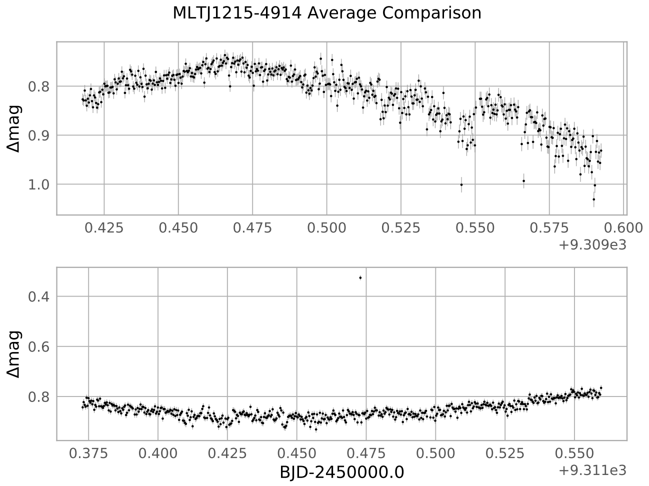

(a) Weighted average differential lightcurve for MLTJ1215–4914 across two nights.

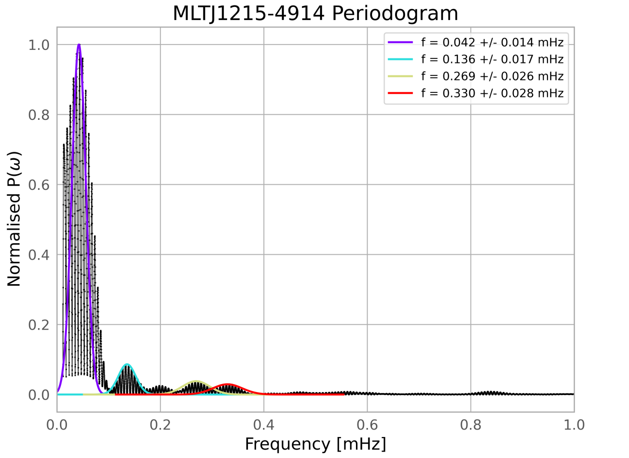

(b) Periodogram produced by Lomb-Scargle analysis for MLTJ1215–4914.

Figure 32: Lightcurve and periodogram for MLTJ1215–4914.

We can see evidence of a changing magnitude over the course of a single observation on both the nights that MLTJ1215–4914 was observed in Figure 32a. Although the variation is low in amplitude, only changing by just over 0.2 magnitudes, it is present in both nights. We can see four clear peaks in the periodogram, the strongest being at 0.042 mHz, followed by much smaller amplitude peaks at 0.136 mHz, 0.269 mHz, and 0.330 mHz. These correspond to periods of 393.212 minutes, 122.989 minutes, 61.944 minutes, and 50.548 minutes respectively.

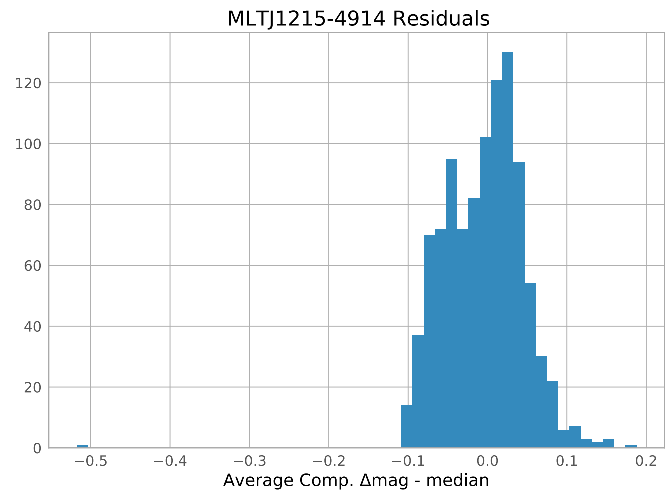

(a) Histogram of $\Delta m -$median for MLTJ1215–4914, showing a relatively narrow spread.

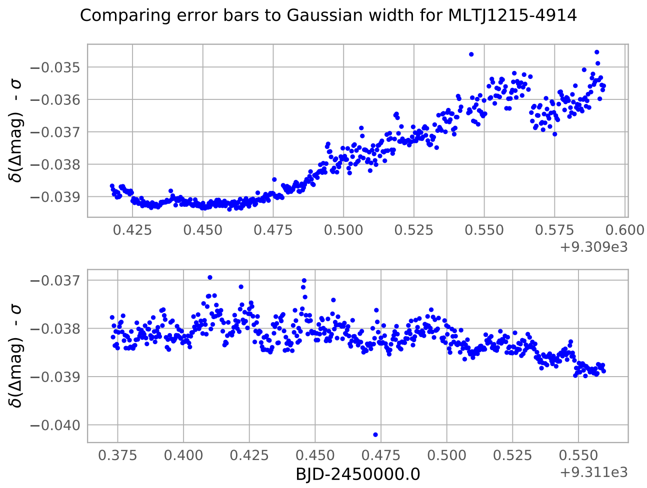

(b) Comparing error sizes to Gaussian width for MLTJ1215–4914.

Figure 33: Histogram of residuals and error comparison for MLTJ1215–4914.

In the histogram in Figure 33a, see a narrow spread around the median, implying that if there is variability, it is low in amplitude. The size of the error bars of the magnitude measurements are also very similar to, although still less than, the width of the Gaussian fitted to the histogram, as seen in Figure 33b. This further confirms the possibility of low-level variability.

3.4.5 MLTJ1446–3056: surprise Delta Scuti

When reducing the data for MLTJ144641.89–305708.2, we noticed that the lightcurves produced by TEA-Phot for the three comparisons did not all have the same structure. The first comparison showed strong variability on a timescale just over an hour, whereas the second and third had no evidence of variability. Thus, we re-reduced the data, this time making the original first comparison star the target star. This star is MLTJ144640.60–305645.9 (MLTJ1446–3056) and is unknown on SIMBAD. The lightcurve has a sawtooth-like shape and shows a period of just over an hour. This evidence is indicative of MLTJ1446–3056 being a possible Delta Scuti pulsating star.

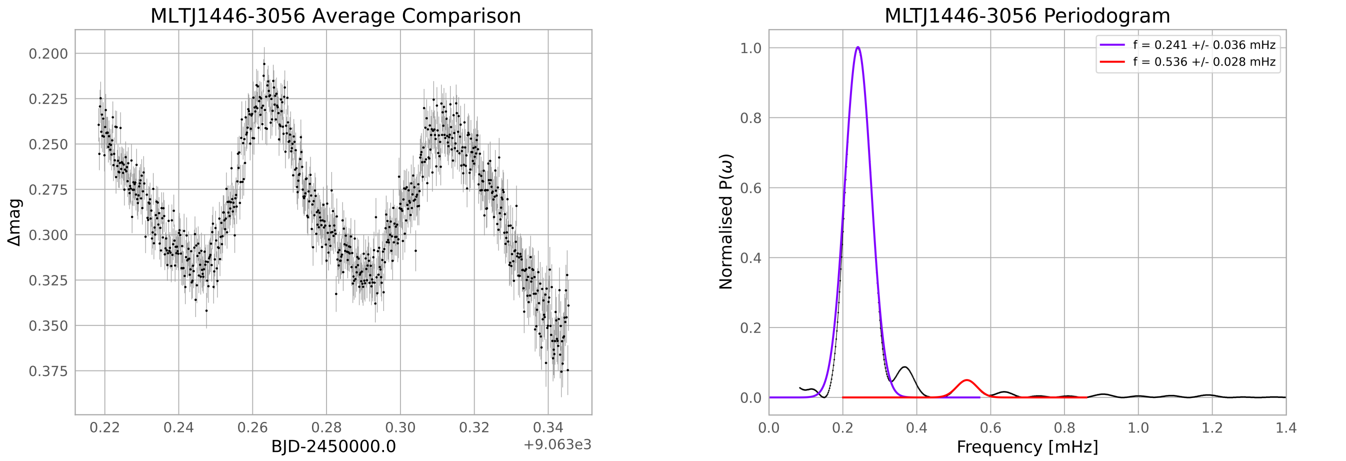

(a) Weighted average differential lightcurve for MLTJ1446–3056 from 3 available comparison stars.

(b) Frequency periodogram produced by VARTOOLS for MLTJ1446–3056.

Figure 34: Differential lightcurve and Fourier power spectrum for MLTJ1446–3056.

The lightcurve in Figure 34a shows clear variability with a period of just over an hour with a sawtooth-like shape. The periodogram for MLTJ1446–3056 in Figure 34b shows a strong spike at a frequency of 0.241 mHz. This corresponds to a period of 69.176 minutes which corresponds to the shape we see in the lightcurve.

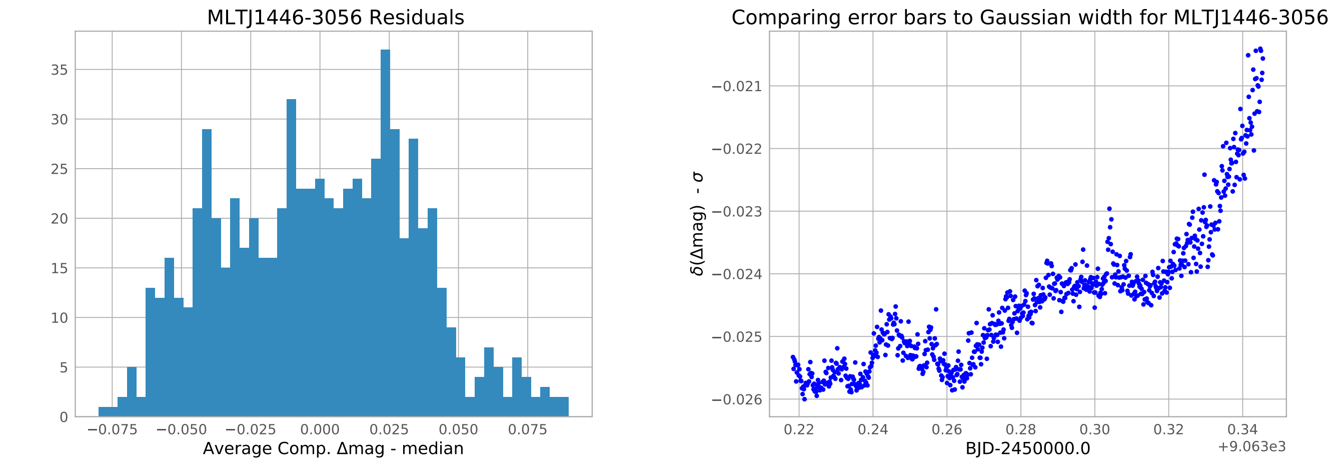

(a) Histogram of Δm$-$median for MLTJ1446–3056, showing a wide and scattered shape.

(b) Comparing error sizes to Gaussian width for MLTJ1446–3056.

Figure 35: Histogram and error comparison plot for MLTJ1446–3056.

The wide and spread-out shape seen in the histogram in Figure 35a is further confirmation of the apparent variability in MLTJ1446–3056. In Figure 35b, the error sizes are consistently smaller than, but still relatively close to, the width of the Gaussian fit implying that the variability is legitimate. The apparent increase of the error size throughout the observation is likely due to an increase in seeing as the night progressed.

3.4.6 MLTJ203654.63–432231.6: Known CV CM Mic

MLTJ203654.63–432231.6 (MLTJ2036–4322) is a known CV, CM Mic. It was selected as one of our candidates through the full $ugriq$ colour selection criteria. MLTJ2036–4322 has a parallax of 1.251 mas and an apparent magnitude in the g-band of 15.431 from the MeerLICHT observation. In Chen et al. [61] they discuss the star's classification as a CV due to its spectral shape and lightcurve properties. We observed it for four nights in a row in June of 2021, starting on the 3rd. The observations were conducted with Lesedi with a cadence of 20 seconds, each exposure lasting between 2.4 and 4.5 hours. The lightcurves show clear evidence of variability.

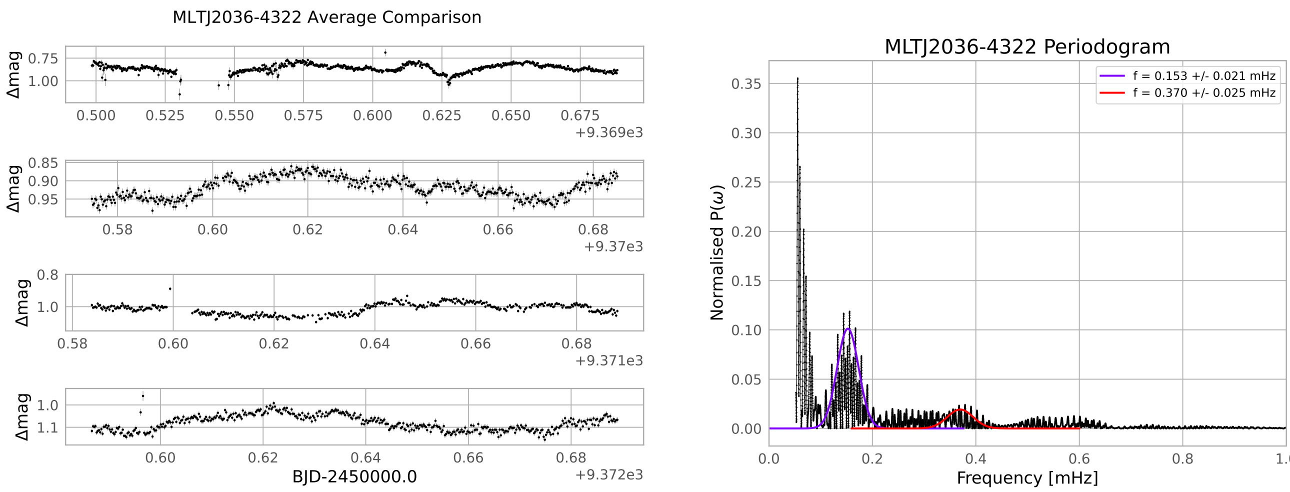

(a) Weighted average differential lightcurve for MLTJ2036–4322 from four consecutive nights.

(b) Frequency periodogram produced by VARTOOLS for MLTJ2036–4322.

Figure 36: Lightcurve and peridogram for MLTJ2036–4322.

The lightcurve in Figure 36a shows that see each night has a clear variability, as well as a general downward trend in brightness across the four nights. This variability on each night is around a 2-hour cycle which would agree with the hump period detected by Chen et al. [61]. The periodogram shown in Figure 36b provides further evidence of this as there is a clear spike at a frequency of 0.153 mHz which corresponds to a period of 109.194 minutes.

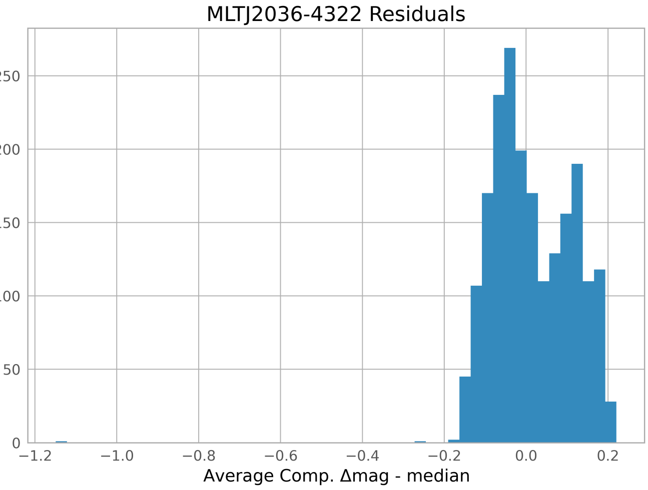

(a) Histogram of Δm$-$median for MLTJ2036–4322.

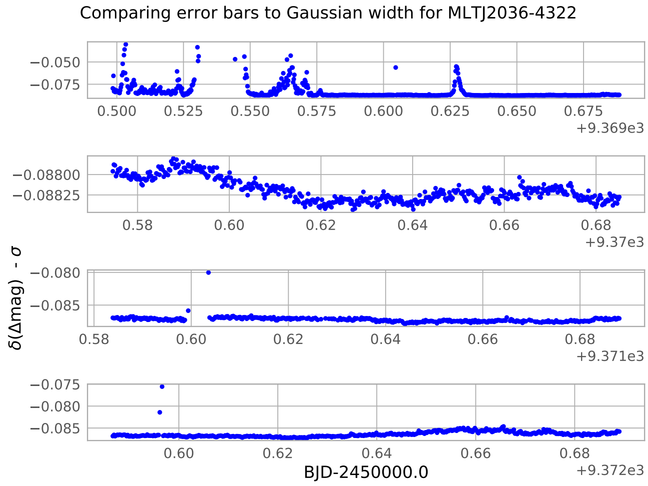

(b) Comparing error sizes to Gaussian width for MLTJ2036–4322.

Figure 37: Histogram and error comparison for MLTJ2036–4322.

The histogram of residuals for MLTJ2036–4322 shows little variation away from the median value, indicating that the variability detected is low in amplitude. This is further evidenced by the minor differences between the error sizes and the Gaussian width as seen in Figure 37b.

3.4.7 MLTJ230816.36–042339.3

On the 29th of November 2020, MLTJ230816.36–042339.3 (MLTJ2308–0423) was first observed with the 1.0-m telescope and a quick inspection of the lightcurve showed interesting variability and thus we observed it again the following night. The lightcurves from both nights show both short-term variability on a timescale of around 30 minutes as well as longer-term fluctuation in brightness over the three hour observations. The lightcurves' shape and structure bear similarities to that of the magnetic cataclysmic variable V1223 Sgr as seen on page 145 of Hellier [33]. In conjunction with the spectra taken for MLTJ2308–0423, we later discuss the possibility of MLTJ2308–0423's status as a potential magnetic CV.

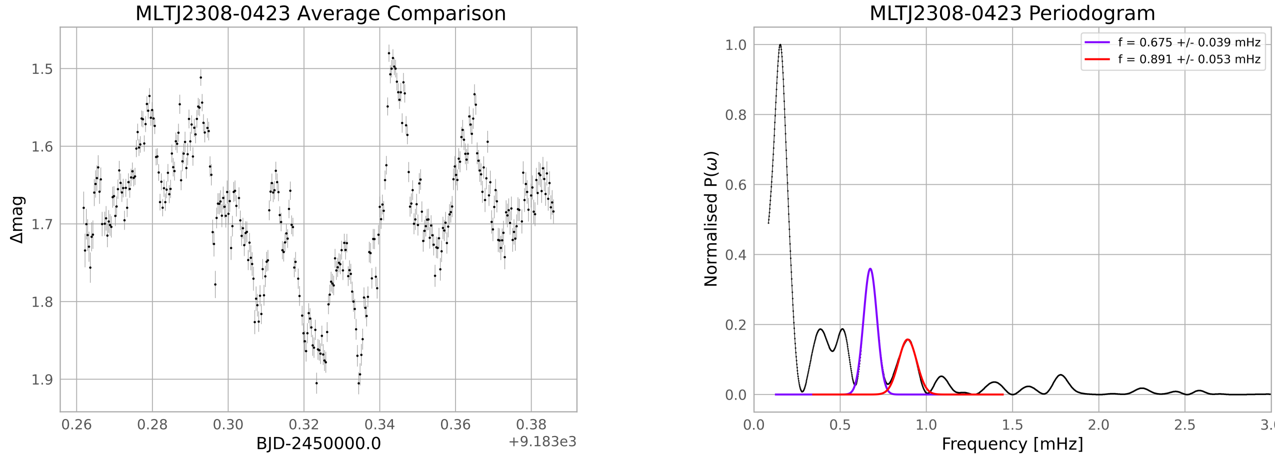

(a) Weighted average differential lightcurve for MLTJ2308–0423 from the first night.

(b) Periodogram produced with Lomb-Scargle analysis for MLTJ2308–0423 from the first night.

Figure 38: Lightcurve and periodogram for MLTJ2308–0423 for the first night.

The lightcurve from the first night of observations shows a clear larger variability as well as a more difficult to detect minor, but faster, variation. There are two clear peaks in the periodogram in Figure 38b, at 0.675 mHz and at 0.891 mHz. These correspond to periods of 24.702 minutes and 18.701 minutes respectively.

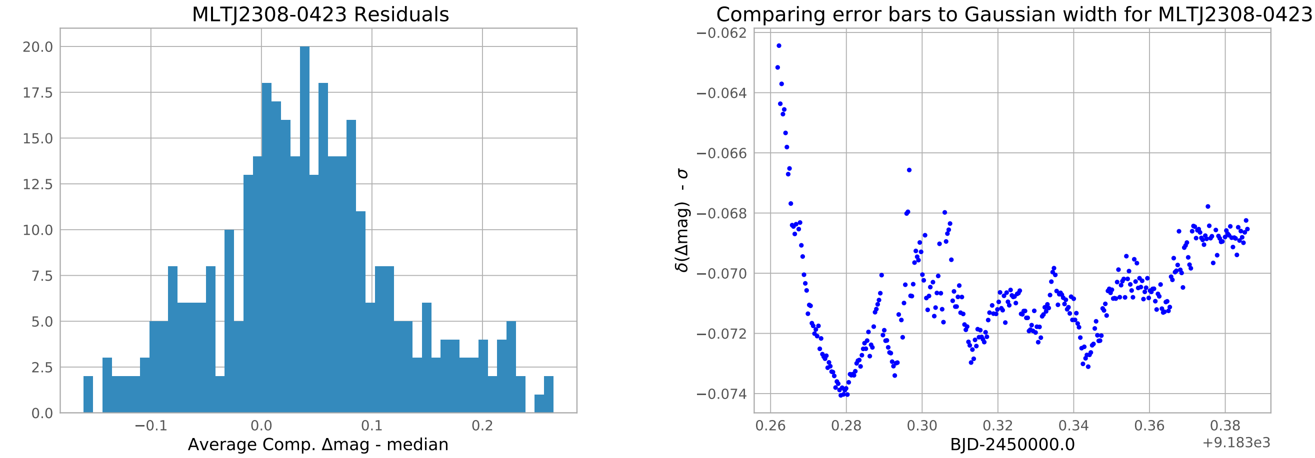

(a) Histogram of Δm−median for MLTJ2308–0423 from the first night.

(b) Comparing error sizes to Gaussian width for MLTJ2308–0423 on the first night.

Figure 39: Residuals histogram and error comparison for MLTJ2308–0423 for the first night.

The histogram of residuals for MLTJ2308–0423 shows a wide spread on the first night, indicative of relatively larger amplitude variations. The small deviations from the Gaussian width for the error sizes seen in Figure 39b are further evidence of variability in the lightcurve.

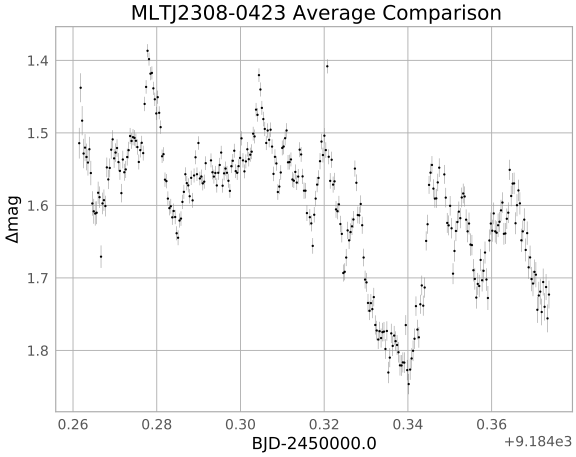

(a) Weighted average differential lightcurve for MLTJ2308–0423 from the second night.

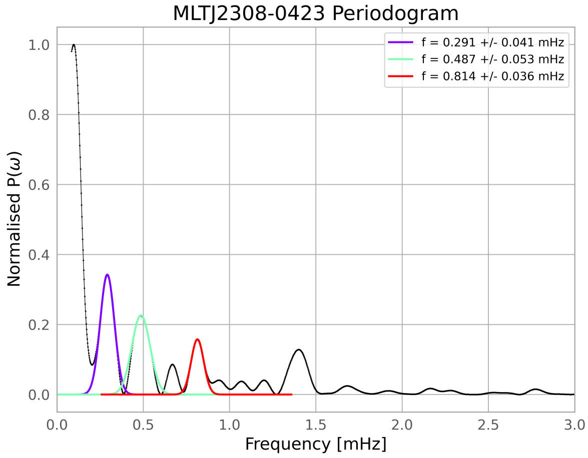

(b) Periodogram calculated with VARTOOLS for MLTJ2308–0423 from the second night.

Figure 40: Lightcurve and periodogram for MLTJ2308–0423 from the second night.

The lightcurve for MLTJ2308–0423 for the second night, seen in Figure 40a, shows the same larger amplitude variability over the course of the whole exposure as well as the minor deviations seen at more regular intervals. This is further seen in the periodogram, Figure 40b, which shows three relatively large spikes at 0.291 mHz, 0.487 mHz, and 0.814 mHz. These frequencies correspond to periods of 57.179 minutes, 34.246 minutes and 20.479 minutes respectively.

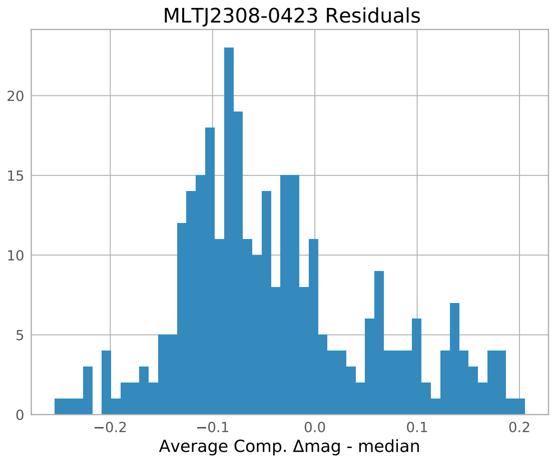

(a) Histogram of Δm$-$median for MLTJ2308–0423 from the second night.

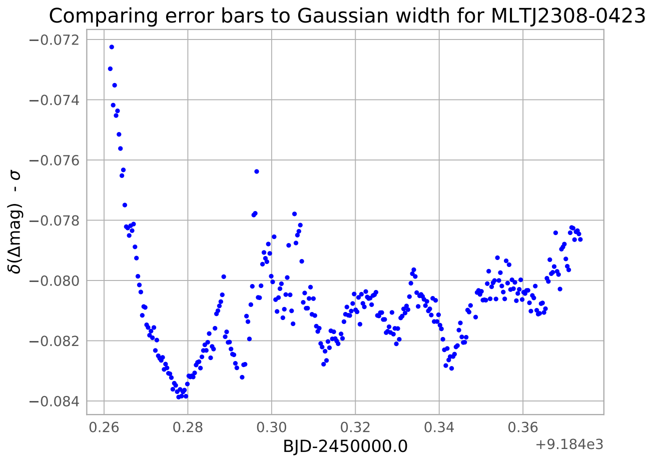

(b) Comparing error sizes to Gaussian width for MLTJ2308–0423 on the second night.

Figure 41: Histogram and error comparison for MLTJ2308–0423 for the second night.

Once again we see a wide spread in the residuals for MLTJ2308–0423 as evidence of the larger amplitude magnitude variations. The plot of error sizes compared to the fitted Gaussian width seen in Figure 41b shows that while the error sizes are smaller than the width, they do not deviate far from the width. This is what we expect with variability present in the lightcurve.

4 Spectroscopy

As part of our follow-up program on the selected candidates, we also obtained spectra with the SpUpNIC spectrograph on the 1.9m telescope at the SAAO site in Sutherland. The purpose of these spectra was to provide us with a rough classification for our candidates. If any of the candidates showed an interesting spectrum, one in which there are strong Helium lines and no hydrogen as is common for AM CVns for example, we would then have a more targeted campaign of follow-up on that specific target. Once again a large portion of these spectrographic observations were done remotely from the SAAO site in Cape Town, although there were some weeks where the observers were able to travel up to Sutherland.

4.1 Observations

The spectroscopic observations were conducted by a team of different observers, Dr Naomi Titus, PhD student Orapeleng Mogawana, PhD student Anke van Dyk, and PhD student Simon De Wet. The spectra were obtained with the SpUpNIC (Spectrograph Upgrade - Newly Improved Cassegrain) instrument which is a recently improved spectrograph on the 1.9-m telescope [62] [63]. SpUpNIC allows for longslit spectroscopy with a wide range of gratings and two different arc lamps, CuAr and CuNe. Aside from some more targeted spectroscopy, only grating 7 (G7) was used in combination with the CuAr lamp. For slightly more targeted spectroscopy, grating 4 (G4) was used also with the CuAr lamp. G4 has 1200 lines per millimeter, a blaze wavelength of 5100 Å, a wavelength range of 1250 Å, a dispersion of 0.62 Å/pixel and a resolving power of 3000. G7 has 300 lines per millimeter, a blaze wavelength of 5000 Å, a wavelength range of 5500 Å, a dispersion of 2.7 Å/pixel and a resolving power of 500. The majority of the spectroscopy was conducted with the G7 grating at a grating angle of 16.2. When G4 was used, it was used at a grating angle of 5.5. In Figure 42, the arc maps for the two gratings used can be seen.

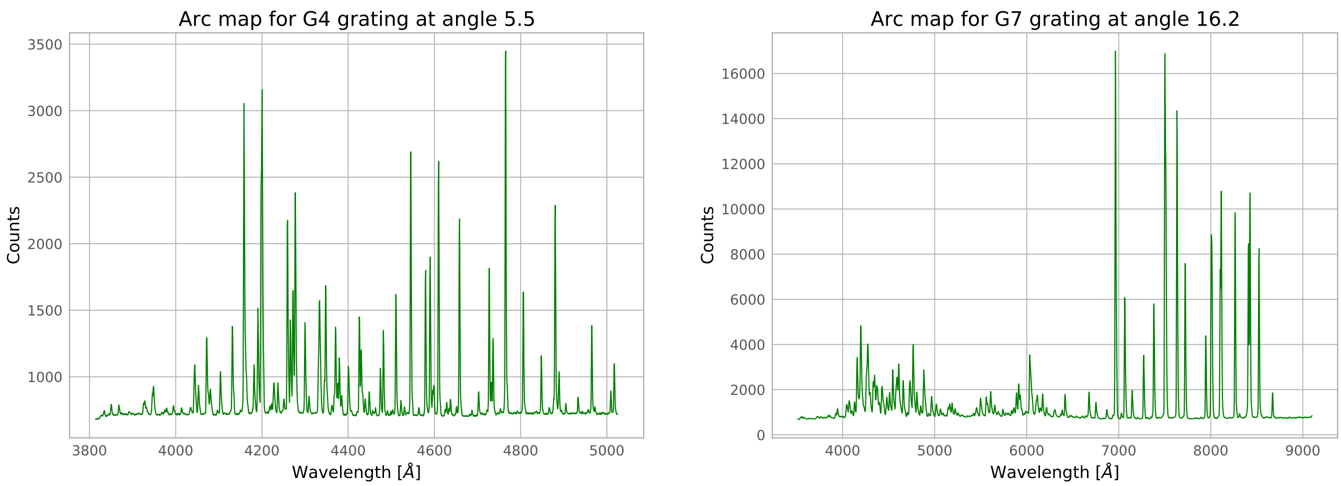

Figure 42: Arc maps for the G4 and G7 gratings.

In Table 4, we see a list of known arc lines used in an initial estimation to prepare the wavelength solution. The "Column" column states roughly what column (pixel value) in the extracted arc spectrum the line is found. These five lines are used to calculate an initial approximation to the pixel-to-wavelength solution. After the initial placement of these lines over a broad range of wavelengths, the rest of lines in the line list are then aligned with the arc spectrum. This line list contains hundreds of potentially identifiable lines for the arc. Once all the lines are aligned, the fit can subsequently be calculated and used for the wavelength solution.

Table 4: Lines used in fitting the arc map to the arc image.

Line	Wavelength [Å]	Column
CuI	4198.317	237
CuI	4764.865	432
CuI	6965.431	1200
CuI	7503.869	1393
CuI	8424.648	1730

4.1.1 1.9-m Telescope

The 1.9-m telescope at Sutherland was built originally for the Radcliffe Observatory in Pretoria in 1948. It has two focal stations, one which is a Cassegrain focus and one which is Newtonian [63]. The Cassegrain focus has an f-ratio of f/18 and a plate scale of roughly 6 arcseconds per millimeter. There are currently three instruments which can be used at the Cassegrain focus, one is SpUpNIC, another is HIPPO, a photo-polarimeter, and the final instrument available is another SHOC camera like those used on the 1.0-m and Lesedi telescopes [64]. The Newtonian focus has an f-ratio of f/4.85 and a plate scale of 22.49 arcsec/mm, however, the secondary mirror is currently not angled towards a Newtonian focus.

4.1.2 Observed Targets

Displayed in Table 5 is all the targets we observed on the 1.9-m telescope. The "Usable" column indicates which of the observed spectra are actually viable; when one is marked as "No" this could either be because the signal-to-noise ratio (SNR) was not high enough, the spectrum was affected by poor observing conditions, or there was an instrumental artefact or issue which ruined the spectrum. The "Lines identified" column displays which of the lines shown in Table 6 can be roughly identified, and whether it is absorption (abs.) or emission (emis.). We also provide a rough classification based on observable features and general shape in each spectra. Several are stars identified to be in the Small or Large Magellanic Clouds (SMC, LMC respectively), others are types of white dwarfs (DA, DB etc.), there are also several subdwarfs (prefix sd), some WDs with main sequence companions (+MS), and a few other types of stars.

Table 5: MeerLICHT selected targets observed with the 1.9-m telescope.

Target	Obs. Date	Grating	Exp. (s)	Usable	Lines	Classification
MLTJ001906.03–432418.6	12/11/2021	G7	1200	Yes	Balmer abs.	DA+MS
MLTJ001906.03–432418.6	22/08/2021	G7	1200	No	-	-
MLTJ003527.38–125706.8	12/11/2021	G7	1800	No	-	-
MLTJ004500.94–732123.2	12/11/2021	G7	1800	Yes	Balmer abs.	sdB?
MLTJ004526.65–732531.4	30/07/2021	G7	300	Yes	Balmer abs.	sdB
MLTJ004526.65–732531.4	11/11/2021	G7	1800	Yes	Balmer abs.	sdB
MLTJ004526.65–732531.4	22/08/2021	G7	1200	No	-	-
MLTJ004809.84–212017.4	20/08/2021	G7	1800	No	-	-
MLTJ005600.70–733100.8	23/08/2021	G7	1200	No	-	-
MLTJ005600.70–733100.8	14/11/2021	G7	1800	No	-	-
MLTJ005842.56–723001.9	23/08/2021	G7	1200	Yes	Balmer abs.	B$\star$ (SMC)
MLTJ010128.84–724337.5	22/08/2021	G7	1200	Yes	Hα emission?	Be$\star$ (SMC)
MLTJ010128.84–724337.5	15/11/2021	G7	1800	No	-	-
MLTJ010255.01–715947.7	23/08/2021	G7	1500	No	-	-
MLTJ011142.36–731232.4	23/08/2021	G7	1500	No	-	-
MLTJ012737.14–740138.2	22/08/2021	G7	1200	No	-	-
MLTJ013424.11–160707.6	29/07/2021	G7	1200	Yes	Balmer abs.	DA
MLTJ013424.11–160707.6	20/08/2021	G7	900	Yes	Balmer abs.	DA
MLTJ014808.36–253244.7	21/08/2021	G7	1200	No	-	-
MLTJ020900.11–735951.6	23/08/2021	G7	1800	Yes	Balmer abs.	sdB

MLTJ022858.36–182839.4	29/07/2021	G7	1200	Yes	Balmer abs.	sdBO
MLTJ022858.36–182839.4	30/07/2021	G7	300	Yes	Balmer abs.	sdBO
MLTJ022858.36–182839.4	11/11/2021	G7	1200	Yes	Balmer abs.	sdBO
MLTJ022858.36–182839.4	20/08/2021	G7	1200	No	-	-
MLTJ022858.36–182839.4	21/08/2021	G7	1800	No	-	-
MLTJ025626.79–172534.7	11/11/2021	G7	1800	Yes	Balmer abs.	sdB
MLTJ032047.03–185527.0	14/11/2021	G7	1800	Yes	None	sdBO or DAB
MLTJ033434.44–640058.0	31/01/2021	G7	1200	Yes	Hα emis., Balmer abs.	DA+MS
MLTJ040830.70–542139.7	14/02/2021	G7	900	Yes	HeI 4471/4921?	sdO?
MLTJ045837.48–685904.4	13/02/2021	G7	1200	Yes	Balmer abs.	DA+MS
MLTJ051841.16–691359.1	15/04/2021	G7	1800	Yes	Balmer emis.	Symbiotic (LMC)
MLTJ052130.06–685156.5	15/02/2021	G7	1200	No	-	-
MLTJ052646.57–685151.6	15/02/2021	G7	1200	Yes	Balmer emis./abs.	Be$\star$ (LMC)
MLTJ053541.03–685734.4	30/01/2021	G7	1800	Yes	Balmer abs.	unknown
MLTJ061835.50–513141.1	16/02/2021	G7	1200	Yes	None	sdB or DC
MLTJ061835.50–513141.1	31/01/2021	G7	600	No	-	-
MLTJ063928.68–402808.4	15/02/2021	G7	1200	Yes	Balmer abs.	sdB
MLTJ064936.83–833153.0	01/05/2021	G7	900	Yes	Balmer abs.	sdB or DA
MLTJ065449.05–791843.1	12/03/2021	G7	1800	Yes	HeI abs., Hβ/γ abs.	sdO
MLTJ070914.31–824005.7	12/03/2021	G7	1800	Yes	Balmer abs.	sdBO
MLTJ070939.87–190720.8	14/11/2021	G7	1800	Yes	Strong Balmer abs.	DA
MLTJ071444.56–323235.0	02/05/2021	G7	1200	No	-	-
MLTJ073110.10–554025.0	13/02/2021	G7	1200	Yes	Balmer abs.	DA
MLTJ073110.10–554025.0	01/05/2021	G7	1800	No	-	-
MLTJ074739.80–332420.3	02/05/2021	G7	1200	No	-	-
MLTJ080401.92–211831.9	14/04/2021	G7	1800	Yes	Narrow Balmer emis.	Reddened Be?
MLTJ083142.28–610030.1	13/02/2021	G7	1200	Yes	Balmer abs.	sdB
MLTJ083142.28–610030.1	16/03/2021	G7	1200	Yes	Balmer abs.	sdB
MLTJ085423.51–493634.1	13/02/2021	G7	1200	Yes	Balmer abs.	sdB
MLTJ085449.77–175705.7	15/04/2021	G7	1200	Yes	Balmer abs.	DA
MLTJ090257.69–075919.8	16/04/2021	G7	1200	Yes	Balmer emis., HeI emis.	CV
MLTJ090824.09–012521.9	18/04/2021	G7	1800	Yes	None	sdB?
MLTJ093238.29–725410.5	15/02/2021	G7	900	Yes	Balmer abs.	DA
MLTJ093453.90–585358.2	18/04/2021	G7	1800	Yes	Balmer abs.	DA
MLTJ094503.82–621540.7	16/04/2021	G7	1800	Yes	Balmer abs.	sdB or DA
MLTJ094739.59–531704.6	16/04/2021	G7	1800	Yes	Balmer abs.	DA+MS
MLTJ100133.23–084250.6	15/04/2021	G7	1800	No	-	-
MLTJ100322.31–610820.2	16/04/2021	G7	1800	No	-	-
MLTJ101043.81–582025.3	15/04/2021	G7	1800	No	-	-
MLTJ101043.81–582025.3	02/05/2021	G7	1200	No	-	-
MLTJ102251.75–322602.6	16/04/2021	G7	1200	Yes	Hα emis., Balmer abs.	DA (nebula?)
MLTJ104626.53–530717.1	16/04/2021	G7	1200	Yes	Balmer abs.	reddened F$\star$?
MLTJ104704.69–352725.3	18/04/2021	G7	1800	Yes	HeI abs., no H	DB
MLTJ104805.98–751745.3	16/04/2021	G7	1200	Yes	Balmer abs.	DA
MLTJ110105.32–355045.3	22/03/2021	G7	1800	Yes	Balmer abs.	DA
MLTJ111610.64–525935.7	29/01/2021	G7	1200	Yes	Balmer abs.	sdB or DA
MLTJ111610.64–525935.7	11/03/2021	G7	1200	Yes	Balmer abs.	sdB or DA
MLTJ111632.74–714049.2	22/03/2021	G7	1800	Yes	Balmer abs.	DA
MLTJ111845.64–420550.0	11/03/2021	G7	1200	Yes	HeI abs., no H	DB
MLTJ111913.45–704853.8	22/03/2021	G7	1200	Yes	Balmer abs.	DA
MLTJ112405.68–431729.4	22/03/2021	G7	1800	Yes	Minor HeI, H abs.	DBA
MLTJ113752.14–580720.6	22/04/2021	G7	1200	Yes	Balmer abs.	sdB
MLTJ114112.44–340146.5	22/04/2021	G7	1800	Yes	HeI abs., no H	DBA
MLTJ114618.09–314101.5	22/04/2021	G7	1800	Yes	Balmer abs.	DA
MLTJ115915.47–140925.3	22/04/2021	G7	1800	Yes	None	DC
MLTJ120752.79–550021.7	22/03/2021	G7	1800	Yes	Balmer abs.	reddened F$\star$?
MLTJ121018.82–554428.5	11/03/2021	G7	1200	Yes	Balmer abs.	sdB
MLTJ121432.53–541942.5	11/03/2021	G7	1200	Yes	Balmer abs.	sdB or DA
MLTJ121558.78–491453.4	14/04/2021	G7	1200	Yes	Balmer abs.	DA
MLTJ123403.30–450133.3	01/05/2021	G7	900	Yes	Balmer abs.	DA+MS?
MLTJ124848.88–344208.5	20/04/2021	G7	900	Yes	Metal emis., Balmer abs.	unknown
MLTJ125002.08–310255.5	11/03/2021	G7	600	Yes	Balmer abs.	sdB
MLTJ125544.63–555351.4	11/03/2021	G7	1200	Yes	Balmer abs.	sdB
MLTJ130106.77–481034.8	07/07/2021	G7	1200	Yes	Balmer abs.	sdB or DA

MLTJ130129.04–515244.5	07/07/2021	G7	1800	Yes	Balmer abs.	DA
MLTJ131438.71–554554.9	12/03/2021	G7	1200	Yes	Balmer abs.	sdBO or DAB
MLTJ132425.35–592124.4	12/03/2021	G7	1200	Yes	Balmer abs.	sdB
MLTJ135103.48–665350.1	01/05/2021	G7	900	Yes	Hα abs., HeI abs.?	sdF?
MLTJ135704.98–510325.9	07/07/2021	G7	1800	No	-	-
MLTJ135917.77–305409.6	12/03/2021	G7	1200	Yes	Balmer abs.	sdB
MLTJ140516.70–434023.6	12/03/2021	G7	1200	Yes	Balmer abs.	sdB or DA
MLTJ141141.49–482900.9	30/04/2021	G7	1200	Yes	Balmer abs.	sdB or DA
MLTJ142706.26–322216.1	17/03/2021	G7	1800	Yes	HeI, Balmer abs.	sdB
MLTJ142909.19–445811.8	30/04/2021	G7	1200	No	-	-
MLTJ144139.77–161530.4	17/03/2021	G7	1200	Yes	HeI, Balmer abs.	sdBO
MLTJ144322.91–335856.9	25/07/2021	G7	1200	No	-	-
MLTJ144700.45–160149.1	17/03/2021	G7	1800	Yes	Minor Balmer emis.	sdB or DA
MLTJ150307.49–502107.2	09/07/2021	G7	1800	Yes	Balmer abs.	sdB or DA
MLTJ151301.40–143457.1	18/04/2021	G7	1800	Yes	Balmer abs.	DA
MLTJ151415.65–012925.3	18/04/2021	G7	1800	Yes	Balmer abs.	sdB
MLTJ151509.15–162102.5	20/04/2021	G7	1800	Yes	Balmer abs.	sdB
MLTJ151913.75–114645.3	18/04/2021	G7	1200	Yes	Balmer abs.	sdB
MLTJ152055.22–112608.0	22/04/2021	G7	1800	Yes	No Hα. Balmer abs.	sdBO
MLTJ152528.92–530611.4	09/07/2021	G7	1800	Yes	Balmer abs.	DA
MLTJ152713.96–641737.4	21/03/2021	G7	1200	Yes	Balmer abs.	sdB or DA
MLTJ152713.96–641737.4	22/03/2021	G7	1800	Yes	Balmer abs.	sdB or DA
MLTJ153346.84–112633.3	18/04/2021	G7	1800	Yes	Broad Balmer abs.	DA
MLTJ153930.73–014351.5	22/04/2021	G7	1800	Yes	None	DC
MLTJ154049.30–542707.7	09/07/2021	G7	1200	No	-	-
MLTJ154049.30–542707.7	30/07/2021	G7	1200	No	-	-
MLTJ154620.07–123228.6	18/04/2021	G7	1800	Yes	Balmer abs.	sdB
MLTJ154956.70–345132.2	10/07/2021	G7	1800	Yes	HeI, Balmer abs.	sdO or DBA
MLTJ154956.70–345132.2	30/07/2021	G7	1200	No	-	-
MLTJ160031.82–445103.2	20/04/2021	G7	1800	No	-	-
MLTJ160038.69–065335.9	22/04/2021	G7	900	Yes	Balmer abs.	sdF?
MLTJ160337.62–374523.1	20/04/2021	G7	900	No	-	-
MLTJ160408.79–370649.5	22/04/2021	G7	1800	Yes	Balmer abs.	sdB
MLTJ160724.20–164451.1	30/07/2021	G7	1200	No	-	-
MLTJ161604.14–794236.8	24/07/2021	G7	900	Yes	Balmer abs.	sdB or DA?
MLTJ161604.14–794236.8	30/07/2021	G7	1200	Yes	Balmer abs.	sdB or DA?
MLTJ161737.30–734440.4	30/07/2021	G7	1200	No	-	-
MLTJ164322.58–334205.5	30/04/2021	G7	800	Yes	Balmer abs.	sdB or DA
MLTJ170507.64–695031.0	22/03/2021	G7	1800	Yes	HeI, Balmer abs.	sdO or DAB
MLTJ170507.64–695031.0	17/04/2021	G7	1200	Yes	HeI, Balmer abs.	sdO or DAB
MLTJ170507.64–695031.0	29/07/2021	G7	1200	Yes	HeI, Balmer abs.	sdO or DAB
MLTJ172737.79–360016.4	30/04/2021	G7	800	Yes	Balmer abs.	DA
MLTJ175253.87–663448.9	30/04/2021	G7	800	Yes	Balmer abs.	sdB
MLTJ181411.28–531653.9	17/04/2021	G7	1200	Yes	Balmer abs.	sdB
MLTJ181411.28–531653.9	29/07/2021	G7	1200	Yes	Balmer abs.	sdB
MLTJ190610.74–373414.1	29/07/2021	G7	1200	No	-	-
MLTJ192433.98–432444.6	22/04/2021	G7	1800	Yes	Minor HeI, Balmer abs.	sdB or DA
MLTJ192433.98–432444.6	29/07/2021	G7	1200	Yes	Minor HeI, Balmer abs.	sdB or DA
MLTJ192617.40–655749.0	01/05/2021	G7	1200	Yes	Balmer abs.	DA
MLTJ193431.86–433643.9	29/07/2021	G7	1200	Yes	Balmer abs.	sdB or DA
MLTJ193431.86–433643.9	15/09/2021	G7	1800	Yes	Balmer abs.	sdB or DA
MLTJ193431.86–433643.9	21/08/2021	G7	1200	No	-	-
MLTJ193431.86–433643.9	22/08/2021	G7	1800	No	-	-
MLTJ203654.63–432231.6	29/07/2021	G7	1200	Yes	Balmer abs.	CV
MLTJ203654.63–432231.6	12/11/2021	G7	1200	Yes	Balmer abs.	CV
MLTJ203654.63–432231.6	22/08/2021	G7	1200	No	-	-
MLTJ205342.93–045943.2	17/09/2021	G7	1200	No	-	-
MLTJ210323.95–335431.5	17/09/2021	G7	1800	No	-	-
MLTJ211329.83–031709.6	17/09/2021	G7	1200	Yes	Minor HeI, Balmer abs.	sdB or DA
MLTJ214314.63–752359.6	11/07/2021	G7	1800	Yes	Balmer abs.	DA
MLTJ220803.20–322800.1	16/11/2021	G7	1800	No	-	-
MLTJ230213.18–315559.1	16/11/2021	G7	1800	Yes	Balmer abs.	DBA?
MLTJ231602.94–324641.6	22/08/2021	G7	1200	No	-	-
TW Pictorius	18/03/2021	G4	600	Yes	HeI, Balmer emis.	CV

TW Pictorius	19/03/2021	G4	600	Yes	HeI, Balmer emis.	CV
TW Pictorius	20/03/2021	G4	600	Yes	HeI, Balmer emis.	CV
TW Pictorius	21/03/2021	G4	600	Yes	HeI, Balmer emis.	CV
TW Pictorius	22/03/2021	G4	600	Yes	HeI, Balmer emis.	CV
TW Pictorius	22/04/2021	G4	600	Yes	HeI, Balmer emis.	CV
TW Pictorius	01/05/2021	G7	600	Yes	HeI, Balmer emis.	CV
TW Pictorius	02/05/2021	G7	600	No	-	-

4.2 Processing with longslit pipeline

To process all the spectra that were obtained, we used a pipeline developed to process an entire night of longslit data in a few minutes. This pipeline was created and written by Dr Naomi Titus in an effort to provide SAAO with an efficient tool to process longslit spectra produced by SpUpNIC, the new Mookodi spectrograph on the Lesedi telescope, and longslit spectra from the Robert Stobie Spectrograph (RSS) on the Southern Africa Large Telescope (SALT). More information on the pipeline can be found at the GitHub page [65] and in the upcoming paper on the pipeline (Titus et al., in prep.).

Current usage of the pipeline requires two Python scripts, (`spectroscopic_routines.py` and `spec_gr#.py` where # is the grating number for SpUpNIC), to be in the same directory as the data which is being processed. It also requires a reference arc spectrum for the relevant grating setup as well as a list of lines to be identified in the observed arcs in order to calculate the wavelength solution. To run the pipeline, one simply has to run `spec_gr#.py` in the terminal. First, we create the master bias and flat files for the given night by opening the script and setting the "`run_pipeline`" and "`apply_flux_cal`" settings to "`False`", and setting the "`construct_bias`" and "`construct_flat`" options to "`True`" - it is also required to supply the script with the exposure time for the flat frames - and then run the script once. After the "Bias.fits" and "Flat.fits" master correction frames have been made, we set the bias and flat construction options back to `"False"` and turn on the pipeline by changing "`run_pipeline`" to `"True"`. If a spectroscopic standard was observed on the night in question then we can also set "`apply_flux_cal`" as `"True"`, however this also requires additional information to be supplied about which spectroscopic standard was observed. Given that on many of the nights our data was obtained a spectroscopic standard was unable to be observed and a flux calibration was not necessary for our purposes, we decided to use only the counts spectra.

One final edit to make to the `spec_gr#.py` file is to set the starting and ending points for the 1D trace extraction. This is not always a necessary change as often if the target is in the middle of the slit, the default values for the "`y0_trace`" and "`yf_trace`" positions are good enough to allow the pipeline's optimal extraction function to work. Occasionally it was necessary to change the "`manual_trace`" value to "`True`" when the target is particularly faint or there are multiple objects on the slit. This then allows for x and y coordinates to be supplied, and a trace width and polynomial order number to be chosen at intermittent steps. Once the changes have been applied to the `spec_gr#.py` script, we run it again through the terminal. It will then trim all the images to be the same size as the master correction frames and apply the corrections. The next step in the automated process selects the first "SCIENCE" target via the fits header information and performs a cosmic ray removal routine with the Lacosmic Python package, a tool designed from the L.A.Cosmic algorithm [66]. Once the cosmic ray removal process is complete, a trace fit is shown for that first science target such as the one seen in Figure 43a and the user is asked if they would like to edit the background sections and the trace width. Once the user is happy with the sky regions and the trace width, the 2D spectrum is shown with the selected regions as seen in Figure 43b.

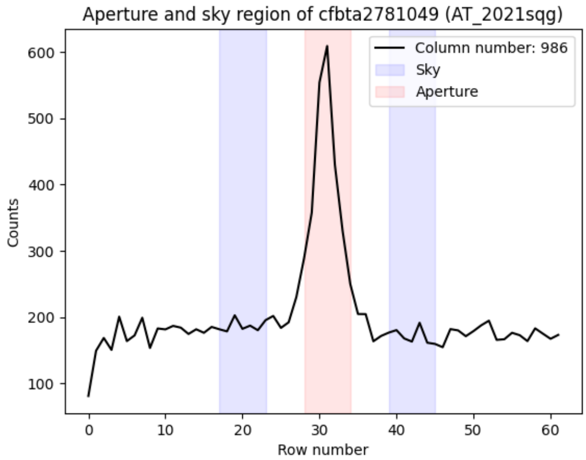

(a) Aperture for the trace and sky regions.

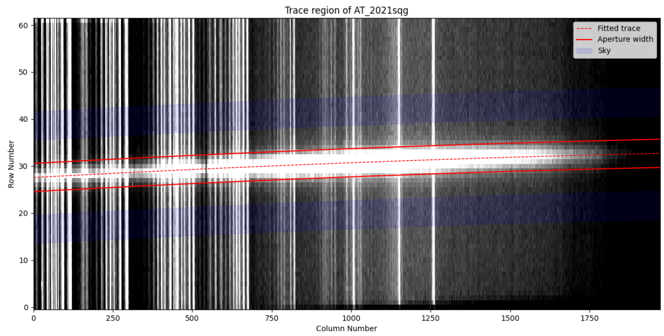

(b) 2D spectrum showing the trace and sky regions.

Figure 43: Aperture extraction for the 2D spectrum of AT 2021sqg example.

The next step is the wavelength solution which is created from an arc spectrum one file number away from the science file, for example if the science file is `a2781049.fits`, the pipeline will look for an arc file at either `a2781048.fits` or `a2781050.fits`, depending on whether the user set the "`ARC`" value as "–1" or "1" respectively in the `spec_gr#.py` file. The default is "–1". Once the wavelength solution is created and applied to the extracted 1D science spectrum, the pipeline outputs the fitted arc, the residuals for the fitted lines of the arc, the SNR for the spectrum, and the wavelength solved 1D spectrum. The output spectrum for the target has both an optimally extracted trace spectrum as well as one based on a summed trace extraction. This entire process is then repeated automatically for the rest of the science frames in the directory in which the pipeline is being run. The user only has to interact with the process during the first target's aperture extraction, the rest happen automatically and through an optimisation process. An example of an extracted and wavelength calibrated spectrum, along with the corresponding fitted arc and residuals (difference between wavelength solution and reference arc spectrum), can be seen in Figure 44.

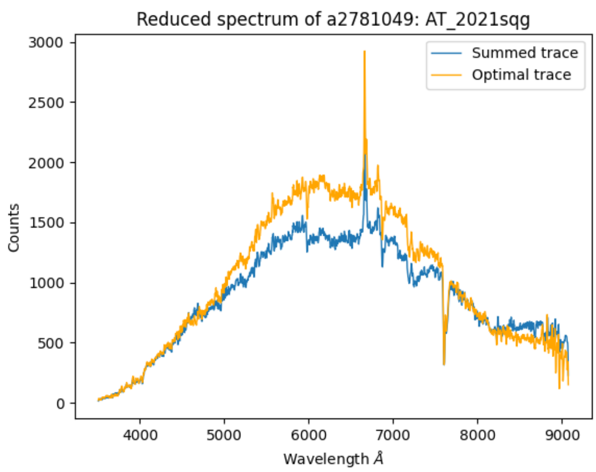

(a) Optimal and summed trace spectra for AT 2021sqg.

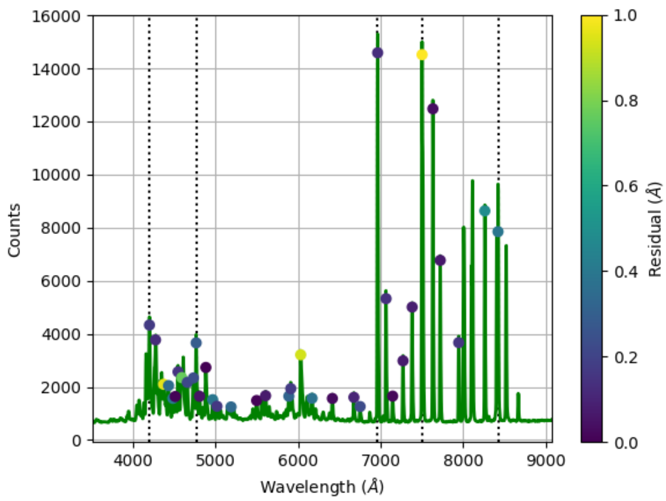

(b) Wavelength solution for AT 2021sqg arc.

Figure 44: Spectra and arc solution for AT 2021sqg.

4.2.1 Quick look line identification

In order to perform a rough identification of emission and absorption lines in all the spectra, several lines of interest were plotted as vertical lines over the spectra. These lines of interest are given in Table 6. The lines chosen were the Balmer series of hydrogen lines, several Helium lines, and a few heavier metal lines. The Helium and metal lines are common lines in AM CVn spectra, and the lack of hydrogen lines is another key feature in AM CVn spectra. An example of using these lines to make quick identification can be seen in Figure 45 in a spectrum obtained for TW Pictoris (TW Pic) with the G7 grating. In the figure one can clearly see strong emission of the Balmer series lines as well as several of the Helium lines. While it may be difficult to distinguish some of the lines in the plot, during the identification procedure we could zoom in to change the scale.

Table 6: Key lines for rough identification of spectra

Line	**Wavelength [Å]**	**Line**	**Wavelength [Å]**	**Line**	**Wavelength [Å]**	**Line**	**Wavelength [Å]**
Hϵ	3970	HeI	4471	HeI	6678	CaII	3969
Hδ	4101	HeI	4713	HeI	7065	FeII	5169
Hγ	4340	HeI	4921	HeI	7281	SiII	6347
Hβ	4861	HeI	5015	HeII	4686	SiII	6371
Hα	6562	HeI	5047	HeII	6560		
HeI	4026	HeI	5876	CaII	3934		

These lines were used to point out the notable features which are marked in the table showing all the observed targets in Table 5. In that table, spectra with notable features have an added comment in the "Lines identified" column.

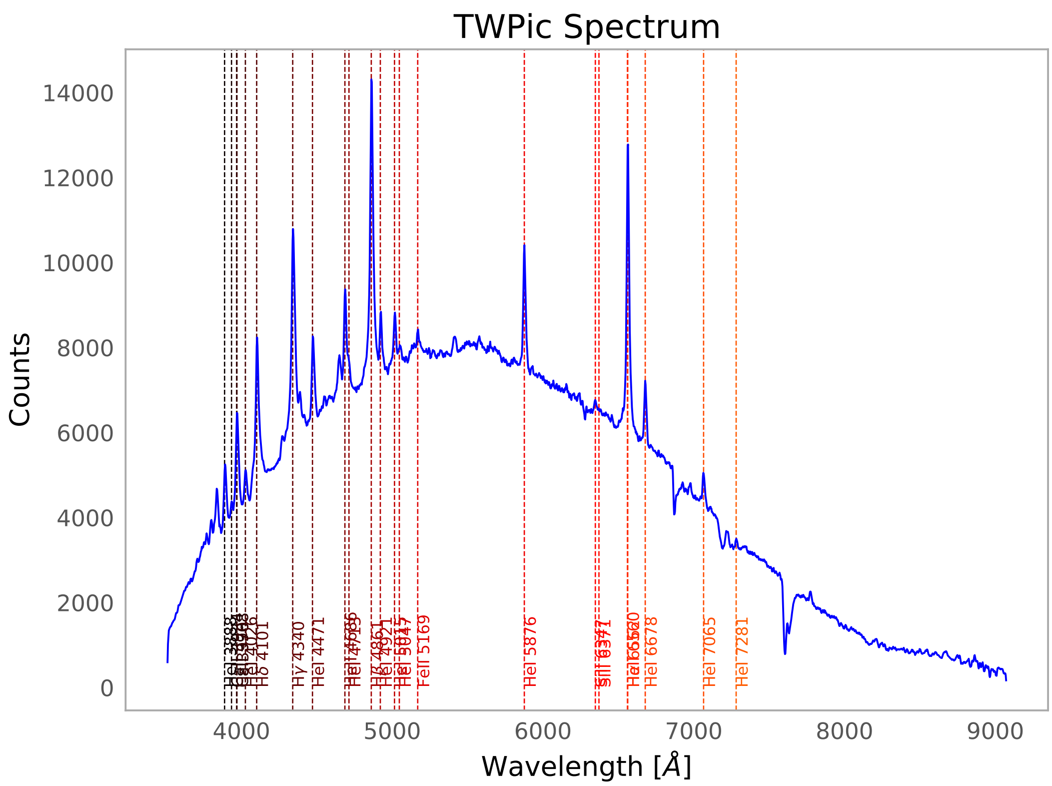

Figure 45: Plotted lines for identification with TW Pic's spectrum.

4.3 Spectra with more than hydrogen

While the majority of the spectra obtained displayed Balmer absorption and no other apparent features as can be seen in Table 5, there were 12 targets which displayed other noteworthy features. These targets all displayed something other than just hydrogen in their spectra, based off of our quick look identification with the lines from Table 6. All of the spectra we obtained displayed the typical atmospheric absorption at roughly 6870 and 7610 Å.

4.3.1 MLTJ040830.70–542139.7

MLTJ040830.70–542139.7 was observed on the 14/02/2021 with an exposure time of 900s. It has a g-band apparent magnitude (g_ML) of 16.878 and a parallax of 10.069 milli-arcseconds (mas). On SIMBAD, it has the potential classification of a white dwarf candidate from Gaia [67]. The spectrum in Figure 46 shows no Balmer lines and HeI absorption at 4471 and 4921 Å. This is a potential sdO subdwarf.

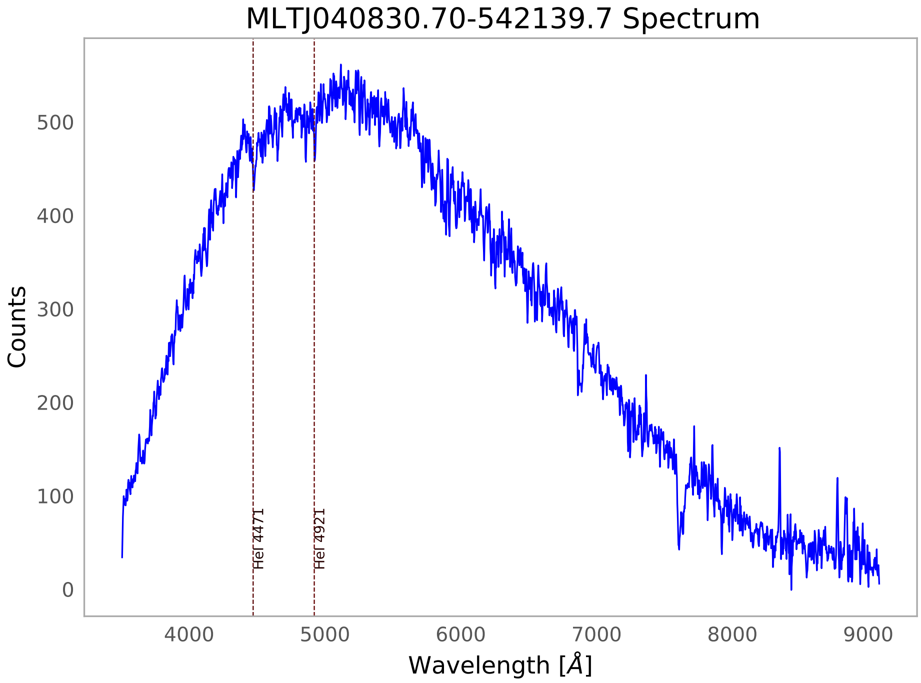

Figure 46: MLTJ040830.70–542139.7.

4.3.2 MLTJ065449.05–791843.1

MLTJ065449.05–791843.1 was observed on the 12/03/2021 with an exposure time of 1800s. It has a mag of $g\_ML = 17.076$ and a parallax of 0.426 mas. Its spectrum displays Balmer absorption lines along with HeI absorption at 4471 and 4921 Å, and HeII absorption at 4686 Å. This is also a potential sdO subdwarf.

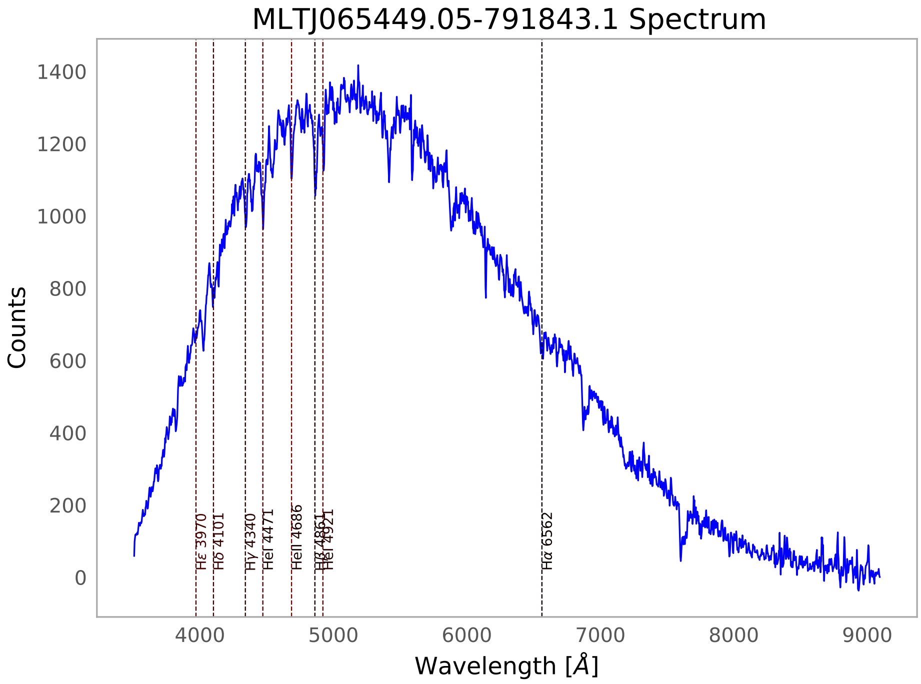

Figure 47: MLTJ065449.05–791843.1.

4.3.3 MLTJ090257.69–075919.8

MLTJ090257.69–075919.8 was observed for 1200s on the 16/04/2021. It has a g-band apparent magnitude of 15.506 and a parallax of 1.373 mas. The spectrum displays strong Balmer emission as well as HeI emission at 4471, 4921, 5876, 6678, and 7065 Å. It also shows emission of the HeII line at 4686 Å. All of these features are highly indicative of MLTJ090257.69–075919.8 being a CV.

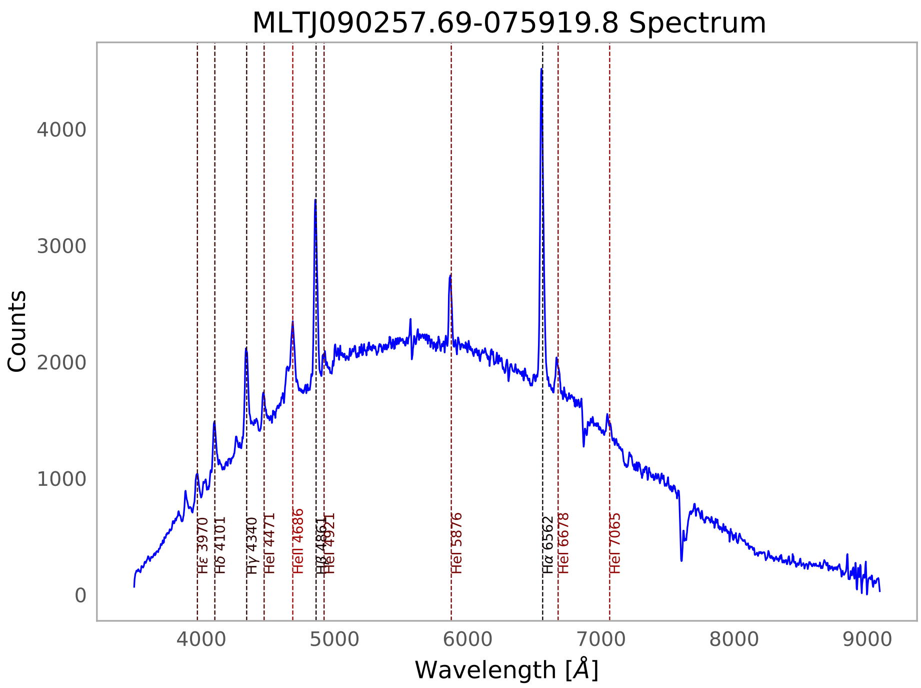

Figure 48: MLTJ090257.69–075919.8: HeI 4471/4686/5876/6678 and Balmer emission lines.

4.3.4 MLTJ104704.69–352725.3

MLTJ104704.69–352725.3 was also observed on the 16/04/2021 for 1200s. Its magnitude is $g\_ML = 17.653$ and it has a parallax of 4.611 mas. The apparent lack of hydrogen combined with the HeI lines at 4026, 4471, 4921, 5015, 5876, and 6678 Å, would indicate this object is a DB WD.

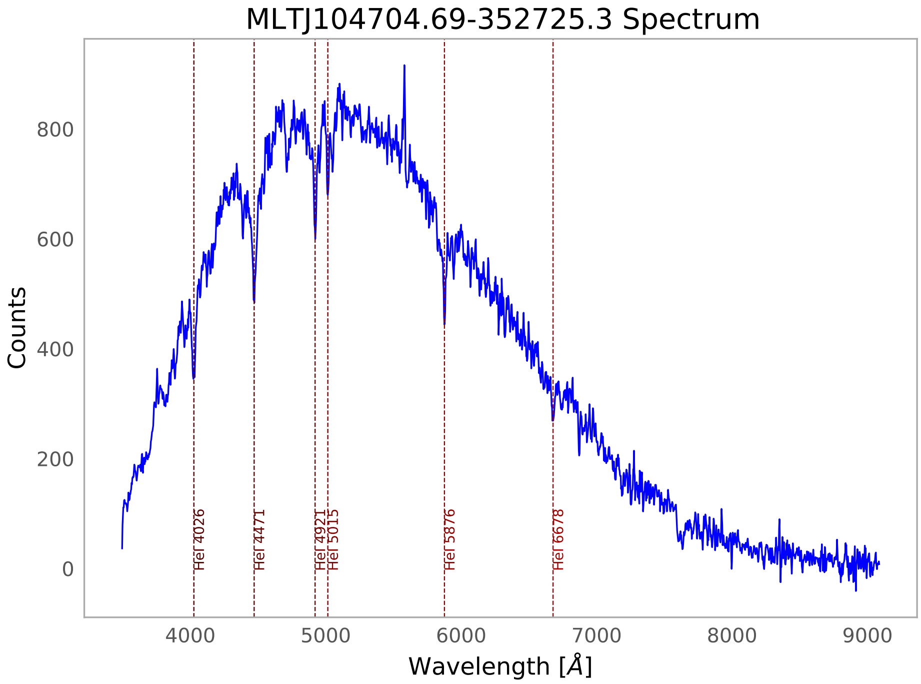

Figure 49: MLTJ104704.69–352725.3.

4.3.5 MLTJ111845.64–420550.0

MLTJ111845.64–420550.0 was observed on the 11/03/2021 for 1200s. Its magnitude is $g\_ML = 16.608$ and it has a parallax of 9.328 mas. The spectrum displays a lack of hydrogen, with HeI lines at 4026, 4471, 4921, 5015, 5876, and 6678 Å. These features are typical for a DB WD. There are also two further atmospheric absorption lines at 5580 and 6300 Å.

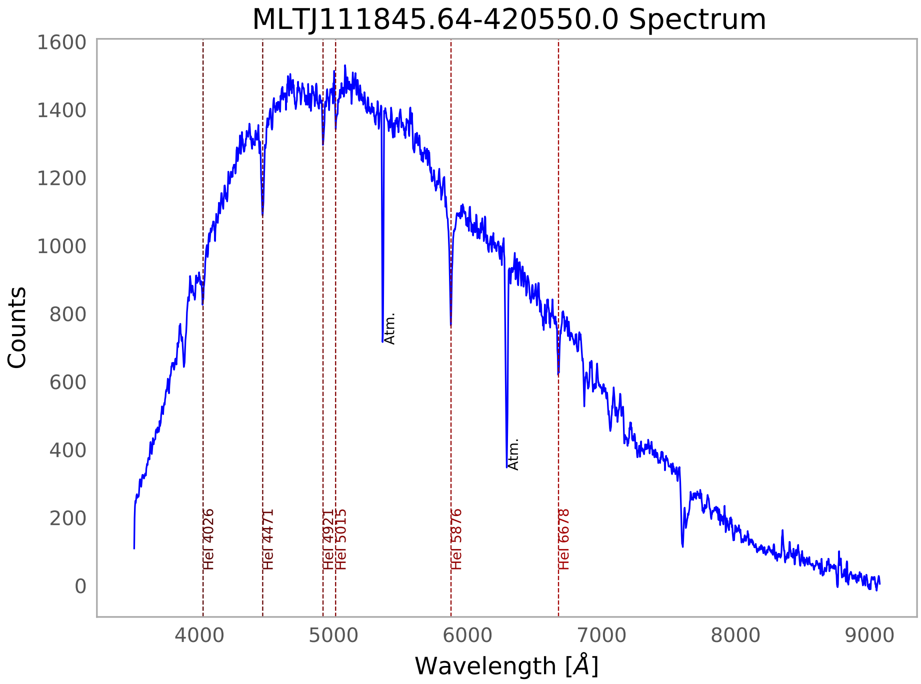

Figure 50: MLTJ111845.64–420550.0.

4.3.6 MLTJ112405.68–431729.4

MLTJ112405.68–431729.4 was observed on the 22/03/2021 for 1800s. Its magnitude is $g\_ML = 16.593$ and it has a parallax of 1.609 mas. The spectrum displays the following absorption lines: HeII 4686 Å, Hβ 4861 Å, and HeI 5876 Å. There are also two non-physical artefacts on the spectrum. This is likely a DBA WD.

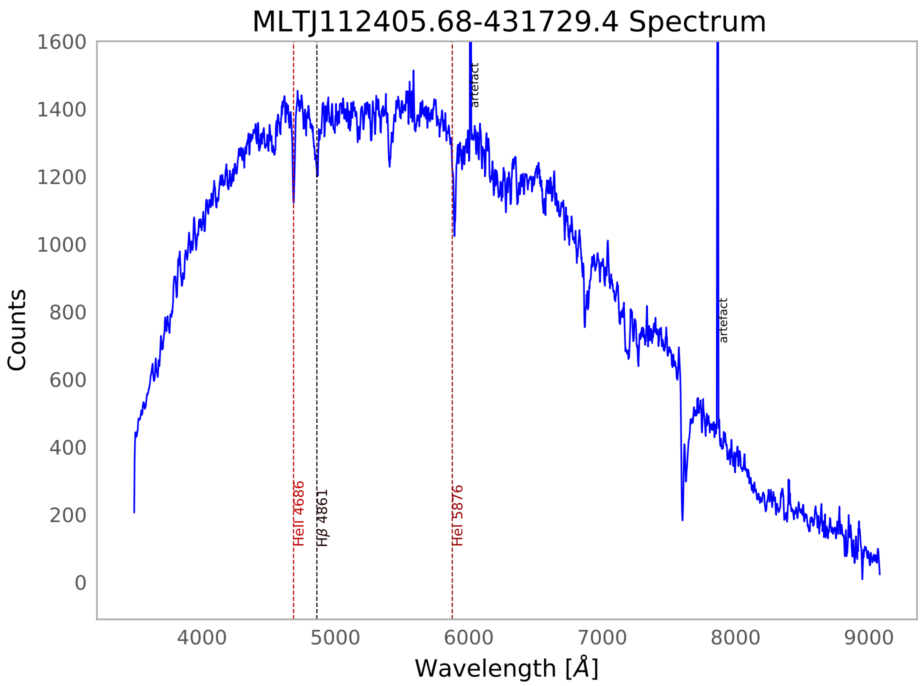

Figure 51: MLTJ112405.68–431729.4.

4.3.7 MLTJ114112.44–340146.5

MLTJ114112.44–340146.5 was observed on the 22/04/2021 with an exposure time of 1800s. Its magnitude is $g\_ML = 16.331$ and it has a parallax of 8.250 mas. The spectrum displays Hα and Hβ absorption at 6562 and 4861 Årespectively. It also shows HeI absorption lines at 4026, 4471, 4713, 4921, 5015, and 5876 Å. These features would indicate that it is likely a DBA WD.

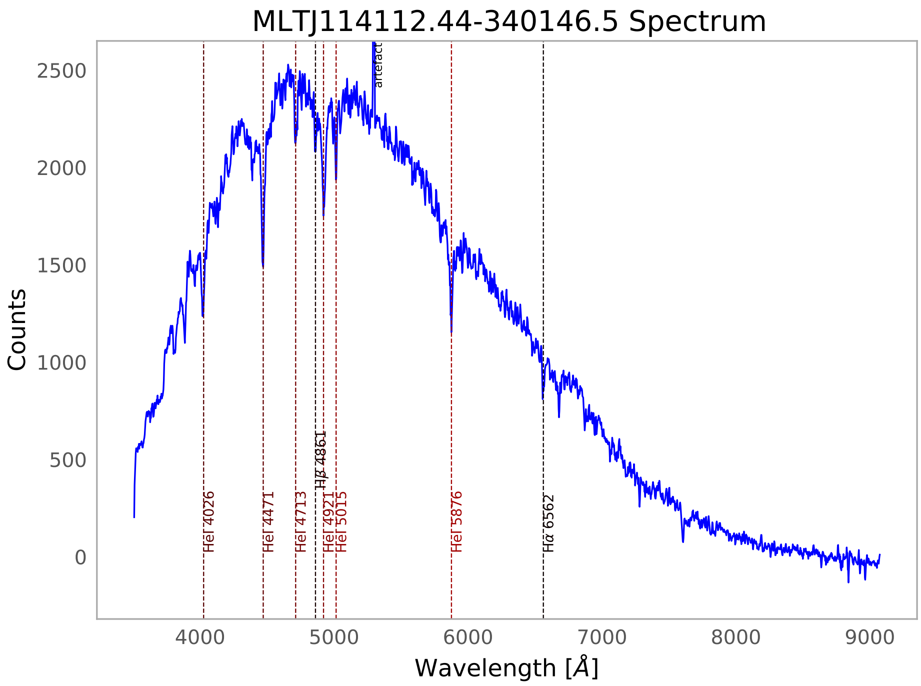

Figure 52: MLTJ114112.44–340146.5.

4.3.8 MLTJ124848.88–344208.5

MLTJ124848.88–344208.5 was observed on the 20/04/2021 with an exposure time of 900s. Its magnitude is $g\_ML = 15.088$ and it has a parallax of 6.002 mas. This object displays the most interesting and unusual of the spectra we obtained. It shows Balmer absorption lines, and the following emission lines: HeI 5047, FeII 5169, SiII 6347, and HeI 6678. There are also several more unidentified emission lines in the spectrum. This object warrants further investigation and potentially higher resolution spectroscopy with the RSS on SALT.

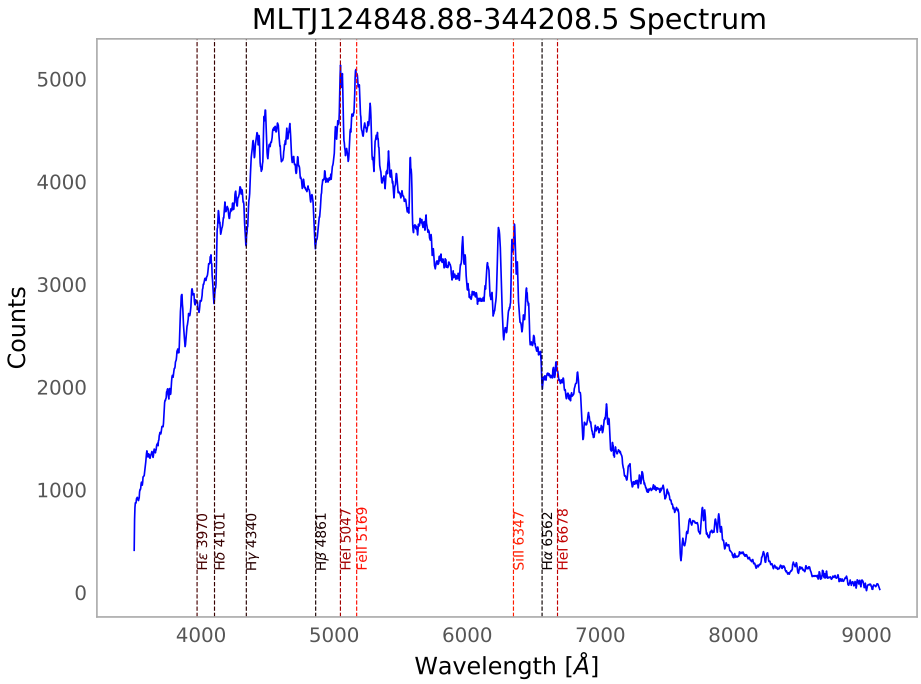

Figure 53: MLTJ124848.88–344208.5.

4.3.9 MLTJ142706.26–322216.1

MLTJ142706.26–322216.1 was observed on the 17/03/2021 with an exposure time of 1800s. Its magnitude is $g\_ML = 16.729$ and it has a parallax of 0.540 mas. The spectrum displays absorption at the Balmer lines, as well as at the HeI and HeII lines of 4471 and 4686 Årespectively. There is also an atmospheric line at 5580 Å, and two artefacts at 4000 and 8943 Å. This is most likely a sdB subdwarf.

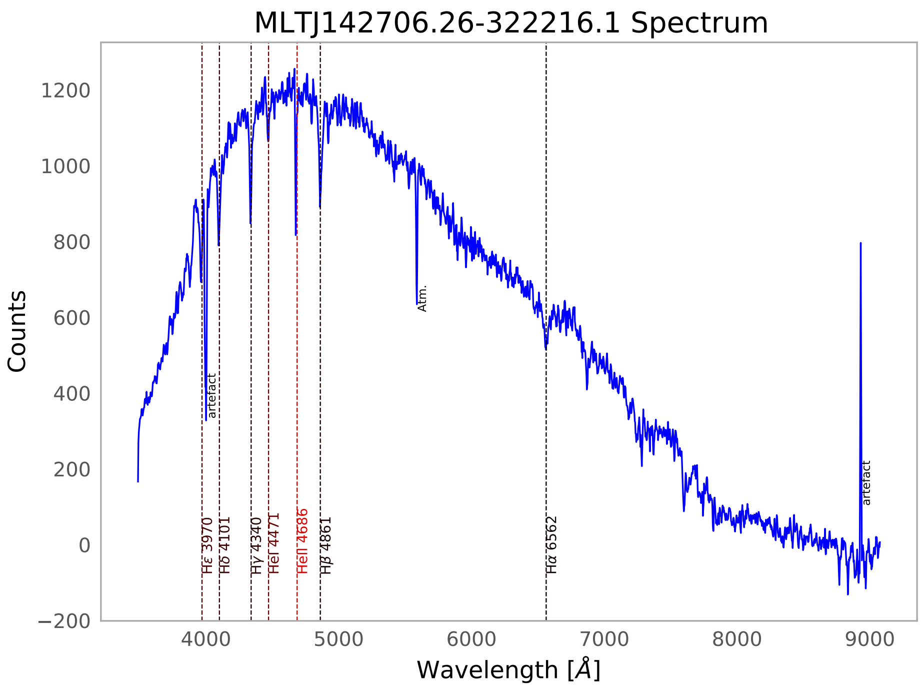

Figure 54: MLTJ142706.26–322216.1.

4.3.10 MLTJ144139.77–161530.4

MLTJ144139.77–161530.4 was also observed on the 17/03/2021, but with an exposure time of 1200s. Its magnitude is $g\_ML = 16.158$ and it has a parallax of 0.723 mas. The Balmer series is present as absorption lines and there are also a number of HeI lines at 4471, 4921, 5015, and 5876 Å. An atmospheric line can be seen at 5580 Å. These features are indicative of a possible sdBO subdwarf.

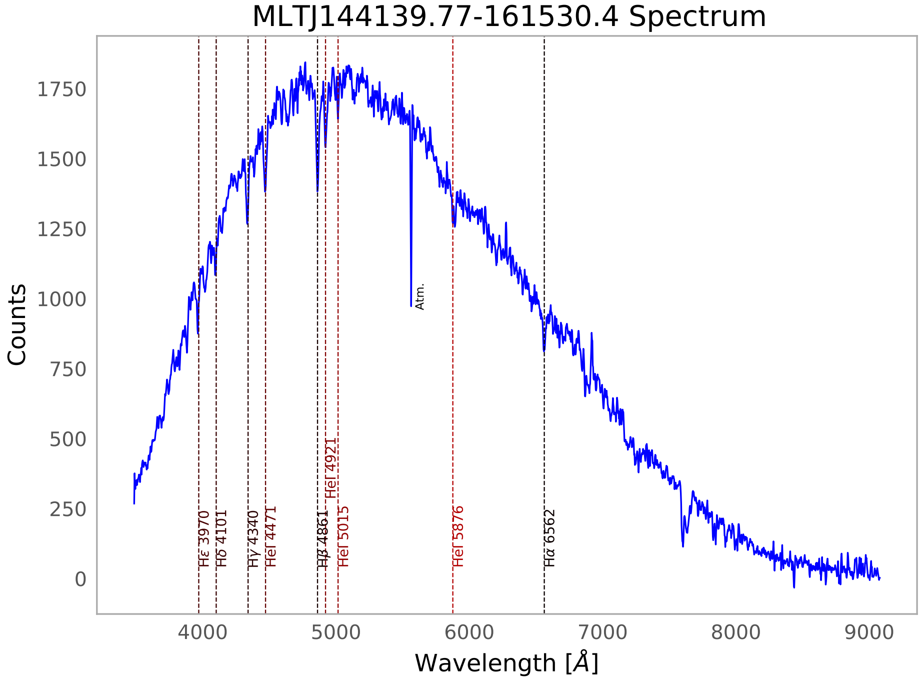

Figure 55: MLTJ144139.77–161530.4.

4.3.11 MLTJ154956.70–345132.2

MLTJ154956.70–345132.2 was observed with an 1800s exposure time on the 10/07/2021. Its magnitude is $g\_ML = 17.044$ and it has a parallax of 0.464 mas. Its spectrum displays Balmer absorption lines, as well as HeI absorption at 4026, 4471, 4921, 5876, and 6678 Å. The HeII line at 4686 Åis also present as absorption. This spectrum is possibly that of a sdO subdwarf or DBA WD.

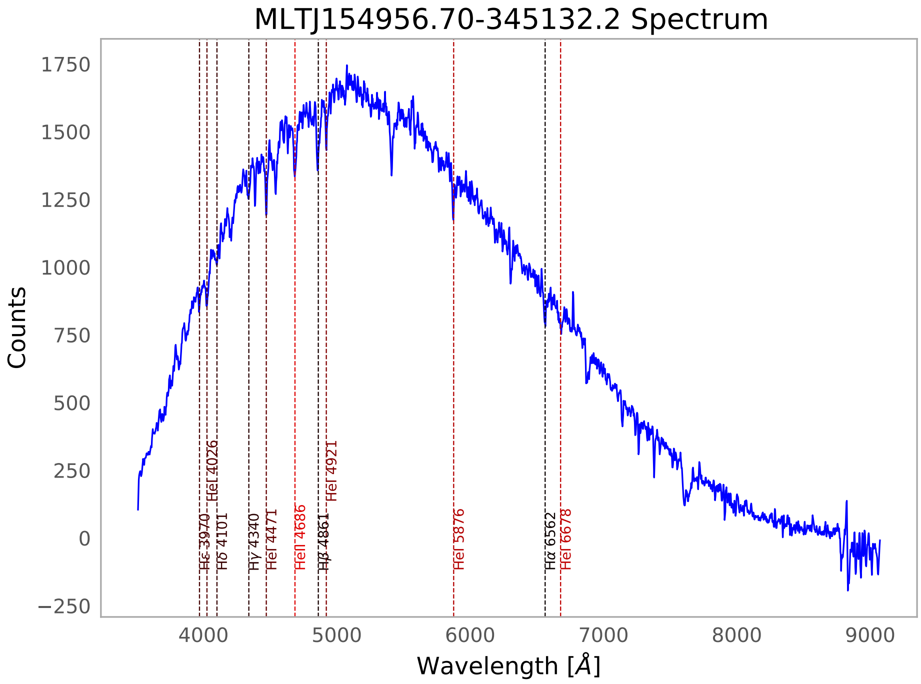

Figure 56: MLTJ154956.70–345132.2.

4.3.12 MLTJ170507.64–695031.0

MLTJ170507.64–695031.0 was observed on three separate occasions successfully. The spectrum displayed in Figure 57 was obtained with at 1200s exposure time on the 17/04/2021. Its magnitude is $g\_ML = 16.354$ and it has a parallax of 0.562 mas. The spectrum shows Balmer absorption, as well as HeI absorption lines at 4026, 4471, 4921, and 5876 Å. This object is most likely a sdO subdwarf or DAB WD.

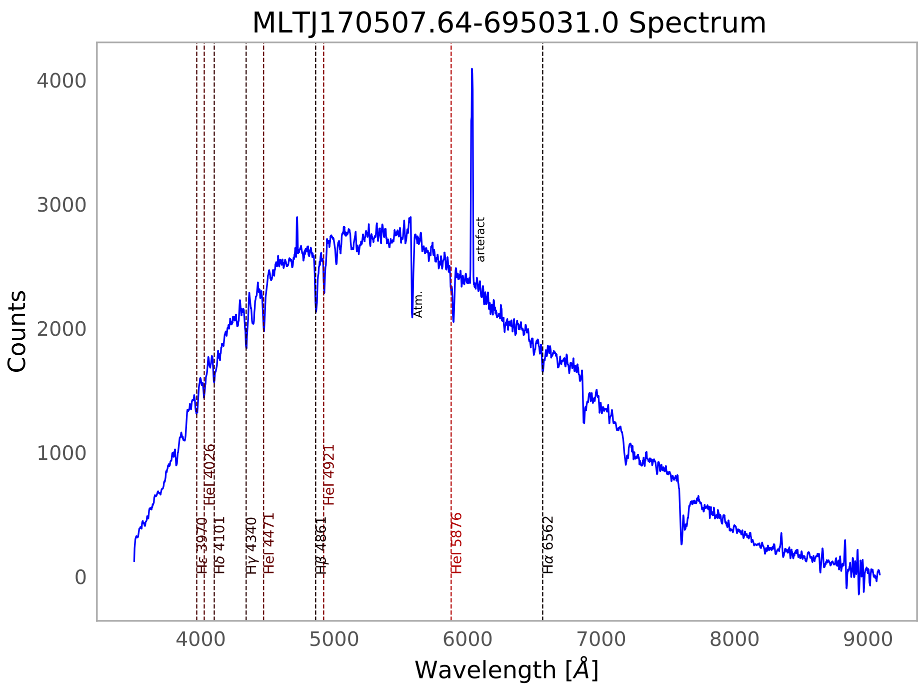

Figure 57: MLTJ170507.64–695031.0.

5 Conclusions and Discussion

5.1 Summary of selection process

5.1.1 Statistics

We performed a colour-based selection process on the MeerLICHT Southern All-Sky Survey (ML SASS) as a means to find candidate AM CVn stars. The criteria for this colour selection were based off of a similar project conducted with the Sloan Digital Sky Survey (SDSS) [21]. Various shifts were applied to the colour criteria in order to make them relevant for the ML SASS data. Our original selection box was slightly under-corrected from the SDSS filter system into the MeerLICHT filter system and was thus out of place and larger than intended. Once the box was corrected as discussed in Section 2.1.3, 79 true primary candidates were found, 77 of which were already in the primary candidates selected previously. The candidate selection process was conducted every few months during the last two years and had yielded 251 primary candidates with the full colour selection and over 300 primary candidates without the i band colours. The last candidate selection process was run in December 2021 and by that time ML SASS had covered ≈ 9041 square degrees in the five filters used for the full colour selection criteria, and ≈ 12254 square degrees when excluding the i band. Each individual MeerLICHT field covers 1.65×1.65 square degrees. The total sample size of stars which were run through the full selection process is roughly 3.5 million stars, and the number of stars in the sample size without the i band is roughly 4.1 million. The percentages of the observable sky which has been observed by ML SASS thus far are shown in Table 7. However, this is a slight underestimate of the percentage covered as there are some fields which overlap.

Table 7: Rough percentages of Southern sky covered by ML SASS

Filters	**Observed Fields**	**Coverage [deg.^{2}]**	**Total Fields**	**Percentage %**
$ugriq$	3321	9041.42	12741	26.06
$ugrq$	4801	12253.97	12741	37.68

5.1.2 Sorting the candidates

The follow-up to this selection process was a campaign of observation with both photometry and spectroscopy. In order to make this more manageable the candidates were sorted into a form of priority. By making use of a table of known AM CVns from Ramsay et al. [4], we had already added an absolute magnitude cutoff to the selection criteria, $M_G > 5$ and $M_U > 5$, allowing us to have primary candidates which were below the cutoff and secondary candidates which were brighter than the cutoff. This was made possible using GAIA parallaxes. A further prioritisation was made by ordering the primary candidates by the percentage error of their parallaxes, with a focus on targets which had parallax errors less than 30% the size of their parallax.

5.1.3 Expectation for space density of AM CVn systems

In order to estimate the approximate number of AM CVn systems we should detect based on our coverage of sky, we made use of the distance modulus to estimate a distance out to which we were sensitive. The faintest star we could observe spectroscopically with the 1.9-m was roughly 17th apparent magnitude (m), and the faintest absolute magnitude (M) star we observed was 12th magnitude. This gives us an approximate distance of sensitivity of:

$$
\begin{aligned}
M - m &= 5 - 5\log d \\
12 - 17 &= 5 - 5\log d \\
-5 &= 5 - 5\log d \\
\therefore \log d &= 2 \\
d &= 10^2 \\
d &= 100 \text{ pc}
\end{aligned}
$$

Thus our distance of sensitivity is $d_{sens} = 100$ pc at 17th magnitude for $M_G = 12$. We then use this distance for calculating the volume of space from which our targets where selected. The formula for this volume is:$V = \frac{1}{3}A \times d_{sens}$. Where A is the total area of sky observed in pc^2. To calculate A, we know that our total coverage in degrees squared is 9041.42 and we know that 1 degree on sky at a distance of 100 pc is $1 \times 3600 \times 100 = 360000$ AU = 1.745 pc. Therefore in square parsecs, the area covered on sky is $A = 9041.41 \times 1.745^2 = 27531.35$ pc^2. Therefore, the volume covered is:

$$
\begin{aligned}
V &= \frac{1}{3}(27531.35 \times 100) \\
V &= 9.18 \times 10^5 \text{pc}^3
\end{aligned}
$$

The current best estimate for the observed space density of AM CVn binary systems is $\rho = 5 \pm 3 \times 10^{-7}$pc^3 which comes from Carter et al. [22]. Therefore, the approximate number of systems we should detect in our observed volume thus far is:

$$
\begin{aligned}
N &= \rho \times V \\
N &= (5 \times 10^{-7}) \times (9.18 \times 10^5) \\
N &\simeq 0.459 \text{ systems out to 100 pc}
\end{aligned}
$$

This is our most conservative lower limit, if we however set our limit for absolute magnitude a bit brighter at say $M_G = 10$, then repeating the above calculations gives us an estimate of $N \simeq 7.275$ systems at 251.18 pc.

5.2 Photometry and Spectroscopy results

From our *ugriq* and *ugrq* primary target lists, we observed over 100 targets photometrically with 98 of them producing clean and usable lightcurves with a few duplicate observations. The photometry was conducted with two 1.0-m telescopes at the SAAO observatory in Sutherland, the new Lesedi telescope and the old 1.0-m telescope (sometimes referred to as the 40-inch telescope). Spectroscopically, we observed 155 targets which produced 94 usable and viable spectra of individual targets. The spectra were obtained with the 1.9-m telescope and a longslit spectrograph in Sutherland. There are 39 targets which have both a lightcurve and a spectrum, which leaves 55 targets with a spectrum without a matching lightcurve and 49 targets with a lightcurve but without a matching spectrum. All the observed targets with both spectroscopy and photometry can be found in Appendix B, those with only photometry in Appendix C, and the targets with only spectroscopy in Appendix D.

5.2.1 Summary of interesting results

In the Photometry chapter, seven targets were picked out for potential variability in their lightcurves, and in the Spectroscopy chapter, 12 targets were displayed for potential Helium lines and other interesting features in their spectra. Here we address the matching spectrum or lightcurve, where available, for those targets which were deemed interesting.

- **MLTJ040830.70–542139.7**: spectrum showing weak HeI absorption lines in Figure 46, however, the lightcurve shows no discernible features and the periodogram has no clear peaks. The lack of helium or metal emission lines in its spectrum combined with the lack of variability in the lightcurve makes it highly unlikely this object is an AM CVn.
- **MLTJ053541.03–685734.4**: MLTJ053541.03–685734.4, which is a well-known CV, TW Pictoris, shows clear variability in its lightcurve and peaks in its periodogram in Figure 26. The spectrum seen in Figure 45 shows clear Balmer and HeI emission.
- **MLTJ065449.05–791843.1**: spectrum showing HeI and Balmer absorption in Figure 47, but the lightcurve and periodogram show no signs of variability. The presence of hydrogen rules MLTJ065449.05–791843.1 out from being classified an AM CVn.
- **MLTJ080401.92–211831.9**: lightcurve and periodogram show some evidence of variability in Figure 30, spectrum shows narrow Balmer emission lines seen in Figure 58. Once again the presence of hydrogen in the spectrum indicates this object is not an AM CVn.
- **MLTJ111845.64–420550.0**: spectrum shows a lack of hydrogen, but HeI absorption in Figure 50, however, the lightcurve and periodogram show no indication of variability. The lack of helium or metal emission lines in the spectrum makes it unlikely to be an AM CVn, however, its spectral features are typical for a DB type white dwarf (WD).
- **MLTJ112405.68–431729.4**: spectrum shows minor HeI and H absorption in Figure 51, however, the lightcurve and periodogram have no clear signs of variability. The lack of helium emission and the presence of Hβ means this object cannot be an AM CVn.
- **MLTJ121558.78–491453.4**: lightcurve and periodogram show strong indications of variability in Figure 32 and the spectrum has clear signs of Balmer absorption as seen in Figure 59. The presence of hydrogen prevents this object being classified an AM CVn.
- **MLTJ144139.77–161530.4**: spectrum shows Balmer and HeI absorption lines seen in Figure 55, but the lightcurve and periodogram display no level of variability. Once again, hydrogen lines in the spectrum means this object is not an AM CVn. However, its spectral features indicate a potential classification as a sdB or sdF subdwarf.
- **MLTJ170507.64–695031.0**: Balmer and HeI absorption lines seen in the spectrum in Figure 57, however, there is no indication of variability in the lightcurve or periodogram. Balmer lines in the spectrum indicates this object is not an AM CVn.
- **MLTJ203654.63–432231.6**: MLTJ203654.63–432231.6 is a well-known CV, CM Mic. It has clear signs of variability in its lightcurve and periodogram as seen in Figure 36, while the spectrum shows Balmer absorption as seen in Figure 60.

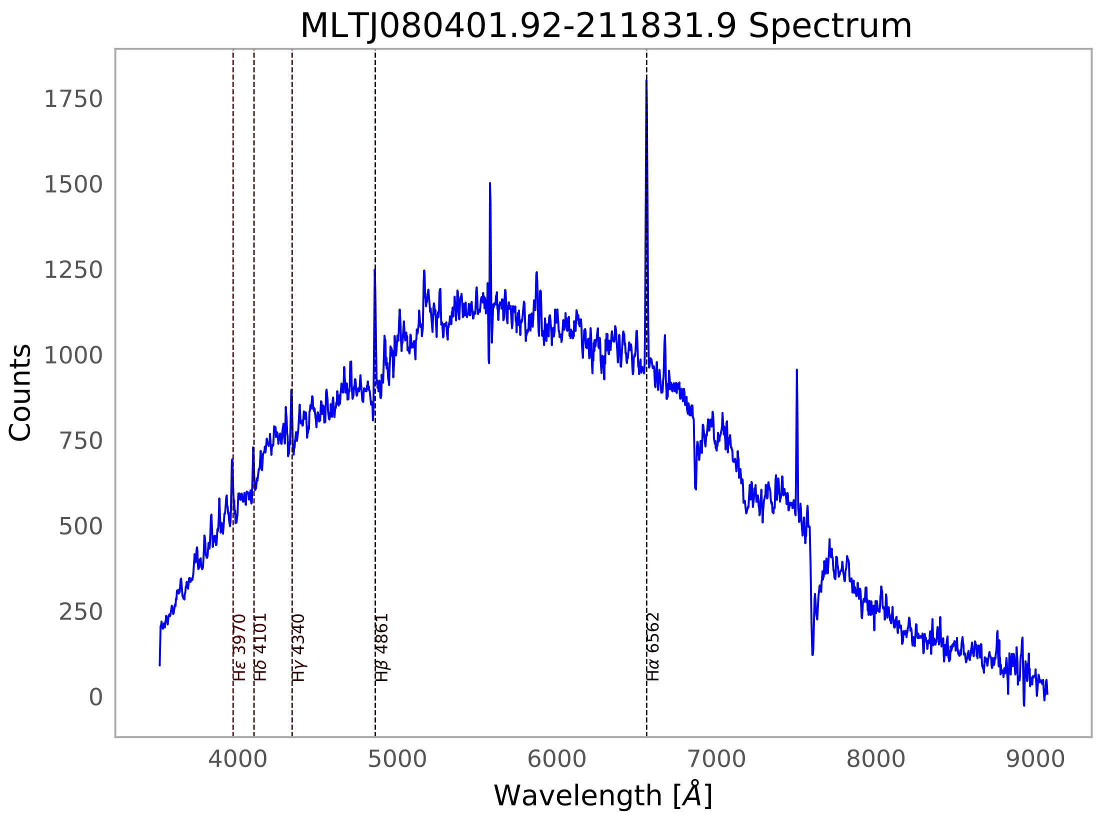

Figure 58: Spectrum of MLTJ080401.92–211831.9.

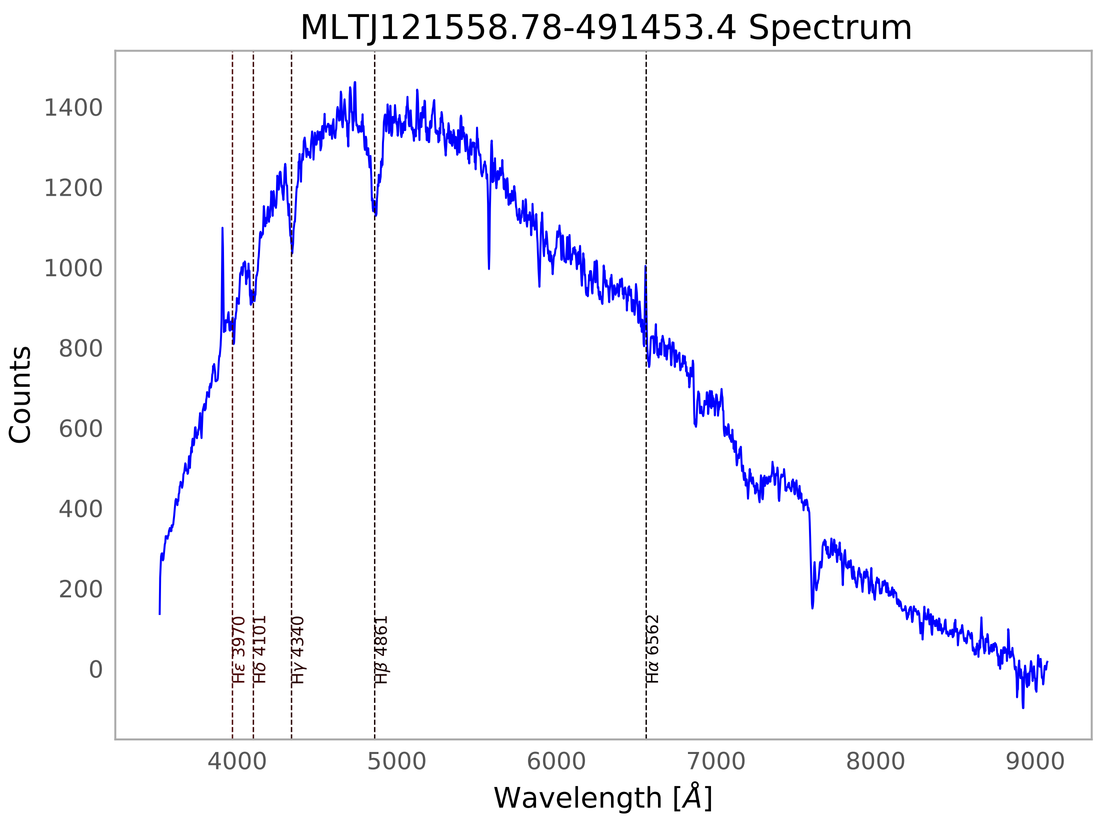

Figure 59: Spectrum of MLTJ121558.78–491453.4.

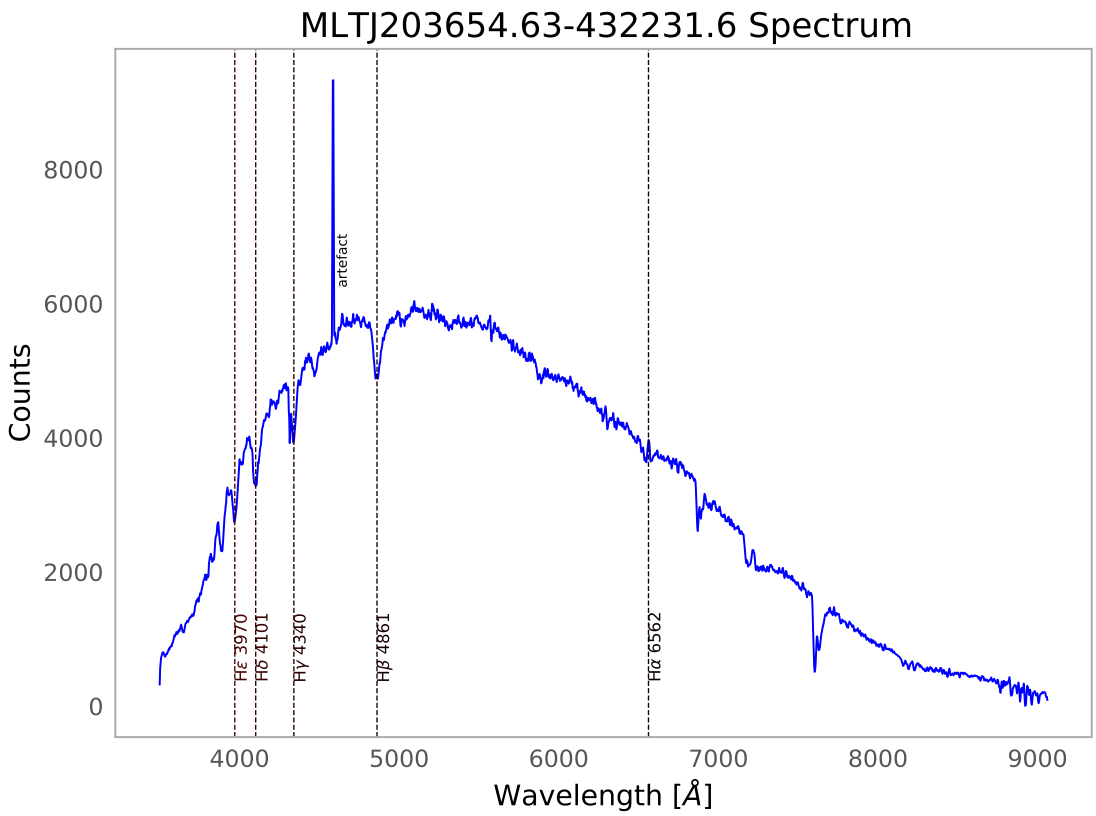

Figure 60: Spectrum of MLTJ203654.63–432231.6.

Three other candidates which deserve a special mention are MLTJ090257.69–075919.8 (MLTJ0902–0759), MLTJ124848.88–344208.5 (MLTJ1248–3442) and MLTJ230816.36–042339.3 (MLTJ2308–0423). These objects were marked as potentially interesting in either the Photometry or Spectroscopy chapter, however, they do not have a matching lightcurve or spectrum.

MLTJ0902–0759 shows a clean spectrum in Figure 48 with strong Balmer and HeI emission lines as opposed to absorption lines. These features are typical of a CV and a direct comparison can be drawn to the known CV TW Pic's spectrum seen in Figure 45. We have not been able to search for any variability as we have not observed this object photometrically yet.

MLTJ1248–3442 has the only spectrum which seems to display lines other than hydrogen or helium, it shows what may be FeII and SiII emission lines as well as HeI emission and Balmer absorption lines in Figure 53. There are also multiple unidentified emission lines. The presence of hydrogen would seem to indicate this object is not an AM CVn, however, the presence of multiple emission lines means this object bears further investigation. Unfortunately, we have not obtained a lightcurve for this object yet so we were unable to search for any photometric variability. It is also unknown in literature.

MLTJ2308–0423 shows some interesting variability as seen in the lightcurves and periodograms in Figures 38 and 40 from two nights of observation, and in Figure 61 we have combined these two nights. The variability seen in its lightcurves is very similar to the variability seen in the lightcurve for TW Pic, a known CV, seen in Figure 26a, which would further ratify MLTJ2308–0423's potential classification as a magnetic CV. Unfortunately, we do not have a usable spectrum for this object yet.

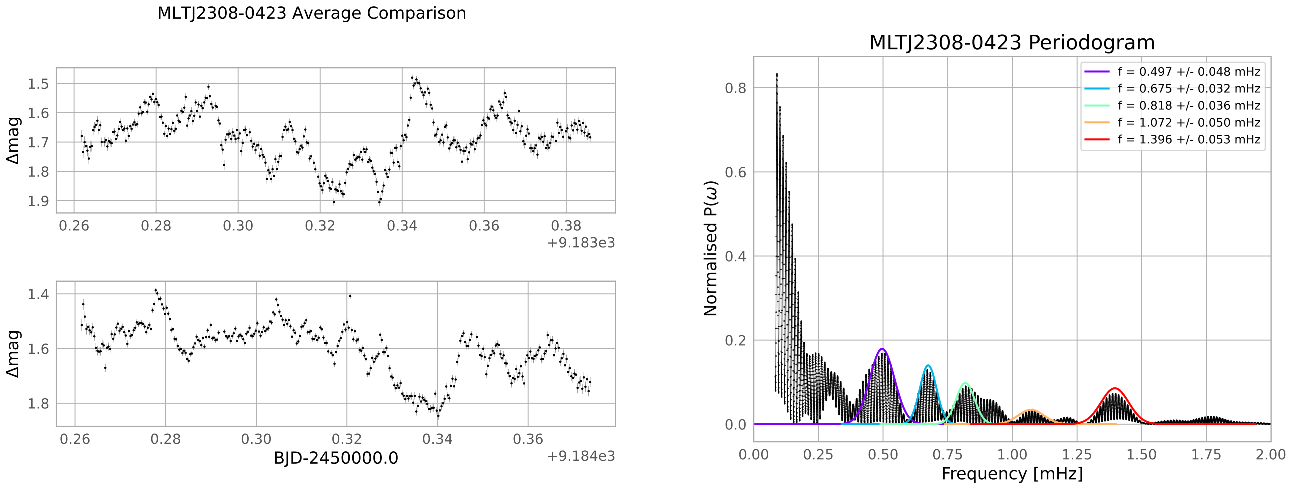

(a) Weighted average differential lightcurve.

(b) Periodogram.

Figure 61: Combined lightcurve and periodogram for MLTJ230816.36–042339.3 for both nights of observations

In Figure 61 we see the combined lightcurve and periodogram of MLTJ2308–0423 showing peaks at f = $0.497, 0.675, 0.818, 1.072, 1.396$ mHz corresponding to periods of $P = 33.560, 24.704, 20.366, 15.545, 11.936$ minutes. We note MLTJ2308–0423 as a potential magnetic CV based off of the lightcurve shape and detected possible periodicity.

5.2.2 Achieved space density of AM CVn systems

Our total number of true primary candidates from the $ugriq$ corrected colour selection criteria was 79 and thus far we have observed 19 of them spectroscopically. For our true primary candidates, the observed ratio is thus 0.24. If we apply that to our approximate range of detected AM CVn systems of 0.459 to 7.275, we should have detected between 0.110 and 1.746 AM CVn systems thus far. However, we have not found any yet which is not unreasonable given our low ratio of coverage for our true primary candidates. There are a further 76 additional targets from the original selection box and from the $ugrq$ colour selection criteria which have also been observed spectroscopically. If we add those to the observed true primary candidates and factor in the total number of candidates across the board we have a smaller ratio of 95/481 which is 0.19, which gives us an even smaller chance of having detected an AM CVn system at this point.

5.3 Methods to improve future work

While we have been unsuccessful in discovering any new AM CVn stars, a great deal has been learnt about the approach to finding these rare ultra-compact binaries. The original project upon which our selection criteria were based had a final candidate sample size of 1523 stars, out of which they theorised, based on available data at the time, Roelofs et al. could detect roughly 40 new AM CVns [21]. That would imply that 1 in approximately every 38 observed candidates could be a new AM CVn. By 2013, further work on this project had narrowed their sample size down to roughly 1100 stars which contained known quasars, white dwarfs, subdwarfs and other known objects [22]. Roughly 400 objects were left as unknown. Given that the campaign of follow-up conducted by Roelofs et al. was largely spectroscopic, a comparison can be drawn between the spectroscopic success rates. Of our 79 true candidates, only 19 were observed spectroscopically and we detected zero new AM CVn binaries. However, it is also worth noting that while the original Roelofs et al. selection criteria could select all those stars which were brighter than $g = 20.5$ apparent magnitude in

SDSS, we were limited by the limiting magnitude of the individual filters of MeerLICHT in a 60s exposure. The most limiting filter was the u band as it has a limiting magnitude of roughly 18/19th magnitude in a single 60s exposure, with our faintest selected target being MLTJ033755.07–351342.3 with $u = 19.10$ and $g = 19.16$. Given the nature of the selection criteria, an object is required to be detected in the u, g, r and i bands. For some fields, this limiting magnitude was fainter as that particular field had more stacked exposures but for the vast majority of fields there was just one or two exposures in each filter. With time and more exposures for each field in the ML SASS, this limiting magnitude will be pushed to fainter magnitudes as more stacking can be done and we can go deeper.

5.3.1 Selection criteria

The selection criteria that the original SDSS project used were based on the available information about known AM CVns, however, the large majority of the known systems at that time were from the northern hemisphere of sky, i.e. a declination of above $0°$. At the time of their selection in 2009, there were only 21 known AM CVns, and only 6 of them had data in the SDSS spectroscopic database. With the much larger sample size of known AM CVn stars of today, including those recently found by surveys such as the search for AM CVns conducted by the Zwicky Transient Facility (ZTF) [32], we could create an entirely new set of colour selection criteria. From our table of the known AM CVn systems detected in MeerLICHT, Table 1 in Section 2.1.2, we see 5 sources with magnitudes in u, g, r, and i, however, none of them were selected with our colour selection technique, as can be seen in Figures 12 and 14. This would imply that the selection box is in need of an update. Two of the known AM CVn sources (V803 Cen and V396 Hya), are clearly too red for the current selection box, however, the other three targets only lie just outside the current box which would imply that a minor increase in the selection region would have caught them. Then with our new colour selection criteria we could begin again, ensuring that if there is any overlap with our old selected and observed targets, we remove them in order to avoid following up on targets we have already ruled out. However, it is also possible that the colour selection process is not the most efficient and that we should rather be performing a similar search for blue, outbursting systems like ZTF, and then using those systems as candidates. After which we could then extract the MeerLICHT photometry where available to create a priority list out of those candidates.

5.3.2 MeerLICHT photometry

One alternative method for searching for candidates is to use the available MeerLICHT photometry on fields which have been observed on multiple occasions. On the MeerZICHT database, one can extract the lightcurves for each filter constructed from available photometric measurements for a given target. Thus the more a field has been observed, the more photometric data there is to populate the lightcurves. To perform an initial check of our candidates, we could extract the long-term lightcurves for candidates which have multiple MeerLICHT observations, as a means of searching for any longer term variability. Or we could use existing databases such as Asteroid Terrestrial-impact Last Alert System (ATLAS) or All-Sky Automated Survey for Supernovae (ASAS-SN) to perform variability checks, which were not publicly available at the start of this project but are now. Alternatively, the approach to finding candidates could start by searching all those fields with multiple observations for stellar objects within which show any variability in their lightcurves and then select those which do as candidates for potential follow-up.

5.3.3 Spectroscopy vs. Photometry

The final question worth addressing is the approach to follow-up after having selected the candidates. Our approach has been largely focused on a photometric analysis, performing Lomb-Scargle periodograms on approximately three hour long lightcurves. The spectroscopy that we obtained served more as a rough classification method to support any classifications we might have been able to make from potential variability in the lightcurves. However, it is possible for AM CVn stars to not show any short-term variability on a timescale of three hours if they are not eclipsing or if they are not in outburst. By the end of our project we had obtained more usable spectra than lightcurves and so our approach might have been more efficient if we had used the spectroscopy as a means of narrowing down our candidates with a rough classification first, and then following up photometrically on those candidates. Alternatively, we could run an initial photometric check on already existing data such as that available with the ATLAS [68] forced photometry server [69] or ASAS-SN. We could increase the size of our initial selection box and create a much larger list of primary candidates and then run those candidates through the server to such for any short- or long-term variability. Those targets which display variability can then be prioritised for more focused photometric and spectroscopic follow-up. One drawback of the ATLAS project is that it currently only surveys the sky north of declinations of –50°, however, with the currently ongoing installation and commissioning of new ATLAS telescopes in Chile and at the Sutherland site in South Africa, soon the whole sky will be visible to ATLAS. Another drawback of this approach using ATLAS or ASAS-SN is that it would find merely the outbursting AM CVn systems which have a orbital range of roughly 20 to 45 minutes and would most likely not find any of the longer period quiescent systems which never go into outburst. These longer period systems have a orbital period of longer than roughly 40 minutes and require spectroscopy to identify helium and metal emission lines. The different methods that can be used to find new AM CVn systems have different subsets of the whole class of systems that they could identify.

References

[1] CSIRO. **Binary Stars**. https://www.atnf.csiro.au/outreach/education/senior/astrophysics/binary_intro.html. Accessed: 23-01-2022.

[2] G. Nelemans. **Ultracompact binary stars.** *Physics Today*, 59(7):7.26, January 2006.

[3] J. E. Solheim. **AM CVn Stars: Status and Challenges**. *Publications of the Astronomical Society of the Pacific*, 122(896):1133, October 2010.

[4] G. Ramsay, M. J. Green, T. R. Marsh, T. Kupfer, E. Breedt, V. Korol, P. J. Groot, C. Knigge, G. Nelemans, D. Steeghs, P. Woudt, and A. Aungwerojwit. **Physical properties of AM CVn stars: New insights from Gaia DR2**. *Astronomy & Astrophysics*, 620:A141, December 2018.

[5] P. A. Mazzali, F. K. Röpke, S. Benetti, and W. Hillebrandt. **A Common Explosion Mechanism for Type Ia Supernovae**. *Science*, 315(5813):825, February 2007.

[6] P. Amaro-Seoane et al. **Laser Interferometer Space Antenna**. *arXiv e-prints*, page arXiv:1702.00786, February 2017.

[7] T. Kupfer, V. Korol, S. Shah, G. Nelemans, T. R. Marsh, G. Ramsay, P. J. Groot, D. T. H. Steeghs, and E. M. Rossi. **LISA verification binaries with updated distances from Gaia Data Release 2**. *Monthly Notices of the Royal Astronomical Society*, 480(1):302–309, October 2018.

[8] H. C. Campbell et al. **Total eclipse of the heart: the AM CVn Gaia14aae/ASSASN-14cn**. *Monthly Notices of the Royal Astronomical Society*, 452(1):1060–1067, September 2015.

[9] D. Levitan, T. Kupfer, P. J. Groot, B. Margon, T. A. Prince, S. R. Kulkarni, G. Hallinan, L. K. Harding, G. Kyne, R. Laher, E. O. Ofek, R. G. M. Rutten, B. Sesar, and J. Surace. **PTF1 J191905.19+481506.2—a Partially Eclipsing AM CVn System Discovered in the Palomar Transient Factory**. *Astrophysical Journal*, 785(2):114, April 2014.

[10] K. Bąkowska, T. R. Marsh, D. Steeghs, G. Nelemans, and P. J. Groot. **Spectroscopy of the helium-rich binary ES Ceti reveals accretion via a disc and evidence of eclipses**. *Astronomy & Astrophysics*, 645:A114, January 2021.

[11] S. F. Anderson et al. **Ultracompact AM Canum Venaticorum Binaries from the Sloan Digital Sky Survey: Three Candidates Plus the First Confirmed Eclipsing System**. *The Astronomical Journal*, 130(5):2230–2236, November 2005.

[12] J. van Roestel, T. Kupfer, M. J. Green, S. Wong, L. Bildsten, K. Burdge, T. Prince, T. R. Marsh, P. Szkody, C. Fremling, M. J. Graham, V. S. Dhillon, S. P. Littlefair, E. C. Bellm, M. Coughlin, D. A. Duev, D. A. Goldstein, R. R. Laher, B. Rusholme, R. Riddle, R. Dekany, and S. R. Kulkarni. **Discovery and characterization of five new eclipsing AM CVn systems**. *Monthly Notices of the Royal Astronomical Society*, August 2021.

[13] G. Nelemans. **AM CVn stars**. In *The Astrophysics of Cataclysmic Variables and Related Objects*, volume 330 of *Astronomical Society of the Pacific Conference Series*, page 27, August 2005.

[14] G. Nelemans, S. F. Portegies Zwart, F. Verbunt, and L. R. Yungelson. **Population synthesis for double white dwarfs. II. Semi-detached systems: AM CVn stars**. *Astronomy and Astrophysics*, 368:939–949, March 2001.

[15] Jr. Iben, Icko and Alexander V. Tutukov. **Helium Star Cataclysmics**. *The Astrophysical Journal*, 370:615, April 1991.

[16] Ph. Podsiadlowski, Z. Han, and S. Rappaport. **Cataclysmic variables with evolved secondaries and the progenitors of AM CVn stars**. *Monthly Notices of the Royal Astronomical Society*, 340(4):1214–1228, April 2003.

[17] K. Inight, Boris T. Gänsicke, E. Breedt, T. R. Marsh, A. F. Pala, and R. Raddi. **Towards a volumetric census of close white dwarf binaries - I. Reference samples**. *Monthly Notices of the Royal Astronomical Society*, 504(2):2420–2442, June 2021.

[18] Gaia Collaboration et al. **Gaia Data Release 2. Summary of the contents and survey properties**. *Astronomy and Astrophysics*, 616:A1, August 2018.

[19] G. H. A. Roelofs, G. Nelemans, and P. J. Groot. **The population of AM CVn stars from the Sloan Digital Sky Survey**. *Monthly Notices of the Royal Astronomical Society*, 382(2):685–692, December 2007.

[20] B. W. Carroll and D. A. Ostlie. ***An Introduction to Modern Astrophysics***. Pearson, 2nd edition, 2014.

[21] G. H. A. Roelofs, P. J. Groot, D. Steeghs, A. Rau, E. de Groot, T. R. Marsh, G. Nelemans, J. Liebert, and P. Woudt. **SDSSJ080449.49+161624.8: a peculiar AM CVn star from a colour-selected sample of candidates**. *Monthly Notices of the Royal Astronomical Society*, 394(1):367–374, March 2009.

[22] P. J. Carter, T. R. Marsh, D. Steeghs, P. J. Groot, G. Nelemans, D. Levitan, A. Rau, C. M. Copperwheat, T. Kupfer, and G. H. A. Roelofs. **A search for the hidden population of AM CVn binaries in the Sloan Digital Sky Survey**. *Monthly Notices of the Royal Astronomical Society*, 429(3):2143–2160, March 2013.

[23] A. J. Drake, S. G. Djorgovski, A. Mahabal, E. Beshore, S. Larson, M. J. Graham, R. Williams, E. Christensen, M. Catelan, A. Boattini, A. Gibbs, R. Hill, and R. Kowalski. **First Results from the Catalina Real-Time Transient Survey**. *Astrophysical Journal*, 696(1):870–884, May 2009.

[24] E. Breedt, B. T. Gänsicke, A. J. Drake, P. Rodríguez-Gil, S. G. Parsons, T. R. Marsh, P. Szkody, M. R. Schreiber, and S. G. Djorgovski. **1000 cataclysmic variables from the Catalina Real-time Transient Survey**. *Monthly Notices of the Royal Astronomical Society*, 443(4):3174–3207, October 2014.

[25] D. Levitan, T. Kupfer, P. J. Groot, S. R. Kulkarni, T. A. Prince, G. V. Simonian, I. Arcavi, J. S. Bloom, R. Laher, P. E. Nugent, E. O. Ofek, B. Sesar, and J. Surace. Five new outbursting AM CVn systems discovered by the Palomar Transient Factory. *Monthly Notices of the Royal Astronomical Society*, 430(2):996–1007, April 2013.

[26] B. Margon, D. Levitan, T. A. Prince, G. Hallinan, and PTF Collaboration. **Magnetic Cataclysmic Variables Discovered in the Palomar Transient Factory**. In *Stellar Novae: Past and Future Decades*, volume 490 of *Astronomical Society of the Pacific Conference Series*, page 389, December 2014.

[27] ASAS-SN Team. **All-Sky Automated Survey for Supernovae**. https://www.astronomy.ohio-state.edu/asassn/index.shtml. Accessed: 02-02-2021.

[28] E. Breedt. **An update on the AM CVn family**. In *The Golden Age of Cataclysmic Variables and Related Objects - III (Golden2015)*, page 25, January 2015.

[29] T. Kato and N. Kojiguchi. **New candidates for AM Canum Venaticorum stars among ASAS-SN transients**. *Publications of the Astronomical Society of Japan*, 73(5):1375–1381, Aug 2021.

[30] E. C. Bellm et al. **The Zwicky Transient Facility: System Overview, Performance, and First Results**. *Publications of the Astronomical Society of the Pacific*, 131(995):018002, January 2019.

[31] F. J. Masci et al. **The Zwicky Transient Facility: Data Processing, Products, and Archive**. *Publications of the Astronomical Society of the Pacific*, 131(995):018003, January 2019.

[32] J. van Roestel, L. Creter, T. Kupfer, P. Szkody, J. Fuller, M. J. Green, R. M. Rich, J. Sepikas, K. Burdge, I. Caiazzo, et al. **A Systematic Search for Outbursting AM CVn Systems with the Zwicky Transient Facility**. *The Astronomical Journal*, 162(3):113, Aug 2021.

[33] Coel Hellier. ***Cataclysmic Variable Stars***. Praxis Publishing Ltd., 2001.

[34] K. P. Singh. **X-ray emission from magnetic cataclysmic variables**. In *Recent Trends in the Study of Compact Objects: Theory and Observation*, volume 8 of *Astronomical Society of India Conference Series*, pages 115–122, 2013.

[35] A. J. Drake et al. **Cataclysmic variables from the Catalina real-time transient survey**. *Monthly Notices of the Royal Astronomical Society*, 441(2):1186–1200, 2014.

[36] G. Chanmugam and G. A. Dulk. **Radio emission from AM Herculis-type binaries**. *The Astrophysical Journal*, 255:L107, 1982.

[37] Brian Warner. ***Cataclysmic Variable Stars***. Cambridge Univ. Press, Cambridge, UK, 2003.

[38] T. R. Marsh, V. S. Dhillon, and S. R. Duck. **Low-Mass White Dwarfs Need Friends - Five New Double-Degenerate Close Binary Stars**. *Monthly Notices of the Royal Astronomical System*, 275:828, August 1995.

[39] W. R. Brown, M. J. Geller, and S. J. Kenyon. **MMT Hypervelocity Star Survey**. *The Astrophysical Journal*, 690(2):1639–1647, January 2009.

[40] W. R. Brown, M. J. Geller, and S. J. Kenyon. **MMT Hypervelocity Star Survey. II. Five New Unbound Stars**. *The Astrophysical Journal*, 751(1):55, May 2012.

[41] W. R. Brown, M. Kilic, S. J. Kenyon, and A. Gianninas. **Most Double Degenerate Low-mass White Dwarf Binaries Merge**. *The Astrophysical Journal*, 824(1):46, June 2016.

[42] W. R. Brown, A. Gianninas, M. Kilic, S. J. Kenyon, and C. Allende Prieto. **The ELM Survey. VII. Orbital Properties of Low-Mass White Dwarf Binaries**. *The Astrophysical Journal*, 818(2):155, February 2016.

[43] L. Bildsten, K. J. Shen, N. N. Weinberg, and G. Nelemans. **Faint Thermonuclear Supernovae from AM Canum Venaticorum Binaries**. *The Astrophysical Journal*, 662(2):L95–L98, June 2007.

[44] R. P. Fender. **Powerful jets from black hole X-ray binaries in low/hard X-ray states**. *Monthly Notices of the Royal Astronomical Society*, 322:31–42, 2001.

[45] E. G. Körding, R. P. Fender, and S. Migliari. **Jet-dominated advective systems: Radio and X-ray luminosity dependence on the accretion rate**. *Monthly Notices of the Royal Astronomical Society*, 369(3):1451–1458, 2006.

[46] E. F. Schlafly and D. P. Finkbeiner. **Measuring Reddening with Sloan Digital Sky Survey Stellar Spectra and Recalibrating SFD**. *Astrophysical Journal*, 737(2):103, August 2011.

[47] Astropy Collaboration. **Astropy: A community Python package for astronomy**. *Astronomy & Astrophysics*, 558:A33, October 2013.

[48] C. Rodrigo and E. Solano. **The SVO Filter Profile Service**. In *XIV.0 Scientific Meeting (virtual) of the Spanish Astronomical Society*, page 182, July 2020.

[49] P. Virtanen, R. Gommers, T. E. Oliphant, M. Haberland, T. Reddy, D. Cournapeau, E. Burovski, P. Peterson, W. Weckesser, J. Bright, S. J. van der Walt, M. Brett, J. Wilson, K. J. Millman, N. Mayorov, A. R. J. Nelson, E. Jones, R. Kern, E. Larson, C. J. Carey, İ. Polat, Y. Feng, E. W. Moore, J. VanderPlas, D. Laxalde, J. Perktold, R. Cimrman, I. Henriksen, E. A. Quintero, C. R. Harris, A. M. Archibald, A. H. Ribeiro, F. Pedregosa, P. van Mulbregt, and SciPy 1.0 Contributors. **SciPy 1.0: Fundamental Algorithms for Scientific Computing in Python**. *Nature Methods*, 17:261–272, 2020.

[50] SAAO. **SHOC: Sutherland High Speed Optical Cameras**. https://www.saao.ac.za/astronomers/shoc/. Accessed: 05-03-2021.

[51] SAAO. **1.0m Telescope**. https://www.saao.ac.za/astronomers/1-0m/. Accessed: 05-03-2021.

[52] SAAO. **Lesedi**. https://www.saao.ac.za/astronomers/lesedi/. Accessed: 05-03-2021.

[53] Joannes Van Roestel. **Eclipsing white dwarfs discovered by the Zwicky Transient Factory**. In G. H. Tovmassian and B. T. Gansicke, editors, *Compact White Dwarf Binaries*, page 17, September 2019.

[54] D. M. Bowman and D. L. Holdsworth. **Adaptive elliptical aperture photometry: A software package for high-cadence ground-based photometry. I. Application to rapid oscillators observed from SAAO**. *Astronomy & Astrophysics*, 629:A21, September 2019.

[55] Kyle Barbary. **SEP: Source Extractor as a library**. *Journal of Open Source Software*, 1(6):58, 2016.

[56] J. D. Hunter. **Matplotlib: A 2D Graphics Environment**. *Computing in Science Engineering*, 9(3):90–95, 2007.

[57] J. D. Hartman and G. Á. Bakos. **VARTOOLS: A program for analyzing astronomical time-series data**. *Astronomy and Computing*, 17:1–72, October 2016.

[58] M. Zechmeister and M. Kürster. **The generalised Lomb-Scargle periodogram. A new formalism for the floating-mean and Keplerian periodograms**. *Astronomy & Astrophysics*, 496(2):577–584, March 2009.

[59] W. H. Press, S. A. Teukolsky, W. T. Vetterling, and B. P. Flannery. ***Numerical recipes in C. The art of scientific computing***. Cambridge University Press, 1992.

[60] A. J. Norton, A. P. Beardmore, A. Retter, and D. A. H. Buckley. **The nature of TW Pictoris**. *Monthly Notices of the Royal Astronomical Society*, 312(2):362–370, February 2000.

[61] A. Chen, D. O'Donoghue, R. S. Stobie, D. Kilkenny, and B. Warner. **Cataclysmic variables in the Edinburgh-Cape Blue Object Survey**. *Monthly Notices of the Royal Astronomical Society*, 325(1):89–110, July 2001.

[62] L. A. Crause, D. Gilbank, C. van Gend, H. L. Worters, C. Sass, E. J. Kotze, S. Potter, A. Sickafoose, R. Sefako, J. Southworth, L. Macri, J. Thorstensen, C. Galan, P. Skelton, C. Engelbrecht, I. Braker, H. Winkler, D. Pieńkowski, D. Sürgit, A. Erdem, and M. Burleigh. **SpUpNIC (Spectrograph Upgrade: Newly Improved Cassegrain): a versatile and efficient low- to medium-resolution, long-slit spectrograph on the South African Astronomical Observatory's 1.9-m telescope**. *Journal of Astronomical Telescopes, Instruments, and Systems*, 5:024007, April 2019.

[63] SAAO. **1.9m Telescope**. https://www.saao.ac.za/astronomers/1-9m/. Accessed: 22-01-2021.

[64] R. Coppejans, A. A. S. Gulbis, M. M. Kotze, D. L. Coppejans, H. L. Worters, P. A. Woudt, H. Whittal, J. Cloete, and P. Fourie. **Characterizing and Commissioning the Sutherland High-Speed Optical Cameras (SHOC)**. *Publications of the Astronomical Society of the Pacific*, 125(930):976, August 2013.

[65] Naomi Titus. **Titus_Saures_Rex_Spectroscopic_Routines**. https://github.com/NaomiTitus/Titus_Saures_Rex_Spectroscopic_Routines. Accessed: 23-11-2021.

[66] Pieter G. van Dokkum. **Cosmic-Ray Rejection by Laplacian Edge Detection**. *The Publications of the Astronomical Society of the Pacific*, 113(789):1420–1427, November 2001.

[67] N. P. Gentile Fusillo, P.-E. Tremblay, B. T. Gänsicke, C. J. Manser, T. Cunningham, E. Cukanovaite, M. Hollands, T. Marsh, R. Raddi, S. Jordan, S. Toonen, S. Geier, M. Barstow, and J. D. Cummings. **A Gaia Data Release 2 catalogue of white dwarfs and a comparison with SDSS**. *Monthly Notices of the Royal Astronomical Society*, 482(4):4570–4591, February 2019.

[68] J. L. Tonry, L. Denneau, A. N. Heinze, B. Stalder, K. W. Smith, S. J. Smartt, C. W. Stubbs, H. J. Weiland, and A. Rest. **ATLAS: A High-cadence All-sky Survey System**. *Publications of the Astronomical Society of the Pacific*, 130(988):064505, June 2018.

[69] ATLAS. **ATLAS Forced Photometry**. https://fallingstar-data.com/forcedphot/. Accessed: 25-01-2021.

A Tables of Primary Candidates

Table 8: 251 MeerLICHT $ugriq$ selected candidates.

MeerLICHT Name	RA (hh:mm:ss)	Dec. (dd:mm:ss)	u_ML	g_ML	r_ML	i_ML	q_ML	Parallax (mas)	Parallax error
MLTJ001758.84–391807.8	00:17:58.8413	–39:18:07.8284	18.638	18.598	18.763	18.945	18.714	5.40249	0.24691
MLTJ003026.87–585638.7	00:30:26.8742	–58:56:38.7007	15.663	15.804	16.078	16.354	15.982	11.92591	0.05509
MLTJ003326.19–733719.5	00:33:26.1994	–73:37:19.5594	16.374	16.285	16.355	16.378	16.278	0.73788	0.15100
MLTJ004526.65–732531.4	00:45:26.6598	–73:25:31.4579	16.321	16.457	16.666	16.865	16.491	0.62818	0.56903
MLTJ004707.65–721659.6	00:47:07.6538	–72:16:59.6093	17.308	17.275	17.425	17.512	17.393	0.35120	0.12222
MLTJ004808.01–731737.9	00:48:08.0192	–73:17:37.9868	16.818	16.937	17.206	17.440	17.199	-	-
MLTJ004809.84–212017.4	00:48:09.8415	–21:20:17.4597	18.568	18.546	18.659	18.846	18.676	4.48898	0.24707
MLTJ004916.80–721424.0	00:49:16.8045	–72:14:24.0185	15.796	15.965	16.310	16.611	16.182	-	-
MLTJ004926.12–731632.6	00:49:26.1213	–73:16:32.6877	15.649	15.769	15.931	16.089	15.926	-	-
MLTJ005012.56–721532.0	00:50:12.5675	–72:15:32.0925	16.003	16.139	16.308	16.391	16.288	-	-
MLTJ005149.73–733011.1	00:51:49.7352	–73:30:11.1864	17.087	17.100	17.213	17.318	17.283	0.60515	0.22267
MLTJ005251.16–731207.7	00:52:51.1675	–73:12:07.7208	16.301	16.410	16.519	16.685	16.534	–0.77415	0.32758
MLTJ005254.67–730315.7	00:52:54.6786	–73:03:15.7965	15.634	15.835	16.073	16.236	16.071	-	-
MLTJ005317.02–732759.7	00:53:17.0228	–73:27:59.7114	17.103	17.039	17.111	17.291	17.143	-	-
MLTJ005353.60–722201.4	00:53:53.6078	–72:22:01.4612	15.375	15.457	15.657	15.866	15.614	-	-
MLTJ005446.17–725750.0	00:54:46.1742	–72:57:50.0684	16.489	16.532	16.698	16.887	16.699	0.00330	0.05490
MLTJ005624.48–714022.0	00:56:24.4808	–71:40:22.0574	15.380	15.740	15.920	16.059	15.895	-	-
MLTJ005640.66–725635.9	00:56:40.663	–72:56:35.9325	17.037	17.077	17.141	17.191	17.116	-	-
MLTJ005703.43–720549.0	00:57:03.4393	–72:05:49.0183	16.765	16.827	17.034	17.211	17.005	-	-
MLTJ005729.58–722135.4	00:57:29.5848	–72:21:35.4219	16.598	16.605	16.661	16.822	16.690	0.50515	0.12689
MLTJ005741.18–721120.0	00:57:41.1817	–72:11:20.0136	14.817	15.005	15.347	15.656	15.211	0.05417	0.04513
MLTJ005816.17–720939.2	00:58:16.1797	–72:09:39.2879	16.486	16.712	16.821	16.944	16.839	-	-
MLTJ010036.86–725103.8	01:00:36.8609	–72:51:03.8431	16.336	16.415	16.654	16.871	16.631	0.74969	0.19861
MLTJ010441.59–720325.4	01:04:41.5927	–72:03:25.4345	16.444	16.527	16.780	17.022	16.664	-	-
MLTJ010507.31–723017.7	01:05:07.3139	–72:30:17.7658	14.930	15.030	15.270	15.436	15.190	-	-
MLTJ010804.95–714235.0	01:08:04.9538	–71:42:35.0769	15.350	15.318	15.437	15.504	15.407	-	-
MLTJ010816.88–722605.4	01:08:16.8889	–72:26:05.4814	15.449	15.665	16.052	16.323	15.924	-	-
MLTJ011332.83–731625.1	01:13:32.833	–73:16:25.1447	16.694	16.711	16.916	17.123	16.839	-	-
MLTJ011449.15–732457.6	01:14:49.1561	–73:24:57.6622	16.778	16.770	16.890	16.974	16.835	-	-
MLTJ011454.49–731254.6	01:14:54.4979	–73:12:54.6496	15.020	15.087	15.365	15.634	15.251	-	-
MLTJ012018.03–721853.7	01:20:18.0333	–72:18:53.7468	14.756	14.875	15.047	15.226	14.978	-	-
MLTJ012222.90–724236.2	01:22:22.9074	–72:42:36.2623	14.899	14.988	15.265	15.528	15.194	-	-
MLTJ012737.11–740138.2	01:27:37.1157	–74:01:38.2829	15.892	15.957	16.110	16.292	16.053	0.80595	0.10208
MLTJ012956.10–305512.3	01:29:56.1068	–30:55:12.3997	15.740	15.694	15.817	16.037	15.817	17.93485	0.04974
MLTJ013424.11–160707.6	01:34:24.1121	–16:07:07.6327	13.455	13.732	14.117	14.132	13.961	10.28166	0.45570
MLTJ020900.08–735951.6	02:09:00.0802	–73:59:51.6269	15.688	16.079	16.439	16.456	15.899	2.75812	0.38880
MLTJ022858.36–182839.4	02:28:58.3682	–18:28:39.4289	15.318	15.551	15.878	16.110	15.751	0.91554	0.09050
MLTJ024901.07–183116.5	02:49:01.075	–18:31:16.5169	16.031	16.184	16.499	16.797	16.369	17.82681	0.12142
MLTJ025307.65–705857.4	02:53:07.6555	–70:58:57.439	15.972	16.026	16.258	16.441	16.172	12.94576	0.04646
MLTJ025626.79–172534.7	02:56:26.7995	–17:25:34.734	16.934	17.023	17.214	17.350	17.149	0.47367	0.14452

MLTJ031158.21–205407.4	03:11:58.2155	–20:54:07.4865	15.623	15.539	15.666	15.880	15.646	21.50258	0.04993
MLTJ032047.03–185527.0	03:20:47.0323	–18:55:27.0607	16.944	16.929	17.060	17.203	17.019	10.17742	0.08620
MLTJ032520.72–604722.5	03:25:20.7298	–60:47:22.5107	16.918	17.347	17.604	17.653	17.505	1.07587	0.21696
MLTJ033755.07–351342.3	03:37:55.0781	–35:13:42.3712	19.105	19.159	19.330	19.498	19.265	3.00962	0.27912
MLTJ034315.70–660204.8	03:43:15.7054	–66:02:04.877	16.425	16.542	16.815	16.972	16.693	8.49889	0.06700
MLTJ034917.85–541825.6	03:49:17.8555	–54:18:25.6391	17.040	17.127	17.282	17.495	17.205	9.96736	0.07392
MLTJ035122.99–254054.7	03:51:22.9909	–25:40:54.729	15.780	15.682	15.798	15.982	15.782	22.14407	0.04388
MLTJ035904.91–231225.1	03:59:04.9108	–23:12:25.1121	15.340	15.651	15.969	16.046	15.858	3.02429	0.07263
MLTJ040830.70–542139.7	04:08:30.7	–54:21:39.7415	16.833	16.878	16.995	17.188	17.000	10.06993	0.05669
MLTJ044309.41–525737.4	04:43:09.4117	–52:57:37.4458	18.536	18.587	18.760	18.994	18.717	4.67753	0.19043
MLTJ044403.48–703939.6	04:44:03.4814	–70:39:39.6102	16.566	16.563	16.740	17.005	16.677	-	-
MLTJ044514.92–694949.3	04:45:14.9205	–69:49:49.3751	16.386	16.410	16.647	16.896	16.560	-	-
MLTJ044821.68–694041.5	04:48:21.6821	–69:40:41.5637	17.062	17.134	17.244	17.396	17.238	-	-
MLTJ044935.22–671013.1	04:49:35.2294	–67:10:13.1123	17.001	16.948	17.082	17.236	17.026	–0.75914	0.16011
MLTJ044937.81–691252.4	04:49:37.8169	–69:12:52.4241	17.339	17.347	17.465	17.699	17.491	-	-
MLTJ045011.53–692253.8	04:50:11.5354	–69:22:53.8108	15.634	15.664	15.805	15.975	15.783	-	-
MLTJ045026.64–690352.1	04:50:26.641	–69:03:52.1241	16.902	16.976	17.125	17.334	17.062	-	-
MLTJ045154.73–714613.6	04:51:54.739	–71:46:13.6577	16.042	16.111	16.348	16.576	16.282	-	-
MLTJ045211.79–671505.3	04:52:11.7933	–67:15:05.3538	17.643	17.645	17.804	17.908	17.713	–0.35141	0.09992
MLTJ045303.28–703755.7	04:53:03.2848	–70:37:55.7605	16.596	16.576	16.676	16.865	16.702	-	-
MLTJ045327.58–684953.3	04:53:27.5832	–68:49:53.3774	16.235	16.115	16.175	16.237	16.182	0.92367	0.33195
MLTJ045418.15–693649.6	04:54:18.159	–69:36:49.6135	16.418	16.396	16.533	16.786	16.525	-	-
MLTJ045746.86–690228.1	04:57:46.863	–69:02:28.1563	15.962	16.137	16.402	16.622	16.322	-	-
MLTJ045823.04–702644.5	04:58:23.0413	–70:26:44.5232	16.142	16.208	16.426	16.561	16.331	-	-
MLTJ045835.96–685311.0	04:58:35.9604	–68:53:11.028	15.409	15.520	15.807	16.021	15.696	-	-
MLTJ045837.48–685904.4	04:58:37.4881	–68:59:04.4363	16.219	16.204	16.341	16.559	16.308	0.85687	0.58590
MLTJ045911.09–654059.4	04:59:11.0905	–65:40:59.4579	15.611	15.705	15.999	16.269	15.917	-	-
MLTJ045926.12–654943.5	04:59:26.1268	–65:49:43.5764	15.935	16.225	16.551	16.663	16.440	1.64140	0.25454
MLTJ045929.42–654644.8	04:59:29.4216	–65:46:44.8752	14.601	14.778	15.139	15.409	15.027	-	-
MLTJ045938.86–654554.4	04:59:38.8623	–65:45:54.4831	13.739	13.929	14.286	14.553	14.154	-	-
MLTJ045945.40–701035.1	04:59:45.4006	–70:10:35.1647	14.784	14.944	15.285	15.544	15.147	-	-
MLTJ050002.81–683421.5	05:00:02.8133	–68:34:21.5648	17.261	17.209	17.241	17.286	17.227	0.50231	0.40685
MLTJ050418.69–671903.9	05:04:18.6908	–67:19:03.9761	16.100	16.245	16.572	16.865	16.464	1.23803	0.16649
MLTJ050420.42–682552.7	05:04:20.4274	–68:25:52.7366	16.100	16.210	16.431	16.641	16.346	-	-
MLTJ050443.13–673350.2	05:04:43.1367	–67:33:50.2882	16.028	16.157	16.252	16.341	16.242	-	-
MLTJ050447.73–674937.2	05:04:47.7325	–67:49:37.2827	16.115	16.182	16.386	16.513	16.325	-	-
MLTJ050511.06–690001.6	05:05:11.0697	–69:00:01.6573	15.979	16.160	16.466	16.610	16.382	-	-
MLTJ050513.81–662456.3	05:05:13.8183	–66:24:56.3107	17.110	17.146	17.321	17.472	17.239	–0.51081	0.39626
MLTJ050555.42–683706.0	05:05:55.4288	–68:37:06.0256	16.974	16.933	17.072	17.088	17.002	0.58494	0.21059
MLTJ050725.00–712044.2	05:07:25.0094	–71:20:44.2377	14.750	14.889	15.127	15.341	15.056	-	-
MLTJ050847.00–681715.0	05:08:47.0067	–68:17:15.0438	17.022	17.077	17.243	17.390	17.165	-	-
MLTJ050916.13–681357.2	05:09:16.137	–68:13:57.271	17.371	17.299	17.343	17.355	17.369	-	-
MLTJ050926.31–651124.1	05:09:26.3148	–65:11:24.1454	15.824	15.787	15.796	15.855	15.847	1.32720	0.48183
MLTJ051037.77–675931.8	05:10:37.7718	–67:59:31.8053	15.149	15.446	15.826	15.920	15.697	-	-
MLTJ051123.60–670446.6	05:11:23.6018	–67:04:46.6376	15.056	15.197	15.465	15.580	15.374	-	-
MLTJ051153.04–711558.7	05:11:53.048	–71:15:58.7713	16.161	16.283	16.452	16.592	16.397	-	-

MLTJ051153.55–673857.7	05:11:53.5573	–67:38:57.7853	15.841	15.912	16.125	16.264	16.073	–0.79828	0.24202
MLTJ051356.74–685801.3	05:13:56.7419	–68:58:01.382	16.031	15.987	16.165	16.378	16.140	-	-
MLTJ051357.88–691339.8	05:13:57.884	–69:13:39.8826	16.614	16.750	16.874	17.010	16.896	-	-
MLTJ051431.17–664021.1	05:14:31.1706	–66:40:21.1418	16.949	16.860	16.948	17.067	16.943	–1.75996	0.37930
MLTJ051446.01–462915.4	05:14:46.0199	–46:29:15.4231	15.426	15.306	15.354	15.417	15.339	-	-
MLTJ051606.12–684656.3	05:16:06.1235	–68:46:56.3713	16.807	16.787	16.944	17.152	16.898	-	-
MLTJ051831.82–680650.9	05:18:31.8293	–68:06:50.9569	17.044	17.016	17.169	17.322	17.124	2.32035	0.30735
MLTJ051841.16–691359.1	05:18:41.1649	–69:13:59.1413	16.519	16.490	16.544	16.666	16.619	0.56878	0.31346
MLTJ052039.78–684106.8	05:20:39.78	–68:41:06.8013	16.829	16.820	16.936	17.104	16.875	-	-
MLTJ052130.06–685156.5	05:21:30.0682	–68:51:56.5353	15.753	15.761	15.938	16.151	15.893	0.76801	0.46318
MLTJ052153.86–654343.6	05:21:53.8668	–65:43:43.6935	16.610	16.671	16.669	16.845	16.684	–0.59019	0.08784
MLTJ052157.40–700247.8	05:21:57.4017	–70:02:47.8376	17.204	17.167	17.312	17.529	17.324	–0.39510	0.16310
MLTJ052306.18–670245.4	05:23:06.1882	–67:02:45.4611	16.270	16.338	16.584	16.648	16.449	-	-
MLTJ052349.94–680159.2	05:23:49.9427	–68:01:59.2721	15.957	16.091	16.394	16.612	16.292	-	-
MLTJ052410.13–684543.7	05:24:10.1332	–68:45:43.7286	17.373	17.319	17.378	17.616	17.380	-	-
MLTJ052414.74–713744.3	05:24:14.7491	–71:37:44.3307	16.006	16.105	16.359	16.561	16.279	-	-
MLTJ052526.97–660123.0	05:25:26.9773	–66:01:23.0653	16.729	16.662	16.813	16.869	16.800	-	-
MLTJ052544.76–690115.8	05:25:44.7673	–69:01:15.8893	16.248	16.309	16.568	16.780	16.476	-	-
MLTJ052646.57–685151.6	05:26:46.5724	–68:51:51.6832	16.518	16.563	16.589	16.633	16.610	0.95900	0.87133
MLTJ052647.13–685505.0	05:26:47.1384	–68:55:05.0417	15.503	15.611	15.840	16.043	15.761	-	-
MLTJ052824.77–323746.1	05:28:24.7748	–32:37:46.1711	15.785	15.919	16.054	16.175	16.020	-	-
MLTJ053237.26–693521.3	05:32:37.2625	–69:35:21.32	15.820	16.040	16.396	16.580	16.339	1.03898	0.30855
MLTJ053353.64–673703.4	05:33:53.6412	–67:37:03.4508	16.662	16.792	16.931	17.128	17.004	-	-
MLTJ053432.79–664330.9	05:34:32.7982	–66:43:30.9738	17.206	17.223	17.302	17.363	17.276	0.60532	0.21864
MLTJ053450.55–580140.6	05:34:50.5507	–58:01:40.6207	14.103	14.191	14.389	14.486	14.986	2.28392	0.02232
MLTJ053541.03–685734.4	05:35:41.0336	–68:57:34.4711	14.333	14.346	14.548	14.798	14.499	0.07640	0.03230
MLTJ053606.04–695519.9	05:36:06.0466	–69:55:19.937	17.021	17.064	17.163	17.205	17.197	-	-
MLTJ053816.50–664744.5	05:38:16.5069	–66:47:44.5483	15.477	15.597	15.848	16.069	15.771	-	-
MLTJ053819.05–690634.5	05:38:19.0592	–69:06:34.534	15.515	15.397	15.488	15.590	15.484	-	-
MLTJ054053.87–693518.8	05:40:53.8747	–69:35:18.8029	16.623	16.658	16.876	17.011	16.825	-	-
MLTJ054100.08–671628.4	05:41:00.0891	–67:16:28.4281	16.218	16.396	16.671	16.897	16.584	-	-
MLTJ054725.58–484720.4	05:47:25.5857	–48:47:20.4753	15.914	15.808	15.892	16.117	15.882	21.45783	0.03996
MLTJ054742.35–344022.6	05:47:42.3545	–34:40:22.6954	16.768	16.813	16.969	17.162	16.956	9.51446	0.07078
MLTJ054806.79–695641.8	05:48:06.7979	–69:56:41.8982	16.765	16.840	17.077	17.230	17.017	–0.70566	0.19810
MLTJ061753.82–362654.4	06:17:53.8257	–36:26:54.4973	16.018	16.009	16.156	16.240	16.109	1.08470	0.18420
MLTJ061835.50–513141.1	06:18:35.5011	–51:31:41.1202	16.971	16.890	16.952	17.242	16.972	11.84959	0.05987
MLTJ062425.79–325731.0	06:24:25.7927	–32:57:31.0249	15.425	15.399	15.530	15.768	15.490	14.45685	0.03326
MLTJ063620.45–150437.0	06:36:20.4503	–15:04:37.0965	15.737	15.829	16.030	16.257	15.989	3.84065	0.06077
MLTJ063732.39–165831.0	06:37:32.391	–16:58:31.046	15.136	15.365	15.646	15.925	15.511	1.04946	0.05537
MLTJ063928.68–402808.4	06:39:28.6877	–40:28:08.4191	16.287	16.282	16.312	16.326	16.317	0.75863	0.30807
MLTJ064004.73–270320.0	06:40:04.7391	–27:03:20.0306	15.678	15.911	16.163	16.265	15.998	0.73701	0.05440
MLTJ064043.28–713031.7	06:40:43.2863	–71:30:31.7464	16.916	17.077	17.365	17.547	17.252	0.87134	0.18177
MLTJ064936.85–833153.1	06:49:36.855	–83:31:53.1578	14.903	14.961	15.225	15.504	15.129	1.23223	0.03377
MLTJ065435.67–180152.2	06:54:35.6783	–18:01:52.2146	16.543	16.550	16.685	16.859	16.654	0.88252	0.09338
MLTJ065449.05–791843.1	06:54:49.0528	–79:18:43.14	16.954	17.076	17.285	17.565	17.243	0.42601	0.07820
MLTJ065943.52–355853.4	06:59:43.5256	–35:58:53.4497	16.689	16.657	16.752	16.967	16.749	0.48023	0.05659

MLTJ070223.63–364243.7	07:02:23.6338	–36:42:43.7543	16.597	16.673	16.916	17.138	16.818	0.64407	0.05433
MLTJ070244.27–194323.8	07:02:44.2716	–19:43:23.8223	16.323	16.289	16.414	16.611	16.398	0.56812	0.06480
MLTJ070902.19–341753.7	07:09:02.1974	–34:17:53.7143	16.957	16.928	17.008	17.183	16.973	12.44138	0.07692
MLTJ070914.31–824005.7	07:09:14.3143	–82:40:05.7568	17.152	17.326	17.622	17.824	17.529	0.37365	0.08671
MLTJ070939.87–190720.8	07:09:39.8701	–19:07:20.8492	16.517	16.559	16.701	16.772	16.466	8.76585	0.06502
MLTJ071143.70+092851.1	07:11:43.7002	+09:28:51.1037	16.534	16.643	16.844	17.094	16.805	8.45952	0.10515
MLTJ071354.61–465306.8	07:13:54.6132	–46:53:06.8189	16.879	17.063	17.381	17.630	17.302	0.53190	0.08614
MLTJ071449.42–465739.1	07:14:49.4287	–46:57:39.1125	16.438	16.756	16.935	17.064	16.865	0.51800	0.10859
MLTJ071546.87–385203.8	07:15:46.8774	–38:52:03.806	15.446	15.519	15.780	16.024	15.683	14.90739	0.03798
MLTJ072051.76–714354.2	07:20:51.7625	–71:43:54.262	15.626	15.777	16.077	16.333	15.968	0.77309	0.05860
MLTJ073110.10–554025.0	07:31:10.1076	–55:40:25.0714	16.726	16.822	17.038	17.249	16.994	0.69574	0.24659
MLTJ073212.80–531036.4	07:32:12.8033	–53:10:36.4379	15.581	15.764	16.111	16.376	16.010	0.86636	0.03680
MLTJ073440.68–601152.0	07:34:40.6867	–60:11:52.0554	16.490	16.400	16.478	16.613	16.460	18.24231	0.04195
MLTJ073903.87–184859.0	07:39:03.877	–18:48:59.0873	16.568	16.460	16.501	16.760	16.507	0.55229	0.05847
MLTJ074703.95–661404.4	07:47:03.9544	–66:14:04.461	16.450	16.352	16.448	16.739	16.531	15.38723	0.04404
MLTJ080146.06–683258.9	08:01:46.0694	–68:32:58.9097	16.955	17.119	17.332	17.454	17.311	1.18723	0.20872
MLTJ081249.97–560027.5	08:12:49.9718	–56:00:27.5995	15.421	15.529	15.734	15.970	15.669	0.88967	0.04714
MLTJ081249.98–560027.6	08:12:49.9837	–56:00:27.6007	15.415	15.519	15.744	15.946	15.650	0.88967	0.04714
MLTJ081530.78–342123.3	08:15:30.7827	–34:21:23.3982	16.700	16.722	16.878	17.081	16.758	0.50348	0.06084
MLTJ081911.36–353521.3	08:19:11.3644	–35:35:21.3378	16.911	16.847	16.996	17.164	16.951	0.44566	0.07154
MLTJ082742.32–420801.4	08:27:42.3213	–42:08:01.4923	15.341	15.329	15.401	15.486	15.413	0.94614	0.03968
MLTJ083142.28–610030.1	08:31:42.2801	–61:00:30.1443	16.140	16.223	16.380	16.405	16.312	0.64604	0.04032
MLTJ084116.30–493704.7	08:41:16.3011	–49:37:04.7279	17.249	17.434	17.486	17.704	17.521	0.49829	0.09548
MLTJ085048.12–415150.8	08:50:48.1278	–41:51:50.831	15.975	15.877	15.915	16.054	15.897	0.71804	0.04051
MLTJ085423.51–493634.1	08:54:23.5131	–49:36:34.1727	16.045	16.045	16.253	16.451	16.180	0.65049	0.05045
MLTJ091029.43+090202.9	09:10:29.4315	+09:02:02.9983	17.134	17.204	17.418	17.620	17.337	6.15234	0.11575
MLTJ091532.33–354042.6	09:15:32.3323	–35:40:42.6861	16.854	16.979	17.268	17.492	17.140	0.44771	0.08120
MLTJ091547.21–541619.6	09:15:47.2145	–54:16:19.6106	17.152	17.054	17.100	17.301	17.096	0.46902	0.06973
MLTJ093238.29–725410.5	09:32:38.2983	–72:54:10.5598	14.385	14.424	14.672	14.951	14.622	1.36557	0.02850
MLTJ094115.19+090152.5	09:41:15.1907	+09:01:52.5732	16.957	16.848	16.868	16.972	16.871	11.17352	0.12539
MLTJ094122.57–541021.4	09:41:22.5709	–54:10:21.4808	17.060	17.129	17.237	17.341	17.215	0.55008	0.08661
MLTJ095032.31–483556.8	09:50:32.3117	–48:35:56.8648	16.835	16.839	16.889	17.036	16.879	0.51606	0.07157
MLTJ100814.09–375754.2	10:08:14.0975	–37:57:54.2744	16.355	16.330	16.367	16.417	16.363	0.63624	0.15084
MLTJ101640.85–010900.7	10:16:40.8565	–01:09:00.7024	16.409	16.335	16.371	16.431	16.374	-	-
MLTJ103133.33–350054.9	10:31:33.3331	–35:00:54.91	17.847	17.848	17.984	18.149	17.947	7.27511	0.13074
MLTJ104715.91–480240.7	10:47:15.9177	–48:02:40.7486	16.133	16.159	16.259	16.327	16.235	–0.65778	0.21623
MLTJ105609.30–451430.5	10:56:09.3035	–45:14:30.5078	17.606	17.524	17.610	17.739	17.598	7.94883	0.13376
MLTJ110105.32–355045.3	11:01:05.3246	–35:50:45.3101	17.249	17.456	17.632	17.756	17.614	0.37351	0.11061
MLTJ111610.64–525935.7	11:16:10.649	–52:59:35.7585	15.831	15.853	15.973	16.071	15.932	0.77848	0.21514
MLTJ111845.64–420550.0	11:18:45.6415	–42:05:50.079	16.511	16.608	16.867	17.083	16.742	9.32847	0.07790
MLTJ112525.07–434939.2	11:25:25.0722	–43:49:39.2329	17.281	17.184	17.280	17.416	17.268	11.20170	0.09113
MLTJ113726.72–144757.1	11:37:26.7238	–14:47:57.1482	15.987	16.176	16.529	16.778	16.384	0.85564	0.10901
MLTJ113752.14–580720.7	11:37:52.1441	–58:07:20.707	15.771	15.959	16.226	16.430	16.122	0.73703	0.04906
MLTJ114006.20+182401.4	11:40:06.2097	+18:24:01.4951	17.923	17.977	18.066	18.243	18.080	10.55275	0.16137
MLTJ114112.44–340146.5	11:41:12.445	–34:01:46.5528	16.200	16.345	16.616	16.897	16.512	8.25012	0.09020
MLTJ121018.82–554428.5	12:10:18.8284	–55:44:28.5655	16.014	16.125	16.265	16.469	16.236	0.70721	0.05552

MLTJ121405.46–313520.9	12:14:05.4635	–31:35:20.9485	16.889	16.962	17.226	17.410	17.177	7.29149	0.11592
MLTJ121432.53–541942.5	12:14:32.5377	–54:19:42.5293	15.222	15.467	15.814	16.110	15.657	0.98143	0.05919
MLTJ121743.73–531831.3	12:17:43.7335	–53:18:31.3713	16.244	16.256	16.418	16.503	16.316	–2.21678	0.27342
MLTJ124631.99–480413.5	12:46:31.9961	–48:04:13.583	15.938	16.248	16.632	16.825	16.474	0.95651	0.18817
MLTJ125002.08–310255.5	12:50:02.084	–31:02:55.5573	13.734	13.741	13.812	13.833	13.785	0.63420	0.27280
MLTJ125544.63–555351.4	12:55:44.6391	–55:53:51.4732	16.858	16.767	16.852	16.960	16.832	0.71403	0.08264
MLTJ130106.77–481034.8	13:01:06.7774	–48:10:34.8366	15.282	15.466	15.711	15.964	15.639	1.13599	0.12764
MLTJ130129.04–515244.5	13:01:29.0452	–51:52:44.5116	16.806	16.759	16.812	16.863	16.869	0.54850	0.11163
MLTJ131438.71–554554.9	13:14:38.7193	–55:45:54.9207	16.284	16.352	16.487	16.662	16.489	0.57801	0.06042
MLTJ131648.10–323744.6	13:16:48.1018	–32:37:44.6955	16.103	16.296	16.553	16.659	16.483	0.61499	0.09296
MLTJ131945.70–620059.9	13:19:45.7025	–62:00:59.9757	17.014	16.917	16.988	17.032	16.919	0.49878	0.06868
MLTJ132425.35–592124.4	13:24:25.3592	–59:21:24.4831	16.203	16.173	16.315	16.412	16.224	0.67789	0.07154
MLTJ133350.07–555418.5	13:33:50.0769	–55:54:18.5303	16.574	16.595	16.613	16.632	16.607	0.53922	0.27202
MLTJ134704.05–310852.4	13:47:04.0562	–31:08:52.4226	17.359	17.593	17.857	18.068	17.765	0.42567	0.15049
MLTJ135704.98–510325.9	13:57:04.9882	–51:03:25.911	16.344	16.324	16.327	16.382	16.364	0.79823	0.10751
MLTJ135917.77–305409.6	13:59:17.7712	–30:54:09.6769	16.505	16.524	16.755	16.884	16.678	0.93932	0.21845
MLTJ140516.70–434023.6	14:05:16.7043	–43:40:23.6844	14.842	14.891	15.053	15.145	15.040	1.27694	0.09676
MLTJ140801.86–331717.0	14:08:01.861	–33:17:17.0254	16.786	16.867	17.021	17.093	16.971	0.62972	0.09885
MLTJ141822.54–303211.9	14:18:22.5466	–30:32:11.9785	16.331	16.320	16.446	16.584	16.408	14.46776	0.08037
MLTJ141847.55–462959.3	14:18:47.5509	–46:29:59.3323	16.753	16.812	16.940	17.154	16.920	–0.96005	0.34605
MLTJ142705.90–361058.6	14:27:05.905	–36:10:58.6914	16.907	16.899	16.898	16.940	16.910	0.51839	0.10092
MLTJ142706.26–322216.1	14:27:06.2625	–32:22:16.1913	16.440	16.729	17.079	17.360	17.020	0.54050	0.11954
MLTJ144139.77–161530.4	14:41:39.7753	–16:15:30.4479	15.919	16.158	16.538	16.841	16.377	0.72348	0.08922
MLTJ144603.78–680359.5	14:46:03.783	–68:03:59.5416	16.846	16.927	17.107	17.231	17.049	1.07878	0.37379
MLTJ144641.89–305708.2	14:46:41.8927	–30:57:08.2421	16.422	16.516	16.788	17.067	16.700	4.28083	0.08108
MLTJ144700.45–160149.1	14:47:00.4547	–16:01:49.1319	16.294	16.510	16.569	16.655	16.833	1.34655	0.10907
MLTJ144730.79–360734.9	14:47:30.7927	–36:07:34.9188	17.297	17.239	17.341	17.494	17.353	0.49685	0.10886
MLTJ150307.49–502107.2	15:03:07.4939	–50:21:07.2122	16.566	16.631	16.769	17.055	16.756	0.54666	0.07741
MLTJ151509.15–162102.5	15:15:09.1558	–16:21:02.5326	16.695	16.906	17.197	17.340	17.096	0.51565	0.10195
MLTJ151629.11–442615.4	15:16:29.1167	–44:26:15.4677	15.896	15.976	16.203	16.391	16.168	0.88104	0.11462
MLTJ151819.60–301440.4	15:18:19.6061	–30:14:40.457	13.734	13.762	13.901	14.062	13.842	1.91270	0.04014
MLTJ152528.92–530611.4	15:25:28.9283	–53:06:11.415	16.154	16.154	16.265	16.365	16.217	0.70528	0.05763
MLTJ152713.96–641737.4	15:27:13.965	–64:17:37.4686	16.296	16.479	16.788	16.992	16.685	0.60428	0.07975
MLTJ153133.70–353213.7	15:31:33.7047	–35:32:13.7306	16.705	16.781	16.946	17.061	16.912	3.22456	0.14820
MLTJ153749.96–312410.9	15:37:49.9605	–31:24:10.9654	17.215	17.354	17.542	17.616	17.463	0.48627	0.19214
MLTJ153930.73–014351.5	15:39:30.7343	–01:43:51.5519	17.009	16.981	17.061	17.210	17.030	15.35962	0.08725
MLTJ154049.30–542707.7	15:40:49.3062	–54:27:07.7475	15.199	15.115	15.117	15.169	15.119	0.97209	0.03427
MLTJ154956.70–345132.2	15:49:56.7018	–34:51:32.2964	16.972	17.044	17.173	17.436	17.223	0.46450	0.09605
MLTJ155149.17–445125.3	15:51:49.1741	–44:51:25.3505	17.576	17.605	17.779	17.958	17.689	0.41457	0.13388
MLTJ155257.46–444303.9	15:52:57.4697	–44:43:03.9713	17.476	17.588	17.751	17.960	17.780	0.54396	0.13597
MLTJ155913.63–165546.6	15:59:13.631	–16:55:46.6331	17.465	17.505	17.652	17.819	17.635	0.63823	0.16104
MLTJ160032.14–320356.9	16:00:32.1497	–32:03:56.9851	16.183	16.380	16.626	16.859	16.504	0.83939	0.07261
MLTJ160647.72–152740.6	16:06:47.7256	–15:27:40.6403	16.670	16.739	17.005	17.228	16.903	4.89001	0.10987
MLTJ160724.20–164451.1	16:07:24.2004	–16:44:51.1121	16.769	16.873	17.118	17.360	17.051	0.48571	0.12509
MLTJ161114.11–305346.4	16:11:14.1106	–30:53:46.4643	16.617	16.638	16.822	16.895	16.775	0.73015	0.09431
MLTJ161416.09–345513.2	16:14:16.0992	–34:55:13.2736	17.038	16.993	17.087	17.179	17.125	0.49594	0.08719

MLTJ161604.14–794236.8	16:16:04.1428	–79:42:36.8869	14.990	15.212	15.515	15.815	15.417	3.04367	0.04481
MLTJ161737.30–734440.4	16:17:37.3003	–73:44:40.4533	16.294	16.211	16.328	16.404	16.281	0.59377	0.06199
MLTJ170507.64–695031.0	17:05:07.6494	–69:50:31.0193	16.308	16.354	16.406	16.453	16.433	0.56219	0.05256
MLTJ173148.74–712039.0	17:31:48.7438	–71:20:39.0205	16.631	16.665	16.716	16.820	16.770	0.47349	0.06968
MLTJ181411.28–531653.9	18:14:11.2832	–53:16:53.9217	16.262	16.274	16.472	16.676	16.426	0.70518	0.09521
MLTJ181723.44–872557.7	18:17:23.4493	–87:25:57.7935	16.207	16.301	16.553	16.814	16.478	0.69851	0.04976
MLTJ182133.48+061321.7	18:21:33.489	+06:13:21.7814	16.907	17.072	17.276	17.533	17.192	0.52198	0.09753
MLTJ185535.63–813507.0	18:55:35.6322	–81:35:07.0589	15.983	16.096	16.280	16.514	16.210	0.90453	0.06728
MLTJ190610.74–373414.1	19:06:10.7401	–37:34:14.1006	16.958	17.144	17.352	17.592	17.297	2.96129	0.12850
MLTJ190752.82–373956.0	19:07:52.8209	–37:39:56.078	15.182	15.151	15.311	15.461	15.290	0.95016	0.05666
MLTJ191736.57–374818.7	19:17:36.5704	–37:48:18.7127	17.215	17.272	17.431	17.626	17.397	0.52364	0.13580
MLTJ192433.98–432444.6	19:24:33.9826	–43:24:44.643	16.035	16.151	16.299	16.387	16.314	0.72612	0.09794
MLTJ192504.69–365151.4	19:25:04.6944	–36:51:51.4572	16.485	16.623	16.782	16.994	16.799	0.56823	0.09499
MLTJ192608.60–352013.2	19:26:08.6085	–35:20:13.2696	16.096	16.131	16.357	16.613	16.338	15.07026	0.08713
MLTJ193431.86–433643.9	19:34:31.867	–43:36:43.9572	15.560	15.603	15.743	15.824	15.699	0.92658	0.05970
MLTJ194311.18–153403.7	19:43:11.1806	–15:34:03.7467	16.574	16.581	16.732	16.954	16.682	0.88562	0.11600
MLTJ194605.98–360341.1	19:46:05.9862	–36:03:41.1116	16.501	16.451	16.505	16.497	16.511	0.70305	0.08034
MLTJ194921.72–684412.2	19:49:21.7235	–68:44:12.2212	16.674	16.879	17.215	17.477	17.108	0.47283	0.07806
MLTJ195722.61–380135.6	19:57:22.6153	–38:01:35.6822	17.047	17.192	17.517	17.785	17.385	0.63842	0.14605
MLTJ195807.17–383546.2	19:58:07.1751	–38:35:46.2584	17.675	17.782	18.073	18.299	17.991	0.43693	0.20559
MLTJ203654.63–432231.6	20:36:54.63	–43:22:31.6344	15.446	15.431	15.593	15.774	15.495	1.25132	0.07614
MLTJ204650.73–071418.9	20:46:50.7325	–07:14:18.9327	17.764	17.683	17.755	17.857	17.762	9.48902	0.13999
MLTJ211648.89–365233.6	21:16:48.8995	–36:52:33.6998	16.487	16.499	16.598	16.768	16.548	13.95466	0.10518
MLTJ220535.14–671448.2	22:05:35.1475	–67:14:48.2254	16.499	16.750	17.114	17.211	17.003	2.22637	0.14578
MLTJ224421.79–401537.7	22:44:21.7934	–40:15:37.7512	16.360	16.320	16.414	16.587	16.408	14.37987	0.13832
MLTJ230345.82–141447.1	23:03:45.8225	–14:14:47.1845	16.634	16.889	17.188	17.281	17.094	2.30753	0.11713
MLTJ232129.59–602302.9	23:21:29.5976	–60:23:02.9598	16.591	16.722	16.929	17.147	16.928	0.54588	0.08316

Table 9: 370 MeerLICHT $ugrq$ selected candidates.

MeerLICHT Name	**RA (hh:mm:ss)**	**Dec. (dd:mm:ss)**	u**_ML**	g**_ML**	r**_ML**	q**_ML**	**Parallax (mas)**	**Parallax error**
MLTJ001906.03–432418.6	00:19:06.03	–43:24:18.6138	15.605	15.519	15.579	15.567	7.53148	0.28226
MLTJ003527.37–125706.8	00:35:27.3758	–12:57:06.8073	16.664	16.988	17.100	17.005	5.47645	0.64536
MLTJ003527.38–125706.8	00:35:27.3851	–12:57:06.8019	16.651	16.964	17.085	17.000	5.47645	0.64536
MLTJ004500.94–732123.2	00:45:00.9454	–73:21:23.2578	15.860	15.914	16.167	16.126	1.01723	0.12812
MLTJ004647.57–730837.9	00:46:47.5794	–73:08:37.9181	16.889	16.855	16.907	16.969	-	-
MLTJ004702.36–731105.1	00:47:02.3681	–73:11:05.1544	16.450	16.647	17.001	16.889	-	-
MLTJ004751.46–730711.9	00:47:51.4666	–73:07:11.9249	16.898	17.020	17.099	16.902	–0.72718	0.11044
MLTJ004751.46–730711.9	00:47:51.4666	–73:07:11.9249	16.898	17.020	17.099	16.902	–0.72718	0.11044
MLTJ004926.12–731632.6	00:49:26.1213	–73:16:32.6877	15.649	15.769	15.931	15.926	-	-
MLTJ005045.23–732105.3	00:50:45.2301	–73:21:05.3664	16.288	16.362	16.511	16.352	–1.20650	0.14073
MLTJ005045.23–732105.3	00:50:45.2301	–73:21:05.3664	16.288	16.362	16.511	16.352	–1.20650	0.14073
MLTJ005254.67–730315.7	00:52:54.6786	–73:03:15.7965	15.634	15.835	16.073	16.071	-	-
MLTJ005351.07–731025.1	00:53:51.0764	–73:10:25.1398	16.731	16.971	17.221	17.059	–0.60585	0.20165
MLTJ005351.07–731025.1	00:53:51.0764	–73:10:25.1398	16.731	16.971	17.221	17.059	–0.60585	0.20165

MLTJ005425.36–371439.8	00:54:25.3631	–37:14:39.8915	17.295	17.339	17.408	17.362	-	-
MLTJ005425.36–371439.9	00:54:25.3605	–37:14:39.9809	17.319	17.313	17.407	17.330	-	-
MLTJ005600.70–733100.8	00:56:00.7076	–73:31:00.8696	17.113	17.215	17.318	17.347	0.51085	0.08661
MLTJ005624.47–714022.1	00:56:24.4769	–71:40:22.1239	15.442	15.729	15.923	15.728	-	-
MLTJ005640.66–725635.9	00:56:40.663	–72:56:35.9325	17.037	17.077	17.141	17.116	-	-
MLTJ005729.58–722135.4	00:57:29.5848	–72:21:35.4219	16.598	16.605	16.661	16.690	0.50515	0.12689
MLTJ005757.84–720755.4	00:57:57.8406	–72:07:55.4198	15.275	15.353	15.549	15.507	-	-
MLTJ005826.08–730816.7	00:58:26.0823	–73:08:16.7889	16.844	17.088	17.215	17.217	–1.49554	0.19364
MLTJ005826.08–730816.7	00:58:26.0823	–73:08:16.7889	16.844	17.088	17.215	17.217	–1.49554	0.19364
MLTJ005826.30–732922.4	00:58:26.3004	–73:29:22.4468	15.746	15.910	16.248	16.130	0.02308	0.05406
MLTJ005842.56–723001.9	00:58:42.5672	–72:30:01.9463	16.017	16.116	16.406	16.346	1.32255	0.36544
MLTJ010128.84–724337.5	01:01:28.8424	–72:43:37.5653	15.810	15.855	16.107	16.034	1.79579	0.74761
MLTJ010255.01–715947.7	01:02:55.0155	–71:59:47.7264	16.774	16.891	17.120	17.047	0.44376	0.14636
MLTJ010709.80–425424.0	01:07:09.8051	–42:54:24.0016	16.713	16.917	16.926	16.972	4.11356	0.08732
MLTJ010709.80–425424.0	01:07:09.8051	–42:54:24.0016	16.713	16.917	16.926	16.972	4.11356	0.08732
MLTJ011142.36–731232.4	01:11:42.3639	–73:12:32.4459	17.293	17.565	17.619	17.617	0.81872	0.20632
MLTJ011449.15–732457.6	01:14:49.1561	–73:24:57.6622	16.778	16.770	16.890	16.835	-	-
MLTJ011526.12–712522.4	01:15:26.1209	–71:25:22.4174	17.115	17.135	17.341	17.293	-	-
MLTJ012737.11–740138.2	01:27:37.1157	–74:01:38.2829	15.892	15.957	16.110	16.053	0.80595	0.10208
MLTJ012737.14–740138.2	01:27:37.1464	–74:01:38.2438	15.860	15.929	16.062	16.043	0.80595	0.10208
MLTJ014808.36–253244.7	01:48:08.3674	–25:32:44.7201	14.409	14.441	14.646	14.579	12.73198	0.03954
MLTJ020900.11–735951.6	02:09:00.1124	–73:59:51.6041	15.652	16.058	16.407	15.830	2.75812	0.38880
MLTJ021732.77–021115.6	02:17:32.7796	–02:11:15.6902	15.930	16.000	16.274	16.155	10.28674	0.10724
MLTJ024901.07–183116.4	02:49:01.0776	–18:31:16.4806	16.029	16.186	16.515	16.384	17.82681	0.12142
MLTJ031158.21–205407.4	03:11:58.2155	–20:54:07.4865	15.623	15.539	15.666	15.646	21.50258	0.04993
MLTJ032520.72–604722.5	03:25:20.7298	–60:47:22.5107	16.918	17.347	17.604	17.505	1.07587	0.21696
MLTJ033434.44–640058.0	03:34:34.4482	–64:00:58.0448	13.852	14.106	14.361	14.304	9.34624	0.02254
MLTJ033434.45–640058.1	03:34:34.456	–64:00:58.109	13.836	14.098	14.364	14.269	9.34624	0.02254
MLTJ033553.58–354923.9	03:35:53.5821	–35:49:23.9308	18.723	18.726	18.821	18.583	0.21727	0.18679
MLTJ033553.58–354923.9	03:35:53.5821	–35:49:23.9308	18.723	18.726	18.821	18.583	0.21727	0.18679
MLTJ034240.48–505021.6	03:42:40.4881	–50:50:21.6625	15.696	15.846	15.999	15.936	0.92056	0.03593
MLTJ034240.49–505021.6	03:42:40.4925	–50:50:21.6668	15.710	15.853	15.980	16.010	0.92056	0.03593
MLTJ034917.84–541825.6	03:49:17.8478	–54:18:25.6549	17.025	17.120	17.280	17.228	9.96736	0.07392
MLTJ035122.99–254054.7	03:51:22.9909	–25:40:54.729	15.780	15.682	15.798	15.782	22.14407	0.04388
MLTJ035904.90–231225.1	03:59:04.9074	–23:12:25.1352	15.344	15.656	15.980	15.865	3.02429	0.07263
MLTJ040830.69–542139.7	04:08:30.6978	–54:21:39.7626	16.840	16.880	17.015	16.963	10.06993	0.05669
MLTJ040830.7s–542139.7	04:08:30.7	–54:21:39.7415	16.833	16.878	16.995	17.000	10.06993	0.05669
MLTJ040935.32–494218.0	04:09:35.3261	–49:42:18.0751	16.262	16.592	16.968	16.835	3.77758	0.07349
MLTJ041652.64–042724.8	04:16:52.6496	–04:27:24.8079	15.183	15.209	15.394	15.346	18.61821	0.05830
MLTJ043125.10–152520.5	04:31:25.1062	–15:25:20.5069	17.018	17.304	17.635	17.514	1.85075	0.11553
MLTJ043253.11–773629.7	04:32:53.1106	–77:36:29.7551	15.609	15.555	15.687	15.596	11.47214	0.50275
MLTJ044514.92–694949.3	04:45:14.9205	–69:49:49.3751	16.386	16.410	16.647	16.560	-	-
MLTJ044821.67–694041.6	04:48:21.6718	–69:40:41.6355	17.050	17.112	17.238	17.218	-	-
MLTJ045011.53–692253.8	04:50:11.5354	–69:22:53.8108	15.634	15.664	15.805	15.783	-	-
MLTJ045150.51–690841.8	04:51:50.5135	–69:08:41.8794	16.632	16.541	16.614	16.608	-	-
MLTJ045302.24–693105.1	04:53:02.24	–69:31:05.1955	16.674	16.699	16.844	16.850	-	-

MLTJ045303.27–703755.7	04:53:03.2744	–70:37:55.7999	16.584	16.586	16.691	16.656	-	-
MLTJ045327.58–684953.3	04:53:27.5832	–68:49:53.3774	16.235	16.115	16.175	16.182	0.92367	0.33195
MLTJ045530.89–690948.4	04:55:30.894	–69:09:48.4154	15.535	15.631	15.809	15.789	-	-
MLTJ045658.55–681147.9	04:56:58.5547	–68:11:47.9638	16.580	16.756	17.071	16.980	-	-
MLTJ045724.81–682054.6	04:57:24.8165	–68:20:54.6037	16.771	16.866	17.142	17.031	-	-
MLTJ045823.04–702644.5	04:58:23.0413	–70:26:44.5232	16.142	16.208	16.426	16.331	-	-
MLTJ045837.48–685904.4	04:58:37.4881	–68:59:04.4363	16.219	16.204	16.341	16.308	0.85687	0.58590
MLTJ045926.12–654943.5	04:59:26.1268	–65:49:43.5764	15.935	16.225	16.551	16.440	1.64140	0.25454
MLTJ045938.86–654554.4	04:59:38.8623	–65:45:54.4831	13.739	13.929	14.286	14.154	-	-
MLTJ050130.58–664355.9	05:01:30.586	–66:43:55.9434	16.506	16.543	16.698	16.661	-	-
MLTJ050257.46–682947.2	05:02:57.4616	–68:29:47.2594	15.967	16.056	16.160	16.115	–0.74433	0.25685
MLTJ050257.46–682947.2	05:02:57.4616	–68:29:47.2594	15.967	16.056	16.160	16.115	–0.74433	0.25685
MLTJ050420.42–682552.7	05:04:20.4274	–68:25:52.7366	16.100	16.210	16.431	16.346	-	-
MLTJ050443.13–673350.2	05:04:43.1367	–67:33:50.2882	16.028	16.157	16.252	16.242	-	-
MLTJ050511.06–690001.6	05:05:11.0697	–69:00:01.6573	15.979	16.160	16.466	16.382	-	-
MLTJ050725.00–712044.2	05:07:25.0094	–71:20:44.2377	14.750	14.889	15.127	15.056	-	-
MLTJ050753.95–795122.2	05:07:53.9573	–79:51:22.2699	14.327	14.766	14.767	14.854	1.78278	0.02491
MLTJ050926.31–651124.1	05:09:26.3148	–65:11:24.1454	15.824	15.787	15.796	15.847	1.32720	0.48183
MLTJ050926.31–651124.2	05:09:26.3122	–65:11:24.2156	15.807	15.796	15.811	15.826	1.32720	0.48183
MLTJ051123.60–670446.6	05:11:23.6018	–67:04:46.6376	15.056	15.197	15.465	15.374	-	-
MLTJ051303.85–674535.9	05:13:03.8594	–67:45:35.9099	16.413	16.423	16.518	16.490	1.60029	0.42902
MLTJ051357.88–691339.8	05:13:57.884	–69:13:39.8826	16.614	16.750	16.874	16.896	-	-
MLTJ051606.12–684656.3	05:16:06.1235	–68:46:56.3713	16.807	16.787	16.944	16.898	-	-
MLTJ051642.96–680939.9	05:16:42.9641	–68:09:39.9262	16.929	16.932	17.028	17.041	-	-
MLTJ051642.96–680939.9	05:16:42.9641	–68:09:39.9262	16.929	16.932	17.028	17.041	-	-
MLTJ051841.16–691359.1	05:18:41.1649	–69:13:59.1413	16.519	16.490	16.544	16.619	0.56878	0.31346
MLTJ051841.47–680122.7	05:18:41.4773	–68:01:22.7141	16.122	16.188	16.439	16.361	-	-
MLTJ052039.78–684106.8	05:20:39.78	–68:41:06.8013	16.829	16.820	16.936	16.875	-	-
MLTJ052144.35–210125.8	05:21:44.3507	–21:01:25.8589	16.871	17.096	17.468	17.313	8.14810	0.08069
MLTJ052153.86–654343.6	05:21:53.8668	–65:43:43.6935	16.610	16.671	16.669	16.684	–0.59019	0.08784
MLTJ052317.13–685325.0	05:23:17.1331	–68:53:25.0893	17.525	17.464	17.592	17.523	-	-
MLTJ052410.13–684543.7	05:24:10.1332	–68:45:43.7286	17.373	17.319	17.378	17.380	-	-
MLTJ052526.97–660123.0	05:25:26.9773	–66:01:23.0653	16.729	16.662	16.813	16.800	-	-
MLTJ052646.57–685151.6	05:26:46.5724	–68:51:51.6832	16.518	16.563	16.589	16.610	0.95900	0.87133
MLTJ052647.13–685505.0	05:26:47.1384	–68:55:05.0417	15.503	15.611	15.840	15.761	-	-
MLTJ052706.79–685811.8	05:27:06.7965	–68:58:11.8534	17.242	17.403	17.662	17.553	-	-
MLTJ052726.7s–692937.6	05:27:26.7	–69:29:37.6381	16.796	16.957	17.180	17.085	–0.75625	0.29040
MLTJ052726.7s–692937.6	05:27:26.7	–69:29:37.6381	16.796	16.957	17.180	17.085	–0.75625	0.29040
MLTJ052824.77–323746.1	05:28:24.7733	–32:37:46.1846	15.784	15.933	16.071	16.026	-	-
MLTJ052907.04–664657.5	05:29:07.0467	–66:46:57.5177	14.686	14.930	15.329	15.286	-	-
MLTJ053141.00–671256.0	05:31:41.0022	–67:12:56.0214	16.705	16.899	17.242	17.189	-	-
MLTJ053210.98–670342.5	05:32:10.9835	–67:03:42.5383	17.041	17.172	17.471	17.435	-	-
MLTJ053222.65–703229.9	05:32:22.6521	–70:32:29.9459	17.174	17.172	17.365	17.350	0.51273	0.75383
MLTJ053241.18–665659.4	05:32:41.1852	–66:56:59.4799	15.404	15.589	15.765	15.816	-	-
MLTJ053303.71–671833.9	05:33:03.7191	–67:18:33.9931	16.456	16.587	16.835	16.828	-	-
MLTJ053349.25–695006.6	05:33:49.2563	–69:50:06.6696	17.057	17.022	17.027	17.058	1.04343	1.16561

MLTJ053429.32–665939.1	05:34:29.3218	–66:59:39.1087	16.454	16.626	16.950	16.870	-	-
MLTJ053447.87–664043.3	05:34:47.871	–66:40:43.3501	16.951	17.065	17.288	17.255	0.53916	0.43245
MLTJ053450.54–580140.7	05:34:50.5463	–58:01:40.7483	14.100	14.194	14.405	14.706	2.28392	0.02232
MLTJ053450.54–580140.7	05:34:50.5463	–58:01:40.7483	14.100	14.194	14.405	14.706	2.28392	0.02232
MLTJ053528.88–672858.0	05:35:28.8844	–67:28:58.0842	15.624	15.823	16.156	16.148	-	-
MLTJ053533.88–664119.5	05:35:33.8838	–66:41:19.5575	15.886	16.163	16.541	16.457	-	-
MLTJ053542.19–665722.1	05:35:42.1972	–66:57:22.1903	16.975	17.131	17.427	17.332	-	-
MLTJ053545.99–672029.6	05:35:45.9967	–67:20:29.6604	15.889	16.133	16.502	16.443	-	-
MLTJ053606.05–695519.8	05:36:06.0512	–69:55:19.864	17.084	17.061	17.203	17.136	-	-
MLTJ053616.93–663635.0	05:36:16.9321	–66:36:35.0768	16.905	17.065	17.363	17.295	-	-
MLTJ053705.29–662924.2	05:37:05.2902	–66:29:24.242	16.952	17.135	17.329	17.256	–0.46320	0.11939
MLTJ053705.29–662924.2	05:37:05.2902	–66:29:24.242	16.952	17.135	17.329	17.256	–0.46320	0.11939
MLTJ053819.05–690634.5	05:38:19.0592	–69:06:34.534	15.515	15.397	15.488	15.484	-	-
MLTJ054100.10–671628.5	05:41:00.1018	–67:16:28.5311	16.220	16.404	16.668	16.601	-	-
MLTJ054122.64–192104.4	05:41:22.644	–19:21:04.4926	16.680	16.868	17.057	16.990	7.50129	0.07546
MLTJ054309.56–690607.0	05:43:09.5628	–69:06:07.0596	15.370	15.379	15.596	15.530	1.10591	0.41248
MLTJ054352.52–690112.0	05:43:52.5238	–69:01:12.0875	14.838	14.793	14.963	14.868	1.10146	0.22144
MLTJ054714.03–334426.0	05:47:14.0362	–33:44:26.0046	16.932	17.007	17.248	17.163	6.38770	0.08788
MLTJ055211.22–495306.3	05:52:11.2251	–49:53:06.3986	17.032	17.164	17.448	17.394	4.75430	0.08992
MLTJ055519.37–704052.4	05:55:19.3778	–70:40:52.409	15.377	15.474	15.773	15.730	-	-
MLTJ055944.00–731227.6	05:59:44.0068	–73:12:27.6264	15.296	15.522	15.779	15.929	1.92752	0.04054
MLTJ055944.01–731227.6	05:59:44.0167	–73:12:27.6914	15.278	15.530	15.763	15.789	1.92752	0.04054
MLTJ062425.78–325730.8	06:24:25.7878	–32:57:30.8494	15.368	15.361	15.498	15.445	14.45685	0.03326
MLTJ062425.79–325731.0	06:24:25.7914	–32:57:31.0606	15.400	15.385	15.523	15.477	14.45685	0.03326
MLTJ062643.97–504537.8	06:26:43.9788	–50:45:37.8849	16.387	16.571	16.630	16.615	2.25796	0.11059
MLTJ062643.98–504537.6	06:26:43.9829	–50:45:37.6706	16.393	16.563	16.623	16.609	2.25796	0.11059
MLTJ063253.06–384329.0	06:32:53.0681	–38:43:29.0909	15.860	16.311	16.634	16.513	3.78569	0.51961
MLTJ063253.07–384329.0	06:32:53.0706	–38:43:29.0372	15.855	16.315	16.610	16.520	3.78569	0.51961
MLTJ063620.45–150437.0	06:36:20.4503	–15:04:37.0965	15.737	15.829	16.030	15.989	3.84065	0.06077
MLTJ063732.39–165831.0	06:37:32.391	–16:58:31.046	15.136	15.365	15.646	15.511	1.04946	0.05537
MLTJ064004.73–270320.0	06:40:04.7391	–27:03:20.0306	15.678	15.911	16.163	15.998	0.73701	0.05440
MLTJ064056.60–185643.6	06:40:56.6014	–18:56:43.6589	16.769	16.988	17.350	17.191	3.49428	0.11361
MLTJ064724.55–312935.2	06:47:24.5547	–31:29:35.2547	16.770	16.817	17.048	16.985	5.43376	0.13983
MLTJ064936.83–833153.0	06:49:36.8363	–83:31:53.0289	14.861	14.922	15.154	15.031	1.23223	0.03377
MLTJ064936.88–833153.0	06:49:36.8844	–83:31:53.0729	14.903	14.926	15.173	15.096	1.23223	0.03377
MLTJ065435.67–180152.1	06:54:35.6793	–18:01:52.1824	16.549	16.574	16.710	16.702	0.88252	0.09338
MLTJ065449.05–791843.1	06:54:49.0528	–79:18:43.14	16.954	17.076	17.285	17.243	0.42601	0.07820
MLTJ070223.62–364243.7	07:02:23.6291	–36:42:43.7883	16.555	16.641	16.855	16.773	0.64407	0.05433
MLTJ070902.19–341753.7	07:09:02.1974	–34:17:53.7143	16.957	16.928	17.008	16.973	12.44138	0.07692
MLTJ071444.56–323235.0	07:14:44.5654	–32:32:35.0764	17.131	17.387	17.676	17.538	5.77587	0.11107
MLTJ071444.56–323235.0	07:14:44.5645	–32:32:35.0442	17.163	17.349	17.609	17.510	5.77587	0.11107
MLTJ072016.20–264458.1	07:20:16.2085	–26:44:58.1392	16.611	16.743	16.985	16.905	0.50446	0.07637
MLTJ072152.89–465305.6	07:21:52.8921	–46:53:05.6475	16.762	16.784	17.012	16.915	0.59980	0.06119
MLTJ073217.76–573454.2	07:32:17.7699	–57:34:54.2297	16.118	16.366	16.643	16.535	0.65927	0.07613
MLTJ074739.80–332420.3	07:47:39.8036	–33:24:20.3762	17.082	17.065	17.130	17.101	0.63116	0.08160
MLTJ075411.87–143916.4	07:54:11.8781	–14:39:16.443	15.117	15.355	15.342	15.197	1.00925	0.03777

MLTJ075411.87–143916.4	07:54:11.8779	–14:39:16.4351	15.123	15.392	15.376	15.188	1.00925	0.03777
MLTJ075928.67–220921.7	07:59:28.6772	–22:09:21.7816	16.597	16.811	17.137	17.050	0.48973	0.08225
MLTJ080146.07–683258.9	08:01:46.0739	–68:32:58.9283	16.972	17.114	17.328	17.333	1.18723	0.20872
MLTJ080401.92–211831.9	08:04:01.9265	–21:18:31.9957	16.721	17.141	17.460	17.354	1.79874	0.07669
MLTJ080401.92–211832.0	08:04:01.9258	–21:18:32.0242	16.724	17.155	17.448	17.328	1.79874	0.07669
MLTJ080401.92–211832.0	08:04:01.9258	–21:18:32.0242	16.724	17.155	17.448	17.328	1.79874	0.07669
MLTJ081023.08–153344.3	08:10:23.0899	–15:33:44.3367	16.522	16.786	16.960	16.898	1.83402	0.12650
MLTJ081023.08–153344.4	08:10:23.0866	–15:33:44.4251	16.516	16.800	16.971	16.903	1.83402	0.12650
MLTJ081249.96–560027.6	08:12:49.9684	–56:00:27.6412	15.428	15.565	15.757	15.694	0.88967	0.04714
MLTJ081249.97–560027.6	08:12:49.9795	–56:00:27.6381	15.396	15.527	15.764	15.673	0.88967	0.04714
MLTJ081530.78–342123.3	08:15:30.7827	–34:21:23.3982	16.700	16.722	16.878	16.758	0.50348	0.06084
MLTJ081835.71–183242.8	08:18:35.7153	–18:32:42.8257	16.013	16.112	16.371	16.301	11.41740	0.06412
MLTJ083142.28–610030.1	08:31:42.2801	–61:00:30.1443	16.140	16.223	16.380	16.312	0.64604	0.04032
MLTJ083700.91–555557.7	08:37:00.9108	–55:55:57.7325	16.058	16.129	16.393	16.329	12.37315	0.04667
MLTJ084907.24+113925.4	08:49:07.2451	=+11:39:25.4832	16.524	16.777	17.151	17.039	1.68766	0.10281
MLTJ085449.77–175705.7	08:54:49.7706	–17:57:05.7302	15.041	15.091	15.353	15.250	0.98936	0.07216
MLTJ090257.69–075919.8	09:02:57.691	–07:59:19.8205	15.564	15.506	15.498	15.571	1.37357	0.07568
MLTJ090257.69–075919.8	09:02:57.6948	–07:59:19.8338	15.568	15.538	15.515	15.583	1.37357	0.07568
MLTJ090824.09–012521.9	09:08:24.0961	–01:25:21.9354	17.186	17.501	17.773	17.587	1.14794	0.13202
MLTJ090824.09–012521.9	09:08:24.0958	–01:25:21.9249	17.140	17.483	17.758	17.536	1.14794	0.13202
MLTJ093453.90–585358.2	09:34:53.907	–58:53:58.2096	16.817	17.039	17.360	17.261	1.50934	0.07591
MLTJ094503.82–621540.7	09:45:03.8226	–62:15:40.7925	16.876	17.162	17.474	17.375	2.93250	0.07823
MLTJ094503.82–621540.7	09:45:03.8226	–62:15:40.7776	16.842	17.150	17.405	17.366	2.93250	0.07823
MLTJ094739.59–531704.6	09:47:39.5906	–53:17:04.698	16.330	16.418	16.524	16.471	4.90883	0.05729
MLTJ094739.59–531704.6	09:47:39.5906	–53:17:04.698	16.330	16.418	16.524	16.471	4.90883	0.05729
MLTJ100133.23–084250.6	10:01:33.2348	–08:42:50.6703	15.831	16.051	16.423	16.297	5.33858	0.10197
MLTJ100322.31–610820.2	10:03:22.3103	–61:08:20.2655	16.860	16.953	17.220	17.126	0.47194	0.07705
MLTJ101043.81–582025.3	10:10:43.8164	–58:20:25.3495	15.365	15.294	15.372	15.337	0.89240	0.05564
MLTJ102251.75–322602.6	10:22:51.7536	–32:26:02.6284	15.203	15.575	15.967	15.818	2.62280	0.08546
MLTJ104626.53–530717.1	10:46:26.5397	–53:07:17.1843	15.404	15.638	15.966	15.828	0.84616	0.04197
MLTJ104704.69–352725.3	10:47:04.6934	–35:27:25.3188	17.617	17.653	17.842	17.882	4.61179	0.17376
MLTJ104805.98–751745.3	10:48:05.986	–75:17:45.3022	14.968	15.183	15.497	15.415	4.32989	0.03699
MLTJ110105.32–355045.3	11:01:05.3246	–35:50:45.3101	17.249	17.456	17.632	17.614	0.37351	0.11061
MLTJ110420.12–541544.5	11:04:20.1274	–54:15:44.5444	16.712	16.822	16.864	16.970	0.46760	0.06094
MLTJ110420.12–541544.5	11:04:20.1274	–54:15:44.5444	16.712	16.822	16.864	16.970	0.46760	0.06094
MLTJ111610.64–525935.8	11:16:10.6453	–52:59:35.8053	15.829	15.860	15.970	15.948	0.77848	0.21514
MLTJ111632.74–714049.2	11:16:32.7495	–71:40:49.2286	16.649	16.790	17.035	16.944	0.55730	0.07475
MLTJ111913.45–704853.8	11:19:13.4506	–70:48:53.8126	14.618	14.871	15.247	15.098	5.90020	0.04255
MLTJ112405.68–431729.4	11:24:05.6825	–43:17:29.4962	16.280	16.593	16.649	16.658	1.60937	0.13452
MLTJ112405.69–431729.5	11:24:05.6901	–43:17:29.5196	16.278	16.587	16.643	16.653	1.60937	0.13452
MLTJ113752.14–580720.6	11:37:52.1463	–58:07:20.686	15.758	15.936	16.181	16.090	0.73703	0.04906
MLTJ114112.44–340146.5	11:41:12.443	–34:01:46.526	16.241	16.331	16.611	16.489	8.25012	0.09020
MLTJ114618.09–314101.5	11:46:18.0955	–31:41:01.5954	16.091	16.416	16.741	16.574	4.76606	0.08328
MLTJ114618.09–314101.6	11:46:18.0965	–31:41:01.6221	16.084	16.433	16.724	16.606	4.76606	0.08328
MLTJ115915.47–140925.3	11:59:15.4722	–14:09:25.3087	17.046	17.023	17.082	17.063	10.83326	0.10465
MLTJ115915.47–140925.3	11:59:15.4755	–14:09:25.3258	17.059	17.046	17.105	17.072	10.83326	0.10465

MLTJ120752.79–550021.7	12:07:52.792	–55:00:21.7422	16.410	16.396	16.566	16.533	0.61266	0.07053
MLTJ121018.82–554428.6	12:10:18.8266	–55:44:28.6186	16.038	16.142	16.286	16.233	0.70721	0.05552
MLTJ121432.53–541942.5	12:14:32.5377	–54:19:42.5293	15.222	15.467	15.814	15.657	0.98143	0.05919
MLTJ121558.78–491453.4	12:15:58.7892	–49:14:53.4411	16.111	16.334	16.630	16.507	3.26349	0.08213
MLTJ123403.30–450133.3	12:34:03.3023	–45:01:33.3182	15.189	15.476	15.796	15.657	3.19427	0.33252
MLTJ123836.35–004042.6	12:38:36.3595	–00:40:42.68	17.145	17.451	17.770	17.658	0.81240	0.60325
MLTJ123836.36–004042.7	12:38:36.3628	0:40:42.7381	17.146	17.470	17.782	17.658	0.81240	0.60325
MLTJ124141.97–745348.9	12:41:41.9761	–74:53:48.9164	16.402	16.589	16.883	16.839	0.57152	0.05980
MLTJ124848.88–344208.5	12:48:48.8821	–34:42:08.5955	14.816	15.088	15.472	15.301	6.00241	0.08107
MLTJ125002.08–310255.5	12:50:02.087	–31:02:55.578	13.717	13.714	13.761	13.759	-	-
MLTJ130222.80–571925.9	13:02:22.8007	–57:19:25.9082	16.840	16.813	16.972	17.007	0.51698	0.08029
MLTJ130821.08–445101.9	13:08:21.0846	–44:51:01.993	17.480	17.507	17.529	17.541	0.50199	0.13444
MLTJ130821.08–445101.9	13:08:21.0846	–44:51:01.993	17.480	17.507	17.529	17.541	0.50199	0.13444
MLTJ131438.71–554554.9	13:14:38.7193	–55:45:54.9207	16.284	16.352	16.487	16.489	0.57801	0.06042
MLTJ131648.10–323744.6	13:16:48.1018	–32:37:44.6955	16.103	16.296	16.553	16.483	0.61499	0.09296
MLTJ132611.45–494345.2	13:26:11.4519	–49:43:45.298	17.308	17.435	17.697	17.589	0.40874	0.14302
MLTJ132856.32–420153.9	13:28:56.3238	–42:01:53.9739	17.131	17.320	17.596	17.473	0.46578	0.12809
MLTJ133619.57–063758.5	13:36:19.5786	–06:37:58.5094	16.136	16.072	16.247	16.169	7.45780	0.09331
MLTJ134147.45–420052.8	13:41:47.4529	–42:00:52.8334	16.810	16.810	16.948	16.893	10.71525	0.18007
MLTJ134147.45–420052.8	13:41:47.4541	–42:00:52.8548	16.807	16.829	16.969	16.934	10.71525	0.18007
MLTJ134930.21–100443.5	13:49:30.21	–10:04:43.5121	16.478	16.528	16.680	16.634	11.70868	0.10649
MLTJ134930.21–100443.5	13:49:30.2131	–10:04:43.5395	16.490	16.537	16.699	16.639	11.70868	0.10649
MLTJ135103.48–665350.1	13:51:03.4814	–66:53:50.1225	16.226	16.225	16.399	16.359	0.61238	0.04636
MLTJ135917.77–305409.7	13:59:17.7747	–30:54:09.7126	16.506	16.582	16.731	16.693	0.93932	0.21845
MLTJ135917.90–851327.8	13:59:17.9061	–85:13:27.8955	15.170	15.238	15.482	15.405	0.98095	0.03703
MLTJ140801.86–331716.9	14:08:01.8651	–33:17:16.9731	16.796	16.879	17.035	16.994	0.62972	0.09885
MLTJ141141.49–482900.9	14:11:41.4998	–48:29:00.9636	16.093	16.192	16.482	16.459	0.61356	0.10786
MLTJ141508.09–025431.1	14:15:08.0952	–02:54:31.1632	16.638	16.758	17.044	16.930	4.75012	0.13482
MLTJ141543.77–672204.0	14:15:43.7748	–67:22:04.018	16.371	16.576	16.755	16.747	1.26287	0.16190
MLTJ141543.78–672203.9	14:15:43.781	–67:22:03.9661	16.367	16.584	16.730	16.681	1.26287	0.16190
MLTJ141950.45–634119.3	14:19:50.4575	–63:41:19.3704	16.813	16.746	16.810	16.763	0.47458	0.06123
MLTJ142401.68–515616.6	14:24:01.6897	–51:56:16.6951	14.997	15.057	15.142	15.163	1.23724	0.07363
MLTJ142822.69–815425.4	14:28:22.6968	–81:54:25.4508	15.468	15.551	15.818	15.738	0.87537	0.04619
MLTJ142909.19–445811.8	14:29:09.1927	–44:58:11.8159	17.045	17.280	17.547	17.506	0.54440	0.16966
MLTJ143036.78–495646.9	14:30:36.7821	–49:56:46.991	17.225	17.476	17.723	17.669	0.61668	0.12654
MLTJ143755.01–444658.3	14:37:55.0191	–44:46:58.3167	17.385	17.422	17.591	17.524	0.45362	0.13669
MLTJ143808.55–482530.1	14:38:08.5573	–48:25:30.1758	17.030	17.135	17.384	17.324	0.44976	0.09735
MLTJ144215.68–055835.6	14:42:15.6891	–05:58:35.676	17.504	17.497	17.596	17.576	8.35110	0.13776
MLTJ144322.91–335856.9	14:43:22.9175	–33:58:56.9264	15.948	16.203	16.587	16.467	0.73082	0.10475
MLTJ144700.45–160149.1	14:47:00.4547	–16:01:49.1319	16.294	16.510	16.569	16.833	1.34655	0.10907
MLTJ144700.46–160149.0	14:47:00.4608	–16:01:49.0803	16.282	16.515	16.580	16.694	1.34655	0.10907
MLTJ144721.96–812748.7	14:47:21.9623	–81:27:48.7542	15.406	15.407	15.530	15.514	0.90999	0.03770
MLTJ144721.96–812748.7	14:47:21.9602	–81:27:48.7183	15.401	15.388	15.513	15.503	0.90999	0.03770
MLTJ144737.03–095009.9	14:47:37.0388	–09:50:09.9346	14.666	14.798	15.106	15.006	16.98017	0.05832
MLTJ144912.93–104536.5	14:49:12.9375	–10:45:36.5675	16.120	16.396	16.758	16.538	0.76790	0.08608
MLTJ145054.35–334146.9	14:50:54.359	–33:41:46.9765	15.578	15.969	16.355	16.276	1.25461	0.07381

MLTJ151301.40–143457.1	15:13:01.4059	–14:34:57.1349	17.301	17.261	17.421	17.374	3.36078	0.13469
MLTJ151415.65–012925.3	15:14:15.6583	–01:29:25.399	16.552	16.805	17.069	17.017	0.62589	0.13386
MLTJ151415.65–012925.4	15:14:15.6584	–01:29:25.4206	16.554	16.824	17.086	17.023	0.62589	0.13386
MLTJ151629.11–442615.4	15:16:29.1167	–44:26:15.4677	15.896	15.976	16.203	16.168	0.88104	0.11462
MLTJ151913.75–114645.3	15:19:13.7555	–11:46:45.3822	15.571	15.636	15.729	15.684	0.77000	0.07477
MLTJ151913.76–114645.3	15:19:13.764	–11:46:45.3912	15.575	15.621	15.723	15.696	0.77000	0.07477
MLTJ152055.22–112608.0	15:20:55.2213	–11:26:08.0977	16.992	17.152	17.472	17.392	0.41298	0.14358
MLTJ153133.70–353213.7	15:31:33.7047	–35:32:13.7306	16.705	16.781	16.946	16.912	3.22456	0.14820
MLTJ153346.84–112633.3	15:33:46.8404	–11:26:33.3333	16.851	16.990	17.303	17.179	5.14618	0.16542
MLTJ154620.07–123228.6	15:46:20.0754	–12:32:28.6899	16.203	16.395	16.712	17.136	0.66590	0.09548
MLTJ154809.96–004931.4	15:48:09.9656	–00:49:31.4896	16.434	16.499	16.648	16.591	0.60354	0.19202
MLTJ154809.96–004931.5	15:48:09.9671	0:49:31.5335	16.410	16.480	16.642	16.614	0.60354	0.19202
MLTJ155103.40–350409.4	15:51:03.4098	–35:04:09.4083	16.553	16.619	16.835	16.824	0.51815	0.07744
MLTJ155255.19–154400.4	15:52:55.1913	–15:44:00.4209	17.090	17.282	17.621	17.479	0.49919	0.12731
MLTJ155440.16–073617.1	15:54:40.1641	–07:36:17.1372	16.351	16.493	16.763	16.673	4.36192	0.08412
MLTJ155558.51–611256.2	15:55:58.514	–61:12:56.2967	17.503	17.567	17.763	17.663	0.33503	0.10584
MLTJ155658.03–353107.6	15:56:58.0309	–35:31:07.674	16.675	16.571	16.672	16.593	0.52999	0.09745
MLTJ160031.82–445103.2	16:00:31.8214	–44:51:03.2216	17.103	17.010	17.021	17.047	2.99916	0.08609
MLTJ160038.69–065335.9	16:00:38.6977	–06:53:35.9122	15.358	15.495	15.797	15.685	0.96975	0.06940
MLTJ160337.62–374523.1	16:03:37.6292	–37:45:23.1224	15.570	15.570	15.587	15.548	0.95216	0.06902
MLTJ160408.79–370649.5	16:04:08.798	–37:06:49.5072	16.462	16.619	16.729	16.725	0.58789	0.07335
MLTJ161259.79–100126.8	16:12:59.7971	–10:01:26.8573	16.910	16.905	16.928	16.962	0.79429	0.11507
MLTJ161259.79–100126.8	16:12:59.7971	–10:01:26.8573	16.910	16.905	16.928	16.962	0.79429	0.11507
MLTJ161416.10–345513.1	16:14:16.1012	–34:55:13.1477	17.075	16.974	17.080	17.096	0.49594	0.08719
MLTJ161604.16–794236.8	16:16:04.1633	–79:42:36.8529	14.994	15.209	15.516	15.432	3.04367	0.04481
MLTJ161607.90–101834.0	16:16:07.9079	–10:18:34.0092	16.062	16.181	16.429	16.359	0.74920	0.08008
MLTJ161954.27–653431.2	16:19:54.2774	–65:34:31.2116	15.797	15.725	15.779	15.818	0.76494	0.05790
MLTJ162218.30–061107.7	16:22:18.302	–06:11:07.7738	16.848	16.971	17.162	17.087	1.19914	0.14021
MLTJ162218.30–061107.8	16:22:18.3049	–06:11:07.8189	16.845	16.990	17.171	17.090	1.19914	0.14021
MLTJ164116.65–002821.3	16:41:16.6511	–00:28:21.3008	15.884	15.790	15.898	15.886	18.44848	0.05654
MLTJ164322.58–334205.5	16:43:22.5892	–33:42:05.5977	13.119	13.091	13.256	13.280	2.91225	0.04509
MLTJ164806.26–044725.3	16:48:06.2694	–04:47:25.3151	15.484	15.504	15.633	15.603	1.30024	0.06481
MLTJ164806.26–044725.3	16:48:06.2691	–04:47:25.3119	15.488	15.469	15.595	15.581	1.30024	0.06481
MLTJ164830.53–091822.2	16:48:30.5338	–09:18:22.212	16.206	16.222	16.453	16.401	10.22917	0.06300
MLTJ165045.75–861435.6	16:50:45.7588	–86:14:35.6591	16.094	16.282	16.611	16.526	2.92820	0.06841
MLTJ170221.91–014736.5	17:02:21.9143	–01:47:36.5279	15.899	15.959	16.184	16.132	0.91277	0.06541
MLTJ170500.81–034153.8	17:05:00.8102	–03:41:53.8101	16.584	16.483	16.567	16.585	1.23977	0.12077
MLTJ170507.66–695030.9	17:05:07.6601	–69:50:30.9947	16.298	16.372	16.422	16.451	0.56219	0.05256
MLTJ170921.73+101027.0	17:09:21.7368	=+10:10:27.083	16.368	16.605	16.987	16.837	0.65782	0.07584
MLTJ172737.79–360016.4	17:27:37.7924	–36:00:16.4858	15.061	15.301	15.690	15.535	18.87358	0.07490
MLTJ172956.06–155000.0	17:29:56.066	–15:50:00.0481	17.178	17.179	17.273	17.273	-	-
MLTJ172956.07–155000.0	17:29:56.0758	–15:50:00.0312	17.189	17.218	17.336	17.298	-	-
MLTJ173148.74–712039.0	17:31:48.7438	–71:20:39.0205	16.631	16.665	16.716	16.770	0.47349	0.06968
MLTJ174606.52–003302.8	17:46:06.5245	–00:33:02.8268	17.198	17.276	17.453	17.423	8.15305	0.12837
MLTJ174606.52–003302.8	17:46:06.5212	0:33:02.8846	17.174	17.286	17.484	17.459	8.15305	0.12837
MLTJ175253.87–663448.9	17:52:53.8788	–66:34:48.9999	16.465	16.560	16.727	16.671	18.54382	0.06814

MLTJ175253.88–663448.9	17:52:53.8886	–66:34:48.9464	16.452	16.578	16.789	16.701	18.54382	0.06814
MLTJ181411.28–531653.4	18:14:11.2851	–53:16:53.4488	16.251	16.349	16.532	16.434	0.70518	0.09521
MLTJ181411.28–531653.4	18:14:11.2851	–53:16:53.4488	16.251	16.349	16.532	16.434	0.70518	0.09521
MLTJ185819.25–143025.8	18:58:19.2573	–14:30:25.8702	16.299	16.362	16.457	16.472	0.77316	0.12460
MLTJ185819.26–143025.8	18:58:19.2668	–14:30:25.8517	16.325	16.468	16.570	16.558	0.77316	0.12460
MLTJ185819.26–143025.9	18:58:19.2696	–14:30:25.9469	16.325	16.405	16.500	16.487	0.77316	0.12460
MLTJ190147.42–140355.0	19:01:47.4218	–14:03:55.0307	15.946	16.028	16.294	16.280	0.67377	0.08838
MLTJ190658.11–120557.4	19:06:58.11	–12:05:57.4708	16.415	16.367	16.363	16.399	0.63432	0.07549
MLTJ190752.81–373956.0	19:07:52.8182	–37:39:56.0548	15.157	15.152	15.302	15.274	0.95016	0.05666
MLTJ191052.96–171437.4	19:10:52.966	–17:14:37.4164	17.260	17.470	17.711	17.652	0.98180	0.28060
MLTJ191052.96–171437.4	19:10:52.9685	–17:14:37.4319	17.260	17.468	17.697	17.603	0.98180	0.28060
MLTJ191421.74–595944.9	19:14:21.7463	–59:59:44.9756	17.103	17.465	17.747	17.746	0.55981	0.14503
MLTJ191910.66–152453.6	19:19:10.6683	–15:24:53.6464	16.458	16.633	16.870	16.851	0.56203	0.09256
MLTJ191910.67–152453.6	19:19:10.6754	–15:24:53.6744	16.465	16.668	16.907	16.862	0.56203	0.09256
MLTJ192007.16–663719.5	19:20:07.1672	–66:37:19.5396	17.255	17.265	17.268	17.228	3.33282	0.07817
MLTJ192007.17–663719.5	19:20:07.175	–66:37:19.5515	17.233	17.241	17.256	17.235	3.33282	0.07817
MLTJ192037.94–132605.7	19:20:37.9443	–13:26:05.736	15.470	15.492	15.696	15.634	0.81085	0.10176
MLTJ192106.61–151444.1	19:21:06.6166	–15:14:44.1189	16.098	16.356	16.703	17.692	3.38025	0.09403
MLTJ192124.89–071752.1	19:21:24.8954	–07:17:52.1685	15.874	15.879	16.098	16.050	0.69403	0.09568
MLTJ192319.66–385419.3	19:23:19.6674	–38:54:19.3857	17.662	17.965	18.193	18.127	3.01174	0.38316
MLTJ192319.66–385419.4	19:23:19.6688	–38:54:19.4267	17.654	17.929	18.120	18.055	3.01174	0.38316
MLTJ192433.98–432444.5	19:24:33.9849	–43:24:44.5972	16.036	16.155	16.310	16.277	0.72612	0.09794
MLTJ192433.98–432444.5	19:24:33.9849	–43:24:44.5972	16.036	16.155	16.310	16.277	0.72612	0.09794
MLTJ192501.61–753046.7	19:25:01.6194	–75:30:46.7257	15.576	15.711	16.016	15.882	3.13410	0.05361
MLTJ192607.66–092045.1	19:26:07.6699	–09:20:45.1536	17.350	17.375	17.561	17.504	0.50139	0.15174
MLTJ192617.40–655749.0	19:26:17.4022	–65:57:49.0142	16.184	16.430	16.818	16.536	3.27944	0.09074
MLTJ193215.25–373604.6	19:32:15.253	–37:36:04.6439	15.889	16.086	16.342	16.230	4.25291	0.10207
MLTJ193215.25–373604.6	19:32:15.2519	–37:36:04.6165	15.874	16.099	16.350	16.258	4.25291	0.10207
MLTJ193238.69–604537.4	19:32:38.6981	–60:45:37.4498	15.172	15.262	15.456	15.379	1.05957	0.10418
MLTJ193431.86–433643.9	19:34:31.8661	–43:36:43.9572	15.522	15.591	15.746	15.702	0.92658	0.05970
MLTJ193625.64–352416.7	19:36:25.6452	–35:24:16.7989	17.008	17.187	17.472	17.431	0.55969	0.11414
MLTJ194000.09–665256.0	19:40:00.093	–66:52:56.0381	17.063	17.283	17.614	17.630	5.39779	0.11493
MLTJ194247.28–044715.9	19:42:47.2837	–04:47:15.9319	15.578	15.544	15.721	15.681	1.22454	0.04713
MLTJ194300.67–005833.4	19:43:00.6783	–00:58:33.4702	17.425	17.597	17.838	17.776	0.44224	0.15091
MLTJ194448.58–070557.1	19:44:48.5802	–07:05:57.1759	16.518	16.461	16.586	16.560	0.68873	0.09859
MLTJ194630.00–045218.5	19:46:30.0028	–04:52:18.5276	16.958	17.101	17.277	17.259	0.41748	0.11743
MLTJ195130.95–322255.9	19:51:30.9564	–32:22:55.9695	16.392	16.704	17.027	16.947	1.21064	0.11464
MLTJ195524.50–314956.3	19:55:24.504	–31:49:56.3201	16.401	16.623	16.901	16.821	0.58941	0.11425
MLTJ195548.17–643413.6	19:55:48.1709	–64:34:13.6974	17.526	17.491	17.626	17.582	10.52182	0.11245
MLTJ195859.94–341055.2	19:58:59.9401	–34:10:55.2951	16.559	16.923	17.182	17.077	1.16619	0.11365
MLTJ195859.94–341055.3	19:58:59.9431	–34:10:55.3011	16.566	16.906	17.151	17.110	1.16619	0.11365
MLTJ200320.40–074152.3	20:03:20.4016	–07:41:52.3084	16.550	16.550	16.718	16.676	0.51189	0.09260
MLTJ200400.44–093228.8	20:04:00.44	–09:32:28.8258	16.839	17.095	17.451	17.351	0.51304	0.12342
MLTJ200604.39–032302.7	20:06:04.3949	–03:23:02.7393	16.686	16.745	16.953	16.946	0.48519	0.10608
MLTJ200710.28–161541.1	20:07:10.2834	–16:15:41.112	16.841	17.063	17.416	17.271	1.25344	0.12049
MLTJ200719.42–133348.6	20:07:19.4274	–13:33:48.6556	16.765	16.969	17.239	17.116	0.50760	0.08832

MLTJ200746.88–445428.0	20:07:46.883	–44:54:28.0037	16.599	17.032	17.390	17.233	0.71119	0.17829
MLTJ200746.88–445428.0	20:07:46.883	–44:54:28.0037	16.599	17.032	17.390	17.233	0.71119	0.17829
MLTJ200909.78–114427.6	20:09:09.7891	–11:44:27.6435	16.214	16.421	16.734	16.663	2.80268	0.08445
MLTJ201148.74–035750.8	20:11:48.7494	–03:57:50.8777	16.823	16.891	17.084	17.038	0.70806	0.11873
MLTJ201204.30–032041.2	20:12:04.3034	–03:20:41.2209	16.910	16.944	17.169	17.098	0.46256	0.13017
MLTJ201221.72–021256.6	20:12:21.7228	–02:12:56.6285	17.038	17.218	17.459	17.389	0.58352	0.11639
MLTJ201221.72–021256.6	20:12:21.7224	–02:12:56.6751	17.049	17.222	17.459	17.414	0.58352	0.11639
MLTJ201414.62–335406.8	20:14:14.6211	–33:54:06.802	16.982	17.117	17.383	17.308	5.82158	0.13550
MLTJ201723.73–010138.7	20:17:23.7347	–01:01:38.7116	17.360	17.714	18.024	17.923	1.16162	0.16293
MLTJ202010.12–114655.7	20:20:10.1219	–11:46:55.7498	16.248	16.150	16.255	16.317	0.62736	0.10319
MLTJ202327.36–033540.0	20:23:27.3661	–03:35:40.0077	17.093	17.257	17.586	17.439	5.37116	0.13095
MLTJ203239.56–153120.4	20:32:39.5662	–15:31:20.4962	16.908	16.830	16.857	18.349	4.28704	0.14213
MLTJ205342.93–045943.2	20:53:42.9351	–04:59:43.2355	15.563	15.542	15.657	15.613	22.37659	0.06049
MLTJ205342.93–045943.2	20:53:42.933	–04:59:43.2812	15.580	15.559	15.655	15.631	22.37659	0.06049
MLTJ210323.95–335431.5	21:03:23.9597	–33:54:31.5763	16.831	16.873	17.057	16.935	0.43255	0.11294
MLTJ211303.15–073822.8	21:13:03.1586	–07:38:22.8983	17.445	17.605	17.845	17.780	0.41201	0.17298
MLTJ211329.83–031709.5	21:13:29.8373	–03:17:09.5913	15.391	15.432	15.528	15.512	0.85497	0.09011
MLTJ211329.83–031709.6	21:13:29.8329	–03:17:09.624	15.390	15.397	15.503	15.501	0.85497	0.09011
MLTJ211648.89–365233.6	21:16:48.8988	–36:52:33.6997	16.495	16.510	16.608	16.559	13.95466	0.10518
MLTJ213300.75–044158.4	21:33:00.7568	–04:41:58.4342	16.245	16.398	16.646	16.595	0.58154	0.10816
MLTJ213840.12–003337.3	21:38:40.1273	–00:33:37.3842	17.052	17.078	17.291	17.230	6.48730	0.12293
MLTJ214314.63–752359.6	21:43:14.6342	–75:23:59.6925	16.160	16.426	16.801	16.661	1.74936	0.06802
MLTJ214510.66–321718.6	21:45:10.6675	–32:17:18.617	15.781	16.003	16.283	16.190	0.75470	0.09149
MLTJ215143.39–050248.4	21:51:43.3985	–05:02:48.4941	15.425	15.432	15.634	15.559	19.82550	0.07932
MLTJ220803.20–322800.1	22:08:03.2008	–32:28:00.153	16.556	16.860	17.206	17.035	2.24749	0.11722
MLTJ225541.54–402619.5	22:55:41.5482	–40:26:19.5459	15.543	15.878	16.208	16.061	0.99963	0.70314
MLTJ225541.54–402619.5	22:55:41.5482	–40:26:19.5459	15.543	15.878	16.208	16.061	0.99963	0.70314
MLTJ230213.18–315559.1	23:02:13.1844	–31:55:59.1443	15.592	15.870	15.938	15.919	2.17276	0.26280
MLTJ230213.18–315559.1	23:02:13.1845	–31:55:59.1617	15.591	15.866	15.924	15.997	2.17276	0.26280
MLTJ230345.82–141447.0	23:03:45.8225	–14:14:47.0715	16.623	16.924	17.199	17.108	2.30753	0.11713
MLTJ230816.36–042339.3	23:08:16.3674	–04:23:39.3137	15.694	15.773	15.824	15.866	0.72678	0.06889
MLTJ231602.94–324641.6	23:16:02.9433	–32:46:41.6876	15.595	15.726	16.034	15.969	2.25715	0.06853
MLTJ232129.59–602302.9	23:21:29.5955	–60:23:02.9807	16.576	16.746	16.952	16.946	0.54588	0.08316
MLTJ233917.06–042425.3	23:39:17.0625	–04:24:25.3534	16.006	16.094	16.330	16.246	11.10778	0.10135

B Targets with photometry and spectroscopy

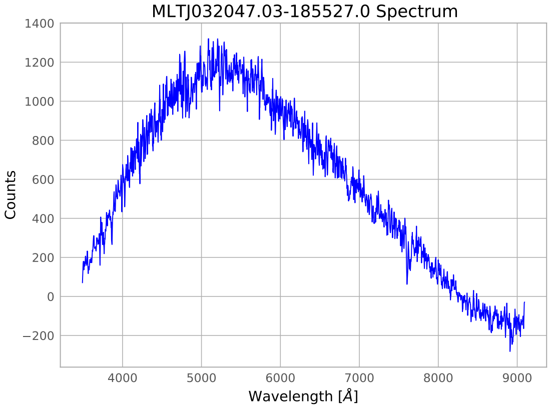

(a) Spectrum.

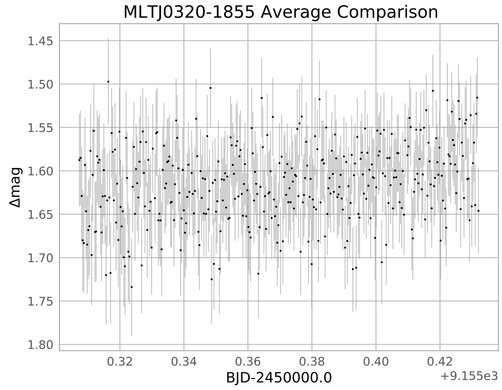

(b) Lightcurve.

Figure 62: MLTJ0320407.03–185527.0.

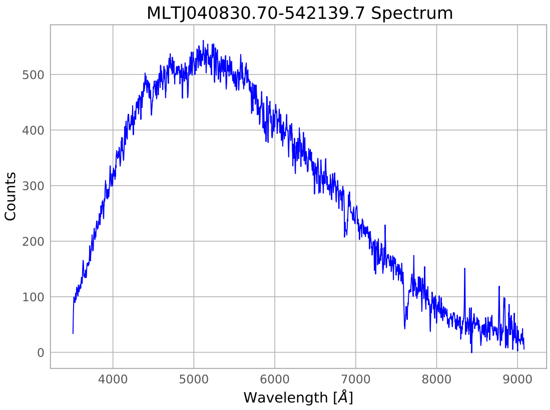

(a) Spectrum.

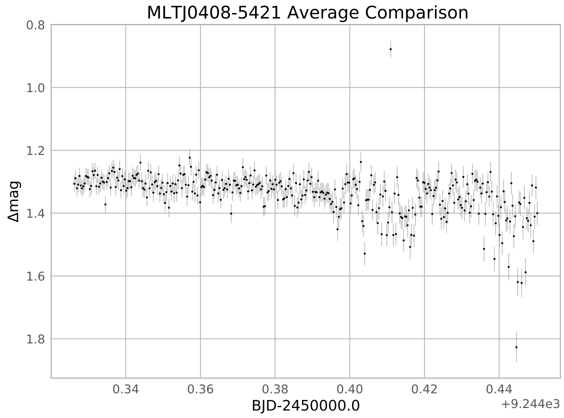

(b) Lightcurve.

Figure 63: MLTJ040830.70–542139.7.

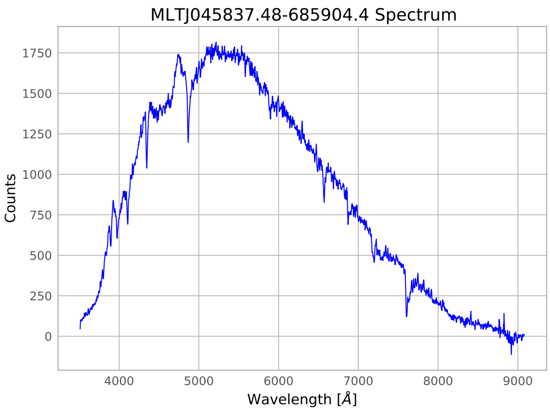

(a) Spectrum.

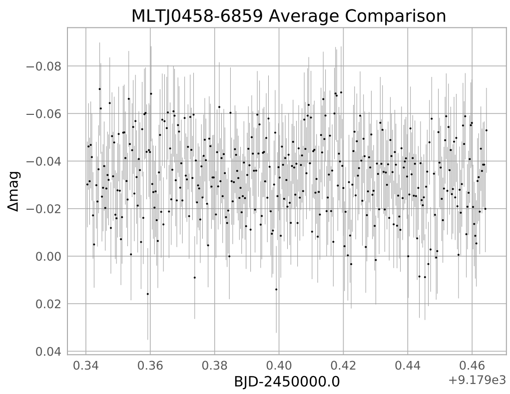

(b) Lightcurve.

Figure 64: MLTJ045837.48–685904.4.

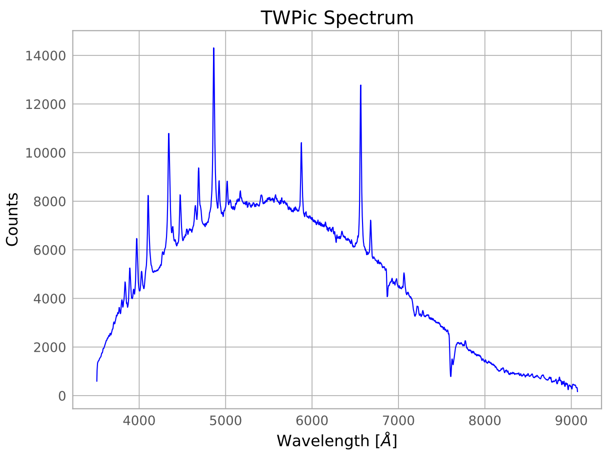

(a) Spectrum.

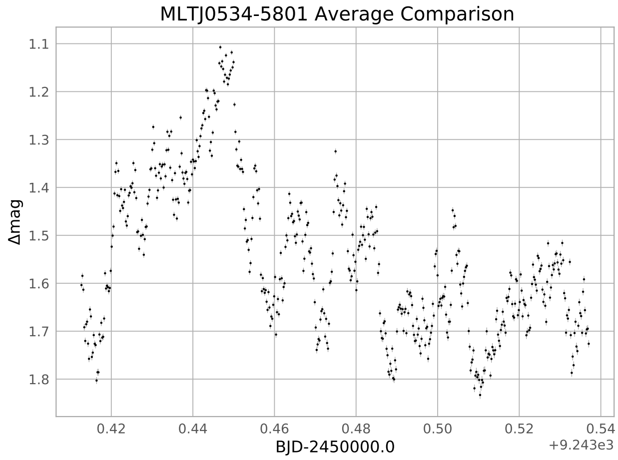

(b) Lightcurve.

Figure 65: MLTJ053450.55–580140.6 (TW Pic).

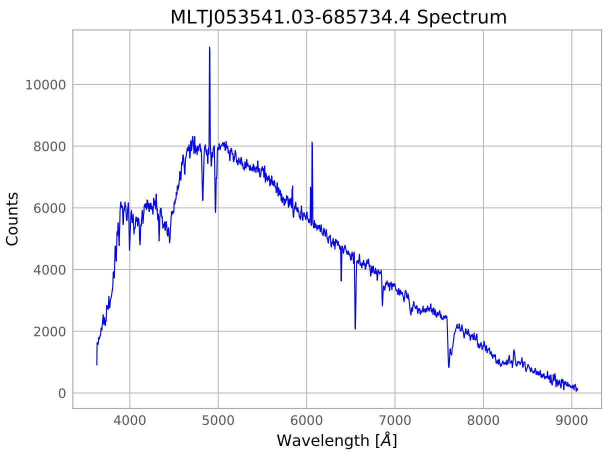

(a) Spectrum.

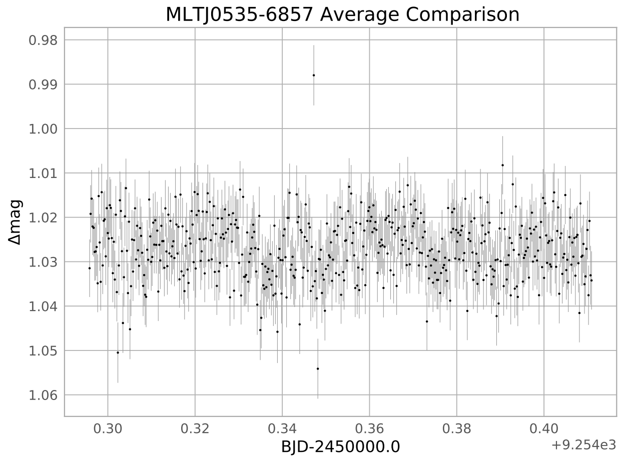

(b) Lightcurve.

Figure 66: MLTJ053541.03–685734.4.

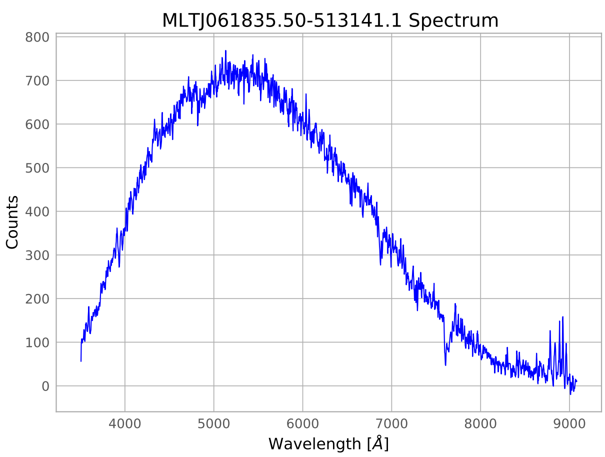

(a) Spectrum.

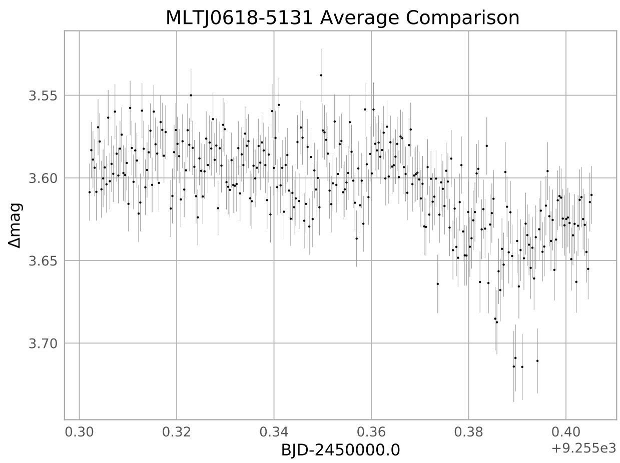

(b) Lightcurve.

Figure 67: MLTJ061835.50–513141.1.

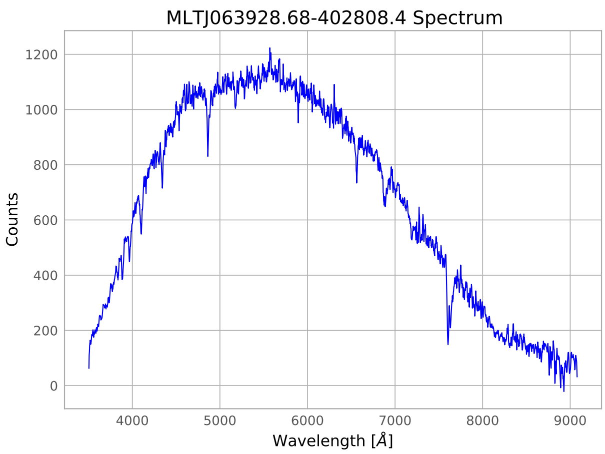

(a) Spectrum.

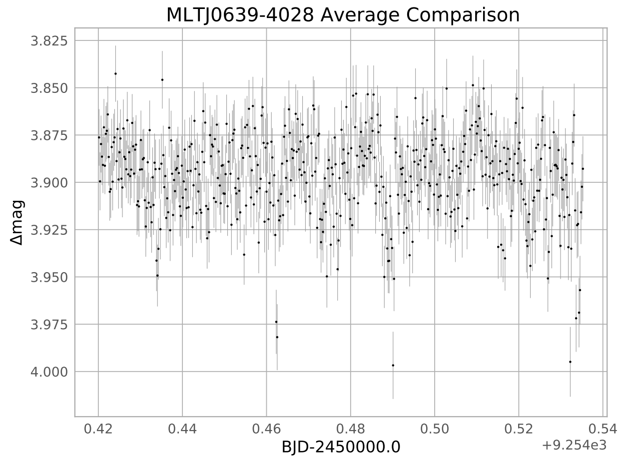

(b) Lightcurve.

Figure 68: MLTJ063928.68–402808.4.

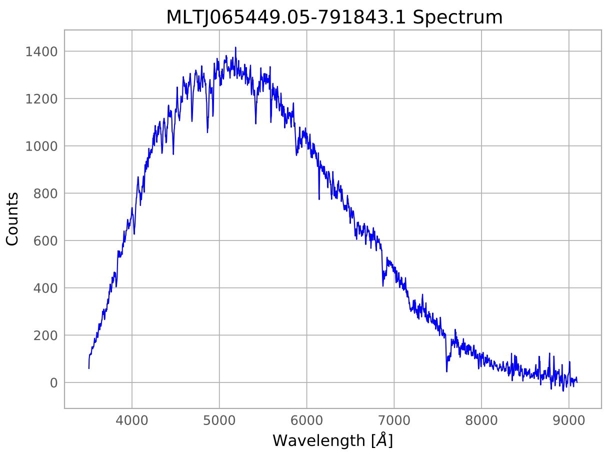

(a) Spectrum.

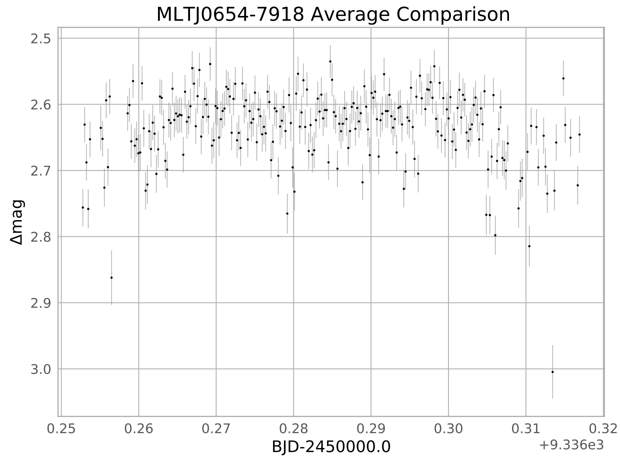

(b) Lightcurve.

Figure 69: MLTJ065449.05–791843.1.

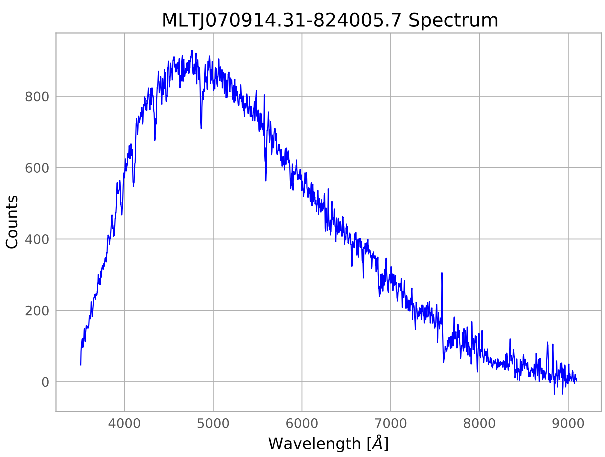

(a) Spectrum.

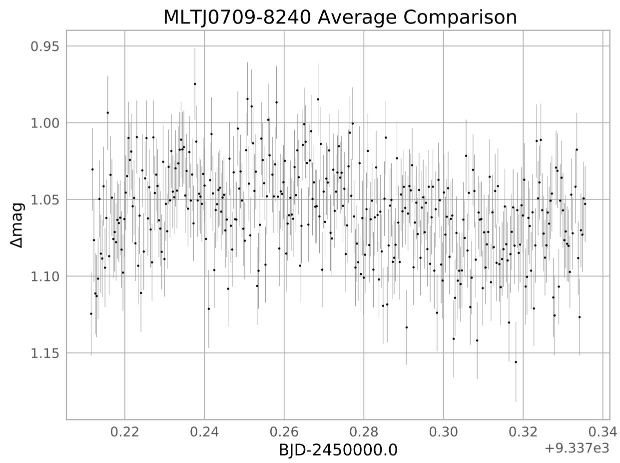

(b) Lightcurve.

Figure 70: MLTJ070914.31–824005.7.

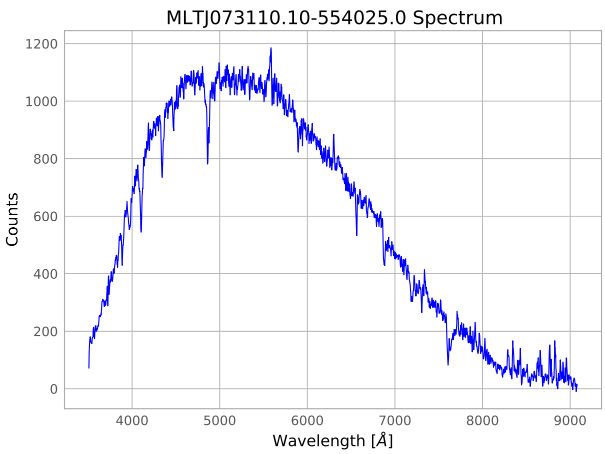

(a) Spectrum.

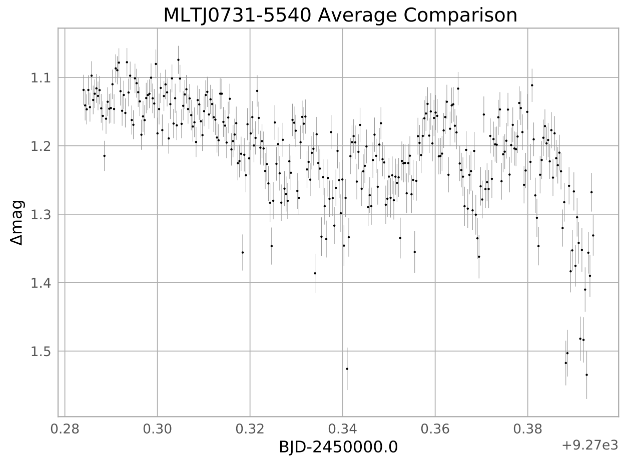

(b) Lightcurve.

Figure 71: MLTJ073110.10–554025.0.

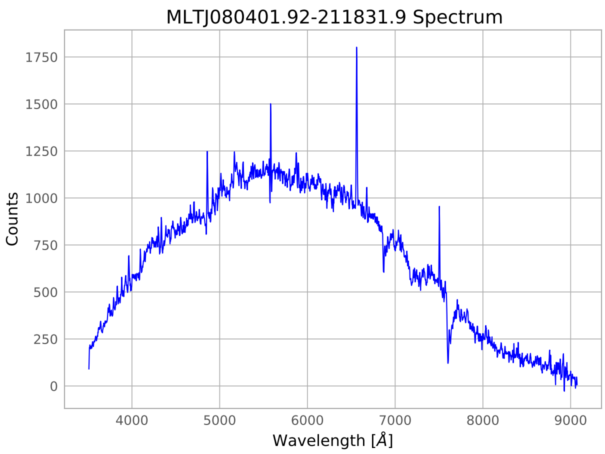

(a) Spectrum.

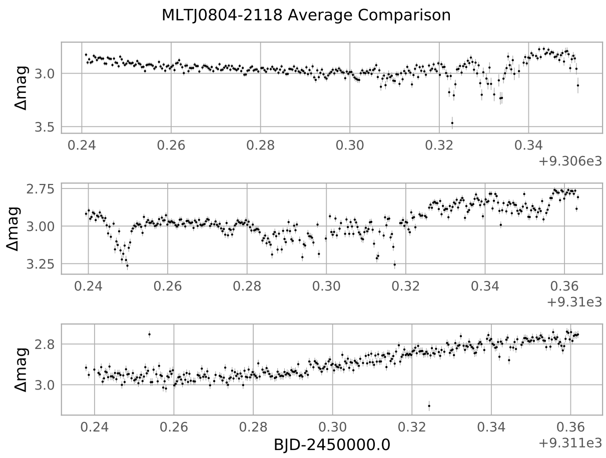

(b) Lightcurve.

Figure 72: MLTJ080401.92–211831.9.

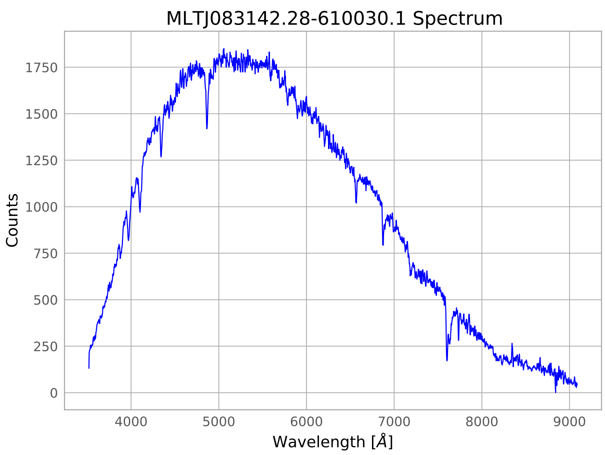

(a) Spectrum.

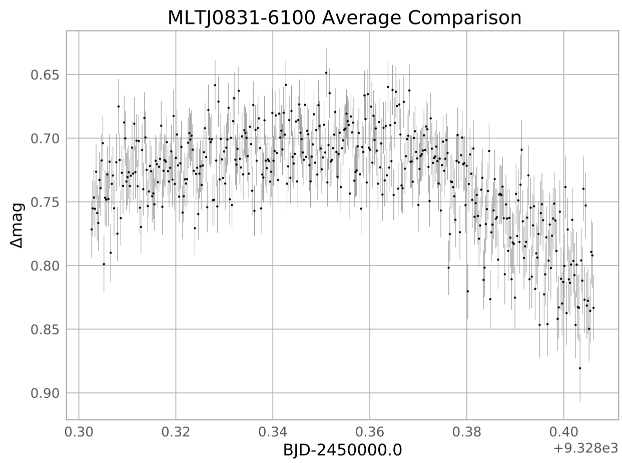

(b) Lightcurve.

Figure 73: MLTJ083142.28–610030.1.

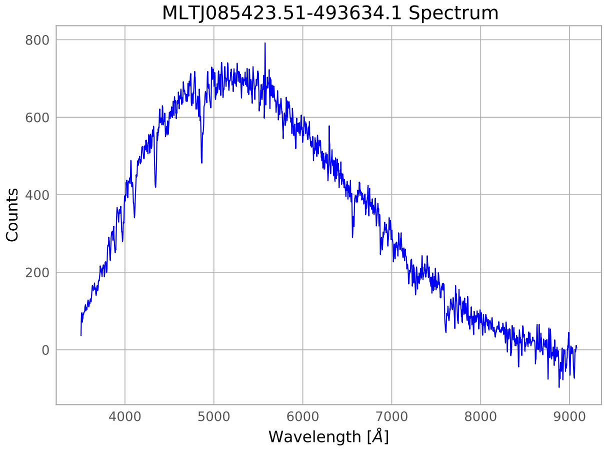

(a) Spectrum.

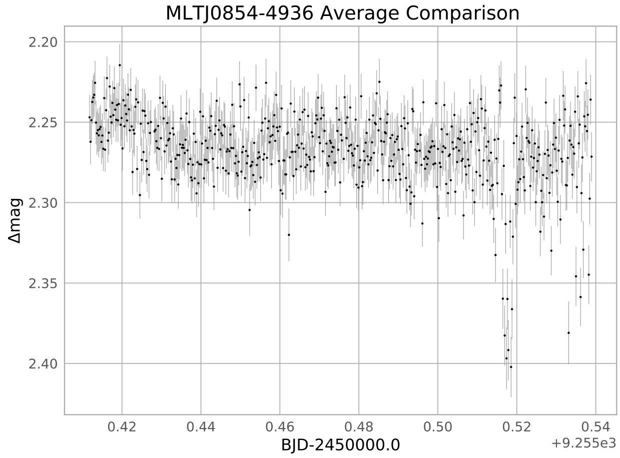

(b) Lightcurve.

Figure 74: MLTJ085423.51–493634.1.

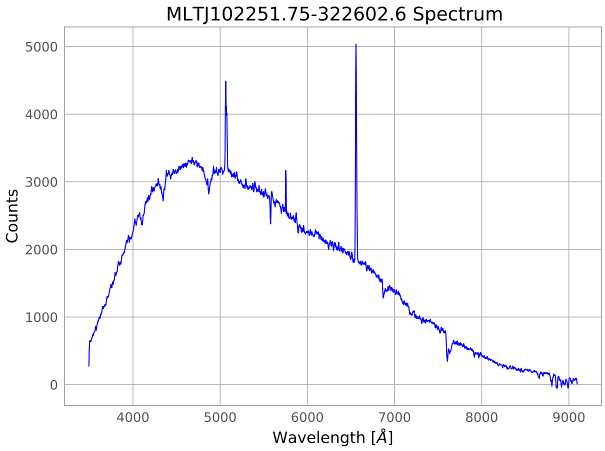

(a) Spectrum.

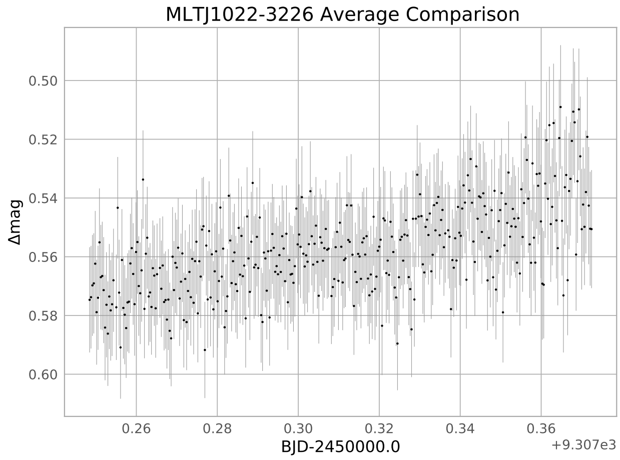

(b) Lightcurve.

Figure 75: MLTJ102251.75–322602.6.

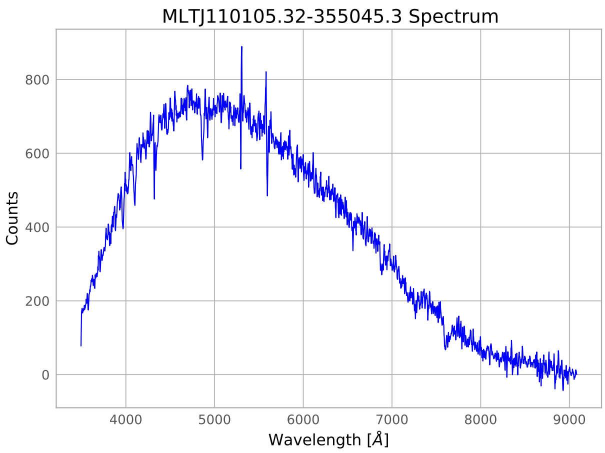

(a) Spectrum.

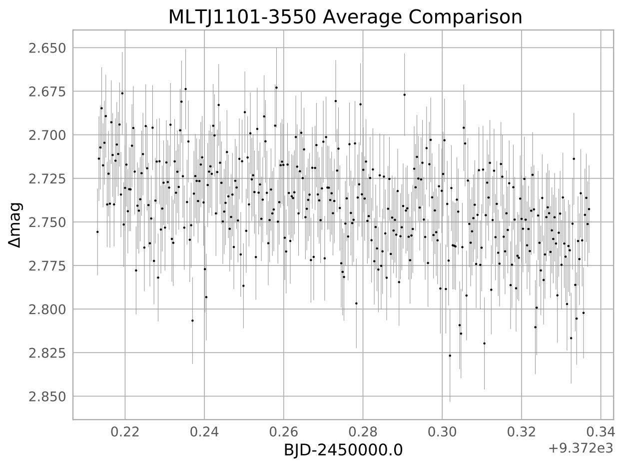

(b) Lightcurve.

Figure 76: MLTJ110105.32–355045.3.

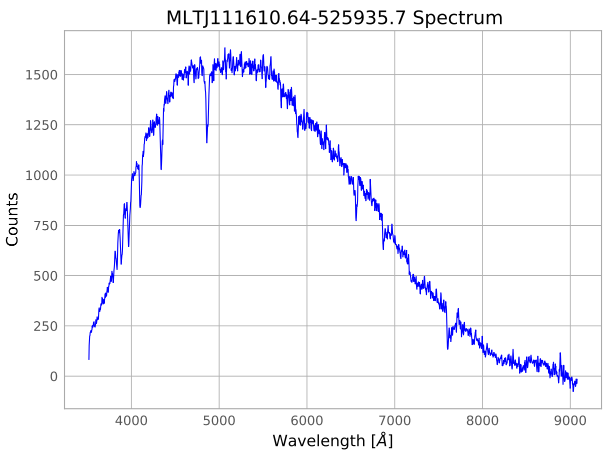

(a) Spectrum.

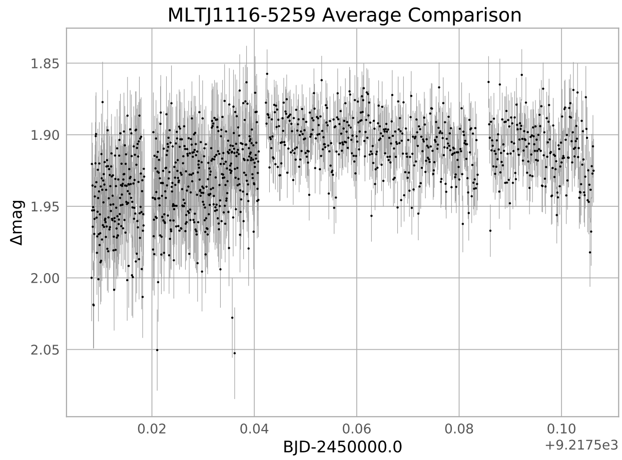

(b) Lightcurve.

Figure 77: MLTJ111610.64–525935.7.

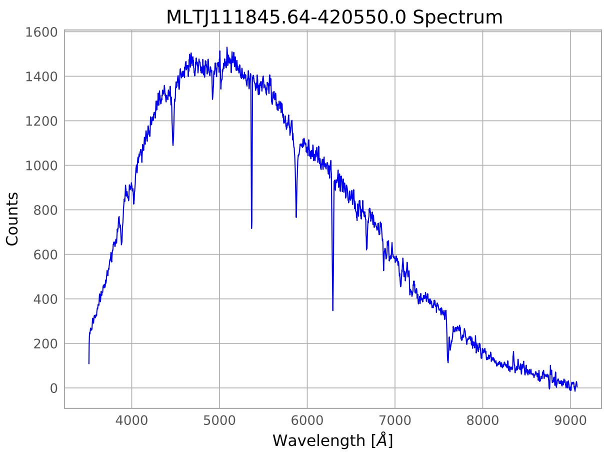

(a) Spectrum.

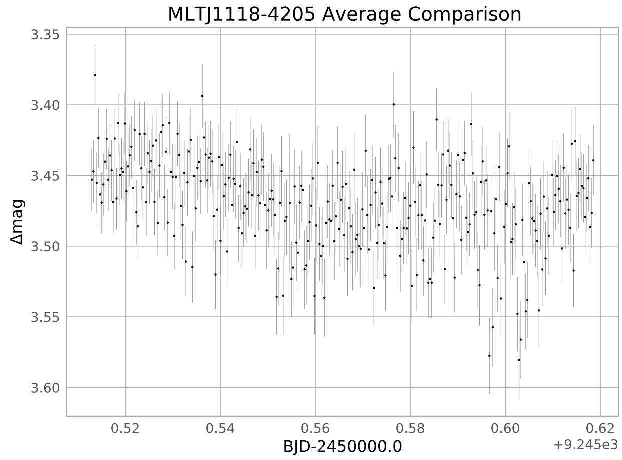

(b) Lightcurve.

Figure 78: MLTJ111845.64–420550.0.

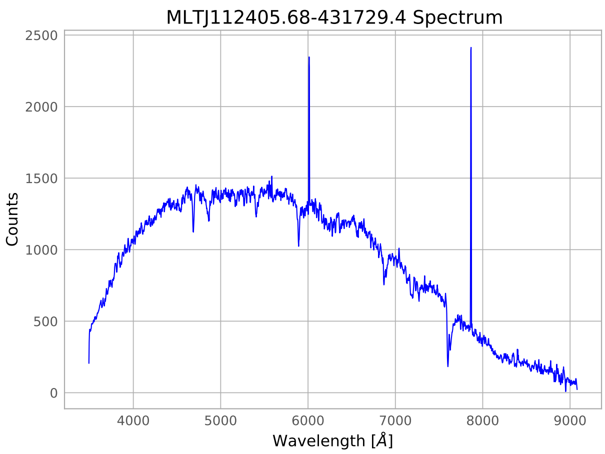

(a) Spectrum.

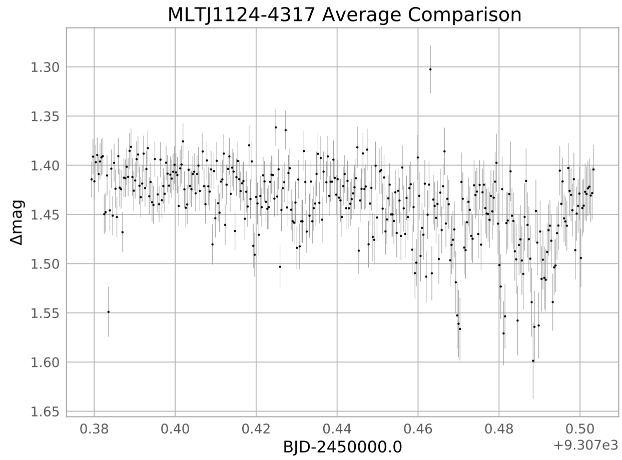

(b) Lightcurve.

Figure 79: MLTJ112405.68–431729.4.

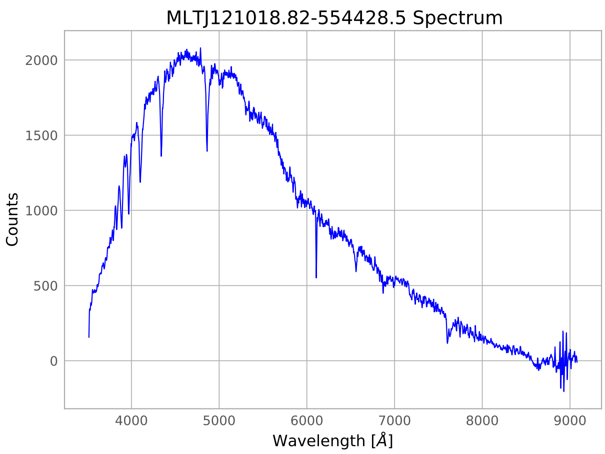

(a) Spectrum.

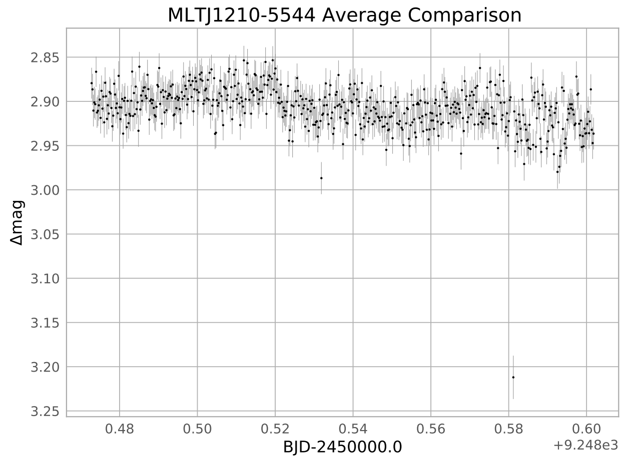

(b) Lightcurve.

Figure 80: MLTJ121018.82–554428.5.

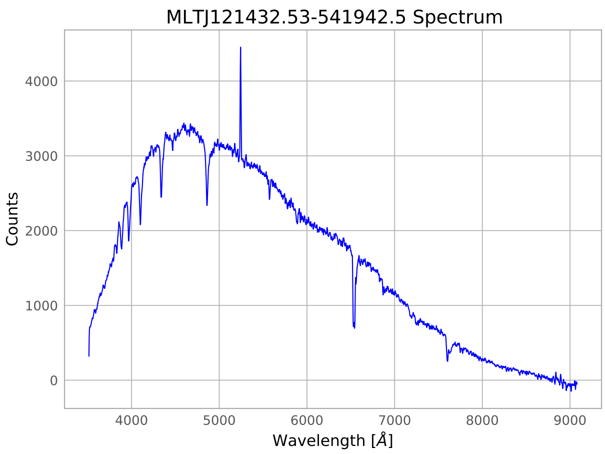

(a) Spectrum.

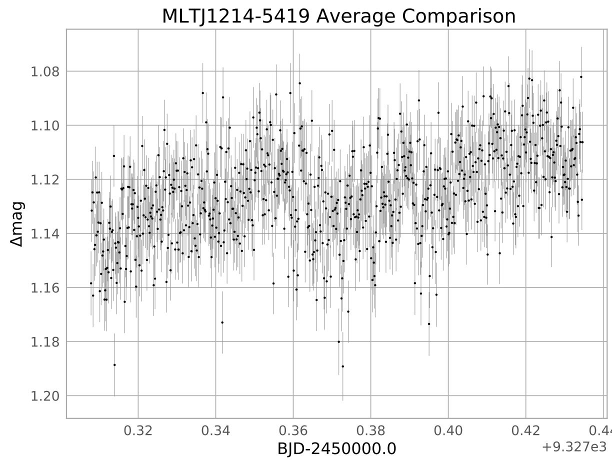

(b) Lightcurve.

Figure 81: MLTJ121432.53–541942.5.

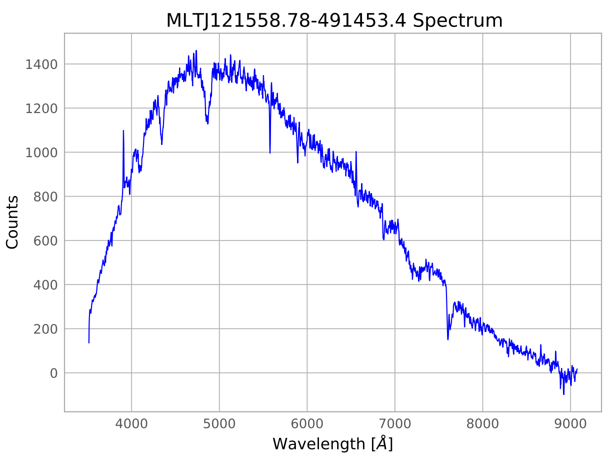

(a) Spectrum.

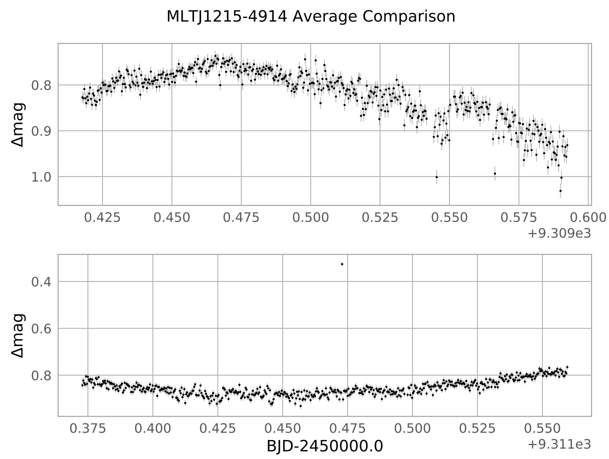

(b) Lightcurve.

Figure 82: MLTJ121558.78–491453.4.

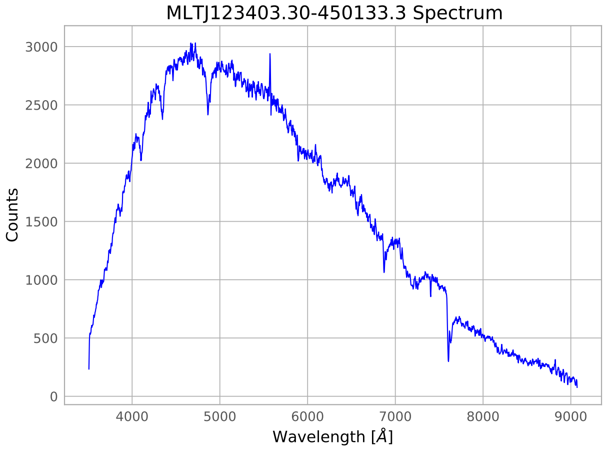

(a) Spectrum.

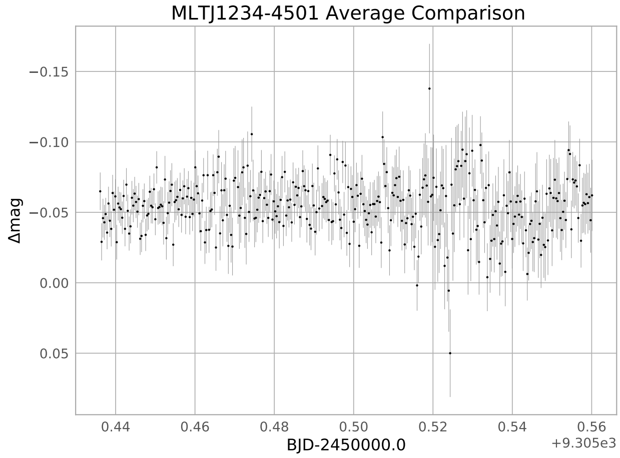

(b) Lightcurve.

Figure 83: MLTJ123403.30–450133.3.

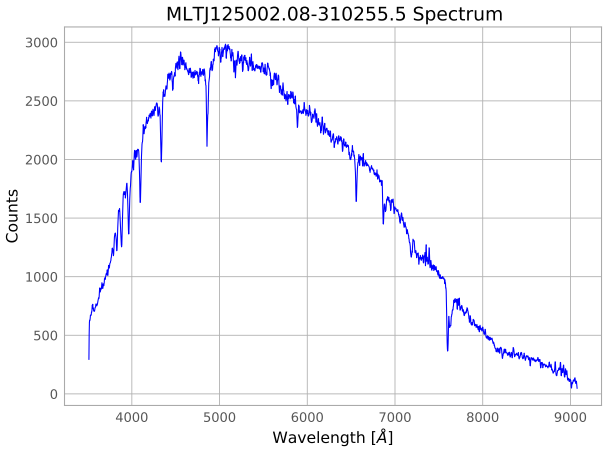

(a) Spectrum.

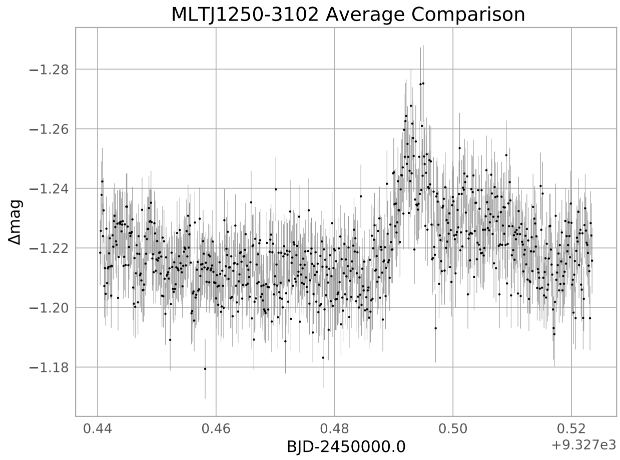

(b) Lightcurve.

Figure 84: MLTJ125002.08–310255.5.

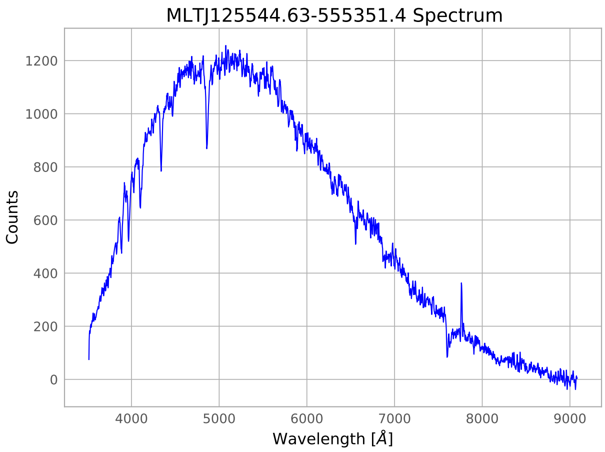

(a) Spectrum.

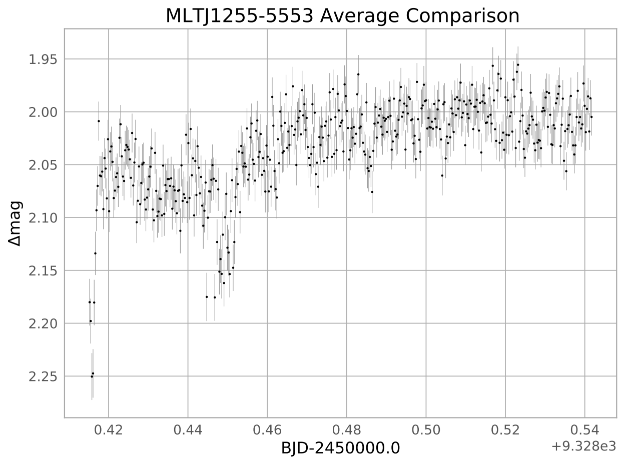

(b) Lightcurve.

Figure 85: MLTJ125544.63–555351.4.

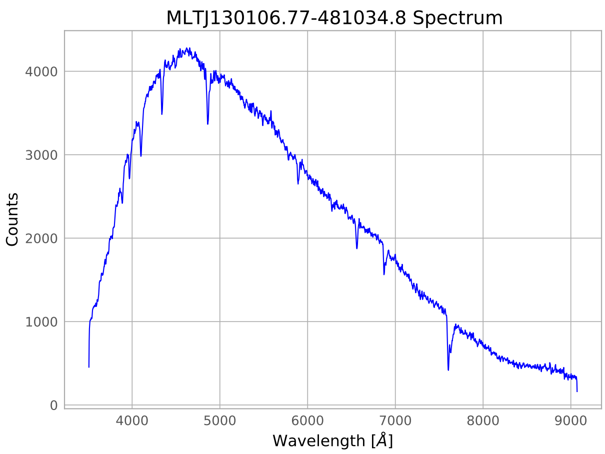

(a) Spectrum.

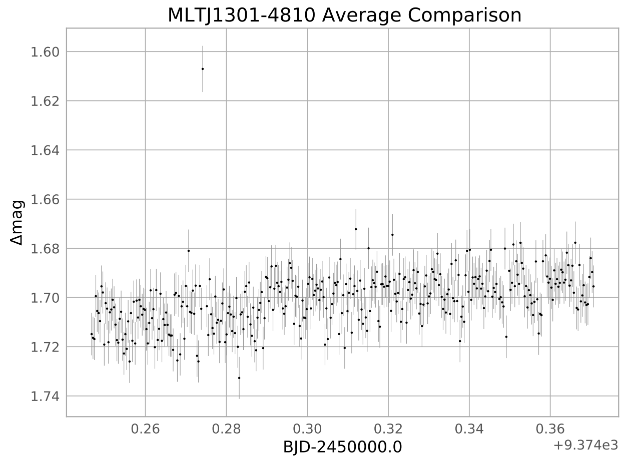

(b) Lightcurve.

Figure 86: MLTJ130106.77–481034.8.

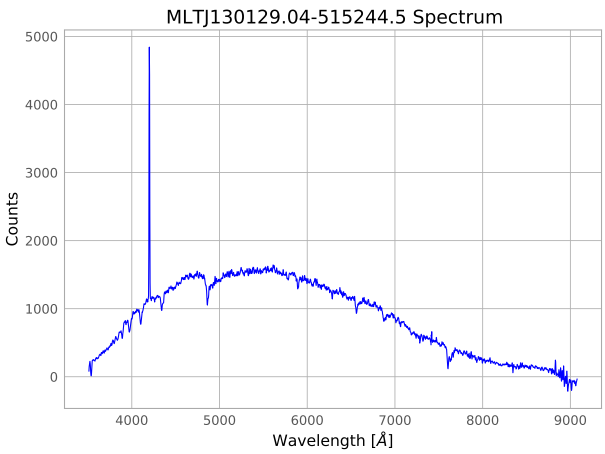

(a) Spectrum.

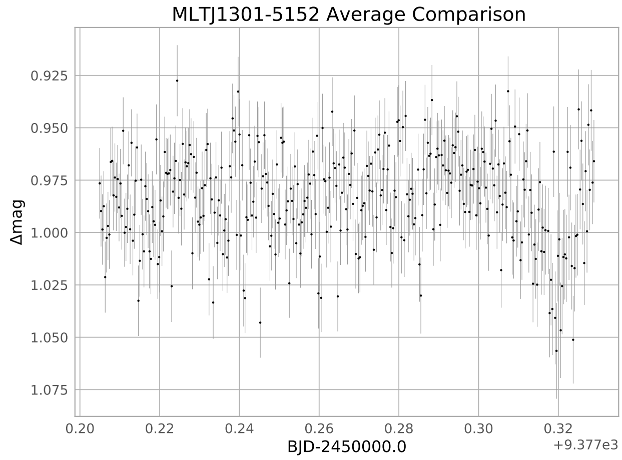

(b) Lightcurve.

Figure 87: MLTJ130129.04–515244.5.

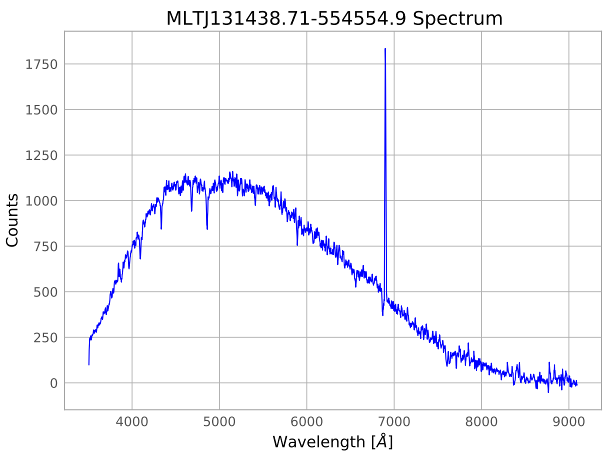

(a) Spectrum.

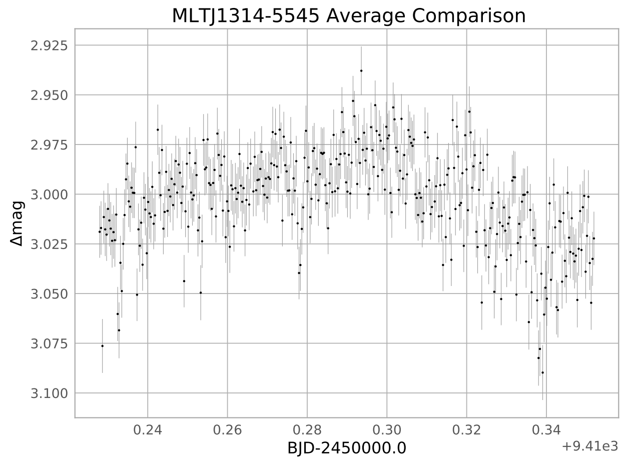

(b) Lightcurve.

Figure 88: MLTJ131438.71–554554.9.

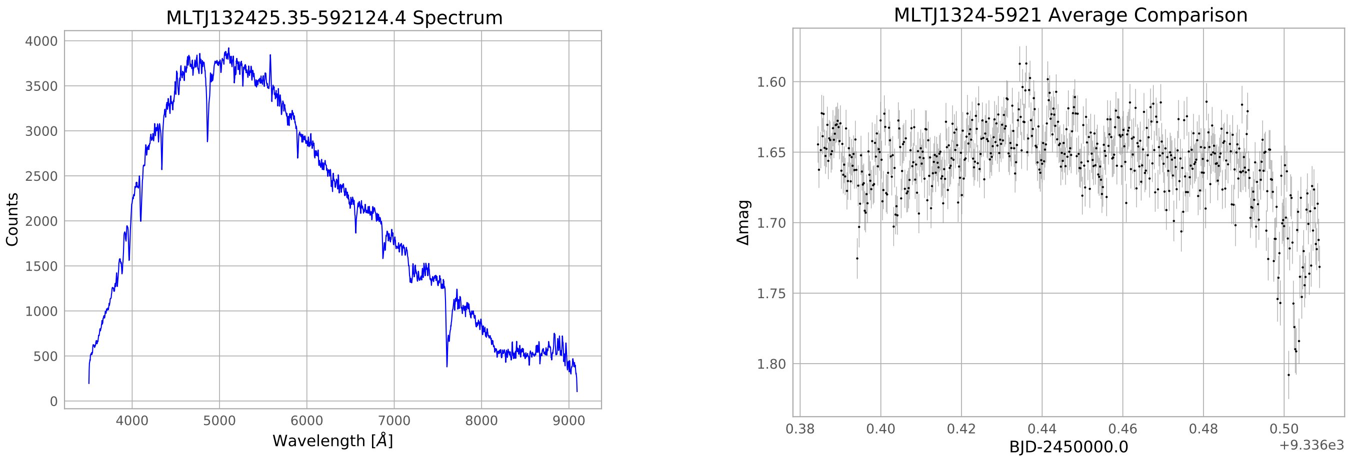

(a) Spectrum.

(b) Lightcurve.

Figure 89: MLTJ132425.35–592124.4.

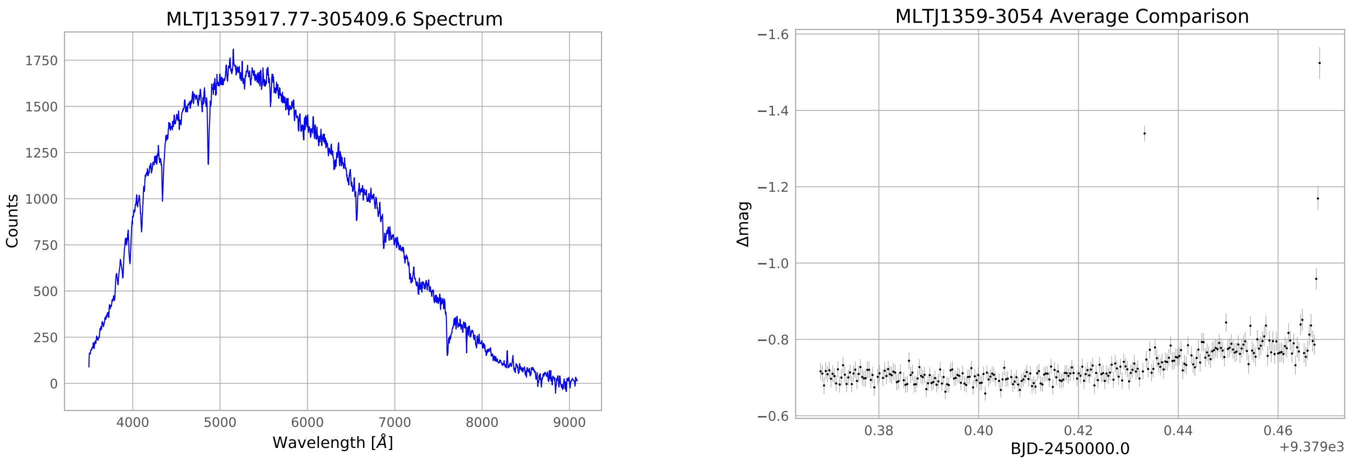

(a) Spectrum.

(b) Lightcurve.

Figure 90: MLTJ135917.77–305409.6.

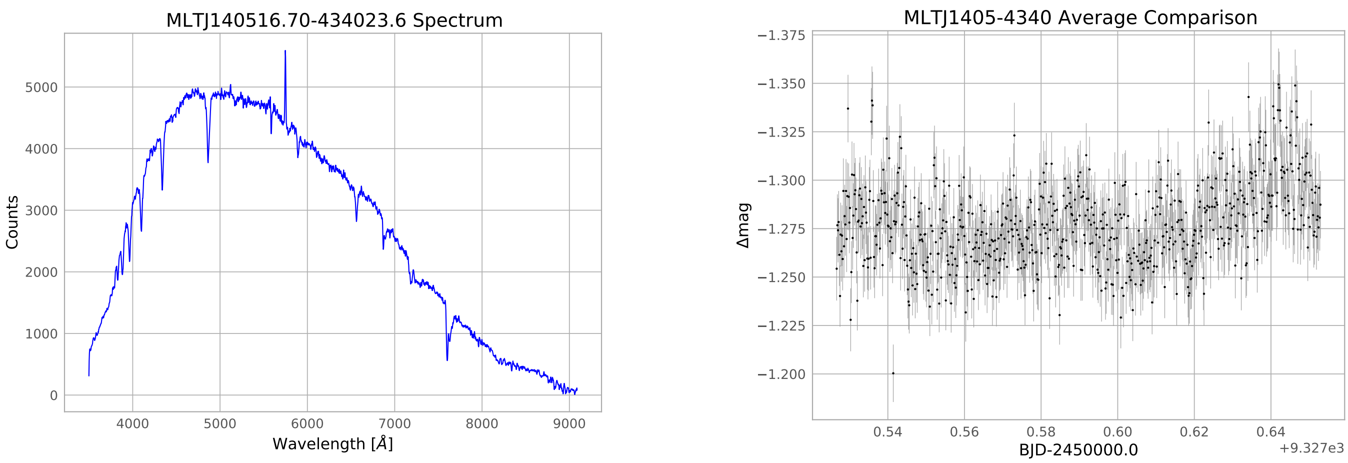

(a) Spectrum.

(b) Lightcurve.

Figure 91: MLTJ140516.70–434023.6.

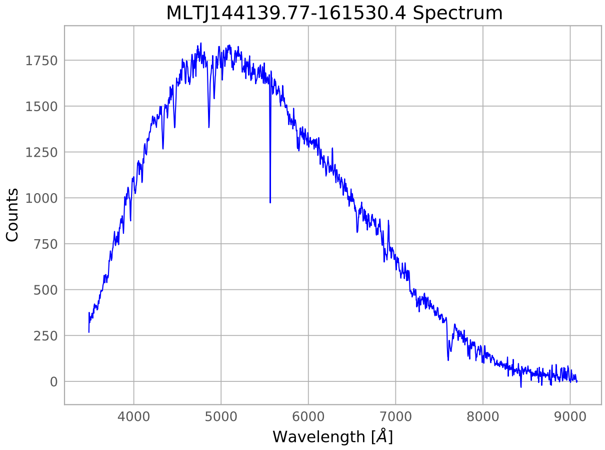

(a) Spectrum.

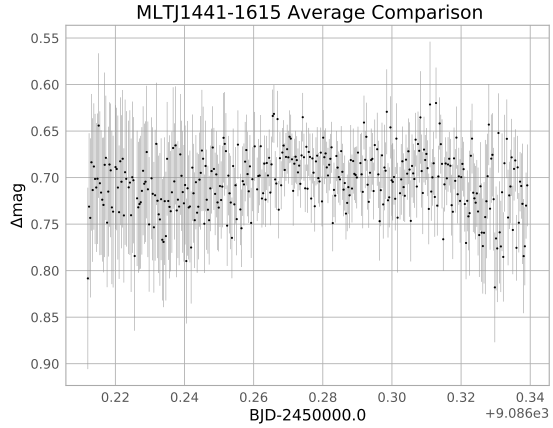

(b) Lightcurve.

Figure 92: MLTJ144139.77–161530.4.

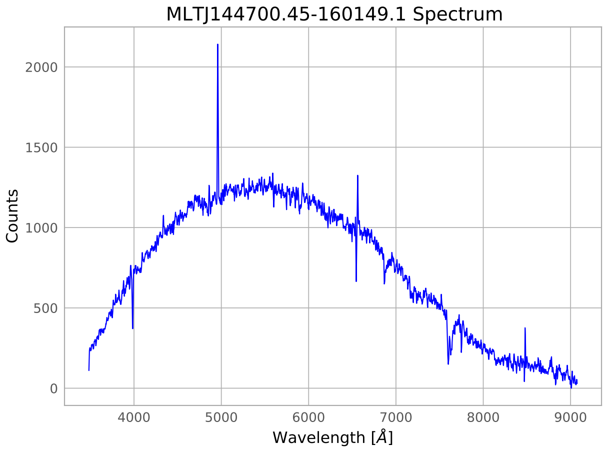

(a) Spectrum.

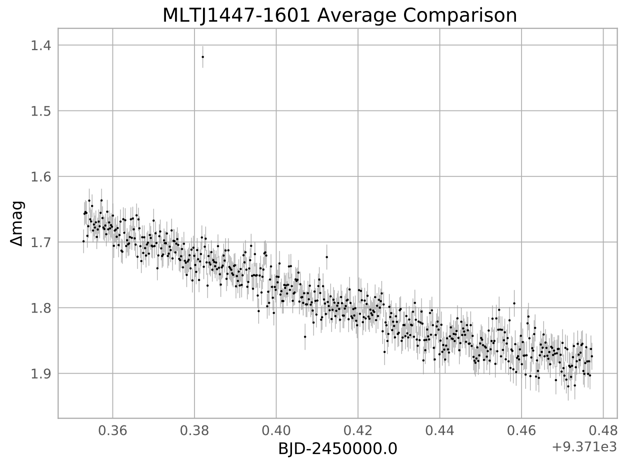

(b) Lightcurve.

Figure 93: MLTJ144700.45–160149.1.

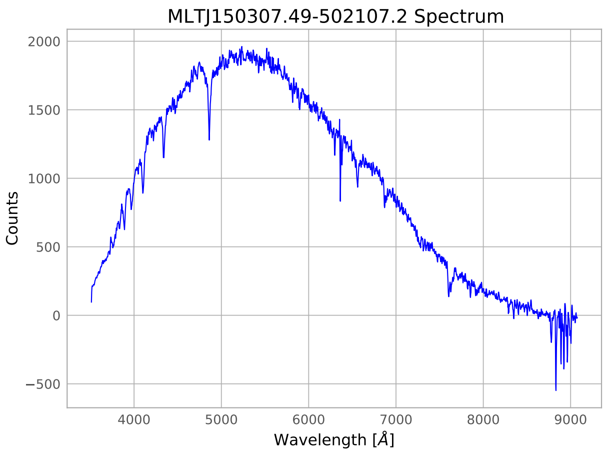

(a) Spectrum.

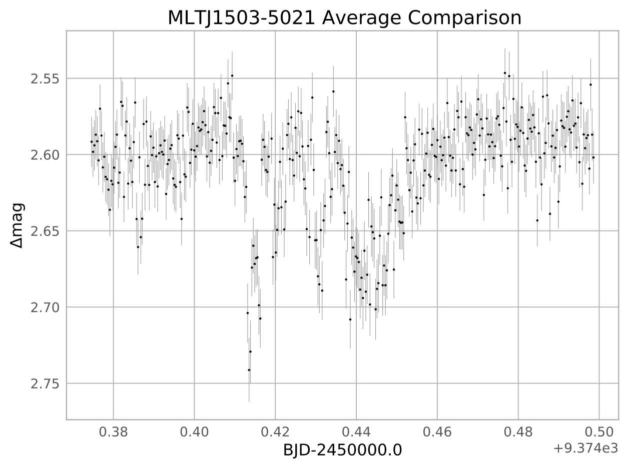

(b) Lightcurve.

Figure 94: MLTJ150307.49–502107.2.

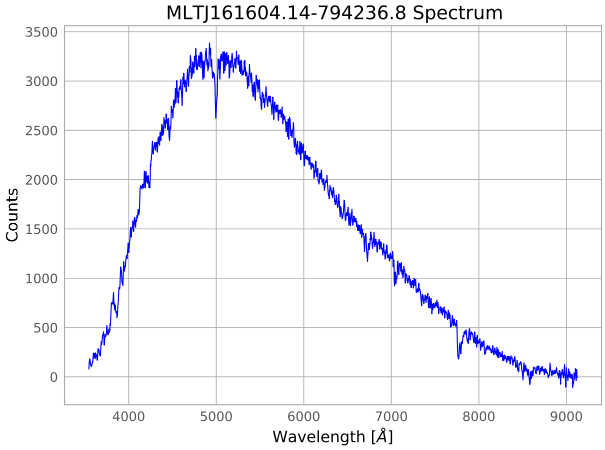

(a) Spectrum.

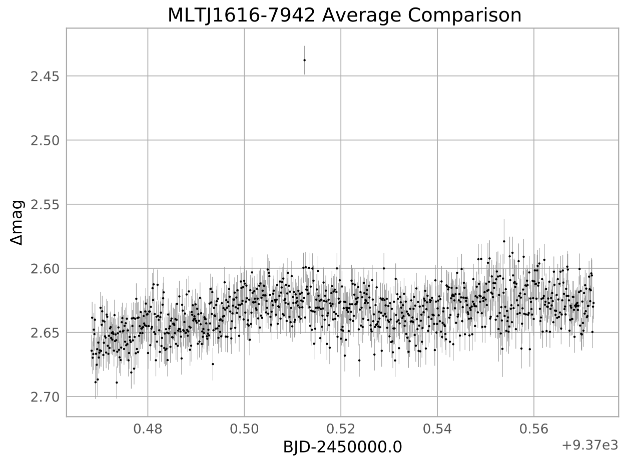

(b) Lightcurve.

Figure 95: MLTJ161604.14–794236.8.

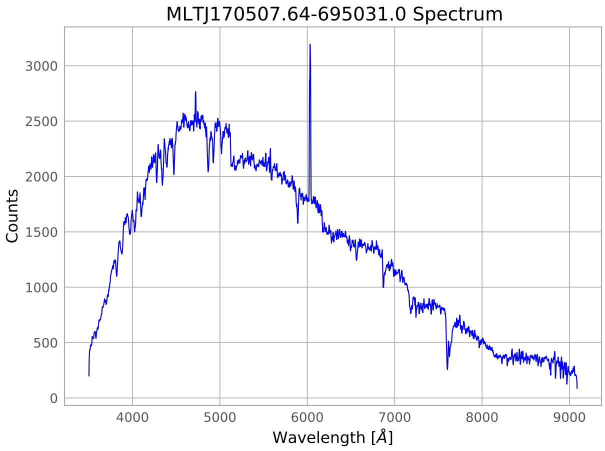

(a) Spectrum.

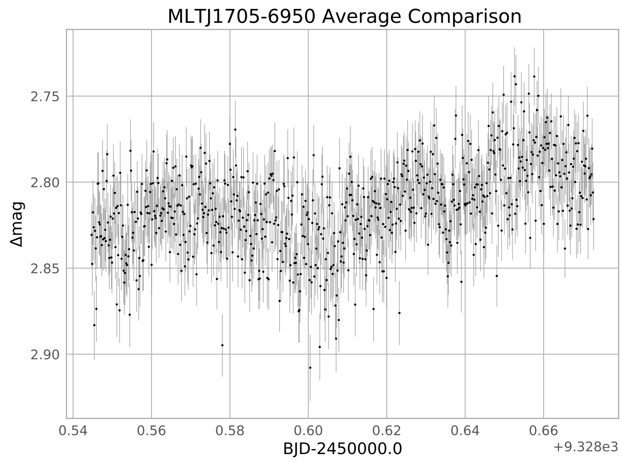

(b) Lightcurve.

Figure 96: MLTJ170507.64–695031.0.

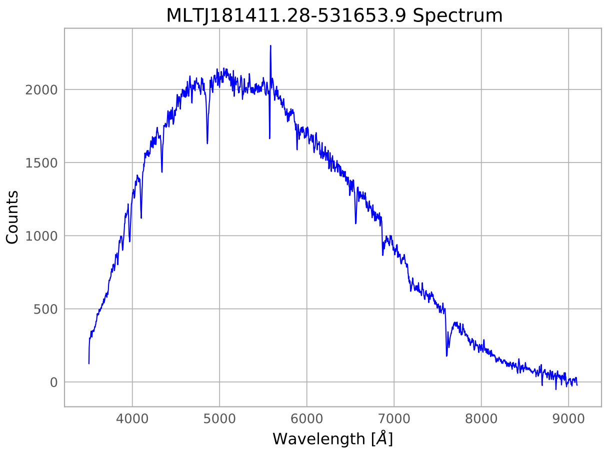

(a) Spectrum.

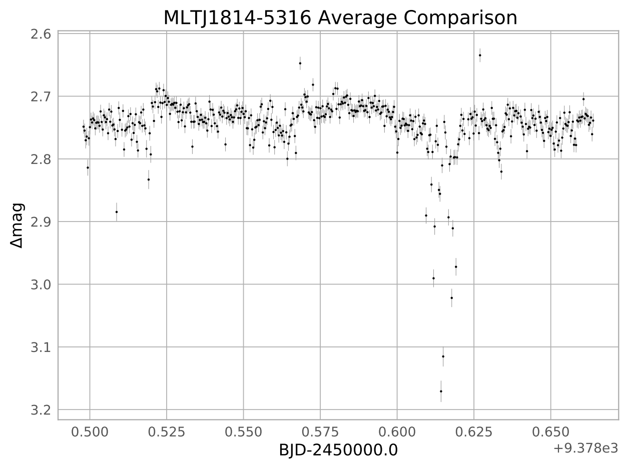

(b) Lightcurve.

Figure 97: MLTJ181411.28–531653.9.

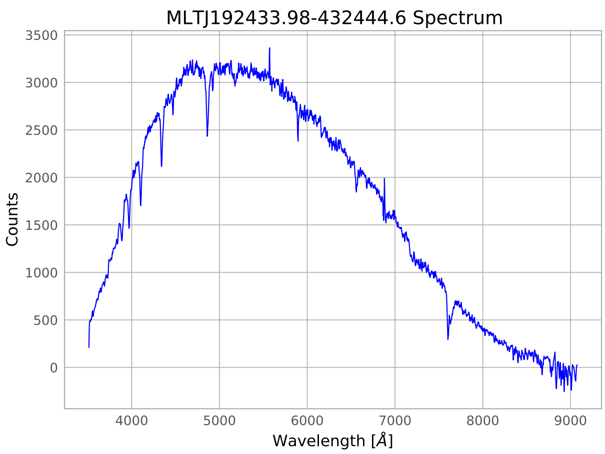

(a) Spectrum.

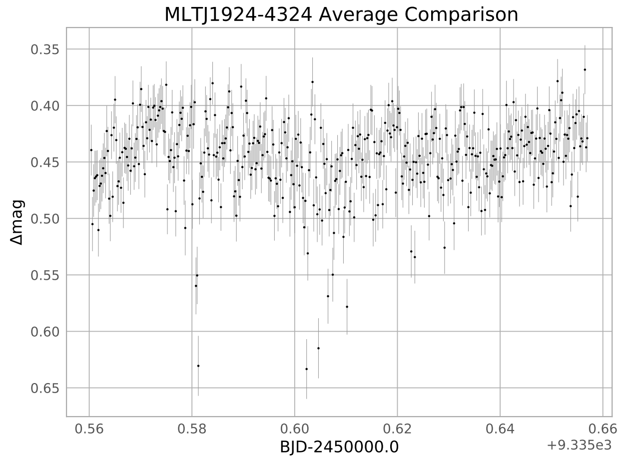

(b) Lightcurve.

Figure 98: MLTJ192433.98–432444.6.

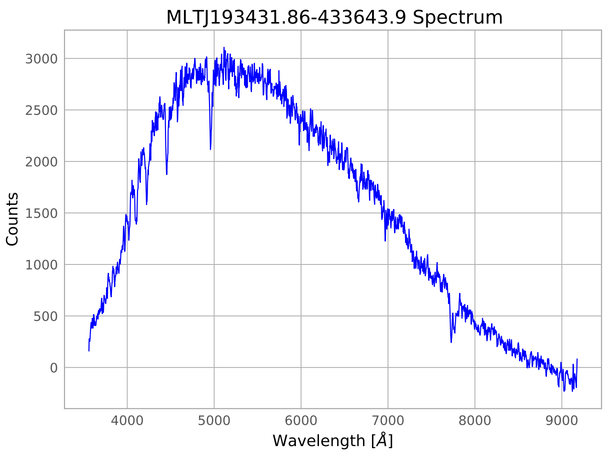

(a) Spectrum.

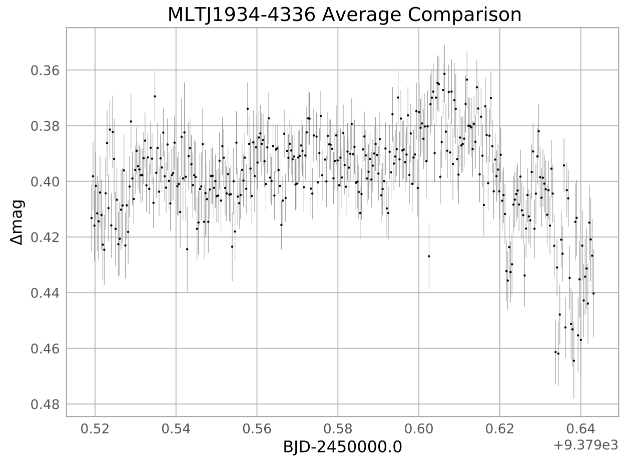

(b) Lightcurve.

Figure 99: MLTJ193431.86–433643.9.

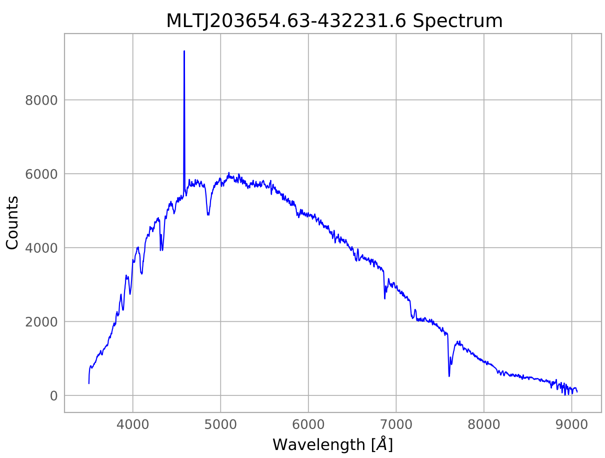

(a) Spectrum.

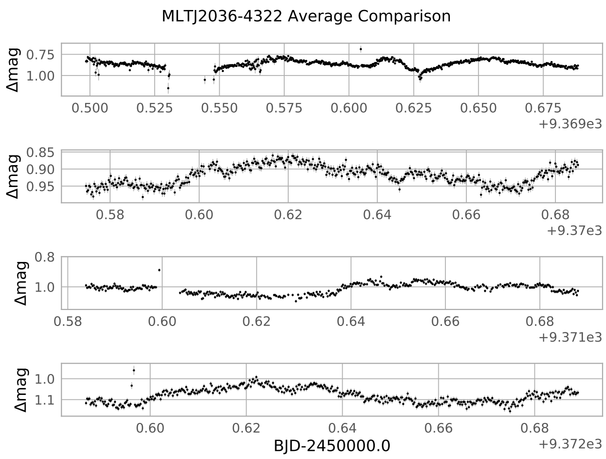

(b) Lightcurve.

Figure 100: MLTJ203654.63–432231.6 (CM Mic).

C Targets with only photometry

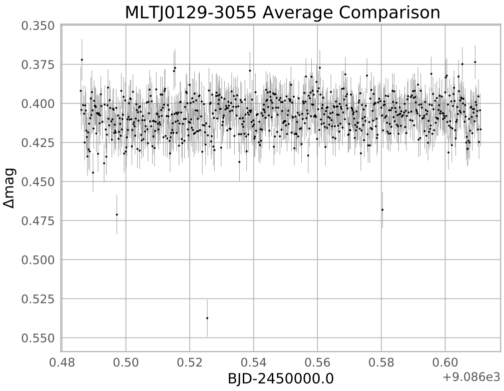

(a) MLTJ012956.10–305512.3.

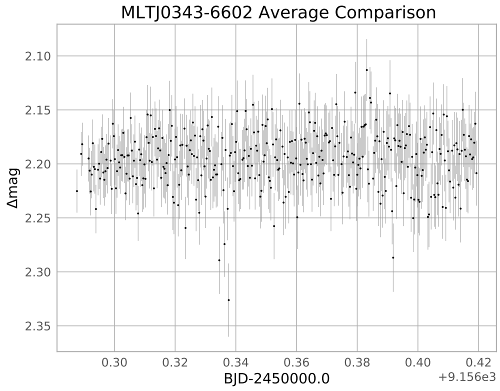

(b) MLTJ034315.70–660204.8.

Figure 101: MLTJ012956.10–305512.3 and MLTJ034315.70–660204.8 lightcurves.

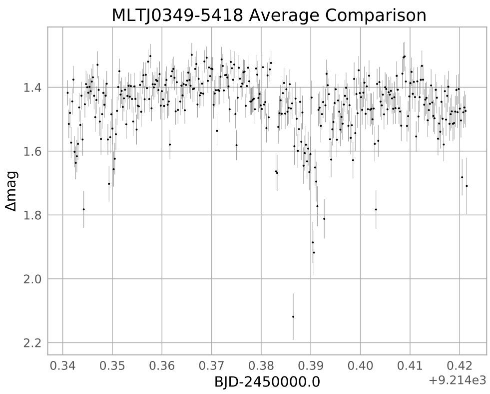

(a) MLTJ034917.85–541825.6.

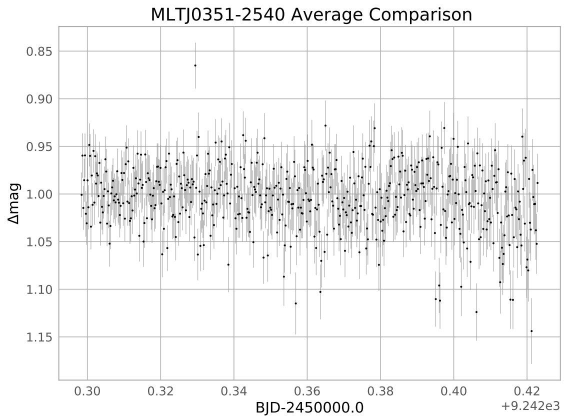

(b) MLTJ035122.99–254054.7.

Figure 102: MLTJ034917.85–541825.6 and MLTJ035122.99–254054.7 lightcurves.

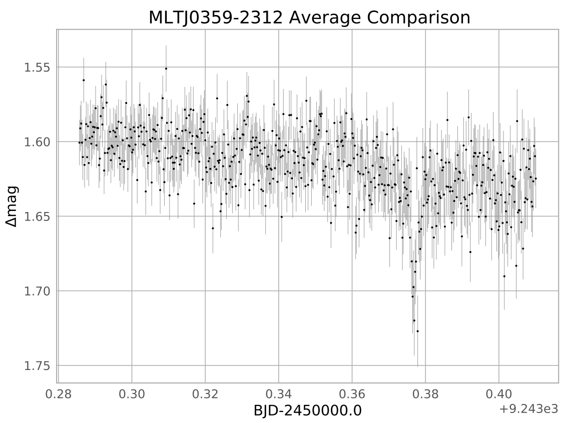

(a) MLTJ035904.91–231225.1.

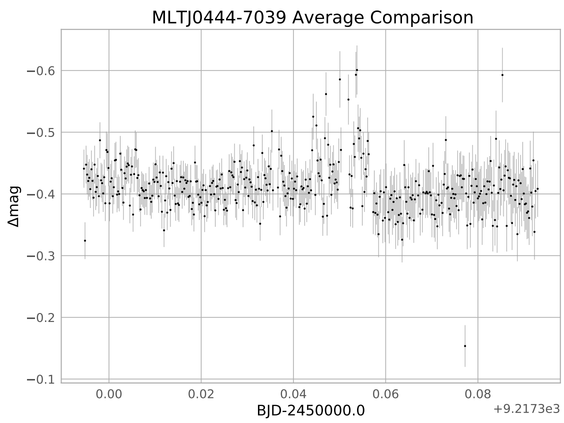

(b) MLTJ044403.48–703939.6.

Figure 103: MLTJ035904.91–231225.1 and MLTJ044403.48–703939.6 lightcurves.

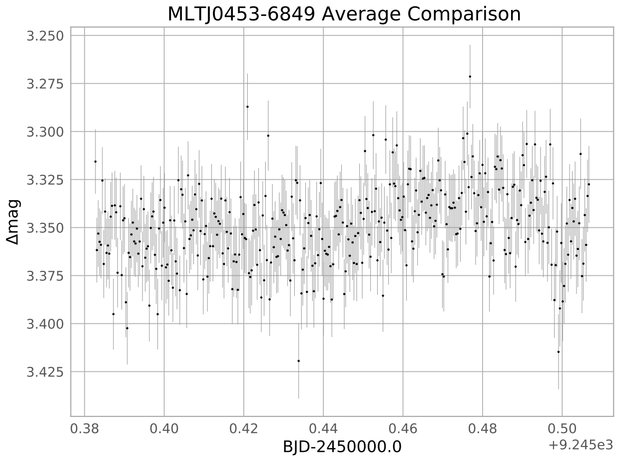

(a) MLTJ045327.58–684953.3.

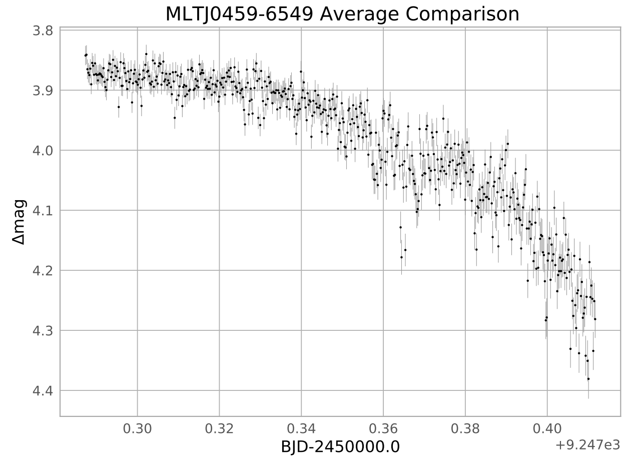

(b) MLTJ045926.12–654943.5.

Figure 104: MLTJ045327.58–684953.3 and MLTJ045926.12–654943.5 lightcurves.

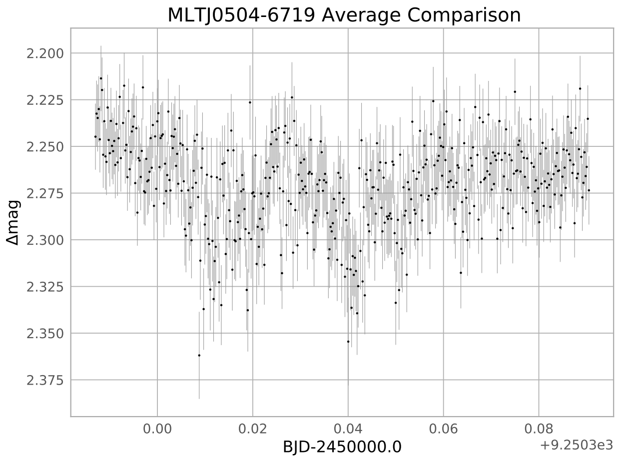

(a) MLTJ050418.69–671903.9.

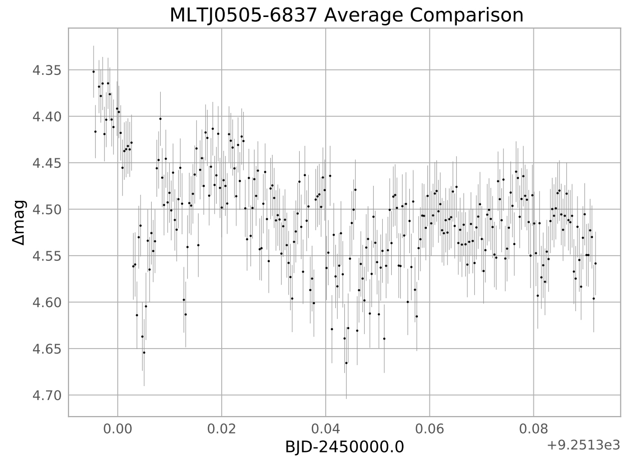

(b) MLTJ050555.42–683706.0.

Figure 105: MLTJ050418.69–671903.9 and MLTJ050555.42–683706.0 lightcurves.

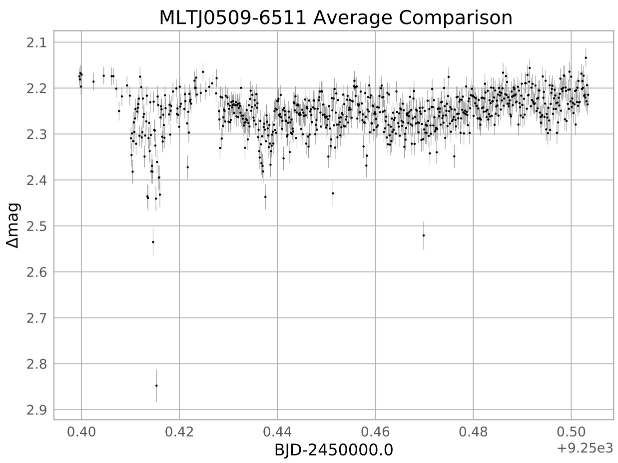

(a) MLTJ050926.31–651124.1.

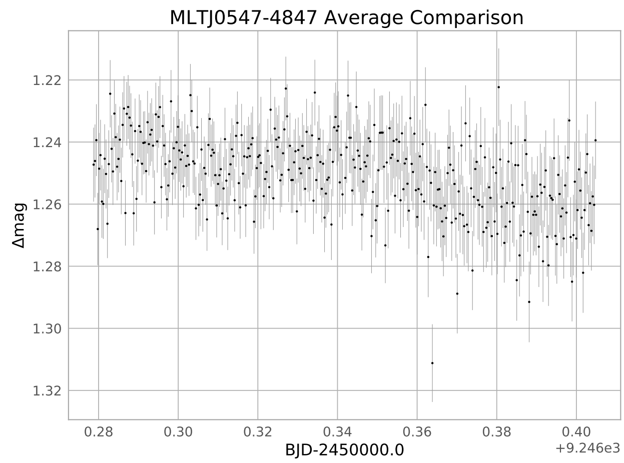

(b) MLTJ054725.58–484720.4.

Figure 106: MLTJ050926.31–651124.1 and MLTJ054725.58–484720.4 lightcurves.

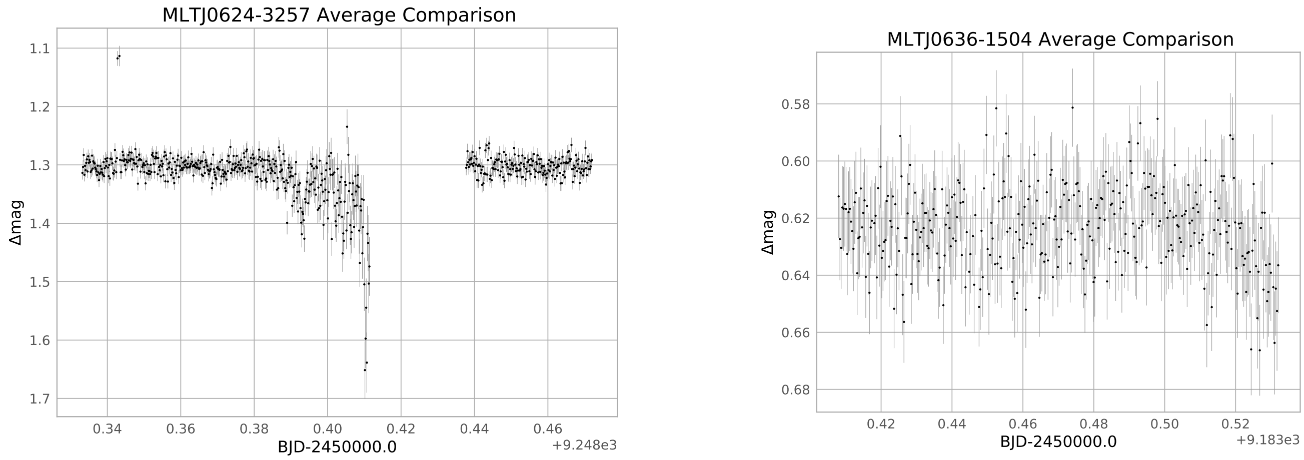

(a) MLTJ062425.79–325731.0.

(b) MLTJ063620.45–150437.0.

Figure 107: MLTJ062425.79–325731.0 and MLTJ063620.45–150437.0 lightcurves.

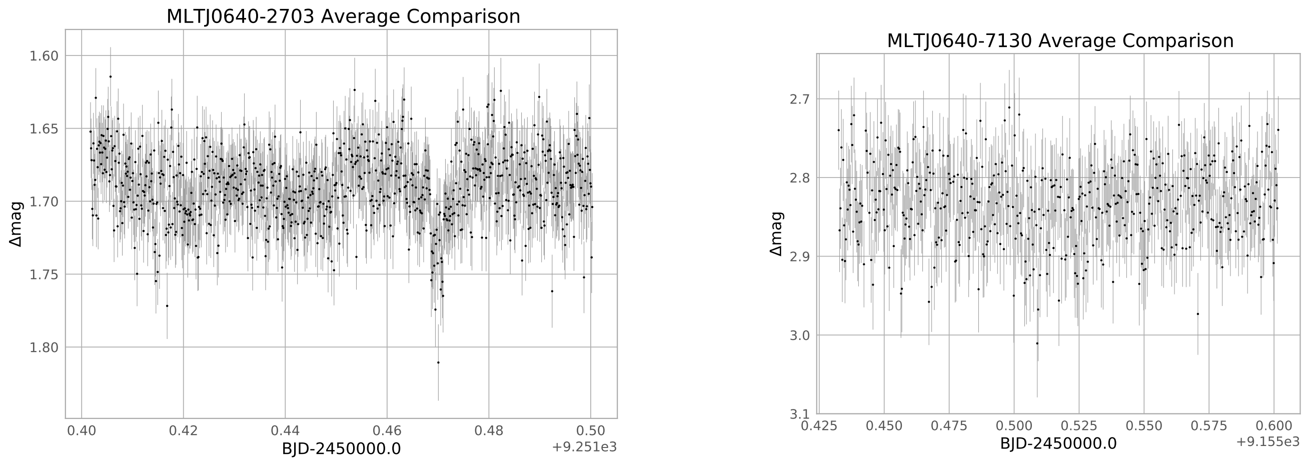

(a) MLTJ064004.73–270320.0.

(b) MLTJ064043.28–713031.7.

Figure 108: MLTJ064004.73–270320.0 and MLTJ064043.28–713031.7 lightcurves.

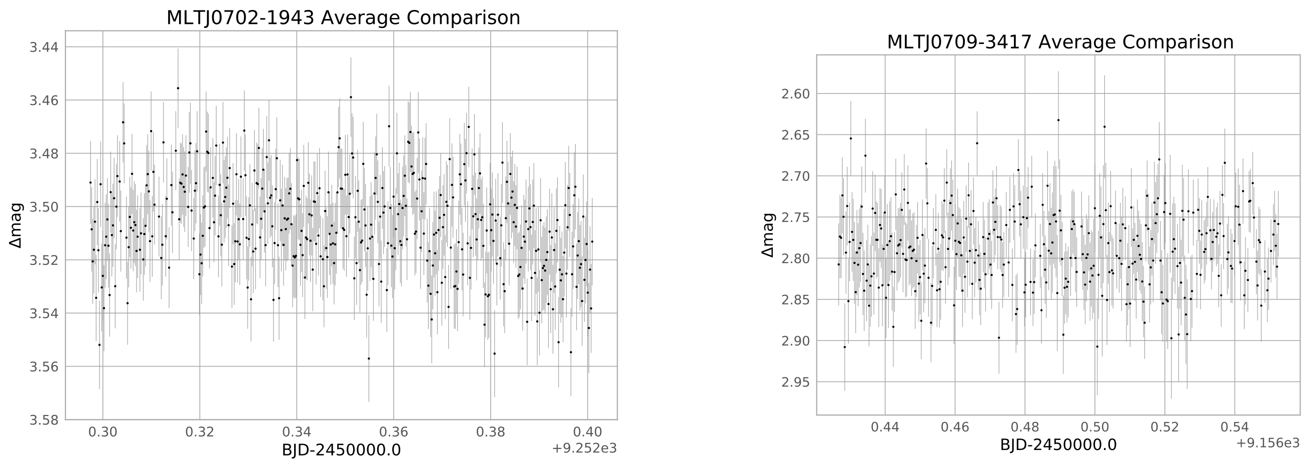

(a) MLTJ070244.27–194323.8.

(b) MLTJ070902.19–341753.7.

Figure 109: MLTJ070244.27–194323.8 and MLTJ070902.19–341753.7 lightcurves.

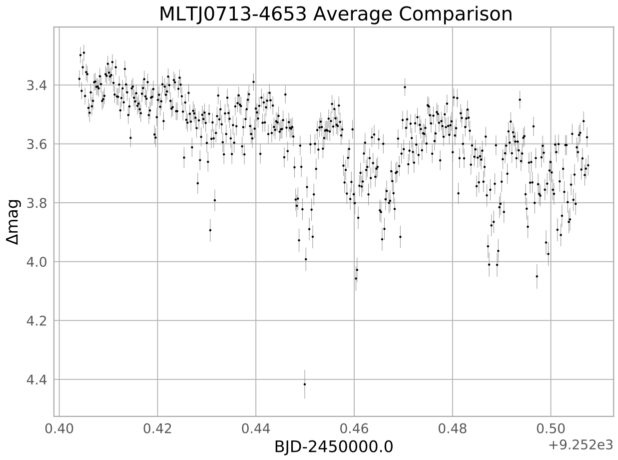

(a) MLTJ071354.61–465306.8.

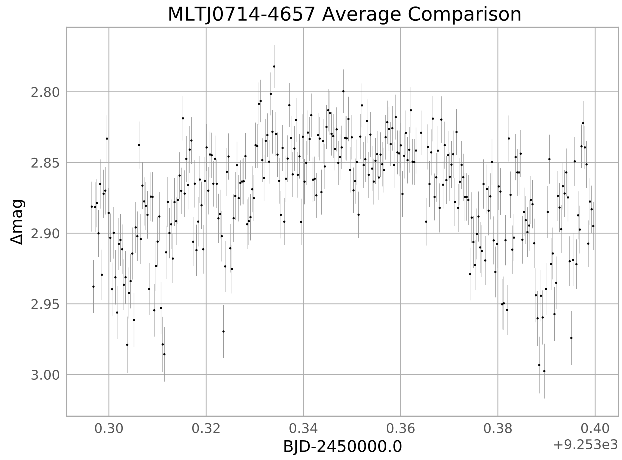

(b) MLTJ071449.42–465739.1.

Figure 110: MLTJ071354.61–465306.8 and MLTJ071449.42–465739.1 lightcurves.

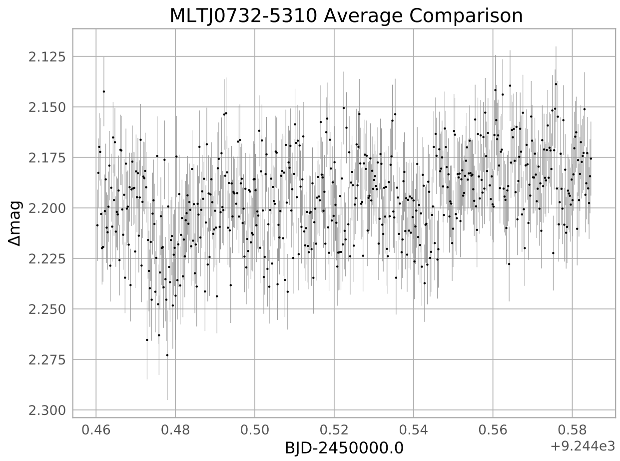

(a) MLTJ073212.80–531036.4.

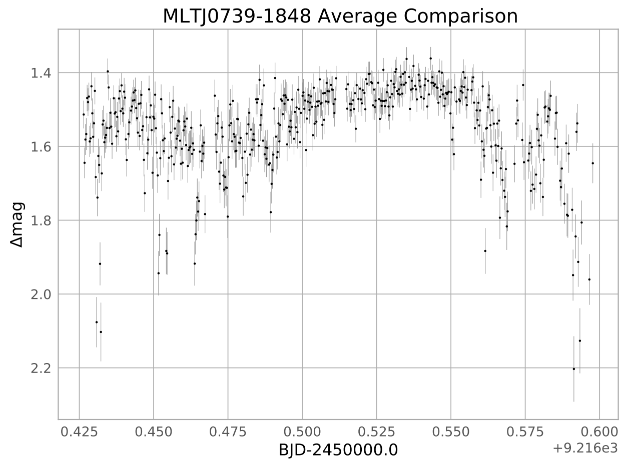

(b) MLTJ073903.87–184859.0.

Figure 111: MLTJ073212.80–531036.4 and MLTJ073903.87–184859.0 lightcurves.

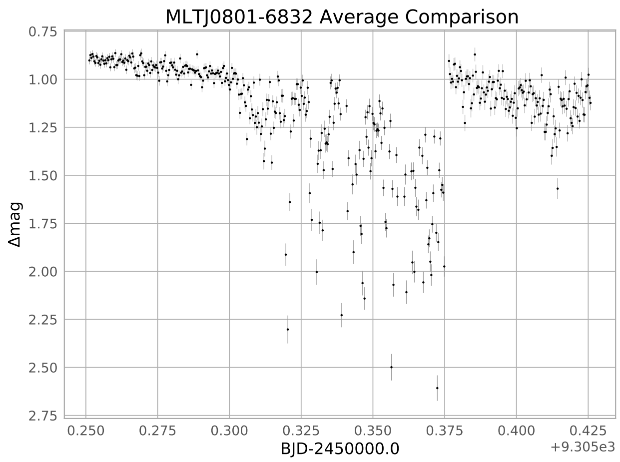

(a) MLTJ080146.07–683258.9.

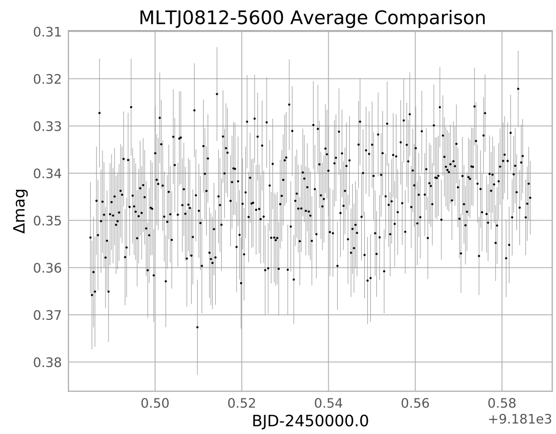

(b) MLTJ081249.97–560027.5.

Figure 112: MLTJ080146.07–683258.9 and MLTJ081249.97–560027.5 lightcurves.

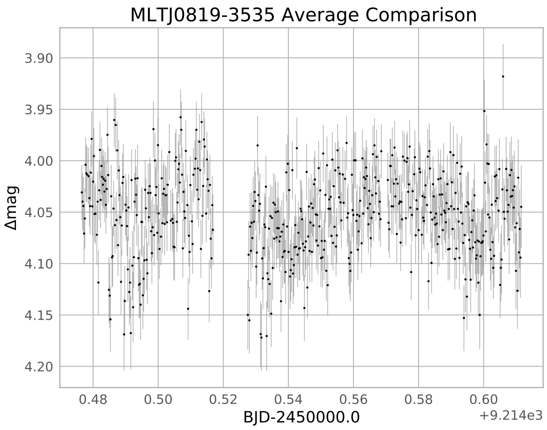

(a) MLTJ081911.36–353521.3.

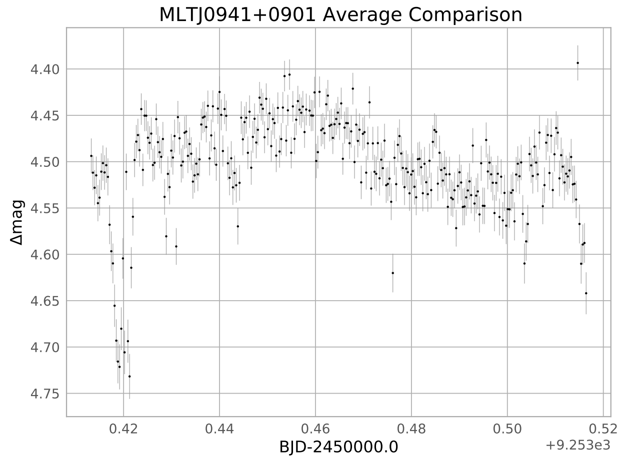

(b) MLTJ094115.19+090152.5.

Figure 113: MLTJ081911.36–353521.3 and MLTJ094115.19+090152.5 lightcurves.

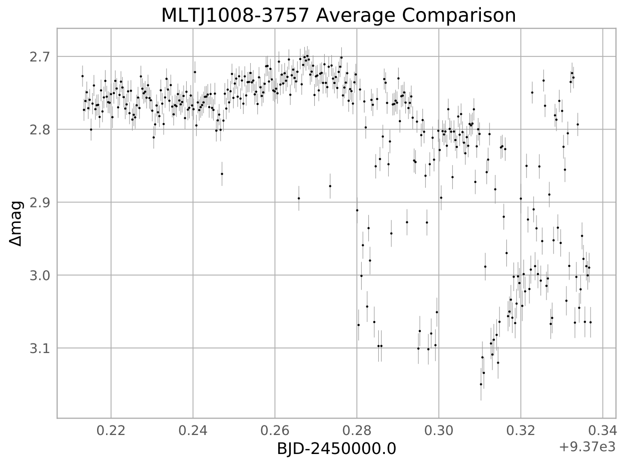

(a) MLTJ100814.09–375754.2.

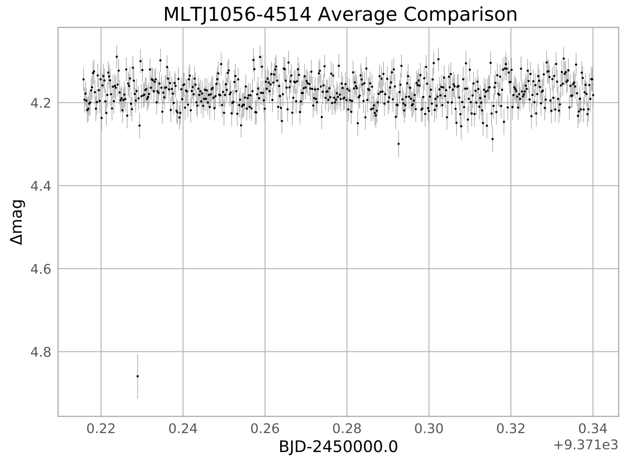

(b) MLTJ105609.30–451430.5.

Figure 114: MLTJ100814.09–375754.2 and MLTJ105609.30–451430.5 lightcurves.

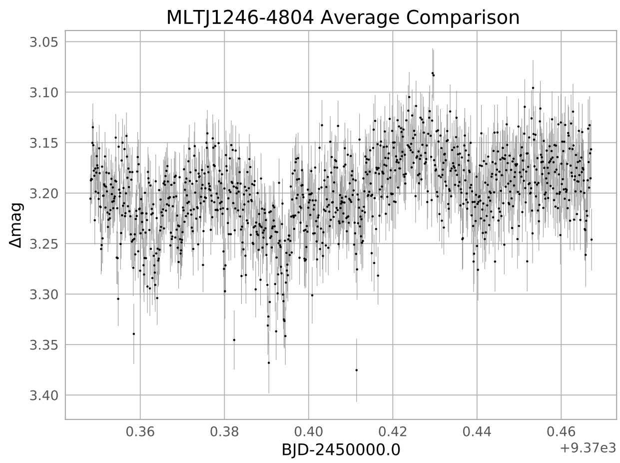

(a) MLTJ124631.99–480413.5.

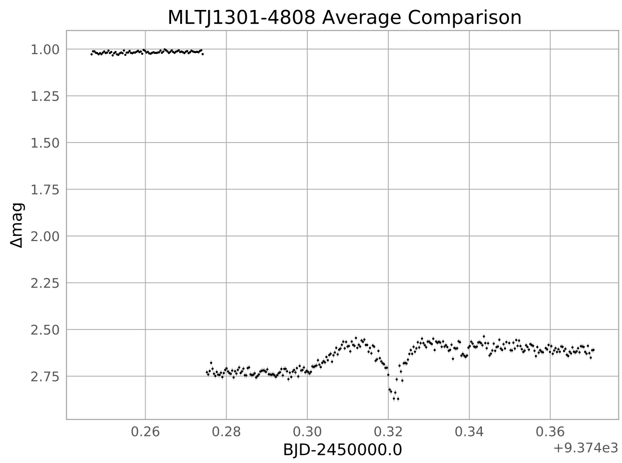

(b) MLTJ130116.33–480811.7.

Figure 115: MLTJ124631.99–480413.5 and MLTJ130116.33–480811.7 lightcurves.

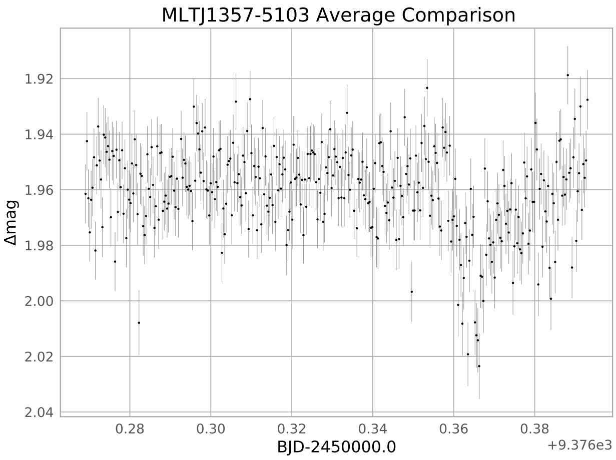

(a) MLTJ135704.98–510325.9.

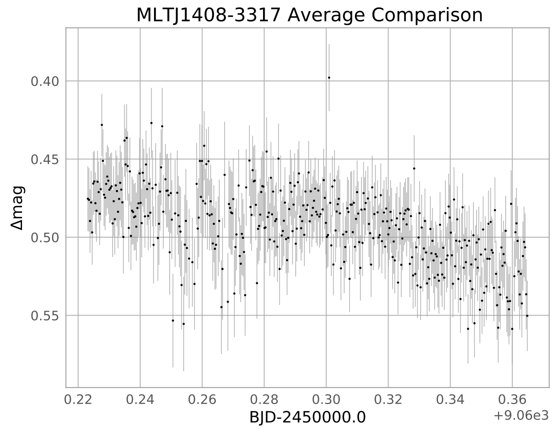

(b) MLTJ140801.86–331717.0.

Figure 116: MLTJ135704.98–510325.9 and MLTJ140801.86–331717.0 lightcurves.

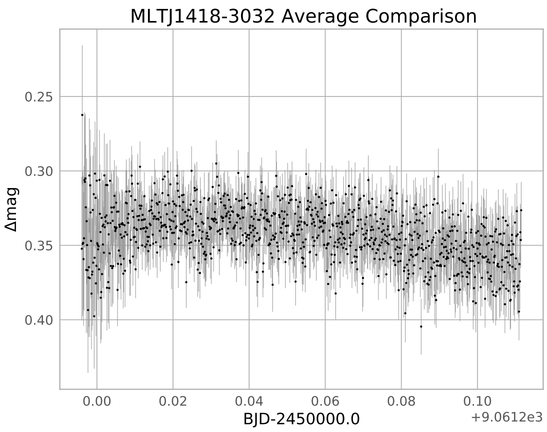

(a) MLTJ141822.54–303211.9.

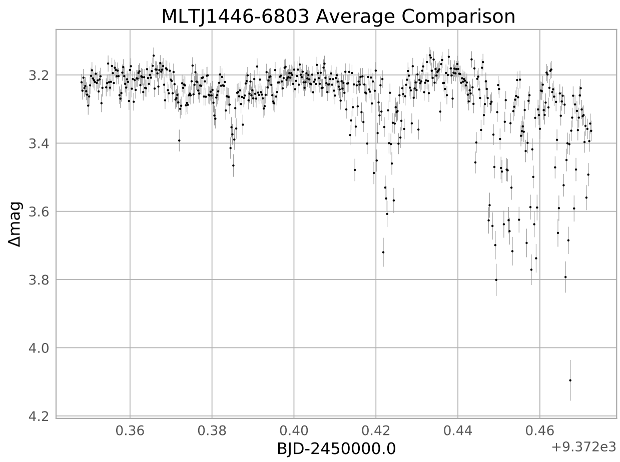

(b) MLTJ144603.78–680359.5.

Figure 117: MLTJ141822.54–303211.9 and MLTJ144603.78–680359.5 lightcurves.

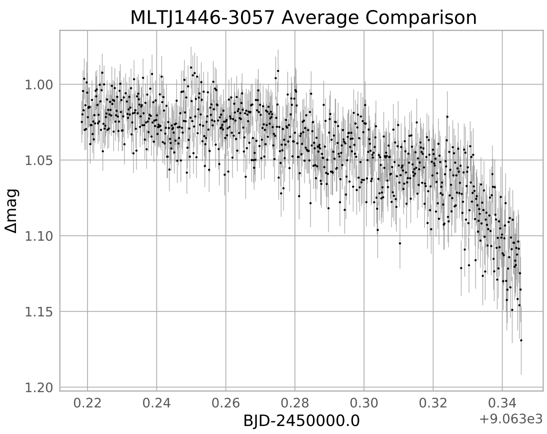

(a) MLTJ144641.89–305708.2.

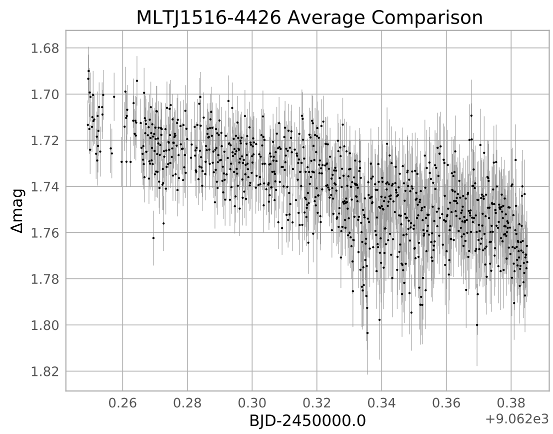

(b) MLTJ151629.11–442615.4.

Figure 118: MLTJ144641.89–305708.2 and MLTJ151629.11–442615.4 lightcurves.

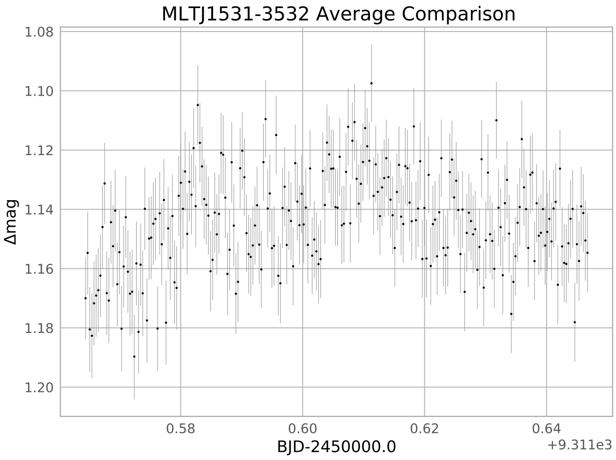

(a) MLTJ153133.70–353213.7.

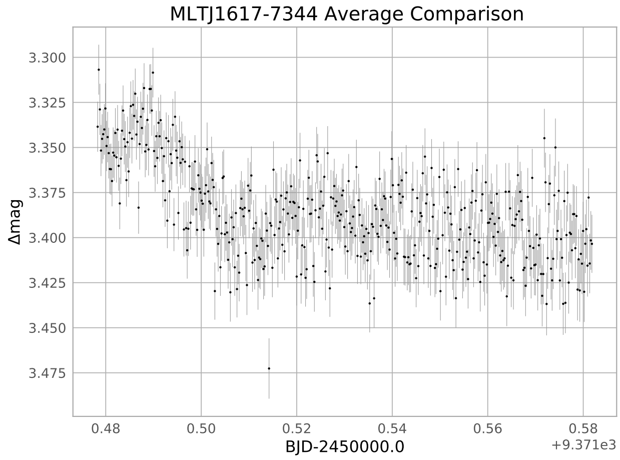

(b) MLTJ161737.30–734440.4.

Figure 119: MLTJ153133.70–353213.7 and MLTJ161737.30–734440.4 lightcurves.

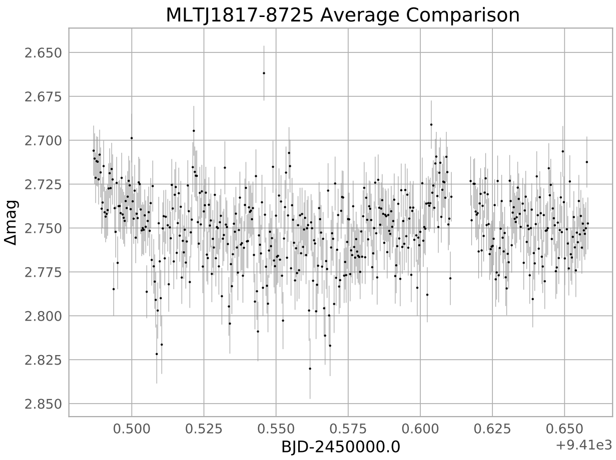

(a) MLTJ181723.44–872557.7.

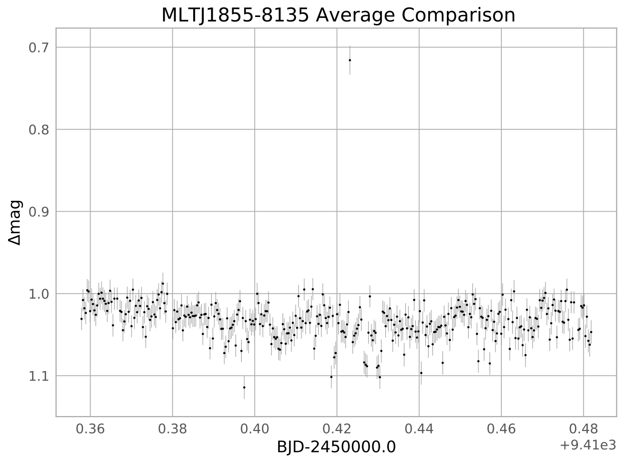

(b) MLTJ185535.63–813507.0.

Figure 120: MLTJ181723.44–872557.7 and MLTJ185535.63–813507.0 lightcurves.

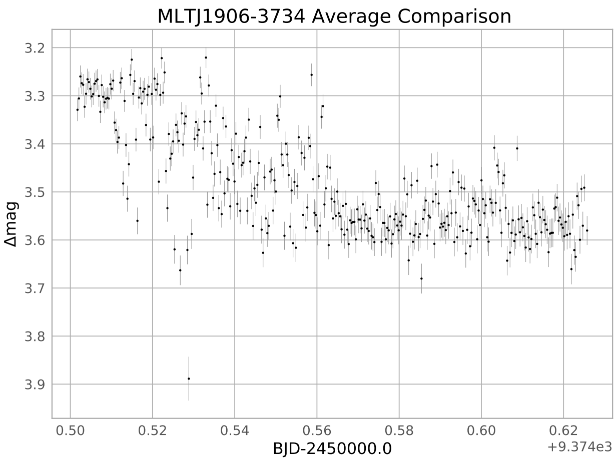

(a) MLTJ190610.74–373414.1.

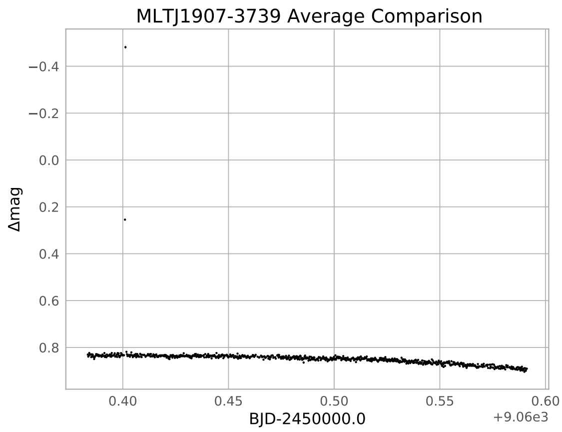

(b) MLTJ190752.82–373956.0.

Figure 121: MLTJ190610.74–373414.1 and MLTJ190752.82–373956.0 lightcurves.

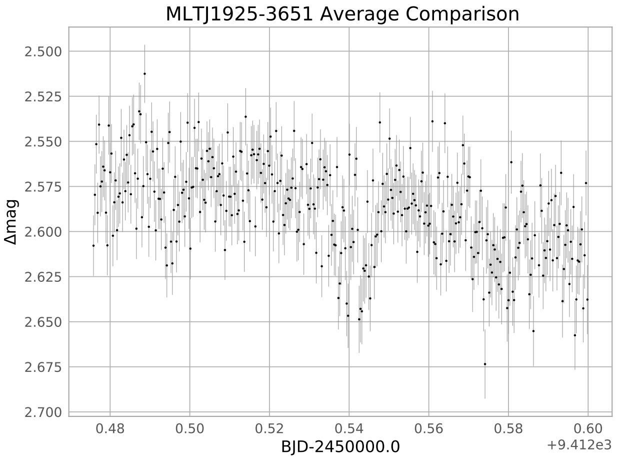

(a) MLTJ192504.69–365151.4.

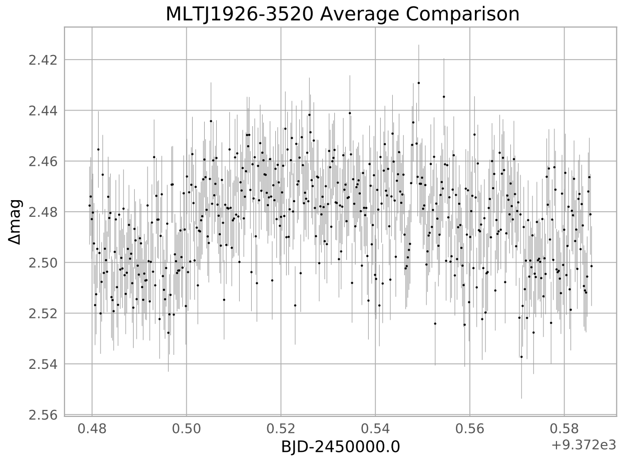

(b) MLTJ192608.60–352013.2.

Figure 122: MLTJ192504.69–365151.4 and MLTJ192608.60–352013.2 lightcurves.

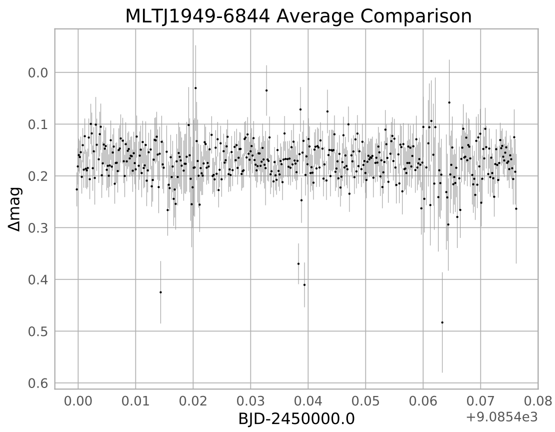

(a) MLTJ194921.72–684412.2.

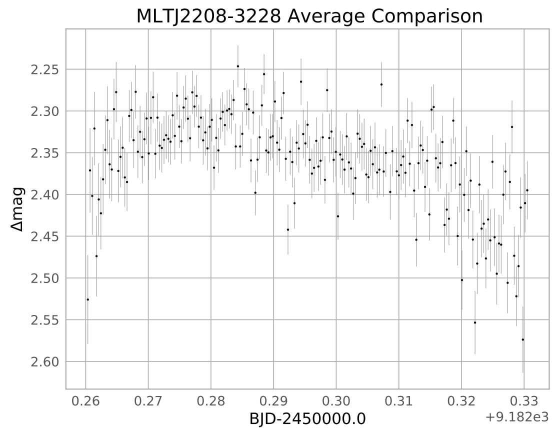

(b) MLTJ220803.20–322800.1.

Figure 123: MLTJ194921.72–684412.2 and MLTJ220803.20–322800.1 lightcurves.

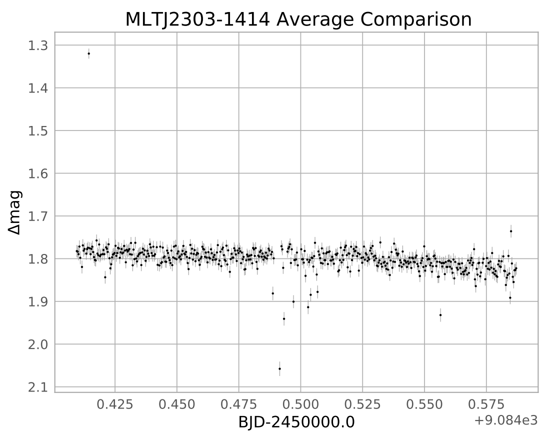

(a) MLTJ230345.82–141447.1.

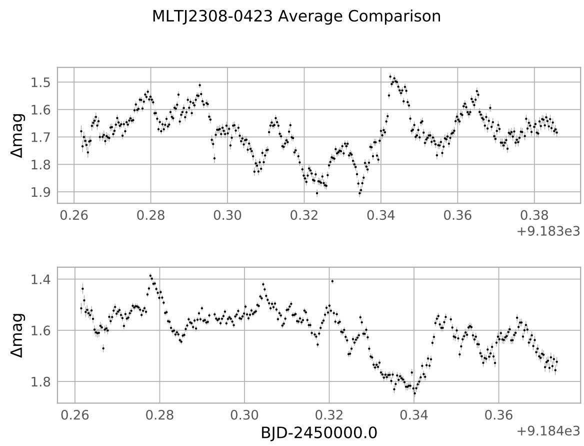

(b) MLTJ230816.36–042339.3.

Figure 124: MLTJ230345.82–141447.1 and MLTJ230816.36–042339.3 lightcurves.

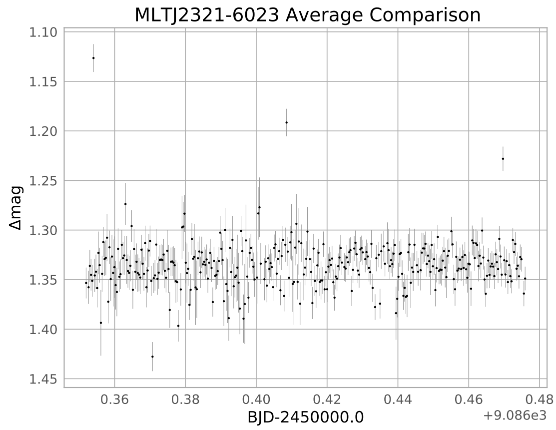

Figure 125: MLTJ232129.59–602302.9 lightcurve.

D Targets with only spectroscopy

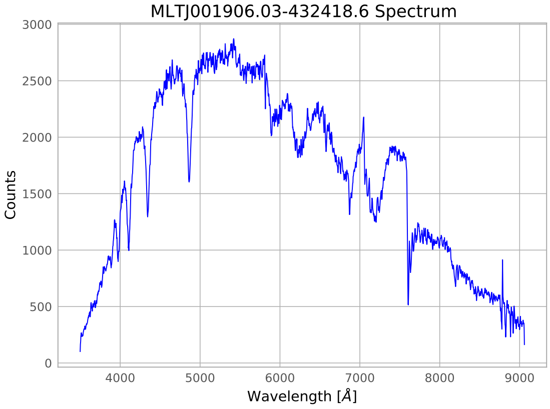

(a) MLTJ001906.03–432418.6.

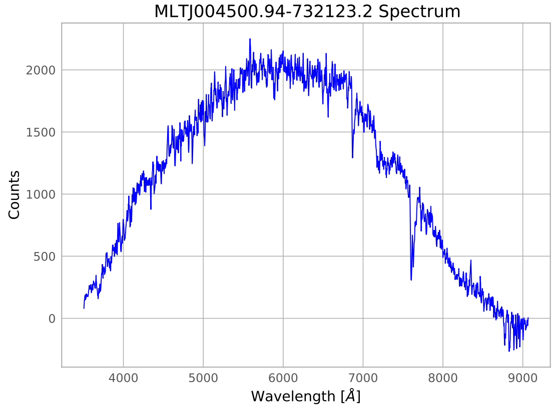

(b) MLTJ004500.94–732123.2.

Figure 126: MLTJ001906.03–432418.6 and MLTJ004500.94–732123.2 spectra.

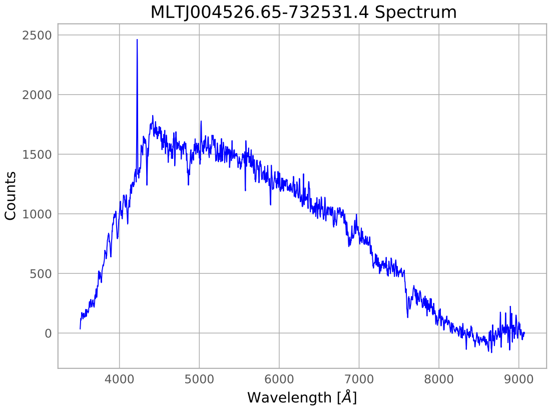

(a) MLTJ004526.65–732531.4.

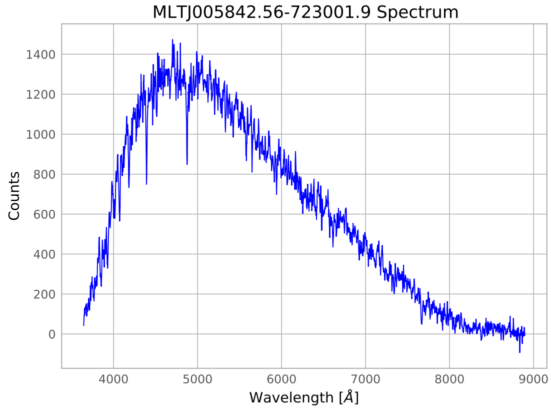

(b) MLTJ005842.56–723001.9.

Figure 127: MLTJ004526.65–732531.4 and MLTJ005842.56–723001.9 spectra.

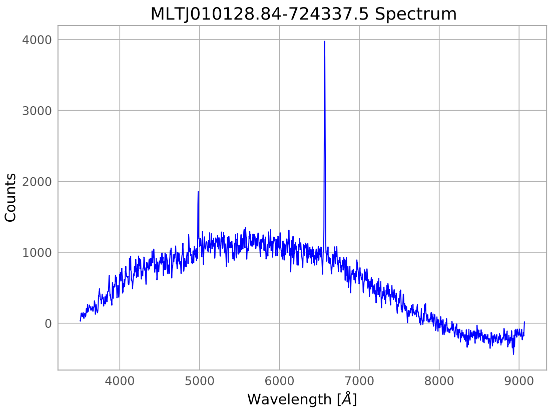

(a) MLTJ010128.84–724337.5.

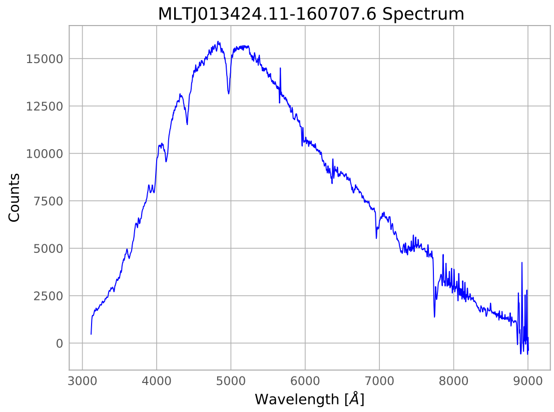

(b) MLTJ013424.11–160707.6.

Figure 128: MLTJ010128.84–724337.5 and MLTJ013424.11–160707.6 spectra.

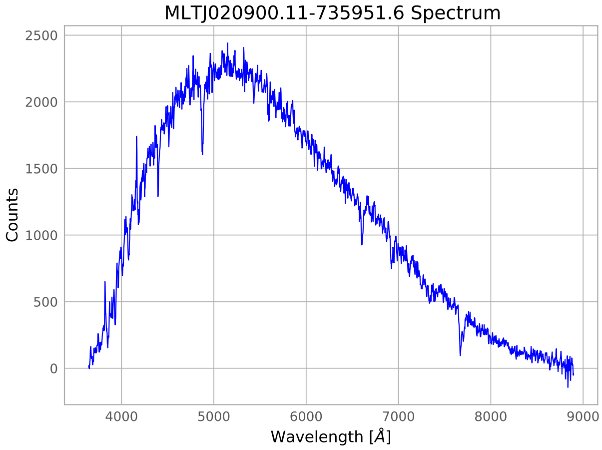

(a) MLTJ020900.11–735951.6.

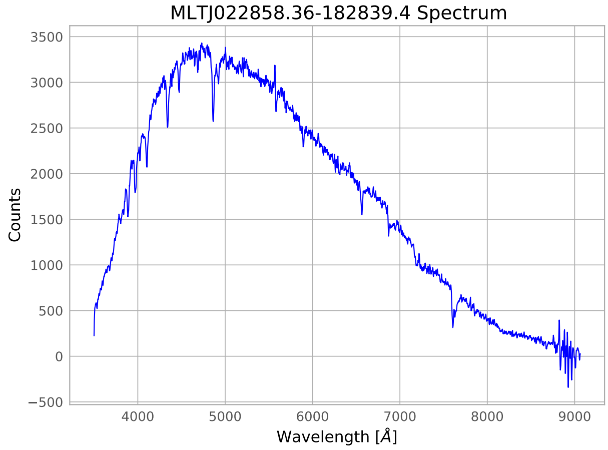

(b) MLTJ022858.36–182839.4.

Figure 129: MLTJ020900.11–735951.6 and MLTJ022858.36–182839.4 spectra.

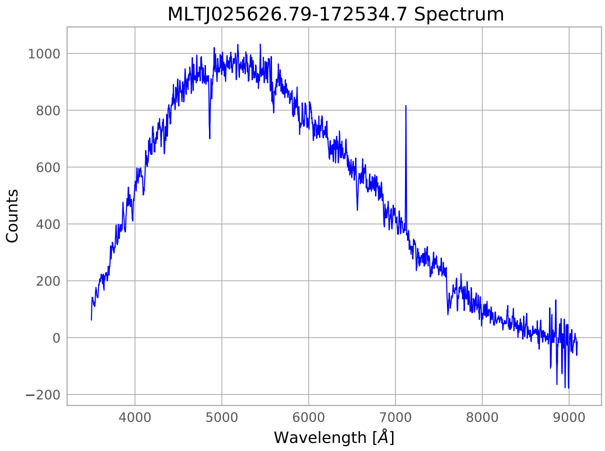

(a) MLTJ025626.79–172534.7.

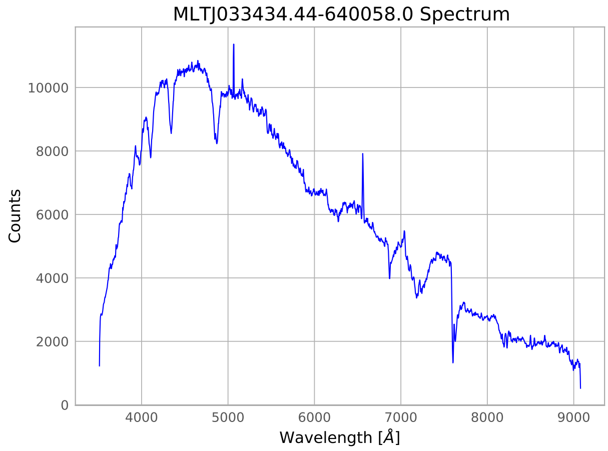

(b) MLTJ033434.44–640058.0.

Figure 130: MLTJ025626.79–172534.7 and MLTJ033434.44–640058.0 spectra.

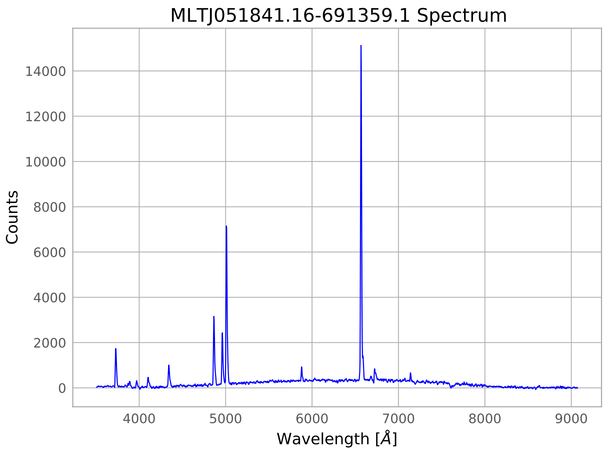

(a) MLTJ051841.16–691359.1.

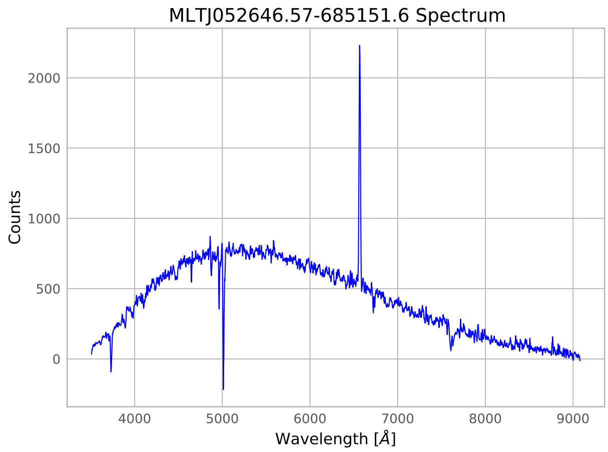

(b) MLTJ052646.57–685151.6.

Figure 131: MLTJ051841.16–691359.1 and MLTJ052646.57–685151.6 spectra.

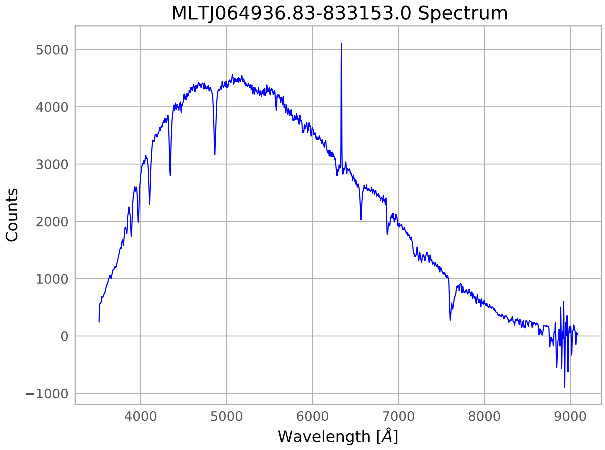

(a) MLTJ064936.83–833153.0.

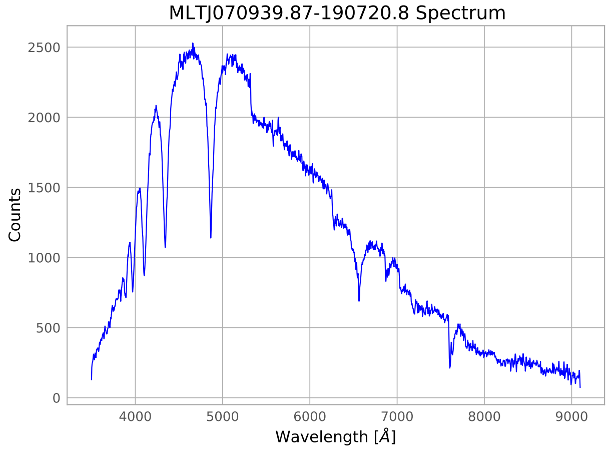

(b) MLTJ070939.87–190720.8.

Figure 132: MLTJ064936.83–833153.0 and MLTJ070939.87–190720.8 spectra.

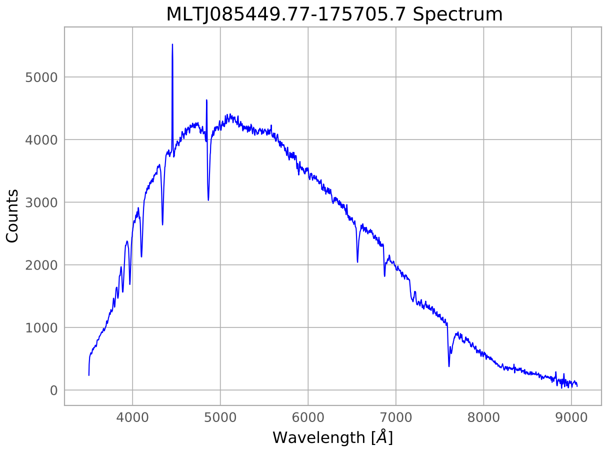

(a) MLTJ085449.77–175705.7.

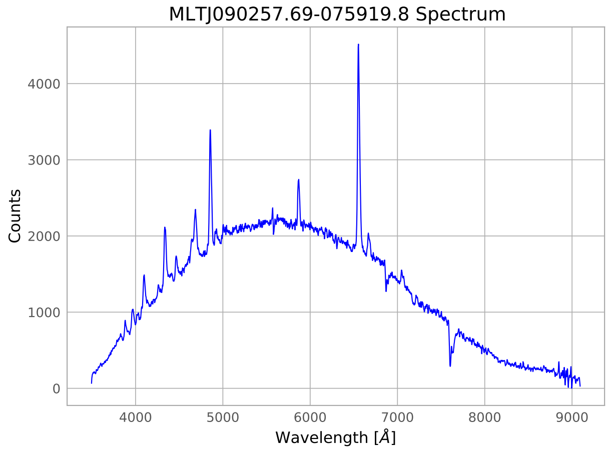

(b) MLTJ090257.69–075919.8.

Figure 133: MLTJ085449.77–175705.7 and MLTJ090257.69–075919.8 spectra.

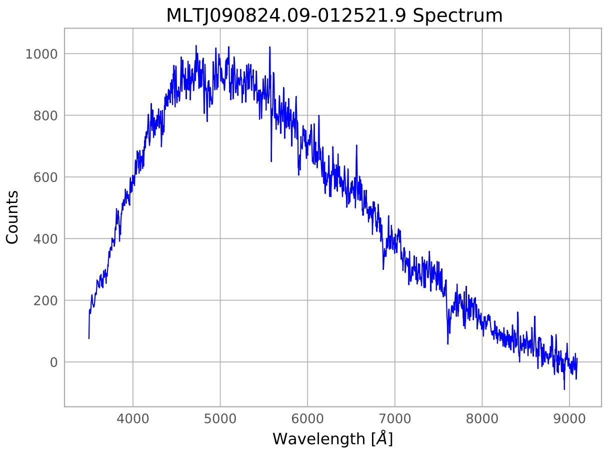

(a) MLTJ090824.09–012521.9.

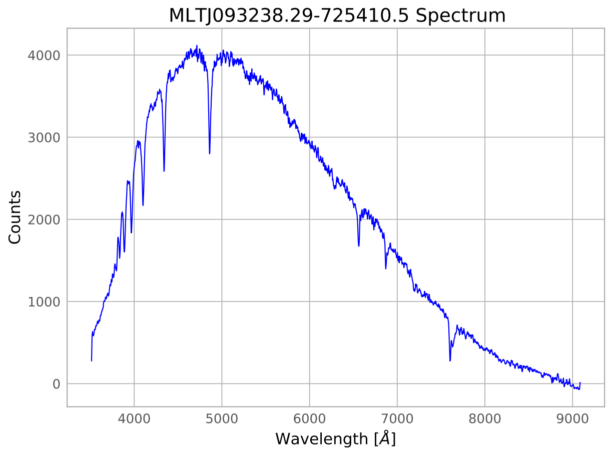

(b) MLTJ093238.29–725410.5.

Figure 134: MLTJ090824.09–012521.9 and MLTJ093238.29–725410.5 spectra.

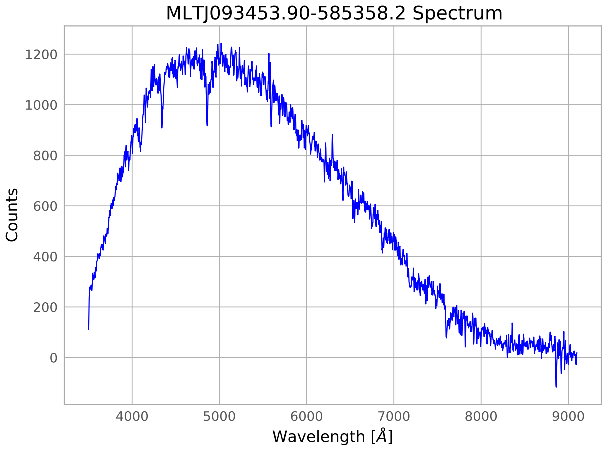

(a) MLTJ093453.90–585358.2.

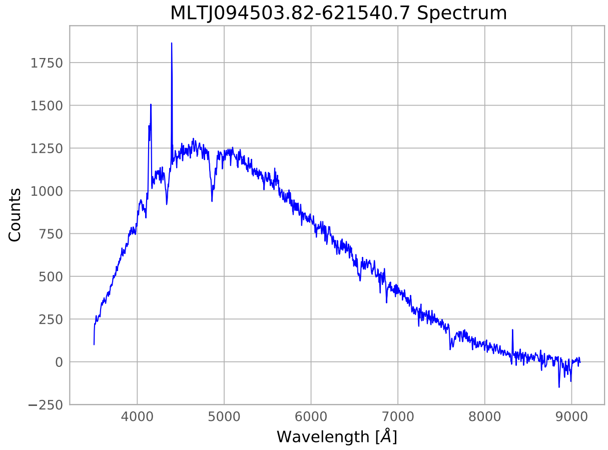

(b) MLTJ094503.82–621540.7.

Figure 135: MLTJ093453.90–585358.2 and MLTJ094503.82–621540.7 spectra.

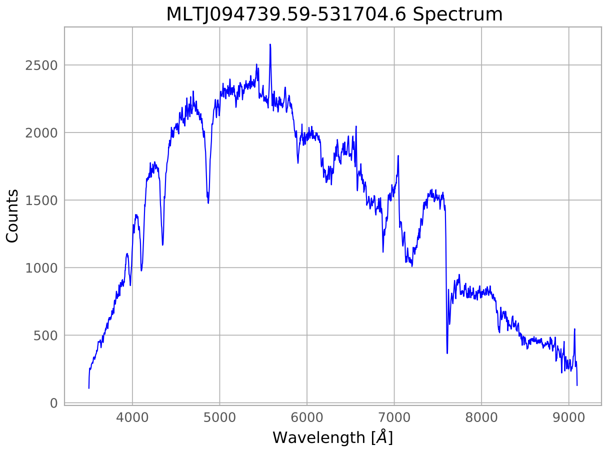

(a) MLTJ094739.59–531704.6.

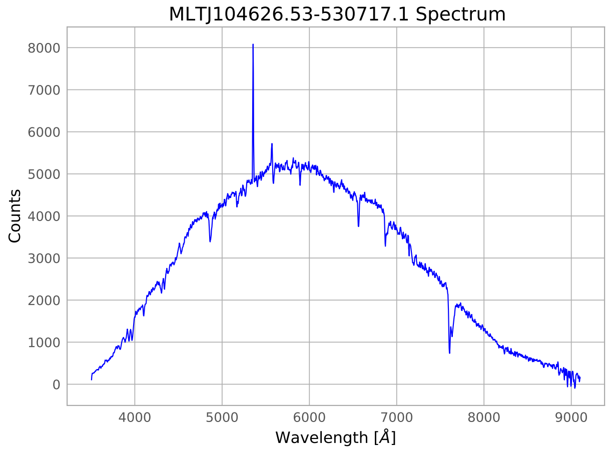

(b) MLTJ104626.53–530717.1.

Figure 136: MLTJ094739.59–531704.6 and MLTJ104626.53–530717.1 spectra.

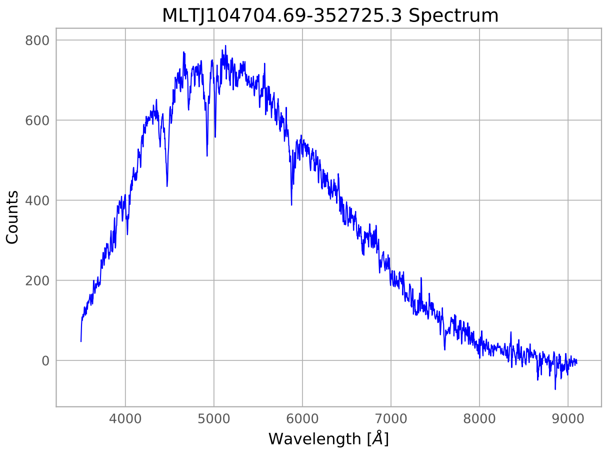

(a) MLTJ104704.69–352725.3.

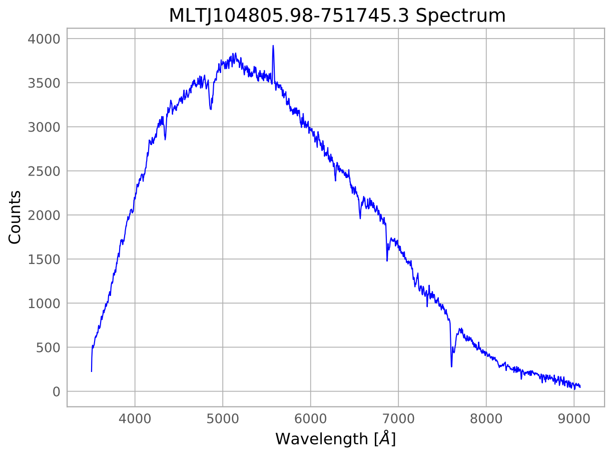

(b) MLTJ104805.98–751745.3.

Figure 137: MLTJ104704.69–352725.3 and MLTJ104805.98–751745.3 spectra.

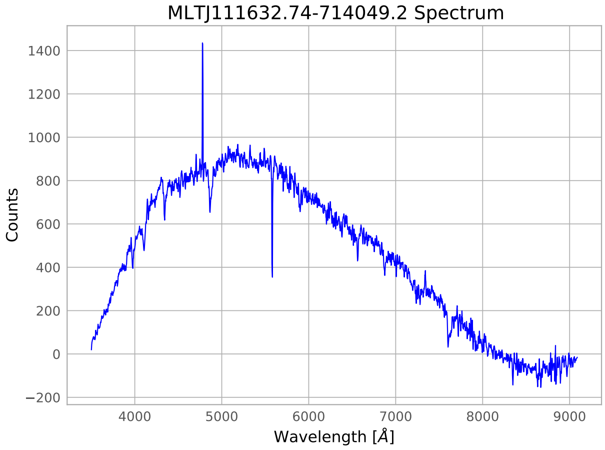

(a) MLTJ111632.74–714049.2.

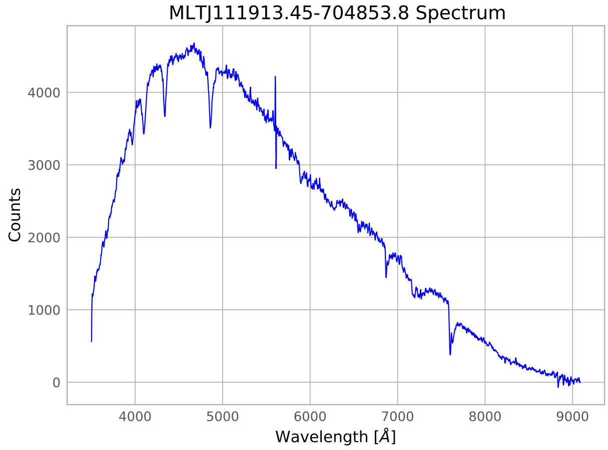

(b) MLTJ111913.45–704853.8.

Figure 138: MLTJ111632.74–714049.2 and MLTJ111913.45–704853.8 spectra.

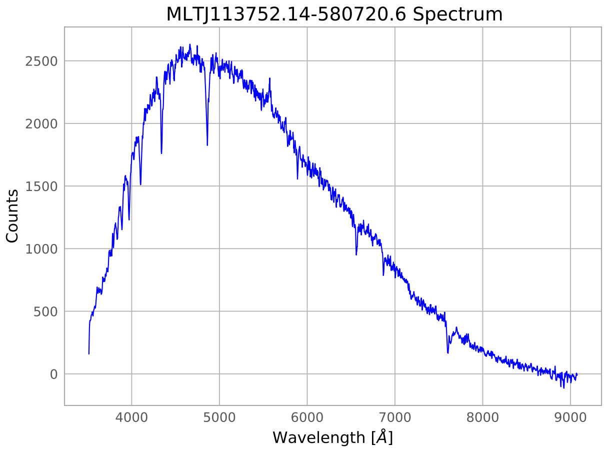

(a) MLTJ113752.14–580720.6.

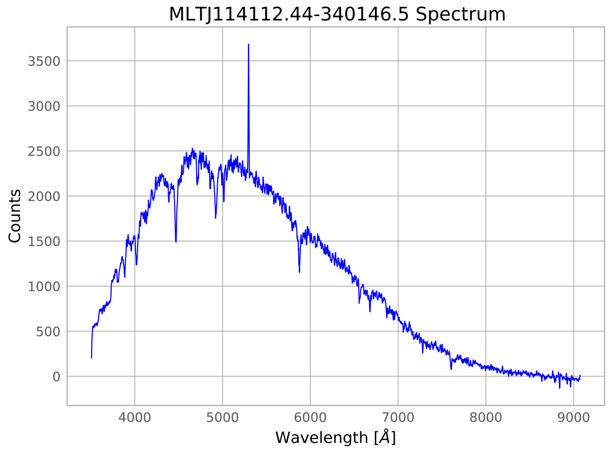

(b) MLTJ114112.44–340146.5.

Figure 139: MLTJ113752.14–580720.6 and MLTJ114112.44–340146.5 spectra.

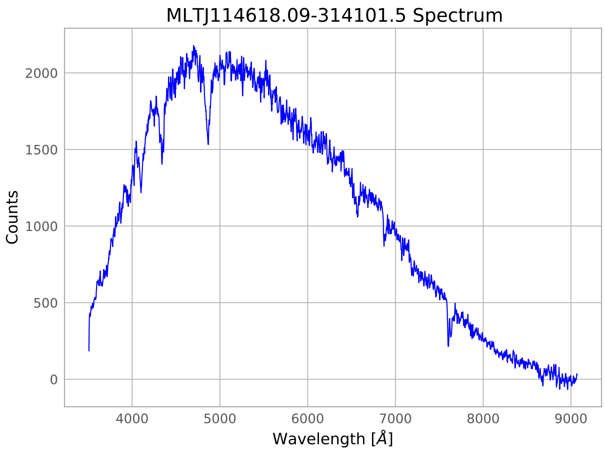

(a) MLTJ114618.09–314101.5.

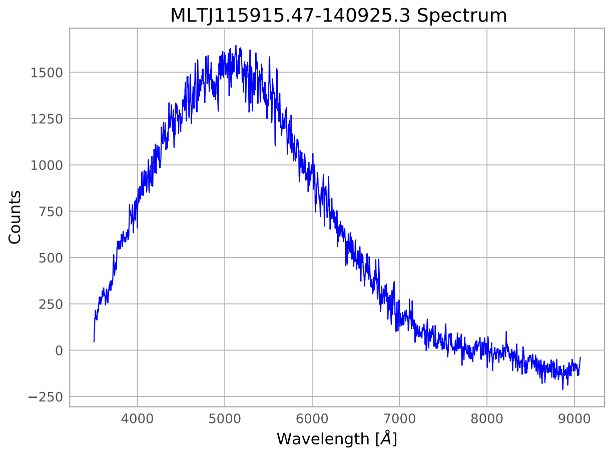

(b) MLTJ115915.47–140925.3.

Figure 140: MLTJ114618.09–314101.5 and MLTJ115915.47–140925.3 spectra.

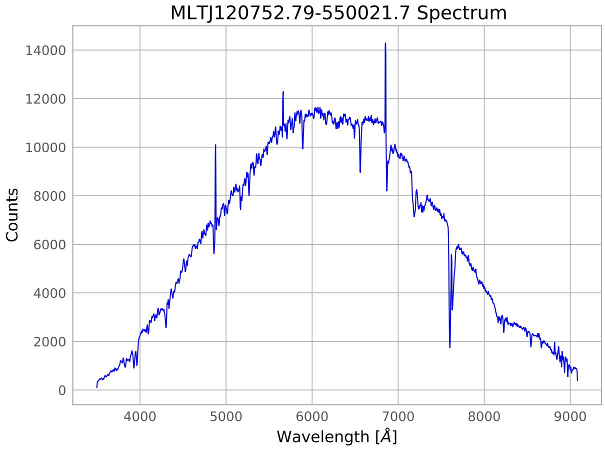

(a) MLTJ120752.79–550021.7.

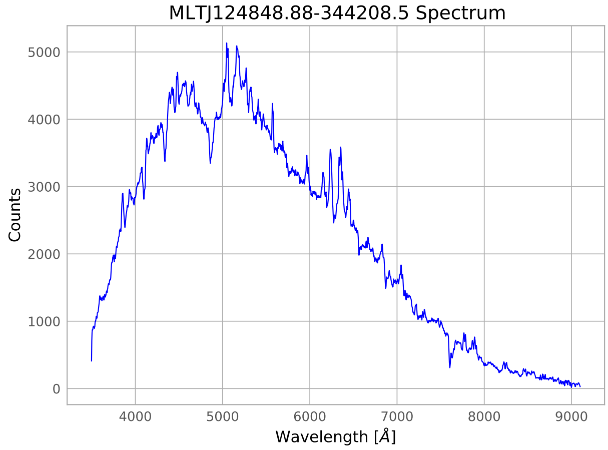

(b) MLTJ124848.88–344208.5.

Figure 141: MLTJ120752.79–550021.7 and MLTJ124848.88–344208.5 spectra.

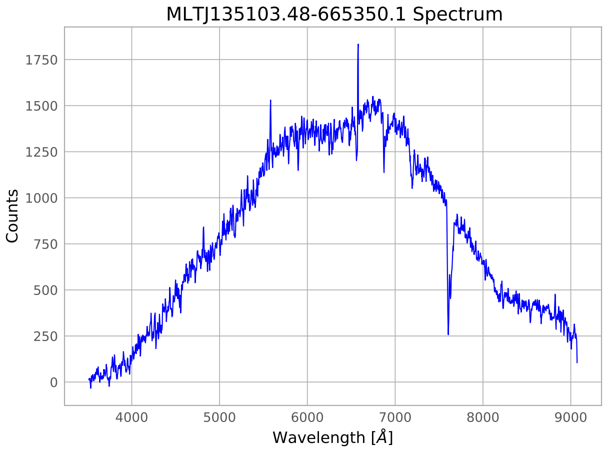

(a) MLTJ135103.48–665350.1.

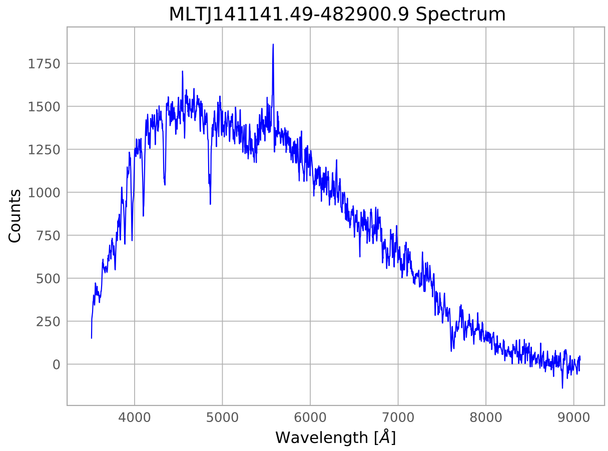

(b) MLTJ141141.49–482900.9.

Figure 142: MLTJ135103.48–665350.1 and MLTJ141141.49–482900.9 spectra.

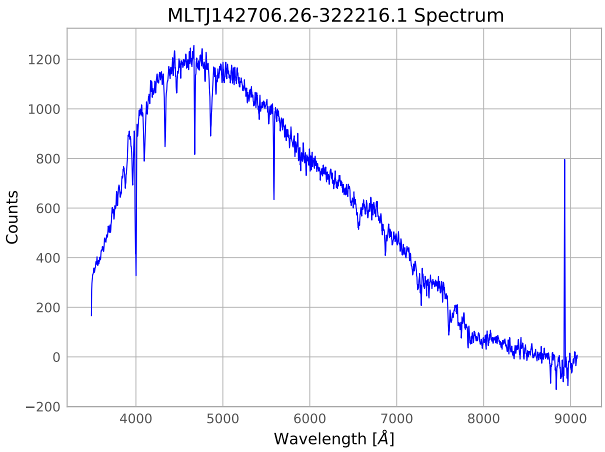

(a) MLTJ142706.26–322216.1.

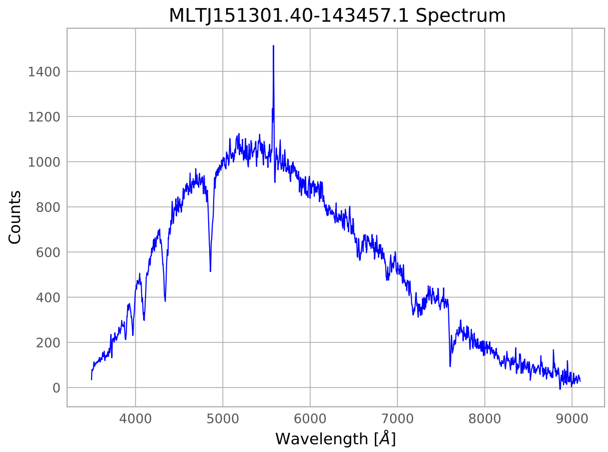

(b) MLTJ151301.40–143457.1.

Figure 143: MLTJ142706.26–322216.1 and MLTJ151301.40–143457.1 spectra.

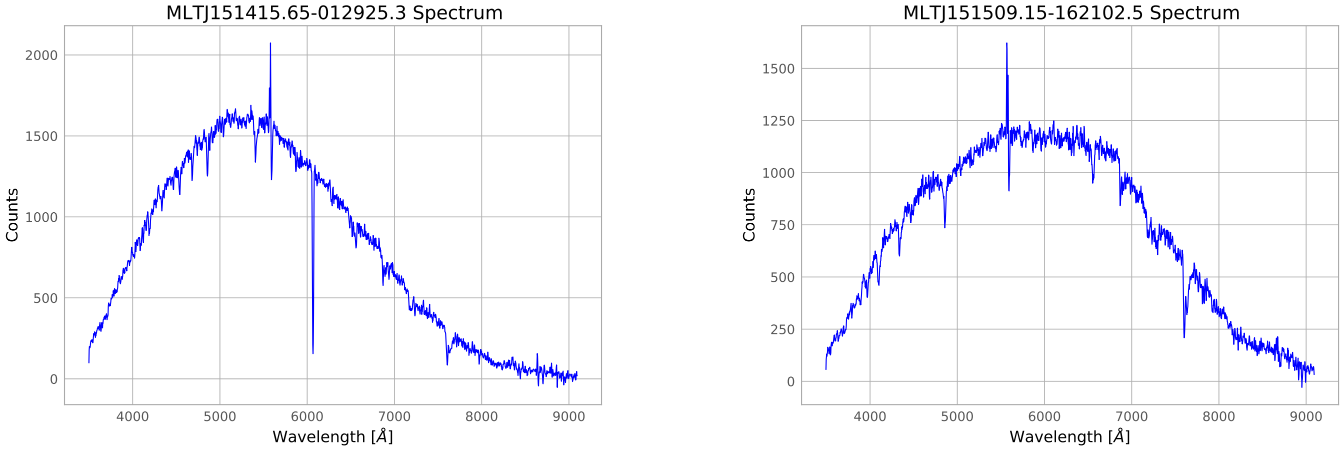

(a) MLTJ151415.65–012925.3.

(b) MLTJ151509.15–162102.5.

Figure 144: MLTJ151415.65–012925.3 and MLTJ151509.15–162102.5 spectra.

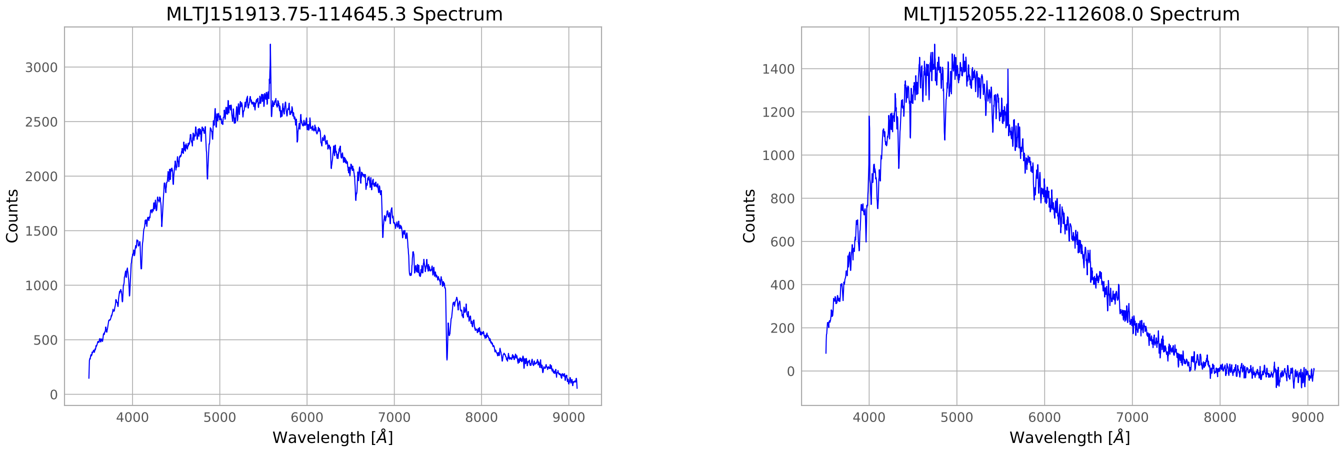

(a) MLTJ151913.75–114645.3.

(b) MLTJ152055.22–112608.0.

Figure 145: MLTJ151913.75–114645.3 and MLTJ152055.22–112608.0 spectra.

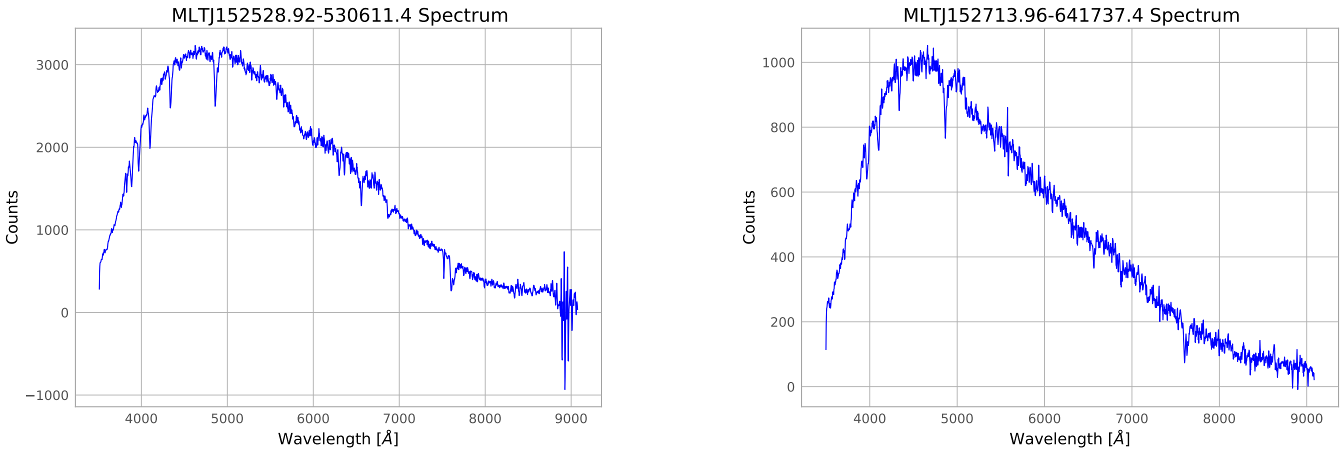

(a) MLTJ152528.92–530611.4.

(b) MLTJ152713.96–641737.4.

Figure 146: MLTJ152528.92–530611.4 and MLTJ152713.96–641737.4 spectra.

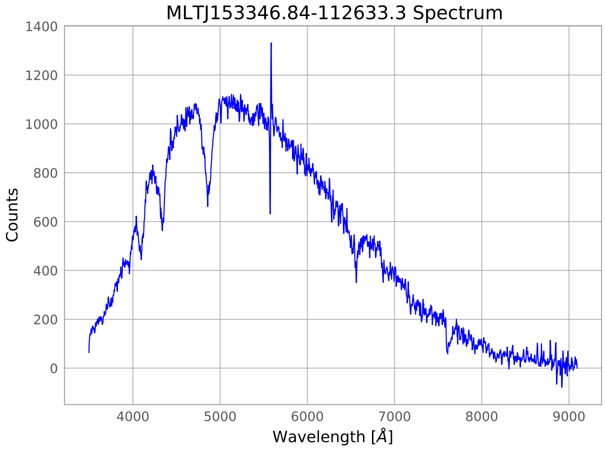

(a) MLTJ153346.84–112633.3.

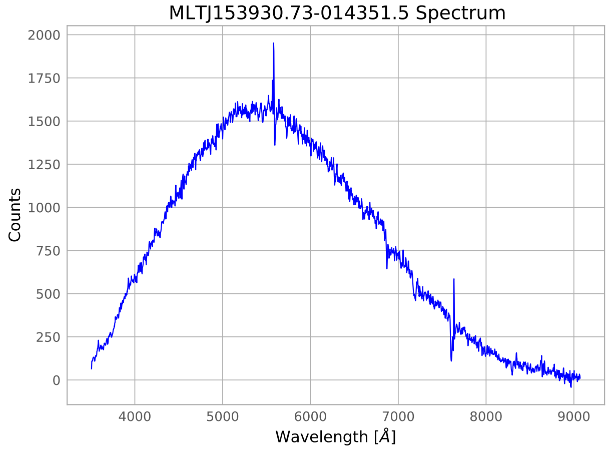

(b) MLTJ153930.73–014351.5.

Figure 147: MLTJ153346.84–112633.3 and MLTJ153930.73–014351.5 spectra.

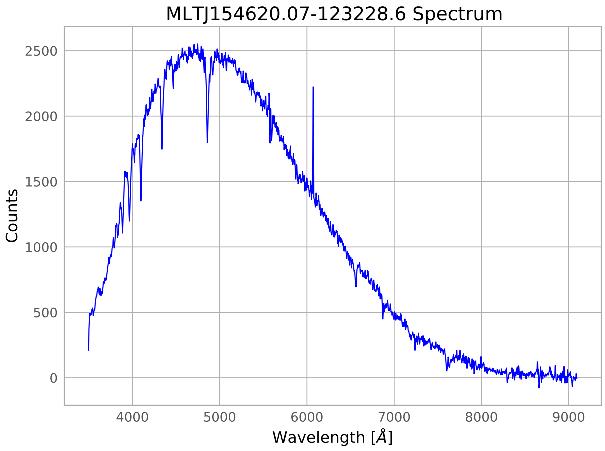

(a) MLTJ154620.07–123228.6.

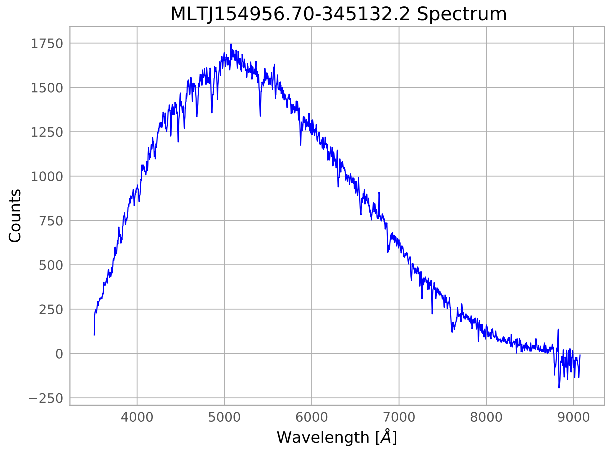

(b) MLTJ154956.70–345132.2.

Figure 148: MLTJ154620.07–123228.6 and MLTJ154956.70–345132.2 spectra.

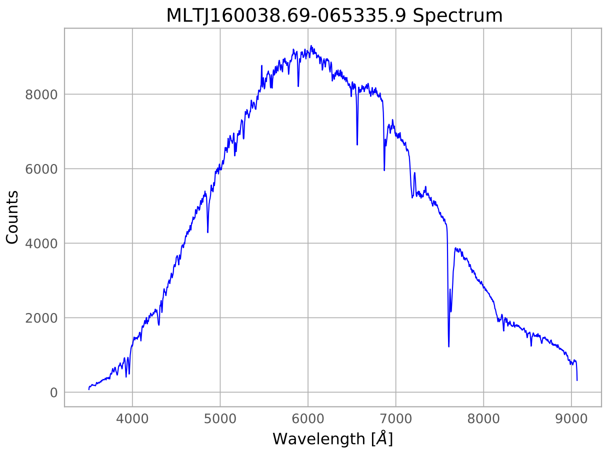

(a) MLTJ160038.69–065335.9.

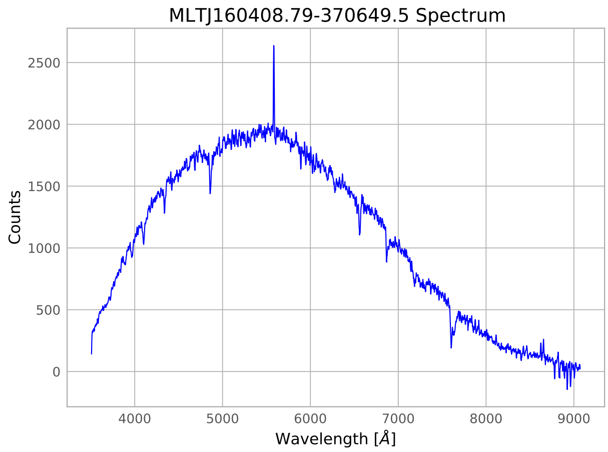

(b) MLTJ160408.79–370649.5.

Figure 149: MLTJ160038.69–065335.9 and MLTJ160408.79–370649.5 spectra.

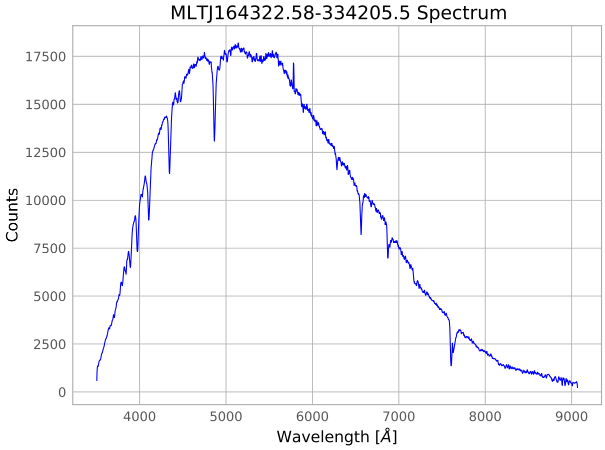

(a) MLTJ164322.58–334205.5.

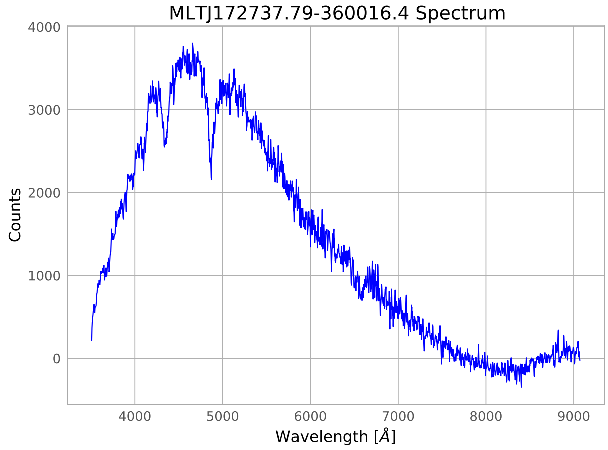

(b) MLTJ172737.79–360016.4.

Figure 150: MLTJ164322.58–334205.5 and MLTJ172737.79–360016.4 spectra.

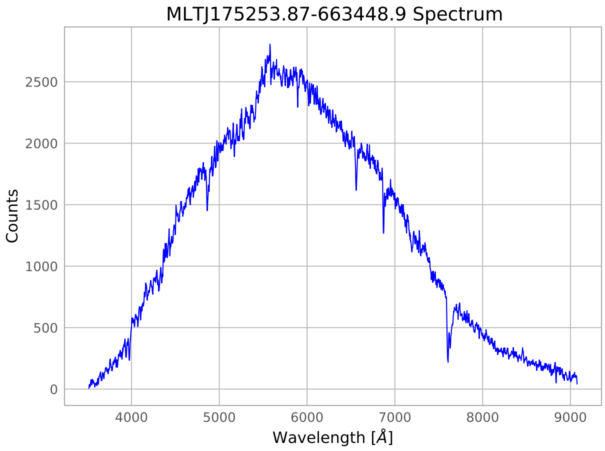

(a) MLTJ175253.87–663448.9.

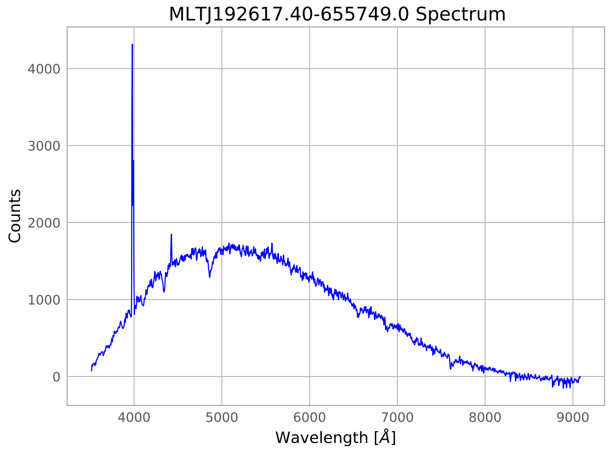

(b) MLTJ192617.40–655749.0.

Figure 151: MLTJ175253.87–663448.9 and MLTJ192617.40–655749.0 spectra.

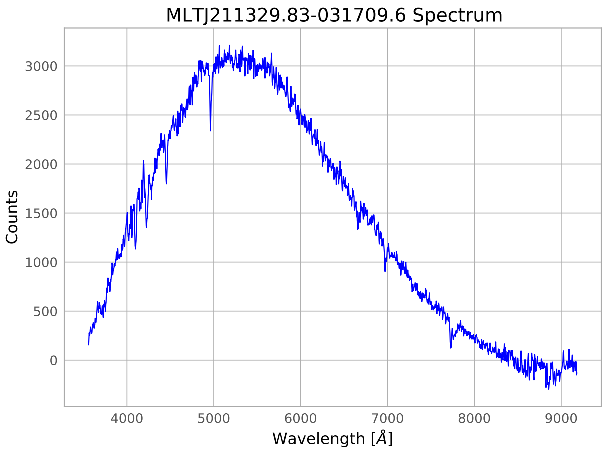

(a) MLTJ211329.83–031709.6.

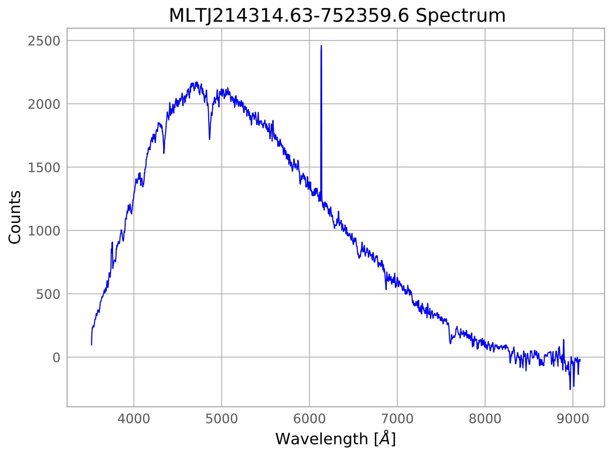

(b) MLTJ214314.63–752359.6.

Figure 152: MLTJ211329.83–031709.6 and MLTJ214314.63–752359.6 spectra.

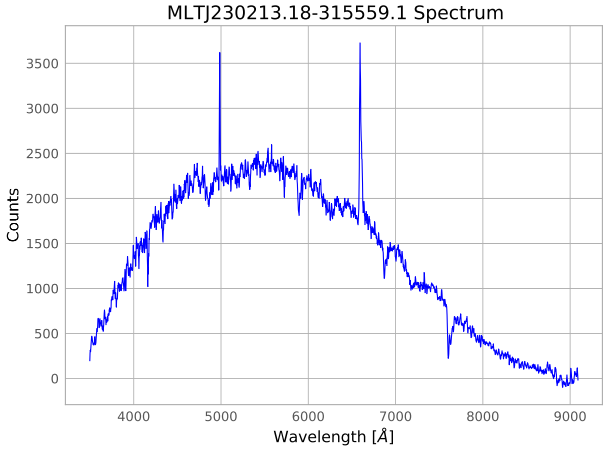

Figure 153: MLTJ230213.18–315559.1 spectrum.